Bertil Osheim

Quantifying Formation Hardness and Pore Pressure using the Bourgoyne-Young Drilling Model

Master's thesis

NTNU
Norwegian University of Science and Technology
Faculty of Engineering
Department of Geoscience and Petroleum

NTNU
Norwegian University of
Science and Technology

Bertil Osheim

Quantifying Formation Hardness and Pore Pressure using the Bourgoyne-Young Drilling Model

Master's thesis in Petroleum Geosciences and Engineering
Supervisor: Pål Skalle
February 2019

Norwegian University of Science and Technology
Faculty of Engineering
Department of Geoscience and Petroleum

NTNU
Norwegian University of
Science and Technology

Summary

Formation hardness and pore pressure are two important factors that must be carefully considered when planning a well and during drilling operations. They are both correlated with drilling efficiency and have the potential to inflict serious problems if deviations from the norm go undetected.

Hard formations reduce penetration rate and are associated with both equipment problems (drill pipe and drill bit failure) and downhole problems (washouts, doglegs and keyseats). The severity may vary, from worn and broken equipment requiring unnecessary tripping, to stuck drill string, which may lead to reaming or the drilling of a new well path. In the worst-case scenario, the hole must be abandoned. Thus, it is in the best interest to map out as much of the formation hardness as possible.

For well control, knowledge of the formation pore pressure and how it evolves throughout the length of the well is crucial. Failure to detect an increase in pore pressure can lead to various problems and instabilities. Well kicks are especially dangerous as they can lead to blowouts or loss of well section if not handled properly. Continuous pore pressure detection while drilling is a tool to prevent and mitigate such circumstances.

This master thesis presents a real-time approach for quantifying both formation hardness and pore pressure. Studies have been done on the correlation between hardness and lithology changes, as well as the effect on penetration rate from changes in formation hardness vs. pore pressure. The computation methods used are based on a simplified form of the Bourgoyne-Young penetration rate equation. Testing have been completed on real-time drilling data from a well in the Norwegian North Sea.

Results show that the method can quantify formation hardness and pore pressure. However, the desired precision of the pore pressure was not obtained when compared with field results in the final well report (FWR). This was reasoned to be caused by the sensitivity of the computed pore pressure to changes in hardness. Some improvements in results are expected if the method is tested on more complete sets of data. The inclusion of full well length data and a lithology indicator such as gamma ray will be especially beneficial.

Two test intervals were selected for hardness analysis. Occurances of hard stringers were shown in the first interval, which was in tune with statements made in the final well report. The second interval also showed tendencies of hard stringers. However, this section was characterized by oscillating hardness values. These oscillations happened to coincide with the lithology transition

between the Sandy Hordaland and Sandfree Hordaland formations. This lithology transition also marks the start of the abnormal pore pressure zone.

The tested well was marred with drilling incidents, causing many anomalies in the drilling parameters used as input data. Though this had a negative effect on the pore pressure results, it was able to highlight the vulnerability of using a solely drilling parameter-based approach such as the Bourgoyne-Young method for pore pressure calculations. Nevertheless, the method is seen as a viable tool if run together with other pore pressure detection methods such as seismic data (acoustic velocity/interval transit time), drilling mud properties and drilled cuttings.

The effect on penetration rate from changes in formation hardness vs. pore pressure was manually studied. In the normal pressured zone, hardness was found to have the most significant effect. In the start of the transition zone, the effect of increased pore pressure was seen. Further work is needed to develop a real-time method which can predict the effect of hardness vs. pore pressure based on penetration rate, and at the same time bypass the problem of pore pressure's sensitivity to changes in hardness.

Sammendrag

Formasjonshardheten og poretrykket er to viktige faktorer som må grundig undersøkes under planleggingsfasen og under boreoperasjonene av en brønn. Begge er korrelert til bore-effektiviteten og har potensial til å påføre alvorlige problemer hvis avvik fra normen forblir uoppdaget.

Harde formasjoner reduserer penetrasjonsraten og er assosiert med både utstyrsfeil (feil på borerør- og borekrone) og nedihulls-problemer (utvasking, doglegs og keyseats). Alvorlighetsgraden kan variere, fra slitt og ødelagt utstyr som krever unødvendig tripping, til at borestrengen blir sittende fast, noe som krever reaming eller boring av en ny brønnbane. I værste fall må borehullet forlates. Det er dermed viktig å kartlegge så mye av formasjonshardheten som mulig.

For brønnkontroll er det kritisk å ha kunnskap om formasjonsporetrykket og hvordan det utvikler seg gjennom hele lengden av brønnen. En uoppdaget økning i poretrykket kan føre til ulike problemer og ustabiliteter. Kick fra brønnen er spesielt farlige ettersom de kan føre til utblåsninger eller tap av brønnseksjon hvis de blir feil håndtert. Kontinuerlig overvåkning av poretrykket under boringen er et verktøy for å forhindre og begrense slike omstendigheter.

Denne masteroppgaven presenterer en sanntidsmetode for å kvantifisere både formasjonshardhet og poretrykk. Studier har blitt gjort på korrelasjonen mellom hardhet og endringer i litologi, samt effekten av penetrasjonsrate fra endringer i formasjonshardhet vs. poretrykk. Beregningsmetodene som brukes er basert på en forenklet versjon av Bourgoyne-Youngs ligning for penetrasjonsrate. Testing har blitt gjennomført på sanntidsdata fra en brønn i norsk del av Nordsjøen.

Resultatene viser at metoden kan kvantifisere formasjonshardhet og poretrykk. Imidlertid, den ønskede nøyaktigheten av poretrykket ble ikke oppnådd sammenlignet med felt-resultater i brønnrapporten. Dette blir begrunnet til å skyldes sensitiviteten av poretrykket til endringer i hardhet. Noe forbedring i resultatet er ventet hvis metoden testes på mer komplette sett av data. Inkludering av hele brønnlengden i dataene og en litologi-indikator slik som gamma-stråling ville vært spesielt nyttig.

To test-intervall ble valgt for hardhets-analyse. Hard stringers ble påvist i det første intervallet, noe som var i samsvar med bemerkninger i brønn-rapporten. Det andre intervallet viste også tendenser av hard stringers. Imidlertid var denne seksjonen karakterisert av oscillerende hardhets-verdier. Disse oscillasjonene sammenfalt med litologi-overgangen mellom Sandy Hordaland og Sandfree Hordaland formasjonene. Denne litologi-overgangen markerte også starten på den anormale poretrykk-sonen.

Den testede brønnen var full av hendelser under boringen som påvirket resultatet, spesielt ved å gi anomalier i bore-parameterne brukt som input. Selv om dette hadde en negativ effekt på poretrykks-resultatene, klarte det å synliggjøre sårbarheten av å bruke en metode kun avhengig av bore-parametere slik som Bourgoyne-Young metoden er for poretrykk-kalkulasjoner. Metoden anses imidlertid som et nyttig verktøy hvis brukt sammen med andre poretrykks-metoder slik som seismiske data (acoustic velocity/interval transit time), borefluid-egenskaper og utboret masse.

Effekten på penetrasjonshastighet fra endringer i hardhet vs. poretrykk ble studert manuelt. I den normale poretrykks-sona, ble hardhet funnet å ha den mest signifikante effekten. I starten på overgangs-sona til høyere poretrykk, ble effekten av poretrykk på penetrasjonshastighet funnet. Videre arbeid trengs for å utvikle en sanntids-metode som kan forutsi effekten av hardhet vs. poretrykk basert på penetrasjonsrate og samtidig omgå problemet med poretrykkets sensitivitet til endringer i hardhet.

Acknowledgements

This is a master thesis in Drilling Technology written at the Department of Geoscience and Petroleum at the Norwegian University of Science and Technology (NTNU). The thesis is written by Bertil Osheim, a 5th year student with specialization within drilling.

I would like to thank my supervisor, Professor Pål Skalle. He has been most helpful with his feedback, advice, knowledge, guidance and patience. I would also like to thank assistant supervisor and PhD Candidate Isak Swahn, who's knowledge in programming was very valuable. IPT and Statoil also deserve to be mentioned for providing real-time drilling data used in this thesis.

Trondheim, 2019

Bertil Osheim

Table of Content

1 Introduction

When drilling a well, the engineer should always strive towards making the job as safe and efficient as possible. However, characteristics of the geological formation encountered may induce various problems affecting the drilling process. The formation hardness and the formation pore pressure are two such triggering factors. To remain in control of the operation, it is in the best interest to be continuously informed on how these parameters change throughout the length of the well. It is also useful to know how these parameters interact and how they affect the penetration rate.

Formation hardness involves the resistance of the sedimentary formation against the compressive and shear forces generated by the rock bit. This means formation hardness is inversely correlated to the rate of penetration (ROP), which ultimately affects drilling time and cost. The drillability, the immediate drilling capacity, will however, be influenced by more than the sedimentary formation itself. Parameters such as those related to the drilling technique and to the specific bit selected for the job, must also be interpreted to maximize drilling efficiency.

Pore pressure is the pressure exerted by the fluids contained in the pore spaces of the formation. The pore spaces can contain fluids such as oil, gas or salt water or a mixture of these (Skalle, 2015). The magnitude of the pressure will vary depending on the type or density of the fluid, and the depth of formation. Abnormal pore pressure is pressure higher than the hydrostatic (normal) pressure. For well pressure control (except for underbalanced drilling) the pore pressure needs to be overbalanced by the pressure exercised by the circulated drilling fluid. Pore pressure detection is highly correlated to ROP and drilling efficiency through the magnitude of this differential pressure between mud and pore pressure. ROP is expected to increase with decreasing pressure differential.

Challenges associated with hard formations are often related to sudden or undesirable changes in the formation hardness. Hard stringers, which are thin layers of well cemented and consolidated rock, can cause such changes. The consequences can be mechanical and down hole problems. Incidents which interfere with the drilling progress include buckled or twisted off drillstring, bit failure, washout, pipe sticking at ledges and shoulders at the borehole wall, development of local dog legs and technical sidetracking (when combined with soft formations).

High formation pore pressure may also cause various problems and instabilities for the drilling operation. Predictions are made in the well planning phase, governing drilling strategy, casing program and mud weights. If values are not according to prognosis, pore pressure may become higher than the well pressure. Kicks and loss of well control are the most critical consequences. If not handled properly this can lead to a blowout or loss of the well section. Even if properly handled,

these instances require valuable time to restore the situation back to normal and thus increases drilling costs.

Another issue is that the formation hardness and formation pore pressure are both detected through the same drilling parameter, namely to rate of penetration. This means changes in penetration rate can be caused by either a change in formation hardness or pore pressure, or both. If for example increases in ROP are seen, the challenge is how to differentiate between an upcoming soft formation and increasing pore pressure.

The solution to the above stated problems today is to evaluate changes in ROP manually with the purpose of detecting immediate changes in hardness, and to use the d_c – exponent or Bourgoyne-Young method for pore pressure detection.

In this thesis, the following goals has been set:

- to show that both formation hardness and pore pressure can be continuously quantified during drilling

- to distinguish between decreased formation hardness and increased pore pressure when the drilling process is subjected to increases in penetration rate

The task will first of all be approached by creating data agents that can interpret and use real-time drilling data (RTDD) to calculate formation hardness and pore pressure.

It should be possible to mathematically detect and determine the drillability and pore pressure of the specific formation by using the Bourgoyne-Young formula for ROP. This formula is based on eight different equations, where each equation represents a different variable in the drilling process.

Manuel interpretations will be made to distinguish between the effects of changes in hardness vs. pore pressure on penetration rate.

2 Published Work Related to Drillability and Pore Pressure

The formation hardness can be detected and potentially separated into soft or hard formations by looking at the behavior of the drillability. As the drillability is influenced by a wider variety of factors than the simplified approach chosen in this thesis, it will be a challenge to evaluate its variation. To achieve good results, it is thus in the best interest to gain as much relevant information as possible on the topic of drillability.

It is also important to understand the geology surrounding the borehole and the potential damage sudden changes in hardness may cause to both the drilling equipment and well.

The pore pressure can either be normal or abnormal. Drilling in abnormal pressure zones can lead to various drilling problems, most notably well kicks. If not handled properly a kick may escalate to a blowout. Continuous pore pressure detection while drilling, as well as kick detection methods are thus essential to avoid such serious circumstances. These topics will be further addressed in this chapter.

Formation hardness can be calculated with the help of the d-exponent method. This method was originally developed to estimate pore pressure but can be used to estimate formation hardness instead. How this is done will be described.

Finally, the theory of the model selected for drillability and pore pressure calculations, the Bourgoyne-Young drilling model, will be addressed.

2.1 Published Work Related to Drillability

2.1.1 Rock geology related to its hardness

2.1.1.1 Main rock types

There exist 3 main classes of rocks: Sedimentary rocks, igneous rocks and metamorphic rocks.

- Sedimentary rocks are formed by the deposition of material on the Earth's surface and within bodies of water. Sedimentation is the collective name for processes that cause mineral and/or organic particles to settle and accumulate or minerals to precipitate from a solution. Examples of sedimentary rocks are coal, shale, clay, sandstone, chert, limestone and dolomite.

- Igneous rocks are formed through the cooling and solidification of magma or lava. The melting of the rock is caused by one or more of three processes: an increase in temperature, a decrease in pressure, or a change in composition. Examples of igneous rocks are granite and basalt.

- Metamorphic rocks are sedimentary, igneous or older metamorphic rocks which have been subjected to a process called metamorphism. This means the rock is exposed to high heat (temperatures greater than 150 to 200 °C and pressures of 1500 bars) causing a change in the original rock form. Examples of metamorphic rocks are quartzite, gneiss and marble.

In general, metamorphic rocks are considered the hardest of the main rock types. Next are igneous rocks, while sedimentary rocks are the softest.

2.1.1.2 Source rocks and reservoir rocks

Of the three main rock types, sedimentary rocks tend to be most interesting in the petroleum industry. Sedimentary rocks such as shale, limestone or coal can be defined as source-rocks. This means they are rocks rich in organic matter and if heated sufficiently will generate oil and gas. Under the right conditions, source rocks may also be reservoir rocks, as in the case of a shale gas reservoir. Reservoir rocks are rocks having sufficient porosity and permeability to store and transmit fluids. Sedimentary rocks are also the most common reservoir rock because they have more porosity than most igneous and metamorphic rocks. They also form under the right temperature conditions at which hydrocarbons can be preserved (Schlumberger[1], 2016).

2.1.1.3 Distinguishing between soft and hard geological formations

The rocks can be mapped in geological formations around the borehole. These formations are continuous body of rocks that are distinctive by their physical properties. Borehole measurements, such as in log or well tests, help to separate between the different formations. Several geological factors exist that will influence what makes a formation soft or hard. The most important causes are the degree of cementing, constituent minerals and mineral composition of the rock:

- Degree of cementing; Well cemented sandstones will be harder than looser cemented sandstones. The degree of cementing increases with depth. Through time, the older and deeper rock formations are exposed to an increasing overburden pressure. The resulting

compression causes mineral grains of the underlying rock to move closer together and pore water seeps out and up through overlying formations. These deep, tightly compacted and low porosity sands can be easily cemented, thus resulting in a higher density rock (Personal comments; Skalle, 2016).

- Constituent minerals; Rocks consisting of harder minerals like quartz, such as quartz sandstone, will be harder than rocks primarily consisting of softer minerals like calcite, such as limestone and dolomite.

- Mineral composition; A pure quartz sandstone will be harder than a sandstone also composed of feldspar or clay minerals in addition to the quartz.

Any physical, chemical and biological changes the sediments are subjected to after its initial deposition and lithification, such as in the compaction and cementing processes described above, are referred to as diagenesis. Diagenesis thus result in alterations to the rock's original mineralogy and texture, converting sediments or existing sedimentary rock into a different sedimentary rock. Important rock parameters such as porosity and permeability are considerably affected by these processes. The term diagenesis does however not include changes from weathering, which only occurs in situ (on site) at the earth's surface. Changes during diagenesis happens during relatively low temperatures and pressures, less than those required during metamorphism and in the formation of metamorphic rocks. No pressure limit between diagenesis and metamorphism exist, so there is no sharp boundary between diagenesis and metamorphism. However, when temperatures reach 200 °C, rock alterations are considered being strictly metamorphic (Wikipedia[1], 2016).

The degree of cementing, constituent minerals and mineral composition of the rock, will influence formation characteristics such as the elastic limit and ultimate strength of the formation. These are considered the most important formation properties affecting penetration rate. The shear strength predicted by the Mohr failure criteria sometimes is used to characterize the strength of the formation. Maurer has reported that the crater volume produced beneath a single tooth is inversely proportional to both the compressive strength of the rock and the shear strength of the rock. Bingham found that the threshold force required to initiate drilling in a given rock at atmospheric pressure could be correlated to the shear strength of the rock as determined in a compression test at atmospheric pressure. The permeability of the formation also has a significant effect on the penetration rate. In permeable rocks, the drilling fluid filtrate can move into the rock ahead of the bit and equalize the pressure differential acting on the chips formed beneath each tooth. This will tend to promote more explosive elastic mode of crater formation. It can also be argued that the nature of the fluids contained in the pore spaces of the rock also affects this mechanism since more filtrate

volume would be required to equalize the pressure in a rock containing gas than in a rock containing liquid. The mineral composition of the rock will affect penetration rate because rocks containing hard, abrasive minerals can cause rapid dulling of the bit teeth. Rocks containing gummy clay minerals can cause the bit to ball up and drill in a very inefficient manner (Bourgoyne et.al., 1986)

A geological formation is seldom completely uniform. In soft formations, thin, discontinuous mineral veins or rock layers consisting of harder and more abrasive rock types, called hard stringers, can be experienced. Likewise, in hard formations, softs stringers may occur (Glossary, 2016).

Hard stringers are formed when compressive forces act on thin veins of calcium carbonate, a common compound with the chemical formula $CaCO_3$. The minerals calcite and aragonite are two polymorphs of $CaCO_3$, both largely making up the composition of the sedimentary rock of limestone. Calcite is not only found in sedimentary carbonate rocks, but also as a cementing material in sedimentary clastic rocks such as shale and sandstone. Aragonite is a high pressure polymorph and thus occurs in high pressure metamorphic rocks such as those formed in subduction zones. Another mineral of calcium carbonate is vaterite, but it is not commonly found because its high solubility makes it very unstable at ambient conditions at the surface of the earth. As soon as vaterite is exposed to water it converts to one of the more common minerals of either calcite (at low temperatures) or aragonite (at high temperatures).

When $CaCO_3$ is subjected to high heat and pressure two processes called calcination and/or metamorphism can occur. During calcination the CO_2 is separated from the $CaCO_3$. During metamorphism the $CaCO_3$ is recrystallized, such as when limestone changes to marble. Both these processes result in the mineral crystals interlocking more closely (into something called granules). Being more concentrated the minerals also become harder, and when found in larger amounts as thin layers or veins they will form hard stringers. In a geologic formation the thickness of hard stringers may vary from half a meter up to two meters. Thus, they can act as a sealing barrier which is lessening the compressive forces on formations located beneath them (Personal comments; Skalle, 2016).

Re-alignment of minerals during metamorphism also produces another distinctive rock texture called foliation. When subjected to pressure the individual minerals align themselves perpendicular to the stress field such that their long axes are in the direction of these planes (which may look like the cleavage planes of minerals). Usually, a series of foliation planes can be seen parallel to each other in the rock. Foliations represent distinct planes of weakness in the rock as they easily brake along these planes (Flexible Learning, 2016).

As the grade of metamorphism increases, resulting from higher temperature and/or pressure, both crystal size and the coarseness of foliation will increase (For example, gneiss represents a higher-grade metamorphic rock than does schist).

Sedimentary rocks may also be laminated. This means the rocks are composed of many fine layers of thin planar structures, usually one centimeter or less in thickness (as opposed to bedding layers, which are greater than 1 cm and up to several meters in thickness). The laminations consist of various sediments, caused by cyclic changes in the supply of sediment to the rock, changes that can occur in grain size, clay percentage, microfossil content, organic material content or mineral content. Laminations can occur as both parallel structures or in different sets that make an angle with each other, called cross-lamination. Either way they tend to cause a reduction in the rock permeability. Shales are naturally laminated, but lamination can occur in many different types of sedimentary rocks, from coarse sandstones to fine mudstones or in evaporites (Wikipedia[2], 2016).

The term laminated formation is commonly used for describing larger scale geological formations with a high frequency of alternating hard and soft rock layers. Typically, only 3-15 meters of thickness separate the different kinds of layers or beddings in these formations (Personal comments; Skalle, 2016).

2.1.2 Drilling problems associated with soft and hard stringers

"While the penetration rate to some degree can be influenced by the operator's choice of drilling-techniques, -bits and -fluids, the geological formation encountered is the only factor truly independent of control" (Head, 1951).

Undetected soft and hard stringers can have serious consequences on the drilling operation. Drilling into harder and more abrasive formations will lead to a reduction in penetration rate and cause more wear on the drilling equipment. For example, if the bit frequently becomes dull or broken, and no longer drills the rock efficiently, round trips to change the bit are necessary. A general estimate for a competent crew is that a round trip requires one hour per thousand feet (304.8 meter) of hole, plus an hour or two for handling collars and bits. At that rate, a trip in a ten thousand-foot (3048 meter) well might take twelve hours (Schlumberger[2], 2016). This lost time will drastically increase total drilling expenses, when considering a drilling operation on the Norwegian Continental Shelf in 2015 would cost between 5-10 MNOK/day (Norwegian Petroleum Directorate, 2016).

Other potential complications besides equipment failure involve downhole problems which can lead to severe damage to the borehole wall and thus potentially mitigate the well integrity.

2.1.2.1 Equipment failure

a) Drillpipe failure related to hard formations

The consequences of drillpipe failure are severe and may include loss of bottomhole assembly (BHA), fishing, bitballing and hole instability. Improper BHA design and wrongly selected drilling parameters in hard rock or sticky formation can lead to intensive vibrations (Abdollahi, 2003).

Potential failure modes of the drill pipe are usually put into four different categories:

1. Twistoff: Occurs when the induced shearing stress caused by high torque exceeds the pipe-material ultimate shear stress. Most common in directional and extended-reach drilling where torques in excess of 80,000 lbf-ft (108.5 kN-m) are frequent and can easily cause twistoff to improperly selected drillstring components.

2. Parting: Occurs when the induced tensile stress exceeds the pipe-material ultimate tensile stress. This may happen when an overpull is applied to free a stuck pipe.

3. Collapse and burst: Seldom occurs, but may arise during extreme conditions of high mud weight and complete loss of circulation.

4. Fatigue: A type of failure induced by repeated (cyclic) dynamic loads. It starts by the development of microcracks which then propagate into macrocracks as a result of the cyclic stresses. Drillstring vibrations, bending-load reversals in curved sections of the hole and doglegs caused by rotation may all lead to fatigue failure. Downhole environments with presence of O_2, CO_2, chlorides and/or H_2S can also corrode the pipe which aggravates the problem (Petrowiki[1], 2017).

The negative effects of hard formations or stringers can be connected to many of these failure mechanisms. The most direct link is to pipe twistoff. As the penetration rate decrease in a harder formation, the driller may seek to restore or increase the ROP by putting more weight on the bit. Higher WOB can induce higher drillstring torque. If the resulting shear stresses go above the pipe ultimate shear stress limit then the pipe will twist off. Wrong torque may also wear the drill string leading to hole in string and pipe wash out (Personal comments; Skalle, 2017). This is a precursor for pipe parting, discussed below. The highest torques occurs in highly deviated wells, so when operating

in such conditions it is important to check for the torsional strength of the pipe during drill pipe selection (Effendi, 2015).

Parting of the drill pipe is another possible outcome caused by hard formations and too high WOB. For this to happen, it will require a series of ill-fated incidents occurring during the drilling process. Incorrect decision-making and job execution by the drilling operators would also be a contributory factor. The order of and involved incidents to cause drill pipe parting would be;

1. Increased rock resistance caused by hard formation.
2. Excessive WOB is applied with means to increase penetration rate.
3. A decrease in penetration rate at the excessive WOB (this behavior is called bit floundering*) occurs because of cutting generation exceeds the capacity of efficient bottomhole cleaning**.
4. Inefficient hole-cleaning lead to accumulation of drilled cuttings in the annular space.
5. Settling of large amounts of suspended cuttings to the bottom of the hole (particularly in deviated wells) when the pump is off or the downward sliding of a stationary-formed cuttings bed on the low side of the hole pack the bottomhole assembly (BHA).
6. Mechanical pipe sticking occurs when tripping out (assuming no circulations of bottom up with the drill bit off bottom to flush out any cuttings bed was done prior to tripping).
7. Overpull is selected as method to free the pipe.
8. Pipe is parted during overpull because the induced tensile stress exceeds the pipe-material ultimate tensile stress***.

Sources: Bit floundering (Bourgoyne et al., 1986), Mechanical pipe-sticking (Petrowiki[2], 2017)
*Bit floundering can also be caused by a complete penetration of the cutting element into the hole bottom. This may lead to change of bit-components (Bourgoyne et al., 1986).
**The poor response of penetration rate at high values of rotary speed (not just at high values of WOB) is also usually attributed to less efficient bottomhole cleaning (Bourgoyne et al., 1986).
***To prevent the drillpipe-parting the pipe need to be checked for its maximum tensional load. This can be calculated from known weights of the drill collars and drill pipe below the point of interest, including the effects of buoyancy. A design factor (usually max pipe tension load multiplied by 1.15-1.3) and a margin of overpull (MOP) should also be added for extra safety. The MOP is the tension in excess of the drill string weight which is exerted when pulling on the string. It may be from 50,000 – 100,000 lbs (22,700 – 45,000 kg). A third potential safety factor for slip crushing can also be added. This allows for the interaction of the hoop stress (S_h) caused by the drill pipe slips with the tensile

stress (S_t) caused by the weight of the string. This effect reduces the allowable tension load by a factor (S_h/S_t) (Effendi, 2015).

Pipe failure because of mechanical collapse and mechanical burst is rare. Pipe burst may however occur under extreme conditions of too high mud weight and complete loss of circulation. Changes in formation hardness are not typically associated with this phenomenon. Lost-circulation can be caused by drilling in formations that are inherently fractured, cavernous (limestones) or have high permeability (usually shallow sands with permeability more than 10 darcies). Maintaining proper mudweight, minimizing annular-friction pressure losses during drilling and tripping, adequate hole cleaning, avoiding restrictions in the annular space, setting casing to protect upper weaker formations in transition zone and updating formation pore pressure and fracture gradients for better accuracy with log and drilling data, are all precautious measures for avoiding lost-circulation. If zones of lost-circulation are anticipated, the operator should treat the mud with loss of circulation materials (LCM) and perform preventive tests such as the leakoff test and the formation integrity test (Petrowiki[3], 2017).

According to Effendi, drill pipe burst pressure resistance is generally considered not of great importance during drill pipe selection. Burst pressures only occur when pressuring up the string on a plugged bit nozzle or during a drill stem test (DST). In these situations, pressure builds up inside the string towards the leakoff pressure. If the pressure becomes too high compared to the annulus pressure, then the pipe will burst (Personal comments; Skalle, 2017). Still, it is very unlikely that the burst resistance of the pipe will ever be exceeded under normal drilling conditions.

The collapse load of the pipe is however more important. Also, in this case for maximum collapse pressure, the DST is involved. The DST is a procedure which tests the geological formation for formation pressure, permeability and productive capacity. During the test the hydrostatic pressure inside the drill string have been reduced by running the string partially full of mud, encouraging the formation fluids to flow into the well bore. The highest external pressure tending to collapse the string will occur at the bottom of the hole when the string is run empty in the hole, which only occurs when running a DST and prior to opening of the DST tool. If a non-return valve is run (preventing upward flow of fluid into the drill pipe) it is normally standard practice to fill up the pipe at regular intervals when running in.

Drillpipe fatigue failure is the most common and costly type of failure in oil/gas and geothermal drilling operations. Drilling in hard formations can induce repeated drillstring vibrations severe enough for micro- and macrocracks to emerge in the pipe and potentially destroy it. Cyclic stress

reversals and bending load reversals due to curved hole sections and bends in dog-legs caused by rotation, also contributes to fatigue failure. The combined action of these cyclic stresses and downhole corrosion can shorten the life expectancy of a drillpipe by thousand folds.

In spite of the vast amount of work that has been dedicated to pipe fatigue failure, it is still the least understood. This lack of understanding is attributed to the wide variations of statistical data in determining type of service and environment of the drillstring, magnitude of operating loads and frequency of occurrence (load history), accuracy of methods in determining the stresses, quality control during manufacturing, and the applicability of material fatigue data.

There are some preventive measures that can be taken to mitigate fatigue failure. These involve minimizing induced cyclic stresses and insuring a noncorrosive drilling environment. Minimizing cyclic stresses is done by controlling dogleg severity and drillstring vibrations. Proper BHA design, correctly selected drilling parameters and continuous downhole vibration monitoring will help reduce intense vibrations in hard rock or sticky formations (Abdollahi 2003). According to Head, the rotational speed should be kept at 40-100 RPM in hard formations such as limestones, quartzite, anhydrite and sandstones to lessen the wear on the drilling equipment. At high rotational speeds severe vibrational conditions exists which can cause premature failure of the drill pipe (Head, 1951). Corrosion can be lessened with corrosive scavengers and controlling the mud pH in the presence of H_2S. The proper handling and inspection of the drillstring on a routine basis are the best measures to prevent failures (Petrowiki[1], 2017).

b) Low ROP/drill bit failure

The wearing mechanism of the drill bit will not be the same in hard as in soft formations. It is especially the mineral composition of the rock which effect the penetration rate and bit wear. For example, rocks containing hard, abrasive minerals can cause rapid dulling of the bit teeth, while rocks containing gummy clay minerals can cause the bit to ball up and drill in a very inefficient matter (Bourgoyne et al., 1986). The wrong choice of bit in regard to the formation characteristics will aggravate these problems, potentially causing complete bit failure.

Bit selection is a difficult challenge, because the best available bit for a job can only be determined by trial and error. The performance of various bits can be compared by computing the drilling cost per unit interval drilled. However, since no mathematical computations allow the same hole section to be drilled more than once, comparisons must be made between succeeding bits in a given well or

between bits used to drill the same formation in different wells. The formations drilled with a given bit on a previous nearby well can be correlated to the well in progress using well logs and mud logging records (Bourgoyne et al., 1986).

If no prior bit records exist, several rules of thumb are used for initial bit selection. These rules include utilizing a classification chart listing bit types applicable in a given formation hardness, in addition to bit cost considerations and bit versatility considerations. Three-cone rolling-cutter bits are the most versatile bit type and are a good initial choice for the shallow portion of the well. Diamond drag bits perform best in nonbrittle formations having a plastic mode of failure, especially in the bottom portion of a deep well, where the high cost of tripping operations favors a long bit life, and a small hole size favors the simplicity of a drag bit design. PCD drag bits perform best in uniform sections of carbonates or evaporites that are not broken up with hard shale stringers or other brittle rock types. PCD drag bits should however not be used in gummy formations, which have a strong tendency to stick to the bit cutters.

To evaluate bit performance, it is important for drillers to make careful inspections of dull bits removed from the well. This can indicate what type of wear the bit has been subjected to, whether it is primarily bit teeth, bit diameter (gauge) or bearing wear. A numerical code exists for reporting the type along with the grade of bit wear, allowing important aspects of bit wear to be quantified and logged quickly in bit reports.

The knowledge of the suitable time interval for bit use and instantaneous rate of bit wear are also important when evaluating the condition of a dull bit. Pulling bits out of hole when there is considerable bit life remaining will waste expensive rig time on unnecessary tripping. On the other hand, if the time interval for the bit is increased too much, the bit may break apart leaving junk in hole. This require an additional trip to fish the junk out of hole or may greatly reduce the efficiency of the next bit if an attempt is made to drill past the junk.

Instantaneous rate of bit wear is divided in rate of tooth- and rate of bearing wear. Rate of tooth wear is affected by drilling parameters such as formation abrasiveness, tooth geometry, bit weight, rotary speed and the cleaning and cooling action of the drilling fluid. Rate of bearing wear is correlated to rotary speed (must be kept low enough to prevent excessive temperature increase), bit weight, mud properties and the hydraulic action of the drilling fluid. Based on the combined action and effect of these parameters, equations for both rate of tooth wear and rate of bearing wear have been developed. These equations will provide a rough estimate of when the bit is completely worn and when to safely pull the bit out of hole.

Bit wear is a contributory factor to a less effective penetration rate. However, the wearing mechanism is a gradual process, meaning it becomes less relevant regarding sudden changes in formation hardness, such as when drilling into hard stringers. In these instances, complete bit failure becomes a probability. For uniform lithologies it is recommended to pull the bit when the penetration rate decreases rapidly as bit wear progresses and the computed cost-per-foot increases rapidly. For non-uniform lithologies, the best chance for avoiding bit failure is to have drilled enough wells in the area to have defined the lithologic variations. For example, it is sometimes desirable to drill an abrasive formation with an already dull bit and then place a sharp bit in the next shale section. Alternately, it may be best to terminate a bit run in order to place a hard formation bit in an extremely hard abrasive section where severe gauge problems are likely to develop.

For more thorough information about drill bits, the reader will be referred to Applied Drilling Engineering, Chapter 5, Rotary Drilling Bits.

Regardless of whether it is the pipe or the drill bit causing the equipment failure, the cost of fishing operations and the sometimes unsuccessful attempts to retrieve the fish out of the hole can lead to the loss of millions of dollars in rig downtime, loss of expensive bottom hole assembly such as directional drilling tools and high-tech logging equipment, or abandonment of the already-drilled section below the fish. Other outcomes are that the well may have to be finished early (if you can use the shallower part of the wellbore to reach your objective), or that cement must be poured on top of the fish and a side-track must be drilled around it.

2.1.2.2 Downhole problems at the borehole wall (Borehole wall damage)

When drilling from softer to harder formations damage to the borehole wall may also occur, such as washouts, doglegs and keyseats. These sorts of problems will be covered in this section.

a) Hole enlargement/Washout

A washout is an openhole section of the wellbore larger than the original hole size or size of the drill bit (Schlumberger[3], 2017). The enlargement is caused by removal of formation grains during drilling or circulation operations. Two mechanisms that can explain this local wall collapse are insufficient mud weight and/or hole erosion due to improper mud design. Other contributing factors to washouts are use of excessive bit jet velocity, soft or unconsolidated formations, in-situ rock stresses,

mechanical damage by BHA-components and chemical attack and swelling or weakening of shale as it contacts fresh water (Agwu and Akpabio, 2012).

As previously mentioned, the driller may increase the weight or the torque on bit to compensate for the decline in penetration rate when entering a harder formation. Too much force or weight on top of the string can lead to buckling of the drill pipe. The most common consequence of tubular buckling is that the drill string breaks leading to a fish in the hole. However, if the formation situated above the harder formation is very soft or weak, the buckled pipe may start to erode into the side of the borehole wall in this softer formation. Erosion increases as the drill string is being rotated and a washout can form at the wall (Odfjell, 2015).

During circulation, a washout leads to lower flow velocity of drilling fluids which can accumulate cuttings and cause inadequate hole cleaning. This can cause restrictions in the hole which may lead to increase in hook load, large overpulls and finally to pipe sticking. Pipe sticking is particularly troublesome during tripping operations in inclined-wells as cuttings accumulate on the low side of the well, packing the BHA-assembly. The pipe can also get stuck at undetected ledges near the washout location. If unconsolidated, the formation may also have collapsed into the hole, which can form a bridge around the drill string. Another effect of washouts and the resulting decrease in hole cleaning capability is that it may lead to the excess cuttings causing an increase in annular pressure. This can result in wellbore fracture and lost circulation. If remaining untreated, washouts become more severe with time. Remedies to minimize washouts include increasing the mud density and choosing appropriate mud types and additives.

b) Dogleg

A dogleg is a particularly crooked place in the wellbore where the trajectory of the wellbore in three-dimensional space changes rapidly. Permissible or controlled doglegs can be created intentionally by directional drillers to reach the desired well target. However, doglegs may also form unintentionally, such as when drilling from a soft to a hard formation or when drilling in alternating soft and hard formations. In such cases the well path can change direction faster than anticipated or desired.

Severe local doglegs are associated with many harmful side effects. First, the wellbore is not located in the planned path. Second is the possibility that a planned casing string may no longer fit easily through the curved section. Third, casing successfully cemented through the dogleg may wear unusually quickly due to high contact forces between the drillstring and the inner diameter of the casing through the dogleg. Wearing of tool joints and worn spots in the casing may lead to collapse

or a hole in the casing. Fourth, doglegs and ledges between hard and soft formations can cause damage to BHA components such as logging tools and drill collars, or it can stick the drill string, particularly when tripping out. This is less of a problem when drilling or tripping in, as the drillstring will be under less tension and more flexible and able to circumvent obstacles. Finally, excessive doglegs increase the overall friction to the drillstring, which also increase the likelihood of getting stuck or not reaching the planned total depth.

Fortunately, problems caused by doglegs are manageable. To reduce the increased torque and drag between the drill string and the wellbore wall, lubricants can be introduced into the mud system. Tension in the drill string can also be reduced by removing excess collars or replacing the collars with heavy-weight drill pipe. The heavy-weight drill pipe is more flexible and reduces the overall string weight while maintaining the same available bit weight. If the dogleg impairs the well considerably, more extensive remedial action can be done, such as reaming or underreaming through the dogleg, or even sidetracking in extreme situations.

Sources: (Schlumberger[4], 2017), (Directional Drilling Technology, 2012)

c) Keyseat

A keyseat is a worn spot or groove in the side of the borehole wall. This condition is created by the repeated abrasion of the rotating drillstring. However, to start cutting into the wall, there also need to be large enough lateral forces acting on the string. Both in undetected ledges near washouts or in doglegs can these circumstances occur. Keyseats will also form more easily in soft formations, as lower lateral forces are required than in hard formations.

Keyseating is another major cause of mechanical pipe sticking. Logging tools, BHA components and other large diameter drilling tools such as tool joints, drill collars and stabilizers often get stuck when pulled out through the keyseat section.

Preventive measures for avoiding keyseats include keeping any turns in the wellbore as gradual and smooth as possible. For stuck pipe in existing keyseats, the remedy involves enlarging the worn channel so that the larger diameter tools will fit through it. Today, this can be done using specialized keyseat wiper and reamer tools.

Tight hole or stuck pipe situations are the most common problem associated with borehole wall damage, whether being caused by washouts, doglegs or keyseats. Since the remedial actions usually are reaming or sidetracking, the main consequence is loss of time. Instabilities may also cause

considerable problems to later operations in the borehole. It may become difficult to run wireline logs, and in particular interpret the logs, since log interpretation is usually based on the assumption of a gauge hole with known size. Irregular borehole shape also leads to large uncertainty in the required cement volume. Poor cementing of the casing can lead to problems for perforation, sand control, production and stimulation. Finally, instabilities may trigger new instabilities.

Sources: (Sclumberger[5], 2017), (Fjær et al., 2008)

2.1.3 Shale and its effect on the drilling operation

Shale is a fine-grained, clastic sedimentary rock composed of mud that is a mix of flakes of clay minerals and tiny fragments (silt-sized particles) of other minerals, especially quarts and calcite. The ratio of clay to other minerals is variable, but from a rock mechanical viewpoint, it is natural to define shale as a rock in which clay minerals constitute a load-bearing framework. In practice this means that the clay content needs to be higher than about 40%. Shale texture is strongly anisotropic and split along planes of weakness into thin laminae or parallel layering or bedding, less than one centimeter in thickness, a characteristic called fissility. The degree of anisotropy may however vary significantly, depending on both depositional environment and post-depositional processes.

Pore sizes in shale are very small, typically between 5 and 25 nm. In addition, the clay minerals contain structurally bound water. This means that it is difficult to measure as well as define the elastic properties of the solid materials contained in shales. The properties depend on which type of clay mineral (kaolinite, smectite, illite) is dominant, and in particular on the adsorbed or bound water present within minerals and on mineral surfaces. This means bulk modulus may range from 5 (bound water) to 51 GPa (dry state, no bound water) and shear modulus in a similar range from 4 to 32 GPa.

Shale porosity may vary from very small (a few %) to quite high (up to 70%). Even with the highest porosities, permeability remains very small. The nanometer sized pores lead to laboratory measured permeabilities in the nano Darcy range, while even lower values may be expected for shale under in situ conditions. Black organic shales are the source rock for many of the world's most important oil and natural gas deposits. In the case of conventional reservoirs, the oil and gas has migrated out and upwards from the shale into an overlaying rock unit such as sandstone. Although conventional drilling can extract large amounts of oil and natural gas from the reservoir rock, much of it remains trapped within the shale, either within the tiny pore spaces or adsorbed onto clay mineral particles. New techniques, such as hydrofracturing, have managed to increase the permeability in shale by pumping water down the well under high enough pressure to fracture the shale. Hydrofracturing has

together with horizontal drilling, which gives a very long "pay zone" through the reservoir rock, revolutionized drilling technology and paved the way for the modern shale gas drilling industry.

75% of drilled formations consist of shale, which is either encountered in the overburden or as a cap rock surrounding the reservoir. Shale can be very problematic during drilling and is reckoned as the cause of more than 90% of wellbore instability problems. Because of the anisotropic nature of shale, it splits more easily when the load is directed parallel to the beddings planes versus normal to the planes. This strength anisotropy influences borehole failure, in particular for deviated holes. Shale instability problems include:

- Increased borehole diameter: Borehole size can be increased due to failure and caving of the wellbore wall in brittle shale. This can also happen by hydraulic or mechanical erosion in weaker and ductile shales. In driller's language, "sloughing shale" is often used, (although not very well defined) to describe fragments or "spallings" generated from the borehole wall. Although often thought to be of a chemical origin, this is first of all a mechanical problem, which to some extent may be influenced by shale-fluid interactions. If the cavings are not transported away, this represents a potential source of stuck pipe situation.

- Reduced borehole diameter: This may occur in very weak (plastic) shales, but also in sandstones, salt and some chalk formations. The case of very soft (plastic) shale is sometimes referred to as "gumbo shale". Such shale is often sticky, contains considerable amounts of swelling minerals (montmorillonite), and may cause problems like bit balling and solids accumulation. Hole closure (sometimes referred to as creep under the overburden pressure) is also associated with increased torque and drag, increased pipe sticking and increased difficulty of casing landings.
  It has traditionally been thought that large hole diameter reductions might be caused by swelling clays. The potential chemical swelling of a shale in downhole stress conditions is however very limited, as was pointed out by Santarelli and Carminati (1995). Large hole deformation is thus a result of primarily plastic shale deformation (Fjær et al., 2008).

- Inappropriate hole cleaning: Hole cleaning is a problem interrelated with hole collapse, as rock fragments produced by the failed formation may not be fully removed by the drilling fluid. This is more problematic in shale than in sand formations, as shale cavings are tougher to remove than sand particles.

Chemical-induced shale instability is caused by the drilling fluid/shale interaction, which alters shale mechanical strength as well as the shale pore pressure in the vicinity of the borehole walls. The mechanisms that contribute to this type of instability include:

- Capillary pressure: During drilling the mud in the borehole contacts the native pore fluid in the shale through the pore-throat interface. This results in the development of capillary pressure ρ_{cap}, which is expressed as

$$\rho_{cap} = \frac{2\sigma \cos \theta}{r}$$

where σ is the interfacial tension, θ is the contact angle between the two fluids, and r is the pore-throat radius. To prevent borehole fluids from entering the shale and stabilizing it, an increase in capillary pressure is required, which can be achieved with oil-based or other organic low-polar mud systems.

- Osmotic pressure: When the energy levels or activity in shale pore fluid, a_s, is different from the activity in drilling mud, a_m, water movement can occur in either direction across a semipermeable membrane (Ions from the drilling mud are hampered from moving across the membrane in to the formation) as a result of the development of osmotic pressure, p_{os}, or chemical/osmotic potential, μ_{os}.

$$\mu_{os} = \frac{RT}{V_w} \ln \frac{a_m}{a_s}$$

Here R is the molar gas constant (8.31 J/(mol K), and V_w is the molar volume of water (0.018 l/mol), T is the temperature (Kelvin), a_m is chemical activity of drilling fluid, and a_s is the chemical activity of pore water in the shale. The activity denotes the effective concentration of water in a solution, such that $a_w = 1$ for fresh water, while $a_w < 1$ for salt water.

To prevent or reduce water movement across this semipermeable membrane that has a certain efficiency, E_m, the activities need to be equalized or, at least, their differentials minimized. If a_m is lower than a_s, it is suggested to increase E_m and vice versa. The mud activity can be reduced by adding electrolytes that can be brought about through the use of mud systems such as seawater, saturated-salt/polymer, KCL/NaCL/polymer or Lime/gypsum. So for instance adding salt to the drilling fluid so that $a_m < a_s$ sets up an osmotic potential $\mu_{os} < 0$, which will tend to drive water out of the shale and hence act as an effective pore pressure reduction. This has an instantaneous stabilizing effect on the borehole. It has however been established that ions do move through shale, which means that the osmotic membrane is leaky. This is accounted for by the membrane efficiency, $E_m < 0$, which reduces the osmotic potential:

$$\mu_c = E_m \frac{RT}{V_w} \ln \frac{a_m}{a_s}$$

The membrane efficiency depends on ionic diffusivity and will hence in general depend both on clay type and on the type of ions present in the drilling fluid. The initial stabilizing effect seen from the addition of salt, will thus due to membrane leakiness, decay with time after drillout.

- Pressure diffusion: This is a phenomenon of pressure change near the borehole wall that occurs over time. The pressure change is caused by the compression of the native pore fluid by the borehole-fluid pressure, p_{wfl}, and the osmotic pressure, p_{os}.

- Borehole fluid invasion into shale: In conventional drilling, a positive differential pressure is always maintained. As a result, borehole fluid is forced to flow into the formation (fluid-loss phenomenon), which may cause chemical interaction that can lead to shale instabilities. To mitigate this problem, an increase of mud viscosity or, in extreme cases, gilsonite is used to seal off microfractures.

- Choice of drilling fluid: It is often observed that oil-based mud (OBM) gives better stability than water-based mud (WBM) when drilling in shale. The capillary entry pressure for pure oil to enter water-saturated shale is around 10 MPa. Thus, an overbalance of 10 MPa is required for oil (or another non-wetting fluid with similar surface tension) to penetrate into intact shale, which means for a lower mud overbalance, the borehole wall will remain impermeable. Oil based muds are however not pure oils. They contain a water phase, and the chemistry of the water phase has an influence on the hole stability.

  Though an OBM gives better stability, water-based muds are often preferred for environmental reasons. Drilling overbalanced through a shale formation with WBM allows drilling fluid pressure to penetrate the formation. Because of the saturation and low permeability of the formation, the penetration of a small mud volume into the formation causes a considerable increase in pore-fluid pressure near the wellbore wall. The increase in pore-fluid pressure reduces the effective mud support, which can cause instability. Several polymer WBM systems have however made shale-inhibition gains on oil-based mud and synthetic-based mud systems through the use of powerful inhibitors and encapsulators that help prevent shale hydration and dispersion.

Sources: (Wikipedia[3], 2017), (Fjær et al., 2008), (Geology.com, 2017), (Petrowiki[4], 2017)

2.1.4 Formation hardness and drillability

In general hardness is defined as a measure of how resistant solid matter is to various kinds of permanent shape change when a compressive force is applied. The hardness of a material depends

27

on variables such as ductility, elastic stiffness, plasticity, strain, strength, toughness, viscoelasticity and viscosity. There exist three common types of hardness measurements, which test for scratch-, indentation- and rebound-hardness. Each of these classes of measurements has individual measurements scales, but for practical reasons conversion tables are used to convert between one scale and another.

When drilling we are interested in the formation hardness. This hardness can be defined as the resistance of the formation versus penetration. The higher the formation hardness, the lower is the drilling penetration rate.

Drillability is a formation characteristic; a measure of how easy the formation is to drill. Higher drillability will increase drilling penetration rate. Though drillability is inversely correlated to the formation hardness, there are other influencing factors. Drillability depends on a variety of parameters such as rock mass parameters, drilling technique parameters, bit-type parameters and parameters related to the drilling fluid.

2.1.4.1 Rock mass parameters affecting hardness

After Uniaxial Compressive Strength (UCS), rock hardness is considered the most important rock property affecting penetration rate. Rock hardness gives a good indication for some rock mass parameters like that of the constituent minerals, cohesive forces, shape and size of grains, homogeneity and water content of the rock (Hoseinie et al, 2007).

In this thesis, the subject formation hardness will be approached by focusing on how it acts as a parameter for drillability. Thus, there will be no further emphasis on the particular parameters influencing rock mass hardness.

2.1.4.2 Rock mass parameters affecting drillability

Hoseinie et al. 2007, listed the various rock mass parameters proven by studies to influence drillability:

1. Origin of rock formation (Drake 2004, Jimeno et al. 1995, Osanloo 1998, Ostovar 2000).
2. Hardness (Ersoy & Waller 1995b, Jimeno et al. 1995, Kahraman et al. 2000, Li 2000, Osanloo 1998, Rao & Misra 1998, Serradj 1996, Thuro 1997, Ung et al 1994, Wilbur 1982).
3. Texture of rock – shape and size of rock grains (Ersoy & Waller 1995b, Jimeno et al. 1995, Rao & Misra 1998, Wilbur 1982).
4. Porosity (Osanloo 1998, Rao & Misra 1998, Thuro 1997).
5. Density (Hoseinie et al. 2006, Osanloo 1998, Rao & Misra 1998, Kahraman et al. 2000).

6. Abrasiveness – Rate of drill bit teeth wear (Drake 2004, Ersoy & Waller 1995b, Osanloo 1998, Rao & Misra 1998, Thuro 1997).

7. Elasticity and plasticity (Jimeno et al. 1995, Kahraman et al. 2000, Osanloo 1998).

8. Uniaxial Compressive Strength – UCS, Point load index and Schmidt hammer (Drake 2004, Ersoy & Waller 1995b, Jimeno et al. 1995, Kahraman et al. 2000, Osanloo 1998, Rao & Misra 1998, Serradj 1996, Singh et al. 1998, Thuro 1997).

9. Tensile strength (Kahraman et al. 2000, Rao & Misra 1998).

10. Rigidity (Osanloo 1998).

11. P-wave velocity (Kahraman et al. 2000).

12. Rock mass specification – joints, cracks and bedding (Drake 2004, Ersoy & Weller 1995b, Hoseinie et al. 2007, Jimeno et al. 1995, Kahraman 1999, Kahraman et al. 2000, Osanloo 1998, Ostovar 2000, Singh et al. 1998, Thuro 1997, Wilbur 1982).

13. Rock Quality Design – RQD (Osanloo 1998).

Some of these parameters are considered more important for drillability than others. This is highlighted in the RDi method and Spider plot method, which are systems that try to classify drillability only based on rock mass parameters. These will be discussed in section 2.1.4.4.a. Note that the listed parameters above are only rock mass parameters affecting drillability, not parameters involving drilling technique such as Rate of Penetration (ROP) and Weight on Bit (WOB), or drill-bit parameters such as bit type and bit diameter. These types of parameters will be discussed later.

2.1.4.3 Classification systems for formation hardness

No general classification systems exist for formation hardness, but three methods are developed which can help to distinguish between different levels of hardness. Each method categorizes formation hardness based on different criteria; Scratch hardness, Indentation hardness, and hardness classified through a roller cone bit classification and naming system.

a) Scratch hardness (Moh's hardness scale)

Moh's hardness scale, developed in 1812, is named after the German mineralogist Carl Friedrich Christian Mohs. His system tests for rock scratch-hardness and uses a scale ranging from 1 to 10, where each grade will scratch the one preceding it. The lowest value of 1 is representative of the softest mineral, which is talc or graphite, while the highest value of 10 represents the hardest mineral, which is diamond (Bestcrystals.com, 2017).

Despite its lack of precision, the Mohs scale is highly relevant for geologists and especially for rock hardness classification in field studies onshore. For this thesis, the value of the system lies in its ability to quantify rock mass hardness. As rock mass hardness is an important parameter for rock mass drillability, this will help in the classification of drillability.

A descriptive form of Moh's hardness scales was presented by Jimeno et al. (1995):

Moh's Hardness:	Description of Hardness:
1-3	Very Soft – Soft
3-4.5	Comparatively Soft
4.5-6	Comparatively Hard
6-7	Hard
>7	Very Hard

(Hoseinie et al, 2007).

b) Indentation hardness (Knoop hardness)

There exist several indentation-hardness tests, such as those of Brinelli (1900), Rockwell (1914) and Vickers (1921). However, the most relevant for measuring formation hardness is the Knoop hardness test developed by Frederick Knoop and colleagues at the National Bureau of Standards of the United States in 1939.

The Knoop hardness test is a microhardness test – a test for mechanical hardness used particularly for very brittle materials or thin sheets, where only a small indentation may be made for testing procedures. A pyramidal diamond point is pressed into the polished surface of the test material with a known (often 100 kg) load, for a specified time, with the resulting indentation measured using a microscope. The geometry of the indenter is an extended pyramid with length to width ratio of 7:1 and respective face angles of 172.5° for the long edge and 130° for the short edge. The depth of the indentation can be approximated as 1/30 of the long dimension. The Knoop hardness HK or HKN, is then given by the formula:

$$HK = \frac{load(kgf)}{impression\backslash area(mm^2)} = \frac{P}{C_p L^2}$$

where:

  L = Length of indentation along its long axis

C_p = correction factor related to the shape of the indenter, ideally 0.070279

P = load

HK values are typically in the range from 100 to 1000, when specified in the conventional units of $kg_f \cdot mm^{-2}$. The SI unit, pascal (Pa) may be used instead 1 $kg_f \cdot mm^{-2}$ = 9.80665 MPa.

The advantage of the Knoop test is that only a very small sample is required, and that it is valid for a wide range of test forces. The main disadvantages are the difficulty of using a microscope to measure the indentation (with an accuracy of 1 micrometre) and the time needed to prepare the sample and apply the indenter. Variables such as load, temperature, and environment also affect this procedure (Wikipedia[4], 2017).

Figure 2.1 shows a comparison between the Mohs and Knoop scales. As evident in the figure, and as expected based on its mathematical formula, the Knoop hardness (HK) manages to more precisely quantify hardness than does the Mohs scale. The Knoop hardness values of the different materials used in Mohs hardness scale (For example, diamond with HK = 7000, and talc with HK = 1) are marked in the figure.
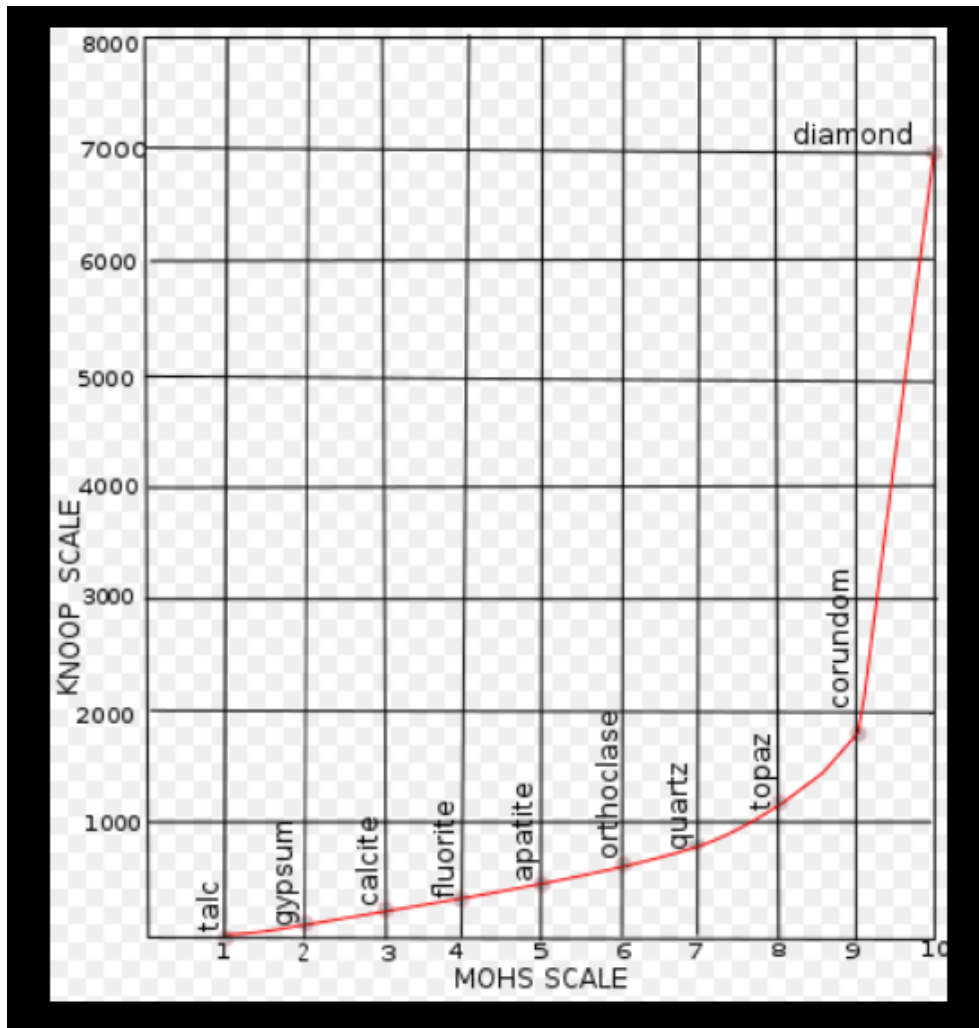
Figure 2.1: Comparison of the Knoop and Moh's hardness scales (Wikipedia[4], 2017).

c) IADC roller cone bit classification system

As discussed earlier, it is crucial to know which bit to choose with respect to the hardness of the formation being drilled. To aid in this matter, the International Association of Drilling Contractors (IADC) introduced a roller-cone bit classification and naming system for drilling bits, which also assist in comparison of similar bits from different manufacturers. The currently used version, approved in 1992, uses a four-digit code. The first three digits in this code are numeric, while the last digit is alphabetic. The first digit represents bit series, the second bit type, the third bit bearing and gauge arrangements and the fourth bit features.

It is the first and second of these digits, the bit series- and type number, which are interesting in helping to classify formation hardness. The series number, ranging from 1 to 8, defines general formation characteristics and also divides milled-tooth bits and insert-type bits. Series 1 to 3 is for

milled-tooth bits; series 4 to 8 for insert-type bits. The lowest number, which is 1 for milled-tooth or 4 for insert-type, represents the softest and most easily drillable formation. The highest number, which is 3 for milled-tooth or 8 for insert-type, represents the hardest and most abrasive formation. A formation hardness sub-classification is further provided by the bit type number. It ranges from 1, the softest, to 4, the hardest, within each series-number.

Unfortunately, as rock hardness is not clearly defined by the IADC system, it only provides a descriptive form of classifying formation hardness. The meanings of "hard" sandstone or "medium-soft" shale will always be subjective and open to a degree of interpretation. Actual rock hardness will vary considerably, depending on factors such as depth, overbalance pressure, porosity, and others that are difficult to quantify. The effect of these factors will be investigated more thoroughly later, so that the method developed in this thesis for determining formation hardness will be as realistic as possible (Petrowiki[5], 2017).

2.1.4.4 Classification systems for drillability

As in the case for formation hardness, there are no general classification systems for drillability which are being used in the industry. Several methods exist, each considering different aspects of what might contribute to better drillability. Some systems are focused on the effect of rock parameters alone. Other systems study the role of the impact force on the bit and the crater volume left behind, to help decide optimal bit- and drilling parameters through mathematical formulas. There is also a method which discusses a broad spectrum of factors influencing penetration rate, aiming to design a drillability classification to aid in optimal bit selection. This method is particularly interesting for this thesis, as it also looks to find a relationship between formation hardness and drillability.

a) Classification systems based on rock parameters (Rockmass Drillability index and Spider plot)

The Rockmass Drillability index (RDi) method was introduced by Hoseinie et al. in 2007. It was originally developed for open pit mining drilling and may thus not be the most relevant method for offshore practices. Still it is an interesting system because it highlights which rock mass parameters its authors consider the most important for drillability.

The RDi is based on the Wilbur classification system. Wilbur classified rock masses for drilling purposes based on Moh's hardness, texture, fracture and structure of rock mass. In the RDi-method more parameters are added, so it becomes six in total. Some of these parameters are related to the rock material while some are related to the rock structure.

In the RDi, the parameters are weighted according to their importance and given a rating for the specified rock mass. The numbers are then added up to a value between 7 and 100. The higher the value, the more drillable the rock is considered. The six parameters, ranked according to their importance for drillability are:

1. Uniaxial Compressive Strength – UCS.   Maximum RDi value of 22.
2. Hardness – Using Moh's hardness.   Maximum RDi value of 18.
3. Joint Spacing.   Maximum RDi value of 18.
4. Texture and Grain Size.   Maximum RDi value of 15.
5. Joints filling (Aperture).   Maximum RDi value of 15.
6. Joints dip.   Maximum RDi value of 12.

However, Hoek & Brown (1994) stated that a classification system must be non-linear in order to classify poor rock masses realistically. To rate the various values of each parameter, the highest weight has been rated for the best mode (fast drilling). Accordingly, and ranked as a percentage of the best mode, the non-linear RDi classification of drillability becomes:

Slow: 0-10% of best mode
Slow-Medium: 10-25% of best mode
Medium: 25-50% of best mode
Medium-Fast: 50-70% of best mode
Fast: 70-100% of best mode

(Hoseinie et al, 2007).

A similar method to the RDi, meaning drillability is expressed and classified for in terms of a number of rock parameters, is the Spider plot method (Prasad, 2009). In this method there are eight physical, mechanical and micro-structural rock properties, retrieved from either log data or from laboratory core testing, being visually displayed. The parameters considered relevant for drillability are: density, porosity, compressional and shear wave velocities, unconfined compressive strength, Mohr friction angle, mineralogy, and grain sizes. These are compiled and normalized in a scale of 1 to 8, with a value of 1 representing very soft rock and a value of 8 representing hard rock, ideally. The real rock is in between depending upon the rock type. The plot is called a "spider plot", which according to the author "characterizes drillability fully in simple enough parameters for use in the industry yet detailed enough to describe drillability issues to a great extent. Further, this gives an excellent tool to optimize the bit and drilling process for a given rock formation while depicting its physico-mechanical and micro-structural properties as a signature plot" (Prasad, 2009).

b) Classification systems based on impact force, crater volume and mathematical formulas (Drillability Index and Stamp test)

"Rock Drillability Related to A Roller Cone Bit" was the name of a drillability study published by Richard I. Morris in 1969, on behalf of the Security Engineering Division of Dresser Industries. They developed a method using the mechanism of a roller-cone rotary bit to measure drillability of hard mining rocks. The goal was to determine a drillability index which along with empirical formulas could help decide important drilling parameters. The parameters sought after were bit type, required bit weight, average penetration rate for a given rotary speed and approximate bit life (Morris, 1969).

The method used a 1/8-inch drill bit element which pushed into a flat surface of a rock hand sample with a hydraulic pump and ram until a crater was formed. The penetrating depth of the crater p', divided by the ram load E, is what constitutes the drillability index:

$$Drillability\ Index = \frac{p'}{E}$$

Unfortunately, this method does not apply well for this thesis as there are no data provided on what rocks are being penetrated.

A newer, and similar method is the Stamp test (Wijk, 1989). In the Stamp test the force and penetration depth required for a tungsten carbide button to fracture a rock surface are determined. From the force and penetration depth one may decide the piston blow velocity and the piston mass/length in a percussive machine capable of drilling the rock material. The stamp strength of the rock is used to define a non-dimensional drilling force F_{rel}, which governs the rock drilling efficiency. The volume of the indented crater is also determined during the test. As well as the stamp strength, the crater volume yields information about the expected drilling rate (Wijk, 1989).

c) **"A Drillability Classification of Geological Formations" and formation drillability versus formation geological hardness**

In 1951, A.L. Head presented a paper called "A Drillability Classification of Geological Formations". Head sought to find a system or scale by which different types of bits could be classified with respect to different types of geological formations. The classification was based entirely upon the relative efficiency at which formations could be drilled with a small rolling-cutter type test bit. To establish the drillability classification, Head studied the factors which affect rate of penetration, citing formation type, bit type, weight on bit, rotational speed, hydraulic action, size of hole and the efficiency of personnel and equipment as the most important factors. Head also conducted limited

tests to determine if there was any relationship between the drillability of a formation and the hardness of it.

Head's idea was based on first classifying various formations with respect to each other, and then, once a drillability classification was established, each type of bit could be graded in accordance with its performance in each formation. The performance of each bit was to be determined by observation of actual field and experimental drilling data over a long period of time. In each formation, there would then be one type of bit which would distinguish itself above all the others. If two or more bits performed equally well, they would have overlapping spheres of application, and one of them should be eliminated. Hence, a schedule of bits showing which formations they drill best could be prepared.

For the apparatus in the drillability study, Head designed and used a small diameter rolling cutter test bit, which would drill in various rock samples. The core sample was held in place on a lathe, while the test bit was secured to a free-rotating spindle of an adapter, mounted in the tailstock of the lathe. Thrust bearings were installed to absorb axial loads applied to the spindle. Rotational movement of the spindle were restrained by attaching a 6-inch lever arm directly behind the threaded connection on the spindle. The torque applied to the spindle could be determined by measurement of the force on the 6-inch lever arm necessary to restrain the rotation of the spindle. Axial force was applied to the bit by turning the tailstock screw. In order to exert a constant axial force on the bit, a constant torque had to be applied to the tailstock screw. To do this, a small drum was made to replace the tailstock hand wheel which turns the tailstock screw. A small wire cable was wound on the drum and threaded through a pully located above the drum. A container for holding weights was attached to the free end of the cable. For any weights placed in the container, a constant force was exerted to the bit. A deflection scale was made to take direct measurements of the force exerted by the bit. Knowing the physical characteristics of the tailstock and the drum, theoretical curves of cable load versus axial thrust of the bit were drawn for three different values of coefficient of friction for the tailstock screw. Then, by use of the deflection scale, the drillability test set-up was calibrated, and the results could be plotted on the same coordinates as the theoretical curves. The axial movement of the bit could be accurately determined by noting the length of cable wound off the drum. The physical characteristics of the tailstock screw and drum magnified the axial movement of the bit approximately 125 to 1, for example if the cable unwinds 1/8 inch, the bit moves axially 1/1000 inch. With this apparatus, Head could take measurements of rotational speed, force exerted by the bit, torque, depth drilled by the bit, and time needed to drill to specified depth.

For 15 different formations, Head measured the time intervals necessary to drill 1/16-inch, with constant rotational speed of 110 RPM and constant bit thrust of 417 pounds. These time intervals in seconds were called the Drillability Classification Numbers of the formations. The Drillability Classification Numbers established for each formation was the average of at least two tests, in most instances three or more tests. Head's results are shown in Table 2.2.

Test data used to determine Drillability Classification Numbers. Bit thrust, rotational speed, and depth drilled were held constant at 417 pounds, 110 revolutions per minute, and $1|_{16}$ inch, respectively.

Formation	Location	Time (min-sec)	Rate of Penetration (ft/hr) $\times 10^{+2}$	Drillability Classification number
Sandstone, Wilcox	Natchez, Miss.	0- 1.9	998	1.9
Lime, Canyon Reef	Snyder, Tex.	0- 2.0	938	2.0
Anhydrite	Gulf Coast Tex.	0- 3.4	552	3.4
Lime, Mississippi.................	Dover, Okla.	0- 3.9	482	3.9
Hard Marine Shale, Hosston	Haynesville, La.	0- 4.3	437	4.3
Crystalline lime	Rotan, Tex.	0-11.6	162	11.6
Carboniferous Shale	West Tex.	0-15.0	125	15.0
Hard Sandstone, First Bromide ...	Lindsey, Okla.	0-19.6	95.7	19.6
Sandy Limestone, Smackover	Haynesville, La.	0-26.0	72.2	26.0
Impure Limestone	Unknown	0-30.1	62.3	30.1
Sandstone	Unknown	0-37.3	50.3	37.3
Syenite	Central Tex.	0-37.7	49.7	37.7
Chert	West Tex.	0-45.8	40.8	45.8
Pink Granite	Central Tex.	1-14.1	25.3	74.1
Quartzitic Sandstone, Hosston.....	Bethany, Tex.	9-15.7	3.4	555.7 *

* This formation was a very hard, consolidated, abrasive sandstone which could not be chipped regardless of the thrust applied to bit. For this reason the DCN is exceedingly high.

Table 2.2: The Drillability Classification Number for 15 different formations, as measured by Head (Head, 1951).

To determine if this classification was consistent with the results obtained from actual bits drilling these same formations under field conditions, the performance of six different types of bits used to drill several of the tested formations was examined. Head stated that since the Drillability Classification Number (DCN) is the time interval required to drill a certain depth, it is equal to the inverse of the rate of penetration if the units are consistent, and in any case inversely proportional to the corresponding rate of penetration of the test bit. Therefore, if the rates of penetration of the actual bits drilling the tested formations under field conditions fell in the same order as the corresponding rates of penetration of the test bit, the drillability classification established would be consistent with actual field drilling practices. The results comparing the rates of penetration of the actual bits with the rates of penetration of the test bit is shown in Table 2.3

Head concluded that the obtained results would indicate that the drillability classification was consistent with actual drilling practices, because when the formations was arranged in the order of their drillability by the DCN, the rates of penetration of the actual bits fell in the same order as the rate of penetration of the test bit. For example, would the DCN-range of 1.9 to 3.4 be most efficiently

drilled by Bit "E", the range of 3.9 to 15.0 by Bit "C" and so on. Head further noted that the reason why Bit "C" could drill two ranges most efficiently, could be explained by certain features of the design of the bit in combination with certain formation characteristics. For unclassified formations, such as when drilling in unknown fields, or "wildcat drilling", Head proposed a reciprocal use of the table. By first conducting drillability tests on a core sample of the formation and classifying the DCN of the formation, a suitable bit for drilling this type of formation most efficiently could then be selected.

Comparison of the rates of penetration of actual bits with the rates of penetration of the test bit

Formation	DCN (e)	Rate of penetration of test bit (ft/hr)×10^{+3}	Rate of penetration of actual bits (ft/hr)						
			Bit "A"	Bit "B"	Bit "C"	Bit "D"	Bit "E"	Bit "F"	Bit "G"
Sandstone, Wilcox	1.9	988					35.0		33.0
Lime, Canyon Reef	2.0	938	13.5	13.8	17.1	14.8	21.0		20.0
Anhydrite	3.4	552	7.0	7.5	8.5	7.8	10.0		10.0
Lime, Mississippi	3.9	482	4.7	4.9	5.4	5.2	4.2	4.6	4.0
Hard Marine Shale, Hosston	4.3	437	4.1	4.0	5.0	5.0		4.2	
Crystalline Lime	11.6	162	3.6	3.8	4.2	4.1		3.4	
Carboniferous Shale	15.0	125	3.5	3.7	4.0	3.9		3.2	
Hard Sandstone, First Brom.	19.6	95.7	2.6	2.7	2.8	3.0		3.0	
Sandy Limestone, Smackover	26.0	72.2	2.5	2.5	2.6	2.5		2.7	
Chert	45.8	40.8	2.0	2.0	2.1			2.0	
Pink Granite	74.1	25.3	1.5	1.8	2.0			1.6	
Quartziferous Sandstone, Hosston	555.7	3.4	0.9	1.2	1.2			1.0	

(e) Drillability Classification Number.

Table 2.3: The Drillability Classification Number (DCN) of the formations, the ROP of the test bit and ROP of the actual bits (Head, 1951).

Finally, Head attempted to determine the relationship between the drillability and hardness of the formations. To do this, specimens of different formations were first mounted in bakelite and polished. Thereafter, micro-hardness tests were made, using a Knoop indenter. The Knoop hardness of each specimen was determined by averaging ten readings. The hardness values were compared with the Drillability Classification Numbers of the formations. Head's results are shown in in Table 2.4.

Comparison of the drillability of formations with their hardness.

Formation	Drillability classification number	Knoop hardness
Sandstone, Wilcox	1.9	813
Lime, Canyon Reef	2.0	630
Anhydrite	3.4	127
Hard Marine Shale, Hosston	4.3	176
Sandstone	37.3	988
Chert	45.8	745
Quartzitic Sandstone, Hosston	555.7	1118

Table 2.4: A comparison between the Drillability Classification Number (DCN) of the formations and the Knoop hardness. No relationship could be established between the drillability and the hardness of the formations (Head, 1951).

As shown, these tests could not establish any relationship between the hardness and drillability of the tested formations. Head did not attempt any further investigations and concluded that "extremely hard crystals were found in most formations, crystals which are in most instances harder than steel. The drillability of formations seems to be more related to the manner which the hard crystals are bound together than to the hardness" (Head, 1951).

2.2 Published Work Related to Pore Pressure

2.2.1 Definition of porosity

Porosity, ϕ, is a measure of the void (i.e. "empty") spaces in a material. In earth sciences (geology, hydrogeology, and soil science), porosity is defined as the quotient between pore volume (void volume around the grains) V_V and total volume V_T.

$$\phi = \frac{V_V}{V_T}$$

Porosity is a fraction between 0 and 1 (or 0-100 %), typically ranging from less than 0.01 for solid granite to more than 0.5 for peat and clay (Wikipedia[5], 2019).

The porosity of a rock, or sedimentary layer, is an important consideration when attempting to evaluate the potential volume of water or hydrocarbons it may contain. Sedimentary porosity is a complicated function of many factors, included but not limited to: rate of burial, the nature of connate fluids, the nature of overlying sediments (which may impede fluid expulsion).

Since sediments are normally deposited in the sea, the pores are normally filled with sea water. As seen in Figure 2.2, the initial porosity will decrease with burial depth (Skalle, 2015).
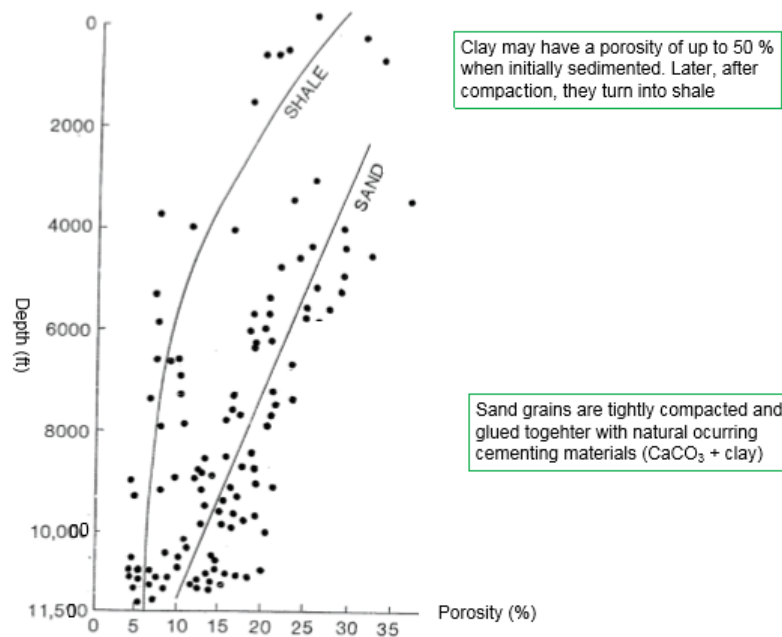
Figure 2.2: Porosity of shale and sandstone vs. depth of burial (Skalle, 2015).

One commonly used relationship between porosity and depth is given by the Athy equation (Athy, 1930):

$$\phi(z) = \phi_0 e^{-kz}$$

Where ϕ_0 is the surface porosity, k is the compaction coefficient (m^{-1}) and z is depth (m).

Alternatively, a value for porosity can be calculated from the bulk density ρ_{bulk}, saturating fluid density ρ_{fluid} and particle density $\rho_{particle}$:

$$\phi = \frac{\rho_{particle} - \rho_{bulk}}{\rho_{particle} - \rho_{fluid}}$$

2.2.2 Capabilities of porosity

2.2.2.1 Sorting and porosity

Well sorted (grains of approximately one size) materials have higher porosity than similarly sized poorly sorted materials (where smaller particles fill the gaps between larger particles). Figure 2.3 illustrates how some smaller grains can effectively fill the pores (where all water flow takes place), drastically reducing porosity and hydraulic conductivity, while only being a small fraction of the total volume of the material (Wikipedia[5], 2019).
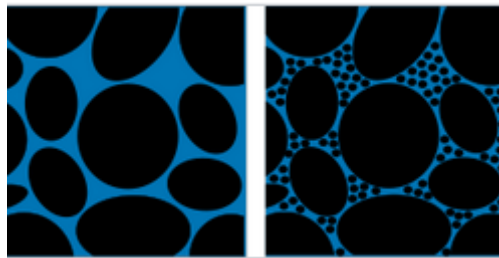
Figure 2.3: Effects of sorting on alluvial porosity. Black represents solids, blue represents pore space.
(Wikipedia[5], 2019).

2.2.2.2 Porosity of rocks

Consolidated rocks (e.g. sandstone, shale, granite or limestone) potentially have more complex "dual" porosities as compared with alluvial sediment. This can be split into connected and unconnected porosity. Connected porosity is more easily measured through the volume of gas or liquid that can flow into the rock, whereas fluids cannot access unconnected pores. The rock porosity is controlled by: rock type, pore distribution, cementation, diagenetic history and composition. Porosity is not controlled by grain size, as the volume of between-grain space is related only to the method of grain packing. Rocks normally decrease in porosity with age and depth of burial. There are exceptions to this rule, usually because of the depth of burial and thermal history (Wikipedia[5], 2019).

2.2.2.3 Types of geologic porosities

- Primary porosity
   - The main or original porosity system in a rock or alluvial deposit
- Secondary porosity
   - A subsequent or separate porosity system in a rock, often enhancing overall porosity of a rock. This can be a result of chemical leaching of minerals or the generation of a fracture system. This can replace the primary porosity or coexist with it.
- Fracture porosity

- o This is porosity associated with a fracture system or faulting. This can create secondary porosity in rocks that otherwise would not be reservoirs for hydrocarbons due to their primary porosity being destroyed (for example due to depth of burial) or of a rock type not normally considered a reservoir (for example igneous intrusions or metasediments)

- Vuggy porosity
  - o This is secondary porosity generated by dissolution of large features (such as macrofossils) in carbonate rocks leaving large holes, vugs or even caves.

- Effective porosity (also called open porosity)
  - o Refers to the fraction of the total volume in which fluid flow is effectively taking place and includes catenary and dead-end (as these pores cannot be flushed, but they can cause fluid movement by release of pressure like gas expansion) pores and excludes closed pores (or non-connected cavities). This is very important for groundwater and petroleum flows, as well as for solute transport.

- Ineffective porosity (also called closed porosity)
  - o Refers to the fraction of the total volume in which fluids or gases are present but in which fluid flow can not effectively take place and includes the closed pores. Understanding the morphology of the porosity is thus very important for groundwater and petroleum flow.

- Dual porosity
  - o Refers to the conceptual idea that there are two overlapping reservoirs which interact. In fractured rock aquifers, the rock mass and fractures are often simulated as being two overlapping but distinct bodies. Delayed yield, and leaky aquifer flow solutions are both mathematical similar solutions to that obtained for dual porosity; in all three cases water comes from two mathematically different reservoirs (whether or not they are physically different).

- Macroporosity
  - o In solids (i.e. excluding aggregated materials such as soils), the term "macroporosity" refers to pores greater than 50 nm in diameter. Flow through macropores is described by bulk diffusion.

- Mesoporosity
  - o In solids (i.e. excluding aggregated materials such as soils), the term "mesoporosity" refers to pores greater than 2 nm and less than 50 nm in diameter. Flow through mesopores is described by Knudsen diffusion.

- Microporosity

- In solids (i.e. excluding aggregated materials such as soils), the term "microporosity" refers to pores smaller than 2 nm in diameter. Movement in micropores is activated by diffusion (Wikipedia[5], 2019).

2.2.2.4 Measuring porosity

Several methods can be used to measure porosity:

- Direct methods
  - Determining the bulk volume of the porous sample, and then determining the volume of the skeletal material with no pores (pore volume = total volume – material volume)
- Optical methods
  - E.g. determining the area of the material versus the area of the pores visible under the microscope). The "areal" and "volumetric" porosities are equal for porous media with random structure.
- Computed tomography (CT) method
  - Using CT scanning to create a 3D rendering of external and internal geometry, including voids. Then implementing a defect analysis utilizing computer software
- Imbibition methods
  - Immersion of the porous sample, under vacuum, in a fluid that preferentially wets the pores.
- Water saturation method
  - Pore volume = total volume of water – volume of water left after soaking
- Water evaporation method
  - Pore volume = (weight of saturated sample – weight of dried sample)/density of water
- Mercury intrusion porosimetry
  - Several non-mercury intrusion techniques have been developed due to toxicological concerns, and the fact that mercury tends to form amalgams with several metals and alloys
- Gas expansion method
  - A sample of known bulk volume is enclosed in a container of known volume. It is connected to another container with known volume which is evacuated (i.e. near vacuum pressure). When a valve connecting the two containers is opened, gas

passes from the first container to the second until a uniform pressure distribution is attained. The volume of the pores is then calculated using the ideal gas law.

- Thermoporosimetry and cryoporometry
  - A small crystal of a liquid melts at a lower temperature than the bulk liquid, as given by the Gibbs-Thomson equation. Thus, if a liquid is imbibed into a porous material, and frozen, the melting temperature will provide information on the pore-size distribution. The detection of the melting can be done by sensing the transient heat flows during phase-changes using different scanning calorimetry – (DSC thermoporometry), measuring the quantity of mobile liquid using nuclear magnetic resonance (NMR cryoporometry) or measuring the amplitude of neutron scattering from the imbibed crystalline or liquid phases (ND cryoporometry) (Wikipedia[5], 2019).

2.2.3 Pore pressure and pressure control

As indicated in Figure 2.4, all formations penetrated by the drill bit are porous to some degree. The pore spaces contain fluids such as oil, gas or salt water or a mixture of these. Pore pressure, P_{pore}, is the pressure exerted by the fluids contained in the pore space (Skalle, 2015).
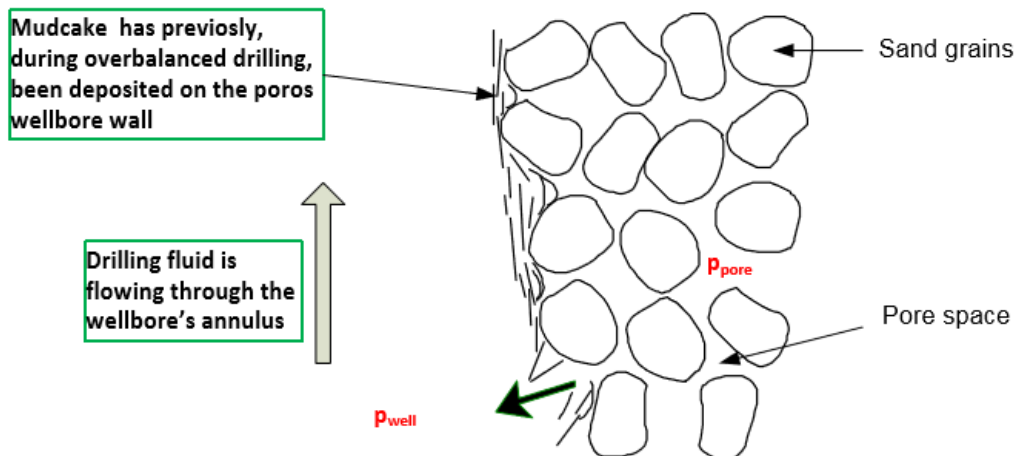

Figure 2.4: Pore fluids will flow into the wellbore when wellbore pressure becomes lower than the pore pressure (Skalle, 2015)

2.2.3.1 Well kick

In normal overbalanced drilling operations, the pressure exerted by the circulating drilling fluid needs to overbalance the formation pore pressure. As seen in Figure 2.4, failure to do so leads to influx of pore fluids into the wellbore. Small influxes will mix with the pumped drilling fluid and cause a minor decrease of the mud density. In such circumstances the drilling fluid is said to be "gas cut", "salt water cut" or "oil cut". When, on the other hand, a noticeable influx occurs, and a noticeable increase in mud pit volume is seen at the surface, we have a well control problem known as a kick. When drilling in normal depth (< 3000 mTVD), it is normal to experience a kick in every 3-7 drilled well. In deep wells (> 3000 mTVD), kick frequency riser to 1-2 kicks per drilled well (Skalle, 2015). When a kick occurs, blowout prevention equipment and accessories are needed to close the well. If the flow is successfully controlled, the kick is considered to have been killed. An uncontrolled kick that increases in severity may result in a blowout (Petrowiki[6]).

a) Factors affecting kick severity

Several factors affect kick severity. One factor is the permeability of the rock, while the porosity is another. A rock with high permeability and high porosity has greater potential for a severe kick than a rock with low permeability and low porosity. For example, sandstone is considered to have greater kick potential than shale, because sandstone has greater permeability and greater porosity than shale.

Another factor affecting kick severity is the pressure differential between the formation fluid pressure and the mud hydrostatic pressure. If the formation pressure is much greater than the hydrostatic pressure, a large negative differential pressure exists. If this negative differential pressure is coupled with high permeability and high porosity, a severe kick may occur (Petrowiki[6]).

b) Causes of kicks

Kicks occur when the formation pore pressure is greater than the wellbore mud pressure. Usually, this happens in the following situations (Skalle, 2015):

- Too low mud density, due to gas cut mud or due to encountering high pore pressure
- Lowering of mud level in annulus due to low circulation or removal of drill pipes from the well during tripping out (improper hole fill-up)
- Swabbing, a suction pressure caused by the drill string being pulled out too fast
- Lost circulation, a decreased mud pressure resulting from a shorter mud column
- Drilling into neighboring producing wells (seldom occurs)

c) Warning signs of kicks

Warning signs and potential kick indicators can be observed at the surface. Each is identified as either primary or secondary warning signs, relative to its importance in kick detection.

- Primary indicators:
    o Flow rate increase
    o Pit volume increase
    o Flowing well with pumps off
    o Improper hole fill-up on trips
- Secondary indicators:
    o Pump pressure decrease and pump stroke increase
    o String weight change
    o Drilling break
    o Cut mud weight

d) Kick detection and monitoring with MWD tools

During circulation and drilling operations, measurements while drilling (MWD) systems monitor:

- Mud properties
- Formation parameters
- Drillstring parameters

The MWD system is widely used for drilling, but it also has applications for well control, including the following:

- Drilling-efficiency data
    o E.g. downhole WOB and torque can be monitored and used to differentiate between ROP changes caused by drag and those caused by formation strength. Monitoring bottomhole, temperature and flow with the MWD tool is not only useful for early kick detection but can also be valuable during a well-control kill operation. Formation evaluation capabilities, such as gamma ray and resistivity measurements, can be used to detect influxes into the wellbore, identify rock lithology, and predict pore pressure trends.
- Monitoring of the acoustic properties of the annulus for early gas-influx detection
    o Pressure pulses generated by the MWD pulser are recorded and compared at the standpipe and the top of the annulus. Full-scale testing has shown that the presence of free gas in the annulus is detected by amplitude attenuation and phase delay between the two signals. For water-based mud systems, this technique has

demonstrated the capacity to consistently detect gas influxes within minutes before significant expansion occurs. Further development is currently under way to improve the system's capability to detect gas in oil-based mud.

- Kick detection through ultrasonic sensors
    o In these systems, an ultrasonic transducer emits a signal that is reflected off the formation and back to the sensor. Small quantities of free gas significantly alter the acoustic impedance of the mud. Automatic monitoring of these signals permits detection of gas in the annulus. It should be noted that these devices only detect the presence of gas at or below the MWD tool.

Kick detection benefits are offered by the MWD tool if the response time is less than the time it takes to observe the surface indicators. The tool can provide early detection of kicks and potential influxes, as well as monitor the kick-killing process. Tool response time is a function of the complexity of the MWD tool and the mode of operation. The sequence of data transmission determines the update times of each type of measurement. Many MWD tools allow for reprogramming of the update sequence while the tool is in the hole. The feature can enable the operator to increase the update frequency of critical information to meet the expected needs of the section being drilled. If the tool response time is longer than required for surface indicators to be observed, the MWD tool only serves as a confirmation source (Petrowiki[6])

e) Kick identification and control

When a kick occurs, the type of influx (gas, oil or salt water) must be noted. Oil or salt water are incompressible fluids, and thus not as difficult to handle as gas. A small volume of gas at the bottom of the well is potentially dangerous because it expands while approaching the lower hydrostatic pressure near the surface. At low pressure it will expand and displace a corresponding amount of mud from the well, thus reducing the bottomhole pressure which in turn allows more gas to flow in from the pores. To regain control of the well it is important to understand the behavior of gas under different well conditions.

In order to create a new overbalance in the borehole, a drilling fluid with a greater density must be pumped into the hole to achieve a mud pressure higher than the pore pressure. Such an operation is called a killing operation or killing procedure. "Kill-weight mud" is the amount of mud necessary to exactly balance formation pressure. A kill mud formula, based on shut-in drillpipe pressure, exists to calculate the mud weight needed. The two main killing methods are the Driller's Method and the Engineer's method. The main difference between these two methods is that in the Driller's Method

the pore fluid is displaced before kill mud is injected, while in the Engineer's Method the mud weight is being increased and pumped into the well immediately.

Other differences between these methods are that the annular pressure becomes higher with the Driller's Method and the choke nozzles erode quicker. If there is a risk of fracturing the casing shoe, the Engineer's Method must be chosen. The Engineer's Method is used in long openhole sections to reduce the pressure in the annulus; otherwise the Drillers Method is preferred.

In situations where the casing shoe is set deep, the gas bubbles will be inside the casing before the kill mud reaches the bit, and the Engineer's Method gives no advantages. The Driller's Method is simple, and the total time it takes is practically the same as for the Engineer's Method. It is important to get started fast with the killing operation to avoid the pressure increase due to gas percolation (Skalle, 2015).

For more thorough information on well kicks and the killing procedures the reader is referred to chapter 4 of Pressure Control During Oil Well Drilling (Skalle, 2015).

2.2.3.2 Well blowout

Statistics indicate that typically every 100th kick results in one blowout (Skalle, 2015). The consequences of a well blowout can be disastrous. While a kick can be controlled, a blowout is an uncontrolled kick with release of crude oil and/or natural gas after pressure control systems have failed. Blowout preventers are intended to prevent such an occurrence. An accidental spark during a blowout can lead to a catastrophic oil or gas fire (Wikipedia[6]). It may take months to stop the blowout, and it is sometimes accompanied by loss of human lives as well as large material and economic losses (Skalle, 2015).

a) Cause of blowouts

Kicks may develop into blowouts for one or more of the following reasons (Skalle, 2015):

- Failure to detect potentially threatening situations during the drilling process
  - This involves not detecting the primary (and secondary) kick warning signs as was described in section 2.2.3.1.c
- Failure to take the proper initial action once a kick has been detected
  - The well must be shut in fast (activate BOPs) to be able to control the kick and to avoid gas percolation
- Lack of adequate control equipment or malfunction of the equipment

- After the first BOP in 1924, BOPs have become standard equipment, assuring that blowouts have become comparatively rare. Still, the well control systems may fail. To ensure fully functioning equipment there are safety requirements in place, such as frequent testing of the equipment

b) Types of blowouts

Well blowouts can occur during the drilling phase, during well testing, during well completion, during production or during workover activities.

- Surface blowouts
  - This is the most common type of blowout, which occurs through the annulus, due to malfunctioning or failed surface BOP equipment. These blowouts can eject the drill string out of the well, and the force of the drilling fluid can be strong enough to damage the drilling rig. In addition to oil, the output of a well blowout might include natural gas, water, drilling fluid, mud, sand, rocks, and other substances.
  - Surface blowouts will often be ignited from sparks from rocks being ejected, or simply from heat generated by friction. A well control company then will need to extinguish the well fire or cap the well and replace the casing head and other surface equipment. If the flowing gas contains poisonous hydrogen sulfide, the oil operator might decide to ignite the stream to convert this to less hazardous substances.
  - Sometimes blowouts can be so forceful that they cannot be directly brought under control from the surface, particularly if there is so much energy in the flowing zone that it does not deplete significantly over time. In such cases, relief wells may be drilled to intersect the well or pocket, in order to allow kill-weight fluids to be introduced at depth. When first drilled in the 1930s relief wells were drilled to inject water into the main drill well hole. Contrary to what might be inferred from the term, such wells generally are not used to help relieve pressure using multiple outlets from the blowout zone.
- Subsea blowouts
  - The two main causes of a subsea blowout are equipment failures and imbalances with encountered subsurface reservoir pressure. Subsea wells have pressure control systems (BOPs) located at the seabed or between the riser pipe and drilling platform.
  - Even with blowout prevention equipment and processes in place, operators must be prepared to respond to a blowout should one occur. Before drilling a well, a detailed

well construction design plan, an oil spill response plan as well as a well containment plan must be submitted, reviewed and approved by a governing safety bureau. (e.g. US: Bureau of Safety and Environmental Enforcement).

- o The 2010 Deepwater Horizon blowout was a subsea blowout at 1500 m water depth, with 11 persons killed after explosions at the rig (Wikipedia[6]).

- Underground blowouts:

  - o Underground blowouts are the most troublesome, occurring when fluids from a high pressure zone flow uncontrolled to lower pressure zones within the wellbore. Usually this is from deeper higher pressure zones to shallower lower pressure formations (where the formation is weaker). There may be no escaping fluid flow at the wellhead (Wikipedia[6]). This situation can ruin valuable reservoirs and charge shallow formations, making further drilling difficult or impossible in this area (Skalle, 2015).

  - o Underground blowouts may also affect the soil around the rig. If the pressure in the annulus exceeds the fracture pressure of the formation, the tensile stress of the sedimentary formation has been surpassed and fractures open up and mud may flow into the formation. If only a short casing string has been set, a fracture can then extend to the surface, causing such a blowout around the rig.

c) Methods of quenching blowouts

- Subsea well containment

  - o After the Deepwater Horizon in 2010, the offshore industry collaborated with government regulators to develop a framework to respond to future subsea incidents. As a result, all energy companies operating in the deep-water U.S. Gulf of Mexico must submit an OPA 90 (Oil Pollution Act of 1990 – a law governing oil spills) required Oil Spill Response Plan with the addition of a Regional Containment Demonstration Plan prior to any drilling activity. In the event of a subsea blowout, these plans are immediately activated, drawing on some of the equipment and processes effectively used to contain the Deepwater Horizon well as well as other that have been developed in the aftermath.

  - o In order to regain control of a subsea well, the responsible party would first secure the safety of all personnel on board the rig and then begin a detailed evaluation of the incident site. Remotely operated underwater vehicle (ROVs) would be dispatched to inspect the condition of the wellhead, BOP and other subsea well equipment. The debris removal process would begin immediately to provide clear access for a

capping stack. While the BOP is the primary method for well control, a capping stack is viewed as secondary method used during well containment operations. This setup can be seen in Figure 2.5.

o Once lowered and latched on the wellhead, the capping stack uses stored hydraulic pressure to close a hydraulic ram and stop the flow of hydrocarbons. If shutting in the well could introduce unstable geological conditions in the wellbore, a cap and flow procedure would be used to contain hydrocarbons and safely transport them to a surface vessel.

o The responsible party works in collaboration with BSEE (Bureau of Safety and Environmental Enforcement) and the US Coast Guard to oversee response efforts, including source control, recovering discharged oil and mitigating environmental impact.

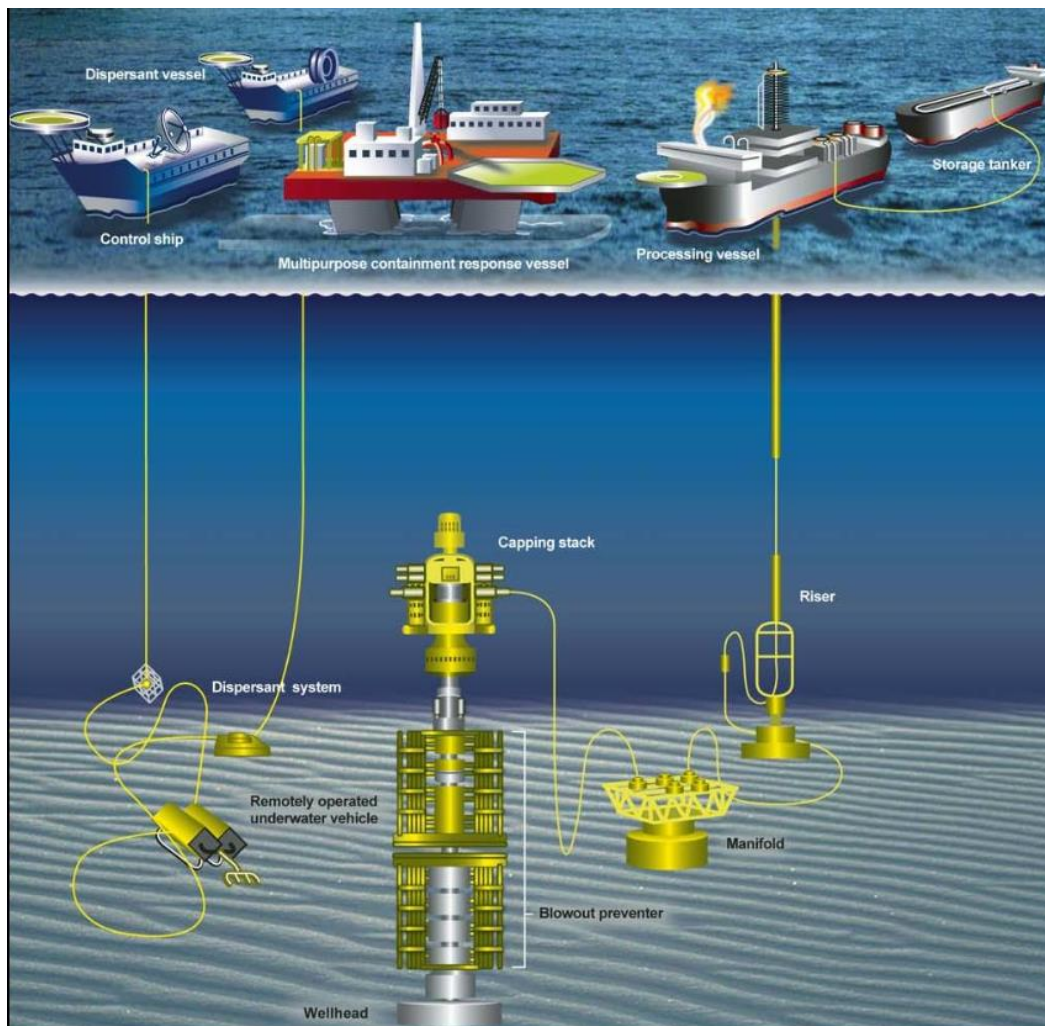o Several not-for-profit organizations also provide a solution to effectively contain a subsea blowout (Wikipedia[6]).

Figure 2.5: Setup for subsea well containment operation (Wikipedia[6]).

- Use of nuclear explosions
  - o This method was first attempted by the Soviet Union in 1966 in an area called Urta-Bulak. A 30 kiloton nuclear bomb was lowered into a 6000 m borehole drilled 25 to 50 meters away from the original rapidly leaking well. A nuclear explosion was deemed necessary because conventional explosive both lacked the necessary power and would also require a great deal more space underground. As the bomb set off, it crushed the original pipe that was carrying the gas from the deep reservoir to the surface and glassified all the surrounding rock. This caused the leak and fire to cease within approximately one minute of the explosion and proved over the years to have been a permanent solution.
  - o Other attempts were not as successful, and today this method is not relevant as the advances in directional drilling technology allows the drilling of relief wells. These wells can intersect the well or pocket in order to introduce kill weight fluids at depth (Wikipedia[6]).

d)   Safety barriers during drilling

With the potential catastrophic effects of blowouts, there are strict rules imposed for pressure control during drilling. One such rule is the principle of redundancy; double up of all equipment systems in order to increase level of safety. This same principle is applied in order to establish two independent barriers to withstand pore pressure (Skalle, 2015):

- Barrier one: The hydrostatic pressure of mud is larger than the pore pressure
- Barrier two: The envelope consisting of the blowout preventer, the well head, the casing, the casing sement and the drill string. This envelope can be closed in case barrier one fails.

2.2.4 Pressure in the sediments

The formation pore pressure can be classified as either normal or abnormal. This section will explain these two terms more thoroughly.

2.2.4.1 Normal pore pressure

Normal pore pressure is equal to the hydrostatic pressure exerted by the pore fluid above the depth of interest. The pressure is proportional to the density of the pore fluids. For water, it varies with

salinity. Salinity is in turn related to geographic and geologic location. For example, the density of fresh water is 1.0, of seawater it is 1.025 and of 20% saline pore water 1.06 kg/m^3.

Pore fluid which is connected to the groundwater table or to the ocean through permeable sediments, are creating a normal pore pressure (Skalle, 2015).

2.2.4.2 Abnormal pore pressure

Pore pressure can both exceed or be less than that of the expected, or normal, formation pressure. Underpressure is what most seldom occurs, but can have severe consequences, e.g. causing the drillpipe to stick to the underpressured formation (Sclumberger[6]). However, in general, high pressure zones are more likely to cause problems for the drilling operation. This is because for well pressure control (except for underbalanced drilling) the pore pressure needs to be overbalanced by the pressure exercised by the circulating drilling fluid. Thus, in this thesis, the focus will be on high pressure zones and the term abnormal pore pressure will be referring to pore pressure higher than normal.

According to Skalle, abnormal pore pressure can exist because of the following reasons (Skalle, 2015):

- Artesian water
  - o A formation which extends to the surface at an elevation higher than the normal groundwater at the drill site, or higher than natural outlet of the formation (higher hydrostatic pressure)
- Rapid sedimentation of clay
  - o Abnormal formation pressure can result from rapid burial of clay. The key processes involved in the forming of high pore pressure and its seal are:
    - ▪ Compaction → porosity reduction
      - • At the time of deposition, the clays and associated minerals have a high volume of water. As the mineral is in the process of being buried, the pore water will tend to be squeezed out due to porosity decrease as a result of increased compaction
    - ▪ Diagenesis → water rich Smectite transforms to Illite, which is more compact
    - ▪ Sealing of formations → both the compaction and diagenesis will come to a halt after the establishment of impermeable boundaries. They are formed by either shale, salt or faults. Impermeable boundaries will hinder water to escape and thus stopping the compaction. The formation is thus termed as

under-compacted. "Rapid" sedimentation of clay increases the probability of the creation of seals.

- Charged formations
  - ○ Shallow sandstones may become charged with gas from lower formations. Once trapped inside a sand layer, the low density of gas causes the gas pressure to be almost constant throughout its vertical column.

Figure 2.6 shows examples of abnormal pressures in sediments. The probability of encountering abnormal pressure increases with depth. Below 2500 m TVD, normal pore pressure is seldom found.
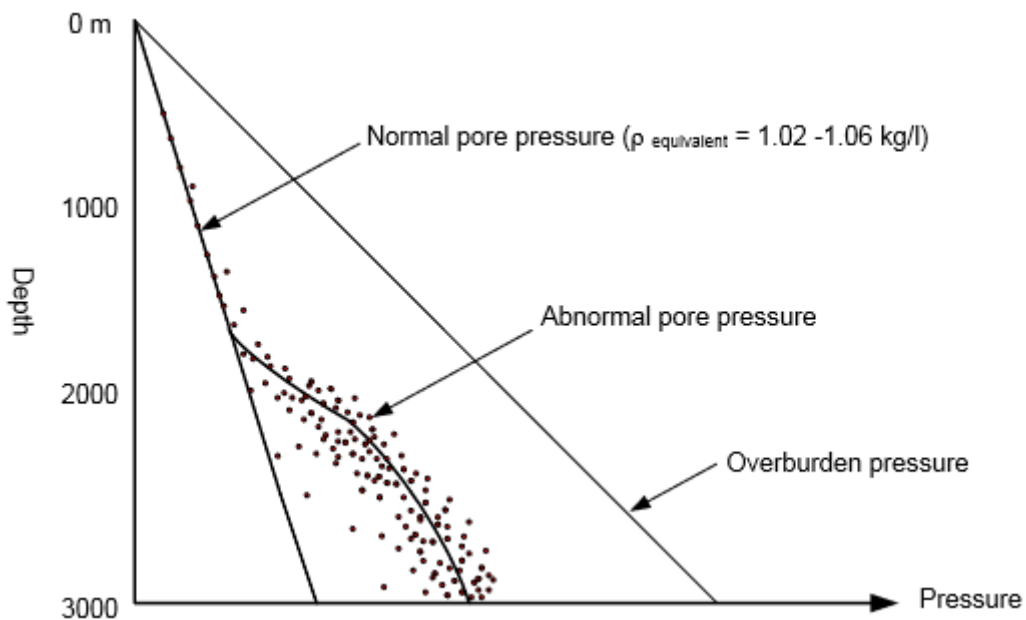

Figure 2.6: Typical pore pressure occurrences in a sedimentary basin (Skalle, 2015)

2.3 Pore pressure estimations during drilling with the help of d-exponent

The methods developed to estimate pore pressure, can be conveniently rearranged to calculate formation drillability instead. This assumes that the local pore pressure is known, or estimations can be made from neighboring wells drilled in the same formation. This chapter will describe the methods which can be tweaked to obtain the drillability.

2.3.1 Methods of pore pressure detection

Abnormal pore pressure conditions may lead to costly and time consuming well killing operations, and in worst case scenarios serious well and personnel damage. It is therefore important to make early and exact pore pressure detections.

The pore pressure can be estimated through either prediction methods or detection methods. Prediction methods are based on data from seismic surveys, offset well logs and well history. Detection methods traditionally utilize drilling parameters and well log information obtained during the actual drilling of the well (Yoshida, 1996).

For redundancy, it is necessary to utilize all available detection methods. Skalle have listed the sources from which pore pressure information can be obtained (Skalle, 2015):

- Seismic data
- Wire-line logs (sometimes replaced by Measurements While Drilling (MWD))
- Drilling Rate of Penetration (ROP)
- Mud properties like gas content and temperature

The seismic data for the prediction methods can be sonic time, resistivity or the d_c-exponent. These parameters are entered into Eaton's equation to estimate the pore pressure.

Direct pore pressure measurements, such as from Wire-line (WL) logs, will give very accurate pore pressure data. The problem with WL-logging is that it is only possible after the formation has been drilled. The tools also must be tripped in-and out of hole, which makes a costly operation. MWD can replace WL, and uses a tool typically placed 15 meters above the bit (Skalle, 2015).

Estimation of pore pressure during drilling, such as MWD, is applying drilling parameters monitored at the surface to different methods. Through the measuring of changes in data such as penetration rate, hook load, rotary speed, torque, drag and hole fill or accumulations of rock fragments in the lower part of the borehole, it is possible to make an estimate of the formation fluid pressure (Bourgoyne et al., 1986). Since the drilling fluid properties and circulating rate affect penetration

rate, they are also monitored frequently. Detection methods for pore pressure from drilling fluid properties are based on analysis of the returning temperature and/or gas content.

2.3.1.1 d_c – exponent

As mentioned in the previous section, drilling rate can be a useful parameter for pore pressure detection. ROP is affected by (Bourgoyne et al., 1986):

1. formation type
2. formation pore pressure
3. bit type
4. bit diameter
5. bit nozzle size
6. bit wear
7. bit weight
8. bit hydraulics
9. string rotary speed
10. mud type
11. mud density
12. effective mud viscosity
13. solids content and size distribution in mud
14. pump pressure
15. pump rate

Assuming all other parameters are kept more or less constant, the magnitude of the differential pressure existing between the formation pore pressure and the hydrostatic pressure in the wellbore, $\Delta P = P_{pore} - P_{mud}$, decides the changes in ROP. The higher the ΔP, the higher the ROP. Therefore, if the mud pressure is constant, increased pore pressure leads to increased ROP (Skalle, 2015).

The physical explanation for the effect of differential pressure on ROP can be attributed to the Hold Down Effect. As chips are produced beneath the bit, the differential pressure will push down on the chips, influencing the ease of their removal. In an overbalanced situation, where the well pressure exceeds the formation pressure, there will be a larger Hold Down Effect, such that the removal of the chips is more demanding, thus reducing the ROP (Bourgoyne et al., 1986).

In an attempt to investigate the relationship between ROP and ΔP, the d – exponent method was proposed by Jorden and Shirley in 1966. The knowledge of this relationship would make it possible to predict changes in pore pressure with respect to obtained drilling data.

The model is based on Bingham's drilling equation for ROP, which also accounts for changes in parameters such as WOB, RPM and bit diameter. K is the drillability constant and includes the effect of rock strength. The main difference from the Bingham equation is that the bit weight exponent, a_5, is replaced by the d-exponent. The d-exponent represents the deviation in ROP caused by differential pressure:

$$ROP = K \cdot RPM \, (\frac{WOB}{d_{bit}})^d \tag{2.1}$$

Jorden and Shirley further rearranged and normalized this relationship:

$$d = \frac{log(\frac{ROP}{60 \, RPM})}{log(\frac{12 \, WOB}{10^3 \, d_{bit}})} \tag{2.2}$$

In the latter equation the formation drillability constant, K, has been assigned a value of unity and a scaling constant, 10^3, has been introduced in the WOB term. Jorden and Shirley felt these simplifications would be permissible in the U.S. gulf coast area for a single formation type as in this area there are "few significant variations in rock properties other than variations due to increased compaction with depth" (Bourgoyne et al., 1986).

From ROP-logs it can be observed that the ROP tends to decrease with increasing depth in a given formation. When entering a transition zone of abnormal pressure and/or low permeability, this usual trend is altered; now the ROP increases with depth. This is felt to result from a decrease in the pressure differential across the bottom of the hole and a decrease in the rock strength caused by undercompaction. During undercompaction, as opposed to normal compaction processes, sediments are buried too fast to allow for sufficient permeability to let pore fluids migrate out and up through the rock. Together with low permeability of claystones and shales, this contributes to trapped water within sediments. As the overlying rocks are supported by both the rock matrix and the interstitial fluids, this leads to an overpressured formation. However, for ROP, the effect of overbalance is much more important than the effect of undercompaction (Bourgoyne et al. 1986).

In a normal pressured zone, increased compaction with depth leads to decreased ROP. The log expression in the numerator of the d-exponent eqn. (2.2) thus turns out < 1. This means the d-

exponent, as opposed to the ROP, increases with depth. When entering a transition zone from normal to abnormal pressure, the d-exponent will depart from the normal pressure trend-line as it increases less rapidly with depth. In some cases, a complete reversal of the trend can happen, and the d-exponent begins decreasing. Studying these trend-lines makes it possible to detect the pore pressure transition zones.

It should be noted that shale is nearly always the formation type selected, and drilling data obtained in other formation types simply are omitted from the calculations (Bourgoyne et al., 1986). This is supported by Skalle, who states that the normal trend line for ROP parameters and other drilling parameters such as the d-exponent, with respect to estimating pore pressure, can only be established in "clean" shale. This shale is found by the means of the gamma ray tool. Requirements for the shale being considered "clean", is that it must have been exposed to normal (slow) compaction and diagenesis, such that pore water have reached equilibrium with surrounding water pressure. With depth, the probability for encountering abnormal pressured zones increases. Normal pressure is seldom found below 2500 mTVD (Skalle, 2015).

An important requirement when using the d-exponent method is that the drilling fluid density must be held constant. In 1971, Rehm and McClendon modified the d-exponent to also include for changes in mud density. The new exponent was called the modified or corrected d-exponent:

$$d_c = d \frac{\rho_{normal}}{\rho_{mud}}$$
(2.3)

ρ_{normal} represents the mud density equivalent to normal formation pore pressure, usually equal to 1.02-1.06 kg/l (Skalle, 2015), while ρ_{mud} is the equivalent mud density at the bit while circulating. By using d_c-exponent values instead of d-exponent values, the deviation from the trend-line will be magnified (Skalle, 2015).

2.3.1.2 Zamora's method

In the d_c-method by Rehm and McClendon the suggestion is to use linear scales for both depth and d_c-values when constructing a graph to estimate pore pressure quantitatively. In 1972, Zamora proposed using a linear scale for depth but a logarithmic scale for d_c. According to Zamora the normal pressure trend lines now "varied only slightly and without apparent regard to location or geological age" (Bourgoyne et al., 1986).

Zamora's empirical relation between the d_c-exponent and the pore pressure gradient was the following:

$$\rho_{pore} = \rho_{normal} \left(\frac{d_{c,normal}}{d_c}\right) \qquad (2.4)$$

ρ_{pore} is the formation pressure gradient at the over pressured zone of interest, ρ_{normal} is the normal pressure gradient for the area, d_c is the value of the d_c on the departed trend line and $d_{c,normal}$ is the d_c - value obtained from the normal d_c- trend line.

2.3.1.3 Eaton's method

In 1975, Eaton presented a method to quantitatively approximate formation pore pressure. The method is based on the assumption that the overburden pressure is composed of the pore pressure and the effective vertical stress. This is shown in Tarzaghi's equation from 1948 (Eaton, 1975):

$$P_{ovb} = P_{pore} + \sigma_z \qquad (2.5)$$

Rearranged and with equivalent pressure gradients:

$$\rho_{pore} = \rho_{ovb} - \rho_z \qquad (2.6)$$

Eaton originally used this relationship to estimate pore pressure on the basis of the logging parameters sonic travel-time and resistivity. However, he discovered that the plots of the corrected d-exponent were very similar to the resistivity log plot and developed a third equation with d_c as the logging parameter (Eaton, 1975). Eaton's equations are as follows:

$$\rho_{pore} = \rho_{ovb} - \left((\rho_{ovb} - \rho_{normal})\left(\frac{\Delta t_{normal}}{\Delta t}\right)^3\right) \qquad (2.7)$$

$$\rho_{pore} = \rho_{ovb} - \left((\rho_{ovb} - \rho_{normal})\left(\frac{R}{R_{normal}}\right)^{1,2}\right) \qquad (2.8)$$

$$\rho_{pore} = \rho_{ovb} - \left((\rho_{ovb} - \rho_{normal})\left(\frac{d_c}{d_{c,normal}}\right)^{1,2}\right) \qquad (2.9)$$

Regardless of which equation is used for the pressure estimation, they all require a trend line calculated in a formation interval that follows the normal pressure regime. As previously discussed, the most typical formation type for this is shale. They also depend on knowing both the overburden gradient and the normal pore pressure gradient in the area.

2.4 The Bourgoyne-Young drilling model

The Bourgoyne-Young drilling model was developed for computing penetration rate when using roller-cutter bits. It can also be used for detection of changes in pore pressure, and for drilling optimization calculations. The model assumes that the different variables affecting ROP are all independent of each other, and that each variable can be represented by its own function. Bourgoyne and Young proposed using eight functions, which composite effect gives an equation for ROP with the form of:

$$ROP = (f_1)(f_2)(f_3)(f_4)(f_5)(f_6)(f_7)(f_8) \tag{2.10}$$

Where:

$$f_1 = e^{2.303a_1} = K \tag{2.10a}$$

$$f_2 = e^{2.303a_2(10,000-D)} \tag{2.10b}$$

$$f_3 = e^{2.303a_3 D^{0.69}(p_{pore}-9.0)} \tag{2.10c}$$

$$f_4 = e^{2.303a_4 D(p_{pore}-\rho_{ecd})} \tag{2.10d}$$

$$f_5 = \left[\frac{\left(\frac{WOB}{d_{bit}}\right) - \left(\frac{WOB}{d_{bit}}\right)_t}{4 - \left(\frac{WOB}{d_{bit}}\right)_t} \right]^{a_5} \tag{2.10e}$$

$$f_6 = \left(\frac{RPM}{60}\right)^{a_6} \tag{2.10f}$$

$$f_7 = e^{-a_7 h} \tag{2.10g}$$

$$f_8 = \left(\frac{F_j}{1,000}\right)^{a_8} \tag{2.10h}$$

In these equations,

   D = true vertical depth, ft,

   ρ_{pore} = pore pressure gradient, lbm/gal,

   ρ_{ecd} = equivalent circulating density,

$(WOB/d_{bit})_t$ = threshold bit weight per inch of bit diameter at which the bit begins to

drill, 1,000 lbf/in.,

h = fractional tooth dullness,

F_j = hydraulic impact force beneath the bit, lbf, and

a_1 to a_8 = constants that must be chosen based on local drilling conditions.

f_1 or K, is the drillability of the formation and models the effects of formation strength and bit type on ROP. It also includes the effects of drilling variables such as mud type, solids content, etc., effects that are not included in any of the other factors. The drillability is numerically equal to the penetration rate that would be observed in the given formation type (under normal compaction) when operating with a new bit at zero overbalance, a bit weight of 4,000 lbf/in., a rotary speed of 60 rpm, and at a depth of 10,000 ft. Using prior drilling data obtained from previous wells in the area, the drillability of the various formations can be computed. Having obtained the drillability, the constants a_1 through a_8 can also be decided with a multiple regression technique (Bourgoyne et al., 1986).

f_2 and f_3 model the effect of compaction on ROP. f_2 accounts for the rock strength increase due to normal compaction with depth, while f_3 models under-compaction in abnormally pressured formations. For a pore pressure gradient of 9.0 lbm/gal and a depth of 10,000 ft, the (f_2,f_3) product is equal to 1.0.

f_4 models the effect of overbalance on ROP. For zero overbalance, that is when the bottom hole pressure is equal to the formation pressure, the f_4 function has a value of 1.0.

f_5 and f_6 model the effect of bit weight and rotary speed on ROP. f_5 is equal to 1.0 when (WOB/d_b) has a value of 4,000 lbf/in. of bit diameter, while f_6 is equal to 1.0 when RPM is 60. This is chosen so that the (f_5,f_6) product has a value near 1.0 for common drilling conditions. The f_5 function involves a threshold bit weight factor, which is the minimum weight on bit to produce cuttings. This factor can be neglected in relatively soft formations, while in competent formations it has to be estimated from drilloff tests terminated at very low bit weight. Drilloff tests can also determine the constants a_5 and a_6. There is also an upper limit to the f_5 function, where increased WOB does not increase the ROP. At this point the ROP may even start to decrease, a behavior called bit floundering. This is attributed to cutting generation exceeding the capacity of efficient bottomhole cleaning or a complete penetration of the cutting element into the hole bottom (Bourgoyne et al., 1986).

f_7 models the effect of tooth wear on ROP. The term f_7 has a value of 1.0 for zero tooth wear. When operating with tungsten carbide insert bits at moderate bit weight and rotary speed, tooth wear is often considered insignificant and f_7 can be neglected. The constant a_7 can be estimated from ROP measurements taken in similar formations at similar bit operating conditions at the beginning and end of a bit run.

f_8 models the effect of bit hydraulics on ROP. With a jet impact force, F_j, of 1,000 lbf, f_8 has a value of 1.0.

In practical applications, it has been shown that for immediate changes in penetration rate only eqn. 2.10a, d, e and f are of importance. This corresponds to the variables caused by drillability, overbalance, bit weight and rotary speed. The other parameters tend to change over larger drilled distances and will therefore not make any significant difference with regard to the detection of changes in drillability (Bourgoyne et al. 1986).

3 Available Field Data

IPT and Statoil provided a data package with RTDD for two wells in the North Sea. The wells were Gullfaks C Well 34/10-48-A (only section 8 ½") and Well 34/10-C-47 (sections 24", 17 ½", 12 ¼", 8 ½"). Included in the data were also final well reports. The RTDD was stored in either Matlab files or the file format H5 and had to be transferred into Matlab for data management and plotting. The data included values for many parameters, such as drilling parameters and pressure gradients.

In this thesis, the focus will be on Well 34/10-C-47. This is because this well was delivered with the most complete data set, containing information from all four well sections above the reservoir.

3.1 General information on Well 34/10-C-47

All information in this section is taken from the final well report compiled by Statoil (2007).

Well C-47 is located in the Gullfaks field in the North Sea and drilled from the rig Gullfaks C. Drilling startup was 25.11.2005 and the well was completed by 30.04.2006. C-47 was drilled intended for oil production from the K2 and K3 segments of the Statfjord Formation (Fm), with water injection being the secondary objective. The well has a deviated well path and becomes horizontal in the reservoir section. Target depth (TD) in the K2 segment is located at 2066 m TVD RKB and 4399 m MD RKB. The RKB height above water level (air gap) is 84.1 m, while the water depth is 216.9 m.

Figure 3.1 shows a 2D-view of planned and actual well path of C-47. Figure 3.2 gives a top view image of the planned well path, showing its location within the Gullfaks field.
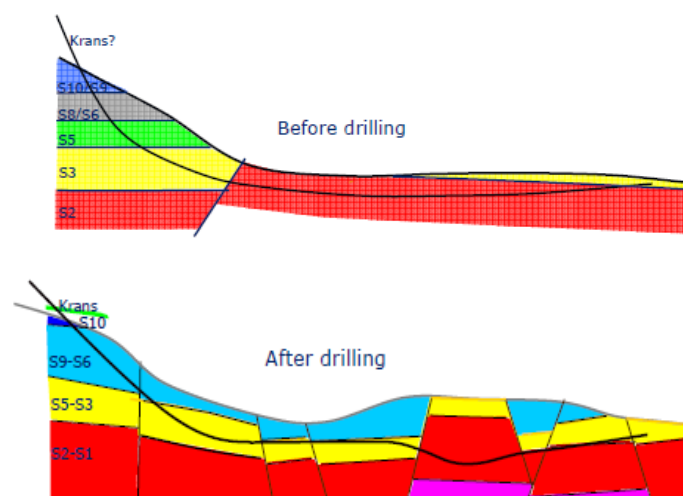

Figure 3.1: Planned and expected well path and stratigraphy for Well 34/10-C-47 before drilling, and actual well path and stratigraphy after drilling (Statoil, 2007).
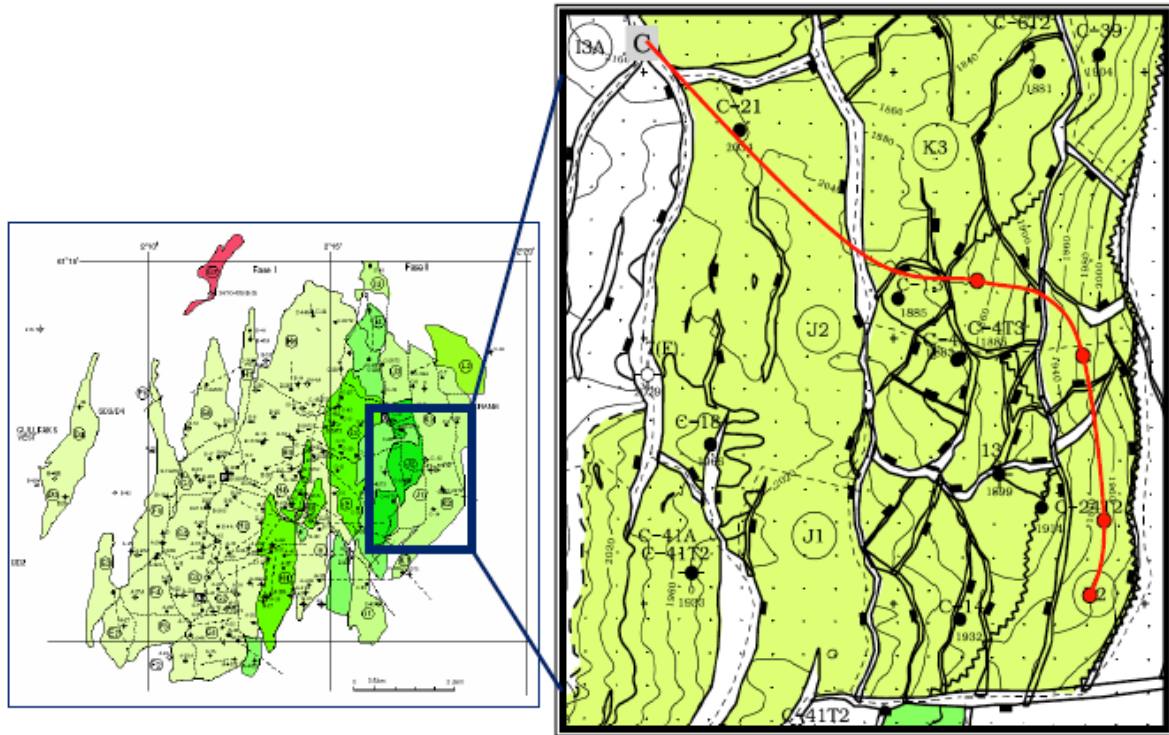
Figure 3.2: Planned well path for Well 34/10-C-47 going into the Statfjord Fm. east of C-13 in the K3 segment and turning south along the east flank of the K2 segment (Statoil, 2007).

The primary target for C-47 was oil production from the eastern flank of the K2 segment in the S2-S1 formations. The secondary target was to produce an attic volume in a small horst at Top Statfjord (S10) and partly water flooded zones (S9-S3), below in the K3 segment. Finally, there was also a possibility for some production from Krans above the Statfjord Fm.

During drilling, as predicted, first oil was struck in a few thin stringers of Krans sand at 2892 m MD RKB/1949 m TVD RKB. Below, at 2929 m MD RKB/1962 m TVD RKB, Top S10 had a thickness of 20 m MD/7 m TVD of oil filled sand.

From S9-S3 partly flooded oil sands with water saturation (SW) of 0.4-0.6 was drilled between 3028 m MD RKB/1998 m TVD RKB and 3810 m MD RKB/2084 m TVD RKB. These zones were found to be highly profitable, with Statoil reporting high NTG (Net-To-Gross Ratio's). The zone S8 was found 20 m TVD deeper than anticipated.

The primary target, the S2 sands, was found at 3810 m MD RKB/2084 m TVD RKB. This was 40 m TVD deeper than the prognosis, with the deviation caused by unexpected faulting. Unfortunately, the S2 sands had a SW of 0.7-0.9. This meant the oil saturation was too low for acceptable production. Thus, the primary objective for the well was not fulfilled.

64

The toe of the well, located in the Top S2/Base S3, was at 4220 m MD RKB/2078 m TVD RKB. The S3 sand had initial oil saturation and vertical thickness of about 4 m.

Results from drilling warranted perforation and completion with DIACS (Downhole Instrumentation and Control System) in the following 3 zones:

1. Krans and S10 in the heal of the well
2. S8-S5/S3 in the mid section
3. S3 in the toe of the well

After production in the 3 zones, the well is to be converted to a water injector.

Table 3.1 gives an overview of the drilled formations and the casing intervals/perforation zones with depth along the length of the well.

Formation	Well Section/Perforation Zone	Bit Size	Casing/Liner Diameter	Measured Depth	True Vertical Depth
	#	[in]	[in]	[m RKB]	[m RKB]
Top Nordland (seabed)	1		32" Casing	301	301
	Casing Shoe 32" Section			436	436
Top Utsira Fm.	2	24"	20" Casing	995	966
Top Sandy Hordaland	2	24"	20" Casing	1050	1011
	Casing Shoe 20" Section			1508	1308
Top Sandfree Hordaland	3	17 1/2"	13 3/8" Casing	1655	1366
Top Balder Fm.	3	17 1/2"	13 3/8" Casing	2050	1570
Top Lista Fm.	3	17 1/2"	13 3/8" Casing	2200	1639
	Casing Shoe 13 3/8" Section			2379	1723
Top Shetland Gp.	4	12 1/4"	9 5/8" Liner	2411	1739
	Casing Shoe 9 5/8" Section			2787	1906
Top Kyrre Fm.	5	8 1/2"	7" Production Liner	2833	1926
Top Krans Mb.	Perforation Zone 1	8 1/2"	7" Production Liner	2892	1949
Top S10	Perforation Zone 1	8 1/2"	7" Production Liner	2929	1962
Top S9	Perforation Zone 2	8 1/2"	7" Production Liner	3028	1998
Top S8	Perforation Zone 2	8 1/2"	7" Production Liner	3047	2004
Top S7	Perforation Zone 2	8 1/2"	7" Production Liner	3058	2009
Top S6	Perforation Zone 2	8 1/2"	7" Production Liner	3075	2014
Top S5	Perforation Zone 2	8 1/2"	7" Production Liner	3150	2041
Top S3	Perforation Zone 2	8 1/2"	7" Production Liner	3202	2057
Top S2	End of Perforation Zone 2	8 1/2"	7" Production Liner	3810	2084
Top S2/Base S3	Perforation Zone 3	8 1/2"	7" Production Liner	4220	2078
TD	Casing Shoe 7" Section	8 1/2"	7" Production Liner	4399	2066

Table 3.1: Location of drilled formations with casing intervals/perforation zones along the depth of Well 34/10-C-47.

3.2 Lithology

The Gullfaks field lies in the northern part of the North Sea and at the western flank of a tectonic area called the Viking Graben. The Viking Graben is a downthrown block of land produced from parallel normal faults. It contains a range of different lithologic groups or formations. This could be seen in Table 3.1, which showed the penetrated formations by Well C-47. In this section, there will be a brief presentation of each type of lithology, mainly highlighting the type of rock and the zone thickness.

All information described in this section is gathered from the online fact-pages of the Norwegian Petroleum Directorate (NPD).

3.2.1 Nordland Group and Utsira Formation

The Nordland Group of the North Sea is dominated of marine claystones. In the upper part, the group consists of unconsolidated clays and sands with glacial deposits. In the Viking Graben area, the Utsira Fm. occurs in the lower parts. The Utsira Fm. consists of fine-grained marine sandstones separated by some claystones and minor siltstones. Thickness of the Nordland Group in the Viking Graben area is about 1000 meter (NPD[1], 2017).

3.2.2 Hordaland Group

The Hordaland Group consists of marine claystones with minor sandstones. The sandstones are generally very fine to medium grained. They are found at various levels in the group, often interbedded with the claystones. In the North Sea, the upper part of the Hordaland Group is classified as sandy, as the upper boundary of the group is placed at the base of the sandstones of the Utsira Fm. The sandstones are less present towards the base of the group, where it is considered as sand-free. The thickness of the Hordaland Group varies by location. In the central and southern part of the Viking Graben it ranges from an average of 1100-1200 meter up to a maximum of 1300-1400 meter. In the northern part, the thickness may only be a few hundred meters (NPD[2], 2017).

3.2.3 Rogaland Group with Balder and Lista Formations

The lithology of the Rogaland Group is highly dependent on location within the group. In the English sector of the North Sea, the group is dominated by sandstones interbedded with shales. In the Norwegian sector, the group consists mostly of claystones and shales (NPD[3], 2017). At Gullfaks position, the Balder Fm. lies in the uppermost part. The Balder Fm. consists of laminated, fissile shales with sandy tuffs (NPD[4], 2017). The Lista Fm., in the lower part, has non-tuffaceous and poorly

laminated shales (NPD[5], 2017). Both the Balder and Lista formations may include stringers of limestone and dolomite, in addition to siderite (in Balder Fm.) and pyrite (in Lista Fm.). There may also be locally developed sandstones within both formations. The thickness of the Balder Fm. varies from less than 20 meter to more than 100 meter, while the Lista Fm. ranges from 100 to 200 meter.

3.2.4 Shetland Group with Kyrre Formation

The Shetland Group is developed in the central and northern North Sea. It consists of the chalk facies of chalky limestone, limestone, marls and calcareous shales and mudstones in the central North Sea. Chert (flint) also occurs throughout the facies (NPD[6], 2017). In the northern North Sea, there are siliciclastic facies of mudstones and shales partly interbedded with limestones. In Well C-47, the lower part of the Shetland Group is made up of the Kyrre Formation. The Kyrre Fm. consists of mudstones with occasional limestone beds. The mudstones are silty to calcareous, occasionally pyritic, gluconic or micaceous (NPD[7], 2017). Thickness of the Shetland Group ranges between 1000 and 2000 meter in the graben areas, with thinning towards and in the platform areas.

3.2.5 Statfjord Group with Krans Member

The Statfjord Group, including the Krans Member, compromises the reservoir section of Well C-47. The basal part of the Statfjord Group consists of a sequence of shale interbedded with thin siltstones, sandstones and dolomitic limestones. There is a "coarsening upward" sequence, such that massive sandstone bodies are interbedded with the shales located further up. The top of the group consists of thick, fossiliferous and glauconitic sandstones (NPD[8], 2017). The Krans Mb., located in the uppermost part of the Statfjord Group in the Gullfaks area, has this type of sandstone lithology. In Well C-47, the Krans Mb. is very thin and only has 13 meters of vertical thickness. The Statfjord Group is 135 meters in Well C-47, but in thicker parts such as in the central Viking Graben, it has been measured up to more than 300 meters.

Table 3.2 summarizes the lithology and thickness of each group/formation drilled in Well C-47.

Formation	Lithology	Vertical Thickness in Well C-47
Nordland Group	Unconsolidated clays and sands.	665 meters
Utsira Fm. (Nordland Group)	Fine grained sandstones seperated by claystones and minor siltstones.	45 meters
Sandy Hordaland Group	Claystones with fine to medium grained sandstones.	355 meters
Sandfree Hordaland Group	Claystones.	204 meters
Balder Fm. (Rogaland Group)	Shales, which are fissile and laminated with sandy tuffs. Ocassional stringers of limestone, dolomite and siderite. Sandstones are locally present.	69 meters
Lista Fm. (Rogaland Group)	Shales, which are poorly laminated and non-tuffaceous. Ocassional stringers of limestone, dolomite and pyrite. Sandstones are locally present.	100 meters
Shetland Group	Siliciclastic facies of mudstones and shales partly interbedded with limestones.	187 meters
Kyrre Fm. (Shetland Group)	Mudstones with occasional limestone beds.	23 meters
Krans Mb. (Statfjord Group)	Sandstones, which are thick, fossiliferous and gluconitic.	13 meters
Statfjord Group	Shales interbedded with thin siltstones, sandstones and dolomitic limestones. Coarser and more massive sandstone bodies interbedded with the shales towards the top of the group.	135 meters

Table 3.2: Lithology and vertical thickness of groups/formations in Well 34/10-C-47.

3.3 Relevant real-time drilling data

To use the models presented in chapter 2 and to calculate drillability and pore pressure, it must be clear which RTDD has been supplied and which still need to be obtained. The RTDD required by the drilling models are as follows:

- Drilling technique parameters:
  - Bit penetration rate, ROP
  - Rotary string speed, RPM
  - Weight on bit, WOB
- Drill bit parameters:
  - Drill bit diameter, dbit
  - Fractional tooth dullness, h
  - Hydraulic impact force beneath the bit, F_j
- Formation fluid and overburden pressure parameters:
  - Normal pore pressure gradient, ρ_{normal}
  - Pore pressure gradient, ρ_{pore}
  - Overburden gradient, ρ_{ovb}
- Drilling fluid parameters:
  - Equivalent circulating mud density, ρ_{ecd}

3.3.1 ROP, RPM and WOB

These are drilling technique parameters recorded in real time while drilling. ROP is the speed at which the drill bit breaks the formation. It is measured in feet per hour (ft/hr) or meters per hour (m/hr). RPM is the measure of the frequency of rotation of the drill string, recorded in revolutions per minute. WOB is the amount of downward force exerted on the drill bit and is normally measured in thousands of pounds or kilograms (tons). It can also be represented as per thousand of weight on bit per inch of bit. In this data package, the WOB unit is in tons.

Data for all the three drilling techniques parameters were found in the supplied data package. Plots of ROP, RPM and WOB versus measured depth in the 17 ½" section of Well C-47 are plotted in Appendix 1 in figures A.1, A.2 and A.3 respectively.

3.3.2 dbit, h and F_j

These parameters are needed for drill bit characteristics. dbit, is the drill bit diameter measured in inches. h, is the fractional bit tooth height that has been worn away. The value h = 0 represents a new bit, while a bit graded T-8 has h = 8/8 = 1, and represents a bit with completely worn out teeth. F_j is the hydraulic impact force beneath the bit and quantifies the effect of bit hydraulics on ROP. F_j is usually measured in pounds and normalized for a value of 1,000 lbf.

Unfortunately, the data package only provides values for the first parameter, dbit. These values are taken from the final well report. For the sake of convenience, and to simplify the drilling model, it was decided to neglect the other two parameters. Thus, the functions f_7 and f_8 from the Bourgoyne - Young drilling model, which models the effect of tooth wear and bit hydraulics on ROP, will have no influence on the final results obtained for drillability.

As previously noted, according to Bourgoyne et al., 1986, only the variables caused by drillability, overbalance, bit weight and rotary speed will have an effect on ROP. The other parameters tend to change over larger drilled distances and will therefore not make any significant difference with regard to the detection of changes in drillability. These statements support the idea that the simplifications should be OK.

3.3.3 ρ_{normal}, ρ_{pore}, ρ_{ovb} and ρ_{ecd}

These are formation fluid (ρ_{normal}, ρ_{pore}), overburden pressure (ρ_{ovb}) and drilling fluid (ρ_{ecd}) parameters. They are presented as pressure gradients and measured in standard gravity, SG, which is the density of the respective fluid divided by the density of water.

69

In the RTDD, there is only data for the equivalent circulating mud density, ρ_{ecd}. The pore pressure gradient and the overburden gradient, ρ_{pore} and ρ_{ovb}, are found from pressure gradient plots in the final well report. There is no data for the normal pore pressure gradient, ρ_{normal}, for the entire length of the well. By extrapolating the normal pore pressure gradient from the top of the well to the final well depth, it should be possible to obtain complete values for ρ_{normal}.

3.4 Collecting and processing data

A goal for this thesis is to investigate if the formation hardness or drillability can be calculated by applying Eaton's method and the Bourgoyne -Young drilling model on RTDD and see if the results are useable for analysis. All four well-sections above the reservoir penetrate different kinds of formations, so there should be enough lithologic variety for the agent to be tested on. In Figure 3.3, shown below, it can be observed that from a depth of 1370 m TVD RKB, the pore pressure starts increasing rapidly from the normal pore pressure trend line. Thus the 17 ½" section is drilled in a zone of both normal and abnormal pore pressure, while the 12 ¼" and 8 ½" are drilled in high pore pressure zones. This variable pore pressure provides another challenge the agent must be designed to overcome.

With the Matlab program delivered by NTNU, all the available and needed RTDD were extracted from the H5 files for interpretation. The chosen parameters were ROP, WOB, RPM at bit, ECD at bit, Mud density out average, Torque and Hole Depth in TVD and MD. When the data from the 24" and 12.25" sections were loaded in Matlab it showed the exact same image and values for all parameters. Vertical depth, DVER, was starting at around 1700 meters and ending at around 1900 meters for both sections. This is the vertical depth data corresponding to the 12.25" section, so the data for the 24" section had to be incorrect. The data for the 17.5" were at first also not possible to run in Matlab. However, after consulting with NTNU and the supervisor, new and accurate data for the 17.5'' were provided. The data for the 8.5" section seemed to be correct.

For the 17.5'', 12.25" and 8.5" sections, those sections which had data that could be used for interpretation, all the loaded parameters except for one seemed to be accurate. The ROP-data was not trustworthy as it stayed completely constant over time intervals when the bit was not moving, which is indicated by constant vertical and measured depth. The ROP data is also recorded too high. Figure 3.3 below shows an example of this trend. The ROP is at a constant value of 7.4 meters per hour when the value should be zero, as no drilling occurs. This defies common sense, so the ROP was instead calculated using an alternative method which involves the velocity of the block during drilling. This method will be presented in chapter 4.
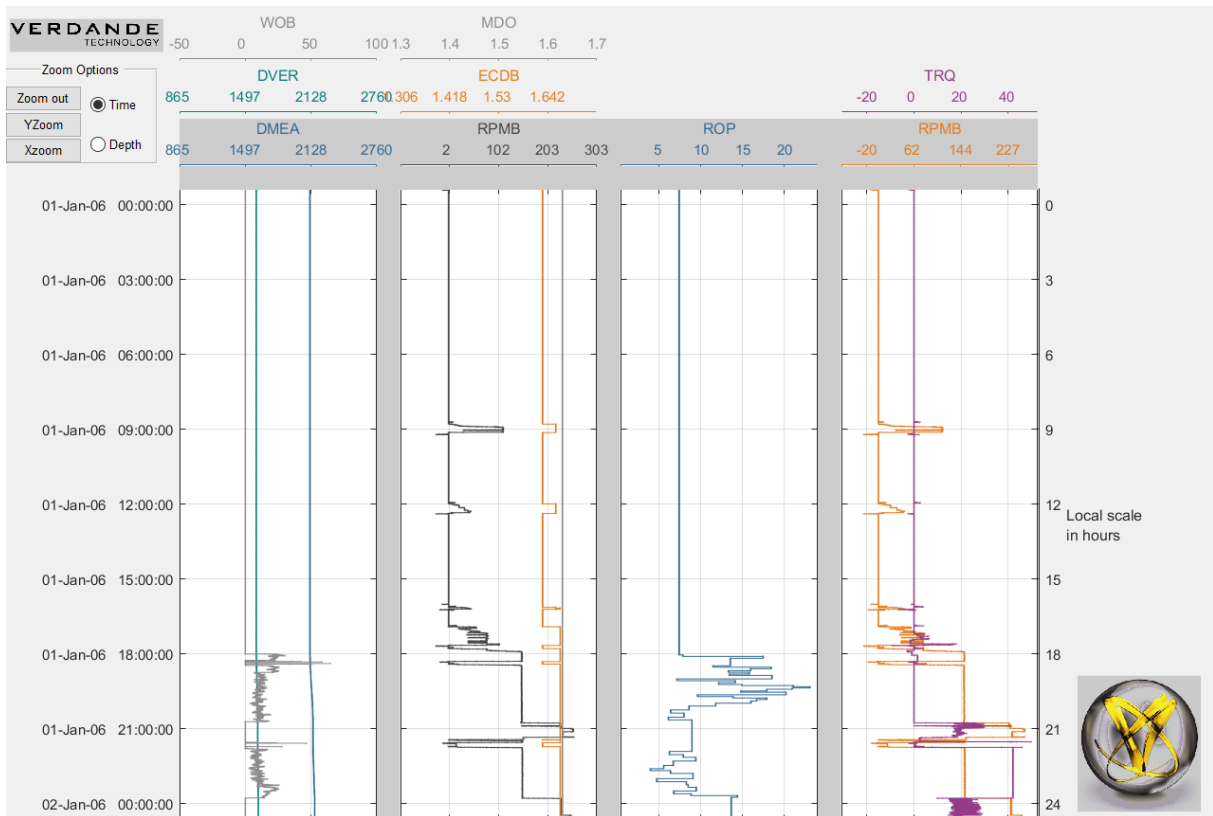
Figure 3.3: Data plot taken from Well 34/10-C-47 dated 1. January 06. It is seen that the ROP has a constant value of 7.4 meters per hour when both vertical depth (DVER) and depth of measured hole (DMEA) are constant.

3.4.1 Pressure gradients

In the final well report, there are plots of the pressure gradient development throughout the length of the wellbore. Figure 3.4 shows the relevant gradients for formation pore pressure, mud weight and overburden pressure for the well interval above the reservoir section.
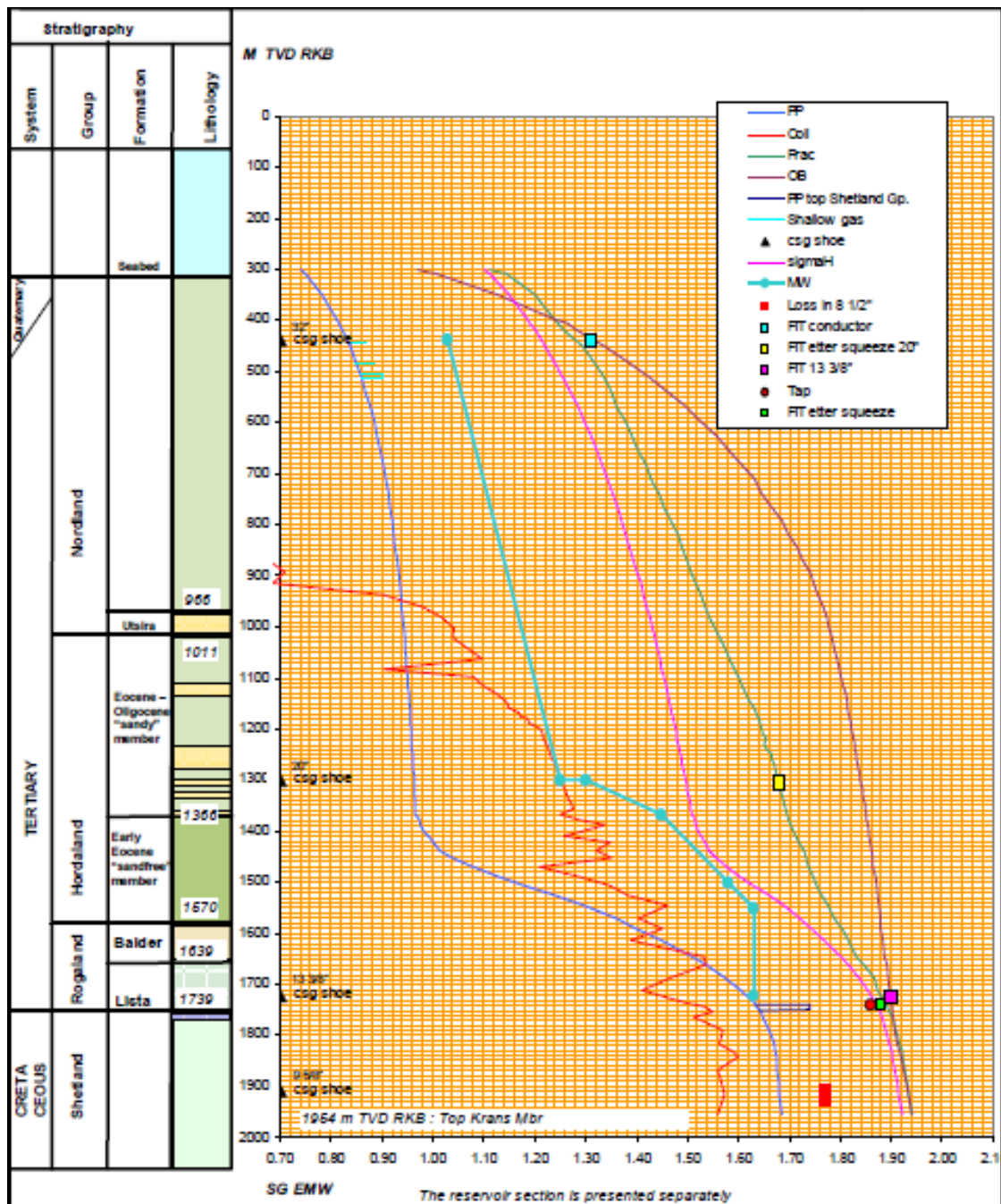
71

Figure 3.4: Pressure gradients above the reservoir for Well 34/10-C-47 (Statoil, 2007).

It can be observed that from a depth of 1370 m TVD RKB, the pore pressure starts increasing rapidly from the normal pore pressure trend line. When penetrating the top of the Shetland Fm., a high pore pressure zone is also encountered, with a reported pore pressure gradient of 1,74 SG. Statoil reported that the 12 ¼" Shetland section was drilled using managed pressure drilling. This means surface pressure was applied in order to keep the well pressure above the pore pressure.

3.4.1.1 Obtaining pore pressure, overburden pressure and extrapolating the normal pore pressure gradient

As mentioned in section 3.3.3, there are no data for the pressure parameters ρ_{pore}, ρ_{ovb} and ρ_{normal} in the RTDD. The pressure data for ρ_{pore} and ρ_{ovb} was attained by evaluating the gradients of Figure 3.4. Starting from 300 m TVD RKB, the values were read for every 100 meters, and then imported to Excel. As noted earlier, the pore pressure becomes abnormal from 1370 meters. By assuming the normal pore pressure continues as a straight line, the normal pore pressure gradient was constructed by using linear extrapolation. Figure 3.5 shows the normal pore pressure gradient and the other relevant pressure gradients of Figure 3.4 after being plotted in Excel.
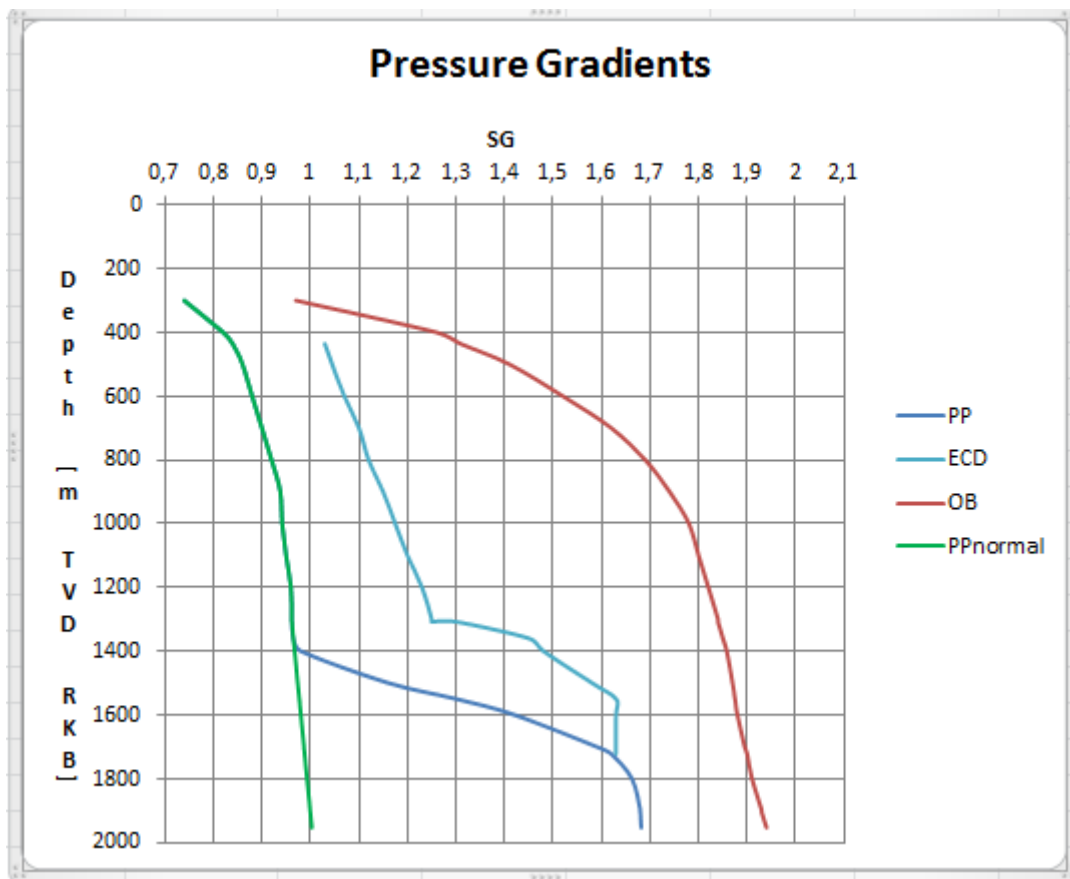

Figure 3.5: Relevant pressure gradients from Figure 3.4, including the extrapolated normal pore pressure gradient.

4 Creating the Agents for Drillability and Pore Pressure Calculations

4.1 Agent for drillability

The data agents created in this thesis will calculate formation drillability based on RTDD and estimations of pore pressure and overburden gradients from Well 34/10-C-47. Three agents have been developed for drillability, the inverse of hardness. Each is representing a different mathematical model. The models chosen, and which were presented in chapter 2, are:

- Zamora's method
- Eaton's method
- The Bourgoyne -Young drilling model

The first two models are both based on the d_c-exponent method, while the Bourgoyne-Young drilling model is based on a ROP-calculation composed of the most influencing drilling parameters. These methods have all been chosen because they are suitable for RTDD. Though this experiment is conducted on already drilled wells and on relevant information gathered during the well planning and drilling operations, it will try to replicate a process performed in real-time. Thus, the methods will be viable as methods of pressure and drillability detection, not prediction.

All three methods presented in the script will replicate a real-time and continuous drillability calculation using mathematical formulas. This is a quantitative approach. However, there exist qualitative methods for formation hardness detection through log interpretation and analysis of RTDD, e.g. gamma ray and sonic logs. For this thesis, it has been chosen a method based on three specific drilling parameters, which will be presented below. Having a qualitative method in addition to the quantitative ones, can help give a better overview of the drilling interval selected for analysis, as well as more redundancy will help in interpreting the obtained results.

4.1.1 Qualitative method based on log interpretation of drilling parameters

Studying the behavior and coherence of the three drilling parameters block positioning (BPOS), weight on bit (WOB) and bit rotations per minute (RPMB), can reveal critical information about the formation being drilled. Figure 4.1 below, shows how the logged curves of these parameters may look like in response to changes in hardness. For example, there is seen a reduction in both BPOS speed (less steep curve) and RPMB, while WOB is increased when transitioning from a soft to a hard formation.
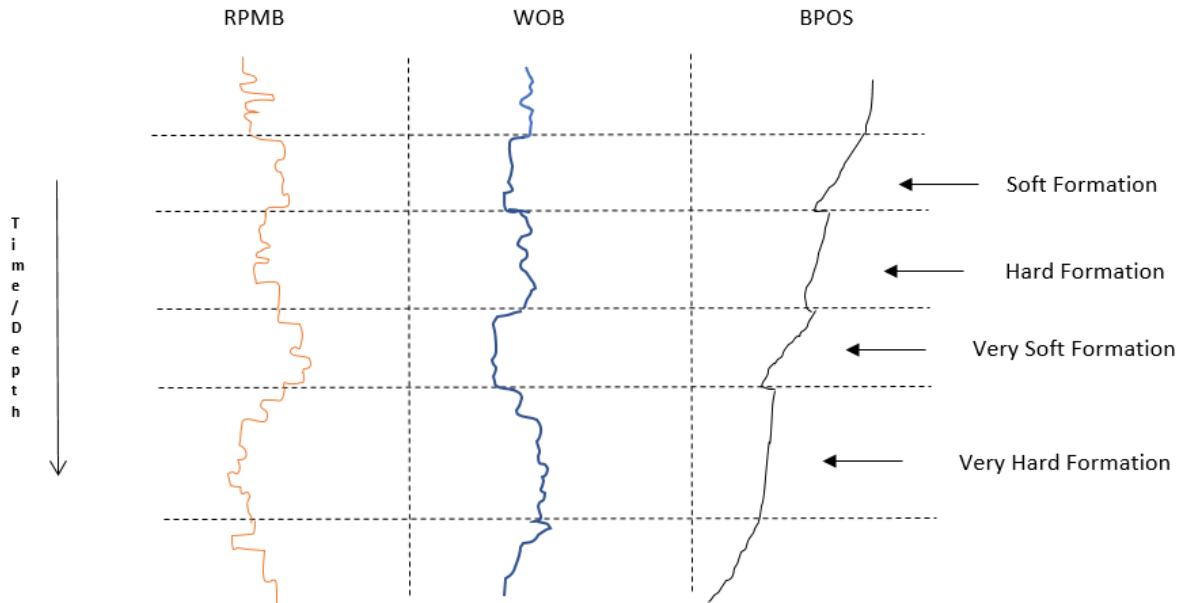
Figure 4.1: Sketched example of how the logged parameters BPOS, WOB and RPMB may behave in response to changes in formation hardness. Hard formations can be indicated by a reduction in BPOS speed, reduction in RPMB and an increase in WOB. In contrast, soft formations are recognized by relatively high BPOS speed and RPMB, while WOB is low.

Hard stringers can be identified by the same means as hard formations. However, when hard stringers are experienced, the changes in the behavior of the parameters happen more abrupt and less gradual compared to a transition from a soft to a hard formation type. This is natural, as hard stringers are thin, hard "veins" within a softer formation. The goal of this thesis is however to be able to spot hard stringers and quantify drillability with the help of mathematical models. Drillability is also essential for the pore pressure model. How to quantify drillability will be addressed in the sections hereafter.

4.1.2 Methods based on the d_c – exponent: Zamora's method and Eaton's method

As made known in section 2.3.1.1, the d-exponent represents the deviation in drilling penetration rate caused by differential pressure. Normalized for common drilling conditions, and with the drillability set at a constant value, the expression for the d-exponent is:

$$d = \frac{log(\frac{ROP}{60\,RPM})}{log(\frac{12\,WOB}{10^3 d_{bit}})} \tag{2.2}$$

The input parameters are ROP, RPM, WOB and d_{bit}, all having values located in the data package.

The corrected d-exponent, the d_c-exponent, includes for changes in mud weight:

$$d_c = d \frac{\rho_{normal}}{\rho_{mud}}$$
(2.3)

This formula depends on the d-exponent, the mud density equivalent to normal formation pore pressure and the equivalent circulating mud density at the bit.

The program will compute a trend line from the assumed normally pressured zones in the upper section of the well, and then present a plot of this trend line compared to the values computed for the full length of the well. As this method only detects at which depth a change of pressure occurs, the methods of Zamora and Eaton will be applied in order to quantify values of the pore pressure gradient. (As discussed earlier, it is important that the normal trendline is computed in a section of competent or "clean" shale. This is to assure that the results from the Zamora and Eaton methods is as accurate as possible.)

Zamora's method expresses the pore pressure gradient by using a linear scale for depth and a logarithmic scale for d_c:

$$\rho_{pore} = \rho_{normal} \left(\frac{d_{c,normal}}{d_c} \right)$$
(2.4)

This expression includes the normal pore pressure gradient, the d_c-exponent on the normal trend line and the actual d_c-exponent which lies on the departed trend line.

Eaton's method is based on the assumption that the overburden pressure is a composite of the pore pressure and the effective vertical stress. Expressed for pore pressure with equivalent pressure gradients and d_c as the selected logging parameter:

$$\rho_{pore} = \rho_{ovb} - \left((\rho_{ovb} - \rho_{normal}) \left(\frac{d_c}{d_{c,normal}} \right)^{1,2} \right)$$
(2.9)

This equation depends on the same parameters as Zamora's method, however it will also require the overburden pressure gradient. The gradients of both the normal pore pressure and the overburden pressure will be based on the values from the Excel plot of Figure 3.5.

4.1.3 Method based on ROP-calculations: The Bourgoyne -Young drilling model

The full Bourgoyne-Young drilling model equation is presented in section 2.4.

The Bourgoyne-Young drilling model is composed of eight different and independent variables or functions affecting ROP:

$$ROP = (f_1)(f_2)(f_3)(f_4)(f_5)(f_6)(f_7)(f_8) \tag{2.10}$$

A large range of parameters are considered in these functions. Based on what parameters are available, as researched in chapter 3.3., only the factors $f_2 - f_6$ will be possible to compute. The f_7 and f_8, modelling the effects of tooth wear and bit hydraulics respectively, will be given values of 1. This is because of the lack of data on the parameters fractional tooth dullness, h, and hydraulic impact force beneath the bit, F_j. As stated earlier, f_7 and f_8 are among those variables not having any immediate effect on ROP. Thus, in theory, their removal from the ROP-equation should not influence the final results on drillability by any large factor.

For the function f_5, modelling the effect of bit weight on ROP, the parameter called threshold bit weight factor, $\left(\frac{WOB}{d_{bit}}\right)_t$, will be given a value of zero. This factor represents the minimum weight on bit to produce cuttings, but as said in section 2.4, it can be neglected in relatively soft formations. For harder formations, it would require calculations from drilloff tests, but since neither any drilloff test data are available, this factor will be overlooked in the drillability calculations.

As mentioned in section 2.4, the effect of overbalance, modeled by f_4, is considered important because it influences immediate changes in penetration rate. In this thesis, the problem with the overbalance factor, is that for it to be considered real-time it should be detected and calculated continuously during the drilling process. This is however not possible to mimic, as there are no RTDD made available for the pore pressure gradient, ρ_{pore}. The only data available for ρ_{pore}, are those which can be obtained from the final well report. These values were predicted in advanced and can be read from the pressure gradients in Figure 3.5. According to the report, pore pressure estimations in the top hole sections were based on drilling parameters, gas readings and general well stability considerations. Pore pressure estimations in the reservoir section was given from Stethoscope pressure points taken while drilling and tripping. Except some abnormal pore pressures in the Shetland Group in the 12 ¼'' section, all estimated pore pressure was stated to be in accordance with the prognosis. However, because no RTDD for ρ_{pore} was provided, in the first edition of this data agent made for drillability detection, the factor of overbalance has been decided to be neglected.

The f_2 and f_3 functions, models the effect of normal compaction and under-compaction on ROP. These are not among those factors having any immediate effect on ROP. Therefore, these two functions are not considered important enough to be included in the model chosen for this thesis. The f_3 function, modeling under-compaction in abnormally pressured formations, has the same issues as the function for overbalance, f_4, meaning it includes the ρ_{pore} parameter. Also, as stated in section 2.3.1.1, the effect of overbalance is much more important than the effect of under-

compaction for ROP, so when it has been decided to neglect the effect of overbalance (initially at least), it is natural to also neglect the fact of under-compaction. The f_2 function is dependent on the true vertical depth, which is available among the RTDD, so this function could in theory have been included in the model and not affect results too such a large extent. However, since the function also depends on the formation coefficient a_2, this adds unnecessary complexity. This coefficient should ideally be decided based on specific formation type characteristics, which can be a difficult process. Because there is one coefficient per function in the ROP equation, wrongly selected values for the formation coefficients may result in a skewed final result, so it is in the best interest to operate with as few coefficients as possible. Methods for deciding the drilling coefficients will be explained in chapter 4.1.4.3.b. The model in the agent should be made to calculate drillability as efficiently as possible, so adding more functions and variables than necessary to the ROP-equation is not considered optimal.

Thus, after these modifications, the simplified Bourgoyne-Young drilling model used hereafter is:

$$ROP = (f_1)(f_5)(f_6)$$

$$ROP = K \left[\frac{\left(\frac{WOB}{d_{bit}} \right)}{4} \right]^{a_5} \left(\frac{RPM}{60} \right)^{a_6} = K \left(\frac{WOB}{4d_{bit}} \right)^{a_5} \left(\frac{RPM}{60} \right)^{a_6} \tag{4.1}$$

4.1.4 Detailed description of data agent

4.1.4.1 Importing and processing data

The data package provided by IPT contains recorded drilling data, available in a format called HDF (Hierarchical Data Format), which most updated version is HDF5. This is a set of file formats designed to store and organize large amounts of numerical data. Each file holds the recorded data for a given time interval of the operation, with the different drilling data stored as one-dimensional arrays which can be read separately by a built-in read-function in Matlab. After reading selected data, Matlab is further used for the programming and plotting.

Data have been stored with time as the indexing variable, where every data point in each different array corresponds to the same time. The time difference between each recording is 5 seconds. However, as data have been recorded over the total time it takes to create the well, it also holds records from periods where the drilling is at a halt. These times can for instance be during tripping operations, when installing new drill pipe or when casing is installed and cemented. Imported data

such as in these instances and which are being considered not relevant have been sorted out and removed. This helps to decrease the load put on the agent and improve the quality of the calculations.

Other data may contain unrealistic values, causing unwanted results. Therefore, sorting is done by giving the agent a command to check if data in a specific data array (e.g. arrays for relevant drilling parameters such as ROP, RPM, and WOB) has values outside given boundary conditions. Only values within the predefined boundaries are kept and used for calculations, while values outside the boundaries are removed.

Plots showing the results should be easy to read and interpret. To do this, the agents are designed to create new data arrays with a predefined depth interval between each data entry. This is done by a loop reading the vertical depth value of a data point, and then checking the following entries until a value with the required depth difference is found.

A consequence of this method for averaging and compressing of data, is that a substantial amount of data entities will be removed before the final calculation is made. The decision on which data is kept is based entirely on the depth parameter, making the data selection from this process random and uncertain with regards to the quality of data being kept. To minimize this risk of error, the program will read multiple data entities and create average values before the depth intervals are made. This process of averaging data will also reduce the amount of calculation the agent must do before its task is complete.

Figure 4.2 shows a simplified flowchart of how the two agents will function to compute hardness.
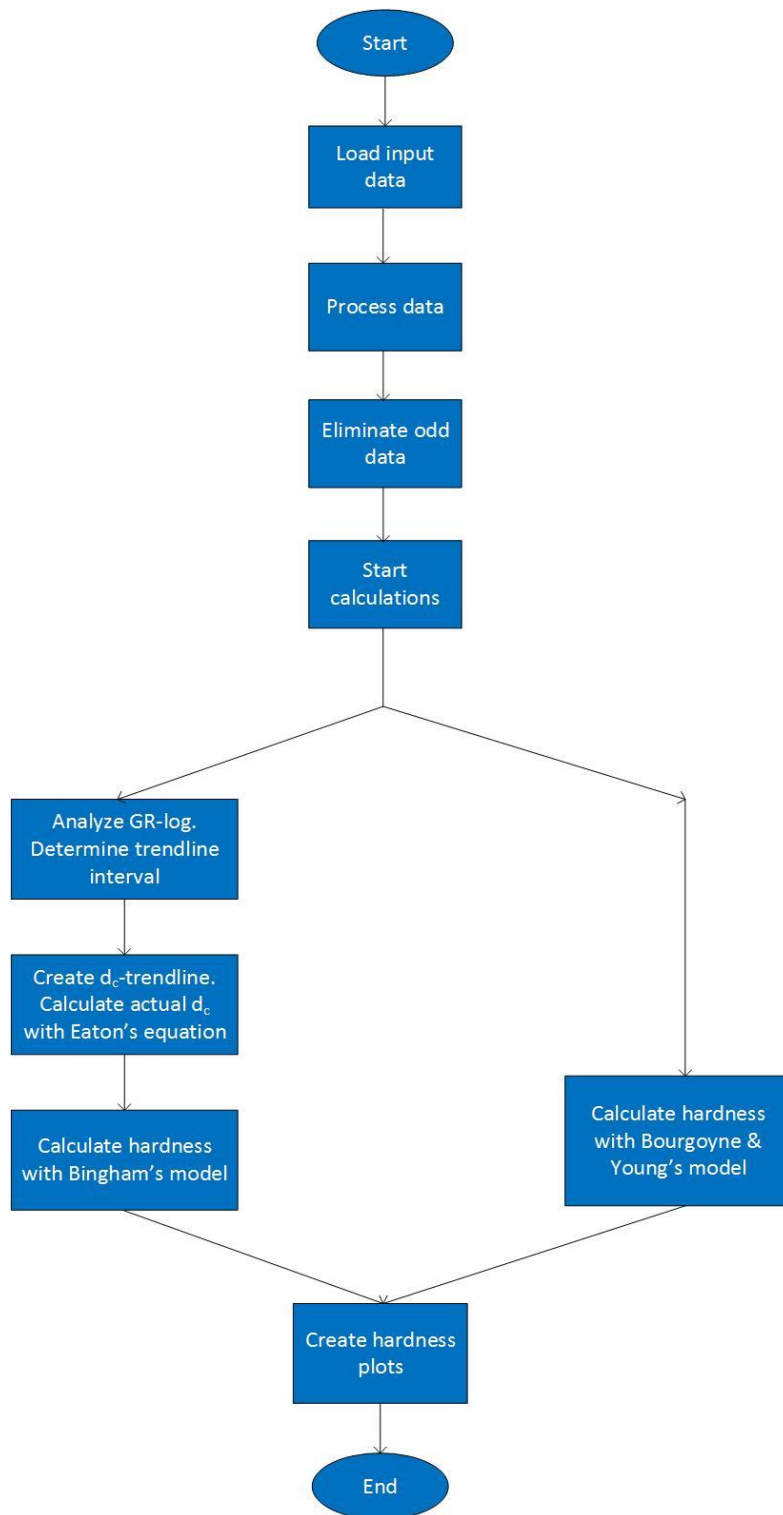
Figure 4.2: Sketched flowchart of the two agents, indicating the commands and flow of data. The output is hardness and hardness plotted vs. measured depth

4.1.4.2 Drillability from reversed Zamora's- and Eaton's method

Both Zamora's method and Eaton's method are normally used to create pore pressure estimations.

Since the task of this thesis is to calculate drillability, the formulas must be reversed to help with this

objective. This means having pore pressure as the input variable and the d_c-exponent as the output variable.

Zamora's method (2.4) solved for the d_c-exponent:

$$\rho_{pore} = \rho_{normal}\left(\frac{d_{c,normal}}{d_c}\right)$$ (2.4)

➔ $$d_c = d_{c,normal}\left(\frac{\rho_{normal}}{\rho_{pore}}\right)$$ (2.4i)

Eaton's method (2.5) solved for the d_c-exponent:

$$\rho_{pore} = \rho_{ovb} - \left((\rho_{ovb} - \rho_{normal})\left(\frac{d_c}{d_{c,normal}}\right)^{1,2}\right)$$ (2.5)

➔ $$d_c = d_{c,normal}\left(\frac{\rho_{ovb}-\rho_{pore}}{\rho_{ovb}-\rho_{normal}}\right)^{\left(\frac{1}{1,2}\right)}$$ (2.5i)

The d_c-exponent value obtained from either Zamora's method or Eaton's method is then run through Rehm and McClendon's equation for the modified d-exponent, eqn. (2.3), to get the "regular" d-exponent:

$$d_c = d\frac{\rho_{normal}}{\rho_{mud}}$$ (2.3)

➔ $$d = d_c\frac{\rho_{mud}}{\rho_{normal}}$$ (2.3i)

Finally, the drillability, K, can be calculated from Jorden and Shirley's modification of the Bingham equation, eqn. (2.1):

$$ROP = K \cdot RPM\left(\frac{WOB}{d_{bit}}\right)^d$$ (2.1)

Solved for K and normalized for common drilling conditions:

➔ $$K = d \cdot \frac{log(\frac{12\,WOB}{10^3 d_{bit}})}{log(\frac{ROP}{60 RPM})}$$ (2.1i)

This procedure requires the agent to access data on the pressure gradients ρ_{pore}, ρ_{ovb} and ρ_{normal}. Under normal circumstances and during real-time drilling, prediction methods and/or detection methods has to be used for pressure estimations. Exact pressure data will only be available after the well has been drilled. In this case, the well has already been drilled so pressure data is available, and the agent acquires the data from Figure 3.5.

A realistic scenario would be more complex. During planning and before reaching target depth, pressure estimations must be based on prediction methods such as data history of neighboring wells or data from seismic surveys. Then, during real-time drilling, the first estimations can be verified or improved upon by detection methods. These methods require the use of advanced MWD-tools continuously recording drilling performances and mud fluid properties, while at the same time being synchronized with data agents performing pressure calculations.

The $d_{c,normal}$-exponent is calculated in a zone where it is assumed that the pore pressure follows the normal pore pressure, ρ_{normal}. This is usually in a clean shale zone or in a shallow sedimentary basin where sedimentation has occurred slowly enough for normal compaction and water expulsion to take place. As mentioned in section 2.3.1.1, a normal pressure situation is indicated on a d_c-exponent vs. depth plot by an increasing trend line of the d_c-exponent, while in an abnormally pressured zone the trend line increases less rapidly or may even become reversed. The next step for the agent is to find such a normal compaction zone and calculate the $d_{c,normal}$-exponent using eqn. (2.2) and then eqn. (2.3). This is done by analyzing the gamma ray log.

First, the agent will remove anomalies from the gamma ray log. It is then assumed that the max gamma ray value represents a clean shale formation, while the minimum gamma ray value represents a sand formation. The agent searches for an interval with shale content exceeding 90%, which is chosen as the base for the trend line calculations. $d_{c,normal}$-exponent values are then computed for this interval. With the help of linear regression functions integrated in Matlab, the trend line can be extrapolated for the whole depth of the well.

Having obtained the $d_{c,normal}$, the agent solves Zamora's method or Eaton's method for the d_c-exponent and runs it through eqn. (2.3) to find the d-exponent. Everything is now in place for the agent to calculate the drillability, K, by solving eqn. (2.1i).

a) Troubles establishing the d_c-exponent trend line because of lack of gamma ray data

As has been mentioned previously, it is essential that the d_c-exponent trend line is established in a clean shale zone. To find such a zone require access to gamma ray data. Unfortunately, there was no gamma ray data provided along with the RTDD. This made it difficult to find such zones. Because of this, it was decided to cancel the work with the method based on the d_c-exponent, such as Zamora's method and Eaton's method. Rather, there will be full focus on computing drillability or hardness from the ROP-method suggested by Bourgoyne and Young.

4.1.4.3 Drillability from Bourgoyne -Young drilling model

a) Calculating drillability

As presented in section 4.1.3, the simplified Bourgoyne – Young drilling model being used is:

$$ROP = K \left(\frac{WOB}{4d_{bit}}\right)^{a_5} \left(\frac{RPM}{60}\right)^{a_6}$$

(4.1)

or in terms of Drillability, K:

$$K = \frac{ROP}{\left(\frac{WOB}{4d_{bit}}\right)^{a_5} \left(\frac{RPM}{60}\right)^{a_6}}$$

(4.1i)

However, some further modifications can still be made to this equation. There is no need to operate with exact values of drillability, as the goal is to eventually normalize the drillability or hardness. The method of how to normalize and classify hardness will be explained in the coming section. Therefore, the constants in the terms for WOB and RPM in the denominator of eqn. (4.1i) can be removed without influencing the result. In the WOB-term, this means the value 4 is removed, which is a conversion constant. However, also the bit diameter, d_{bit}, can be removed from this term, as the bit diameter will be constant throughout the interval being used for computations. For the RPM-term, the conversion constant 60 is removed.

Thus, the final term for drillability, K, and which is used during the calculation process, is:

$$K = \frac{ROP}{WOB^{a_5} RPM^{a_6}}$$

(4.1ii)

During the calculation process, the agent will first calculate drillability according to eqn. (4.1ii). Finally, its inverse, the formation hardness, H can be found according to the simple relation between drillability and hardness:

$$H = \frac{1}{K} \tag{4.2}$$

b) Determining relevant coefficients

Ideally, in the original Bourgoyne-Young drilling equation, the coefficients a_1-a_8 should be chosen based on local drilling conditions. This means selecting the best average values for a_1-a_8 representing the formation type at the depth interval of interest. Frequent changes in lithology with depth can make it difficult to evaluate the correct values. The process of how to determine these coefficients will have great impact on the accuracy of the model.

Bourgoyne and Young (1974) suggested applying a multiple regression analysis to determine the coefficients. This technique requires prior drilling data obtained in the area. The exponential expression for f_1, the drillability, also must be known. Furthermore, this method does not guarantee reaching physical meaningful results and is limited to the number of data points (Bahari, Bahari, Moharrami and Sistani, 2008). Bahari and Baradaran (2007) applied non-linear least square data fitting with trust-region method to solve this problem. This method is one of the optimization algorithms which minimize the sum of square errors function. However, computed coefficients using this scheme did not result in sufficiently accurate models in practice (Bahari, Bahari, Moharrami and Sistani, 2008).

Bahari, Bahari, Moharrami and Sistani (2008), applied a Genetic Algorithm (GA) to determine the coefficients of the Bourgoyne-Young model. GA is a method able to handle linear constraints and bounds, not limited to number of data points and is considered more accurate in comparison with the multiple regression technique and the trust-region method. Testing was performed on sensory drilling data of nine different wells in the Khangiran Iranian gas field. The researchers concluded that: "Simulation results confirm that suggested approach not only provides meaningful results but also leads to more accuracy in comparison with conventional methods."

While it generally requires historical drilling data and complex calculations to reach accurate results for determining a_1-a_8, the values of a_5 and a_6 can be decided by a simpler approach. This is done analyzing data from drilloff tests. Unfortunately, data from such tests are not available in this case, so average values of coefficients must be chosen based either on an example from a previously drilled well or from a range of values. An example from a previously drilled well is given in Table 4.1, which shows average values for a_2-a_8 in a shale formation drilled in the U.S. Gulf of Mexico:

Regression Coefficient	Average value
a_2	0,000090
a_3	0,000100
a_4	0,000035
a_5	0,9
a_6	0,5
a_7	0,3
a_8	0,4

Table 4.1: Average values of regression coefficients of Bourgoyne-Young drilling model for shale formation drilled in the U.S. Gulf of Mexico (Bourgoyne et al., 1986).

Though not an optimal approach, average values can be taken from this formation, where the value for a_5 is 0.9, and the value for a_6 is 0.5. However, reported values of a_5 range from 0.5 to 2.0, and reported values of a_6 range from 0.4 to 1.0 (Bourgoyne et al. 1986). For these ranges, lower values (a_5 = 0.5, a_6 = 0.4) represent extremely hard formation exponents, while higher values (a_5 = 2.0, a_6= 1.0) represent extremely soft formations exponents. Because formations in the range of the extremities are less common, a better solution and the one which has been preferred in the agent when calculating drillability, is to operate with three different sets of a_5 and a_6. The first and initial selection of values will be based on the average of the extreme of the ranges, thus:

$$a_{5-avg} = \frac{(a_{5-hard}+a_{5-soft})}{2} = \frac{(0.5+2.0)}{2} = 1.25 \tag{4.3}$$

$$a_{6-avg} = \frac{(a_{6-hard}+a_{6-soft})}{2} = \frac{(0.4+1.0)}{2} = 0.70 \tag{4.4}$$

These exponents will be used to acquire the first set of results and gain some knowledge about the formation type. Then, the idea is to refine the calculation and see if more distinct differences in hardness are detectable if perhaps one is using sets of exponents that are suited to the specific formation. These exponents can be classified as either moderately hard formation exponents or moderately soft formation exponents. First, however, from the initial drillability results, the plan is to normalize hardness in the range from 0 to 1 by dividing all hardness values throughout the well section by the largest one in the section. This hardness classification will help to classify the formations with respect to hardness and help decide which set of formation coefficients to use in each case. E.g. if the hardness classification becomes more than 0.5, this will mean we are dealing with a hard formation. As such, the agent will be programmed to select coefficient for a_5 and a_6 suitable for moderately hard formations. If the hardness classification is less than 0.5, the story will

be vice versa, now the agent will pick coefficients suitable for a moderately soft formation. The set of a_5 and a_6 values for expected moderately hard formations are:

$$a_{5-mod\_hard} = \frac{(a_{5-hard}+a_{5-avg})}{2} = \frac{(0.5+1.25)}{2} = 0.875 \quad\quad (4.5)$$

$$a_{6-mod\_hard} = \frac{(a_{6-hard}+a_{6-avg})}{2} = \frac{(0.4+0.7)}{2} = 0.55 \quad\quad (4.6)$$

and the set for what is expected to be moderately soft formations are:

$$a_{5-mod\_soft} = \frac{(a_{5-soft}+a_{5-avg})}{2} = \frac{(2.0+1.25)}{2} = 1.625 \qu\quad (4.7)$$

$$a_{6-mod\_soft} = \frac{(a_{6-soft}+a_{6-avg})}{2} = \frac{(1.0+0.7)}{2} = 0.85 \quad\quad (4.8)$$

Having decided the formation exponents a_5 and a_6, along with the values for WOB, RPM and dBPOS, everything is in place to calculate drillability or hardness according to equations (4.1ii) and (4.2).

4.1.5 Plotting

The last task for the agent is to plot the resulting normalized hardness graphs vs. depth (TVD or MD). This compares the different hardness values along the selected well section with each other (or with other added parameters), so changes in hardness can be detected.

4.2 Agent for pore pressure

The derivation of the model for pore pressure is quite similar to that of the derivation for drillability/hardness and many of the same principles apply. However, more accuracy is required for the pore pressure model. The hardness model is mostly used for detecting changes in hardness and studying its effect on penetration rate, such that only the most relevant parameters influencing immediate changes in ROP are utilized. However, the pore pressure model needs to quantify the pore pressure accurately, so it is advantageous to include more functions from the Bourgoyne-Young equation in this model.

The functions f_7 and $f_{8,}$ which models the effects of tooth wear and bit hydraulics on ROP, must also be discarded from the pore pressure equation because of the mentioned lack of data on the

parameters fractional tooth dullness, h, and hydraulic impact force beneath the bit, F_j. On the other hand, the constants involved in the functions could be imported from other, similar wells. Then we need to first evaluate typical variation in said constants. Such evaluation we leave for the follow-up version of present work.

The WOB and RPM-functions, f_5 and f_6, must be included in the equation of the pore pressure. As discussed earlier, these are drilling technique parameters considered important for sudden changes in penetration rate. The term $\left(\frac{WOB}{d_{bit}}\right)_t$ in the WOB-function, the threshold bit weight factor, is still, as in the derivation of the drillability, given a value of zero.

f_2, modeling the effect of normal compaction with depth, should now be included. This factor accounts for the normal decrease in penetration rate with depth from a reference depth of 10,000 feet:

$$f_2 = e^{2.303a_2(10,000-D)} \tag{2.1b}$$

However, it must be modified from its original form in the Bourgoyne-Young equation. The reference depth of 10,000 feet, needs to be altered such that is compatible with a depth where a normal formation pore pressure is found in the test well used in the analysis. A more typical depth for this to occur is 5,000 feet. Ideally the reference depth, D_{ref}, needs to be located at a depth slightly above the transition zone where the pore pressure starts increasing to abnormal values. The method for finding where the pore pressure starts departing from the normal trendline will be explained later. The modified f_2, f_{2-mod}, can now be written as:

$$f_{2-mod} = e^{2.303a_2(D_{ref}-D)} \tag{4.9}$$

Pore pressure, or ρ_{pore}, is included for in the ROP-equation through the factors f_3 and f_4. f_3 models the effect of under-compaction in abnormally pressured formations on ROP while f_4 models the effect of overbalance on ROP:

$$f_3 = e^{2.303a_3D^{0.69}(p_{pore}-9.0)} \tag{2.10c}$$

$$f_4 = e^{2.303a_4D(p_{pore}-\rho_{ecd})} \tag{2.10d}$$

In theory, for computing pore pressure, it is possible to insert one of these or both equations into the Bourgoyne-Young equation and solve for ρ_{pore}. As previously discussed, the effect of overbalance, represented through equivalent densities by ($\rho_{pore} - \rho_{ecd}$) in f_4, is much more important for immediate changes in ROP than the effect of under-compaction in abnormally pressured formations, represented through f_3. To compute pore pressure this can lead to the conclusion that only f_4 is needed. However, to obtain accurate results, both factors should be included for.

The original f_3 equation needs to be modified as the value 9.0 represents a normal pore pressure gradient of 9.0 lbm/gal. This is a common value for the normal pore pressure gradient in the U.S. Gulf of Mexico. For the test well, located in the North Sea, a frequently used value is 8.71 lbm/gal (1.044 g/cm^3). However, for now, the normal pore pressure gradient will be denoted as ρ_{normal}, such that the modified f_3 takes the form:

$$f_{3-mod} = e^{2.303 a_3 D^{0.69}(p_{pore} - p_{normal})} \tag{4.10}$$

It should be noted that as precise values for the formation exponents a_2, a_3 and a_4 cannot be acquired because of lack of data from the test well, uncertainties are linked with these variables. These data will instead be based on average values from shale formations drilled in the U.S. Gulf of Mexico area. However, pore pressure calculations must be made before evaluating the effect of these variables. The coefficient values used are those which were listed in Table 4.1.

After the discussed modifications, the Bourgoyne-Young drilling model used for calculating pore pressure is:

$$ROP = (f_1)(f_{2-mod})(f_{3-mod})(f_4)(f_5)(f_6)$$

$$ROP =$$

$$e^{2.303 a_1} e^{2.303 a_2 (D_{ref} - D)} e^{2.303 a_3 D^{0.69}(p_{pore} - p_{normal})} e^{2.303 a_4 D(p_{pore} - \rho_{ecd})} \left(\frac{WOB}{4 d_{bit}}\right)^{a_5} \left(\frac{RPM}{60}\right)^{a_6} \tag{4.11}$$

Solving eqn. (4.11) for ρ_{pore} gives:

$$p_{pore} = \frac{\log\left(\frac{ROP}{\left(\frac{WOB}{4d_{bit}}\right)^{a_5}\left(\frac{RPM}{60}\right)^{a_6}}\right) - a_1 - a_2(D_{ref} - D) + a_3 D^{0.69} p_{normal} + a_4 D \rho_{ecd}}{a_3 D^{0.69} + a_4 D} \tag{4.12}$$

What is interesting to note from the expression for pore pressure is that the term $\dfrac{ROP}{\left(\frac{WOB}{4d_{bit}}\right)^{a_5}\left(\frac{RPM}{60}\right)^{a_6}}$,

defined as the simplified drillability K in the previous section, is represented here inside a common logarithm term. The a_1 coefficient from the original or real drillability definition of $f_1 = e^{2.303a_1}$ is also represented in the pore pressure equation. a_1 is found at the reference depth D_{ref}, and thus represents a normally compacted formation with a normal pore pressure gradient. Equation (4.12) shows that the pore pressure is highly connected with both the simplified and the original definition of drillability.

It may be difficult to distinguish between the two effects of drillability and pore pressure on penetration rate because of this correlation between the two factors. However, testing of the individual models should first be done.

5 Results from testing of Models

5.1 Results from hardness model

In this section, the results from the qualitative method and quantitative methods for hardness and drillability detection will be presented and analysed. The discussion and conclusion will be based on the results in this section. Before starting on the results, there will be given a short explanation of what and how the available data were used in both the descriptive method and by the agent during calculations.

5.1.1 Available data used in analysis

As mentioned, and shown examples from above, a final well report for Well 34/10-C-47 were among the available data delivered by Statoil. If inspecting this report, an approximate time and depth interval for where hard stringers were hit can be found. From Appendix 2.1, page 45, the following excerpt is copied (report date 23.12.2005): "Drilled 17 ½" hole from 1515.5 m to 1593 m. Several hard stringers from 1556 m to 1587 m." (Christophersen, Gjerde and Valdem, 2007). Thus, an area for which to focus on and for which can be used to test the quality of both models is pointed out by the report.

From the log interpretation example and the simplified Bourgoyne-Young drilling model in chapter 4, given by Figure 4.1 and eqn. (4.1) respectively, it becomes clear what of the available RTDD are required in the analysis. Block positioning (BPOS), weight on bit (WOB) and bit rotations (RPMB) have been applied in both methods. ROP was originally needed in the Bourgoyne-Young drilling model, but the issues with the ROP recordings, which were discussed in section 3.4, means that ROP has instead been calculated from the derivative of BPOS. The velocity of the block is a valid method for representing penetration rate, as the velocity decreases when encountering harder formations and increases when encountering softer formations. From the block movement, one can also get information about what part of the drilling operation is being performed. For example, when the block positioning is increasing, it indicates the block is being pulled up to make new connections. A constant block position for a longer period of time, might be due to performing a connection. Examples comparing the derivative of BPOS with ROP and how to derive penetration rate from the derivative of BPOS will be presented in the coming sections.

Depth and time data are needed for correlating with the more specific drilling parameters such as BPOS, WOB and RPMB. True vertical depth (here abbreviated DVER), which is the vertical distance from the surface to the bottom of the hole, is not needed for any specific calculations besides for

graphical presentations. Measured depth (here abbreviated DMEA), which is the actual borehole and its length, represents the deepest position of the open hole at all time. Bit depth (DBTM), is the measured depth at where the bit appears inside the well. Measured depth (DMEA) and bit depth (DBTM), will be equal when there is an ongoing drilling operation, as the bit is located at the hole bottom. This fact is exploited in the script to sort and remove data at times when there is no drilling occurring, as these periods are of no interest during drillability calculations.

Lastly, as discussed in section 4.1.4.1, the RTDD is stored with time as the indexing variable. Every data point in each different array corresponds to the same time, with a time difference between each recording of 5 seconds. As the derivative of BPOS is dependent on time, calculations in the script on BPOS has been done with original time data rather than with modified time data. This is to ensure that rate of penetration calculations will be as exact as possible, so to not affect the final drillability result. Otherwise, sorting and removal processes of data in the script due to times of non-drilling, odd values of BPOS, WOB and RPMB, and averaging of data points for better plot readability, can reduce the numbers of time-data to such an extent that accurate rate of penetration data is hard to obtain.

5.1.2 Qualitative method: Detection of hard stringers by log interpretation

As discussed in section 4.1.1, hard stringers are indicated through a reduction in BPOS speed and RPM, with fairly constant or high WOB. This can be observed several places in the drilling section shown below in Figure 5.1.
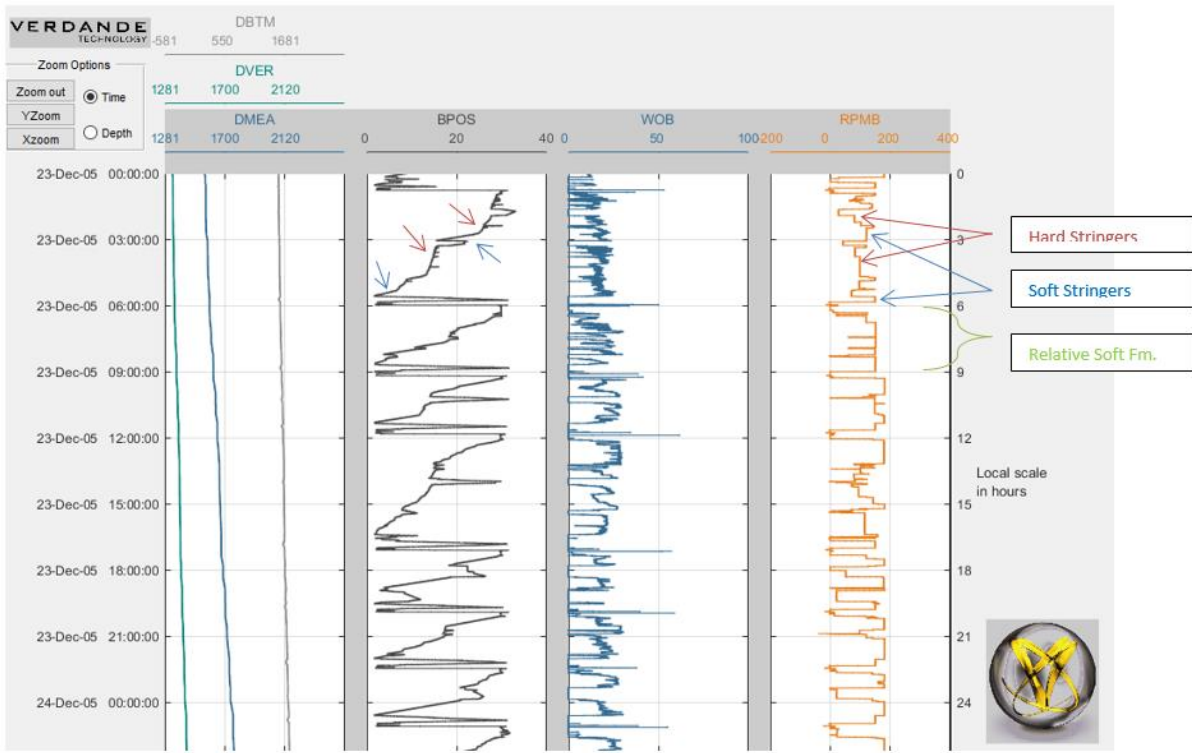
Figure 5.1: RTDD from Well C-47 bit section 17 ½'' dated 23 December 2005. DBTM, DVER and DMEA are drilling depth data measured vs. time. BPOS, WOB and RPM are also plotted vs. time in different real-time drilling windows. In the uppermost well section, hard stringers were found several places (red arrows), most easily observed by the low RPM and BPOS speed. Some soft stringers are also highlighted (blue arrows), indicated by high RPM and BPOS speed. Marked below the upper well section, is a section which was drilled relatively easily, indicating a soft formation.

It can be observed from Figure 5.2 that during these 24 hours of drilling the block was lowered seven times, which means seven stands were completed. Each stand is 27 meters, so a total of 27 times 7, equaling 189 meters of hole were drilled. However, as can be seen by the difference in block speed, not every section is drilled at the same rate. Section 1 and 4 was notably more time-consuming than the other sections. These lower average penetration rates are most likely attributed to the occurrence of harder formation types. Hard stringers have already been identified in section 1, and the same types of characteristics seem to indicate there are hard stringers in section 4. In both sections, there are no long or continuous distances being drilled with low RPM and BPOS speed. This could have indicated a more permanent shift in formation type from soft to hard. Instead there only seems to be anomalies of harder rocks in softer formations, again supporting the notion that hard stringers exist in both section 1 and 4.
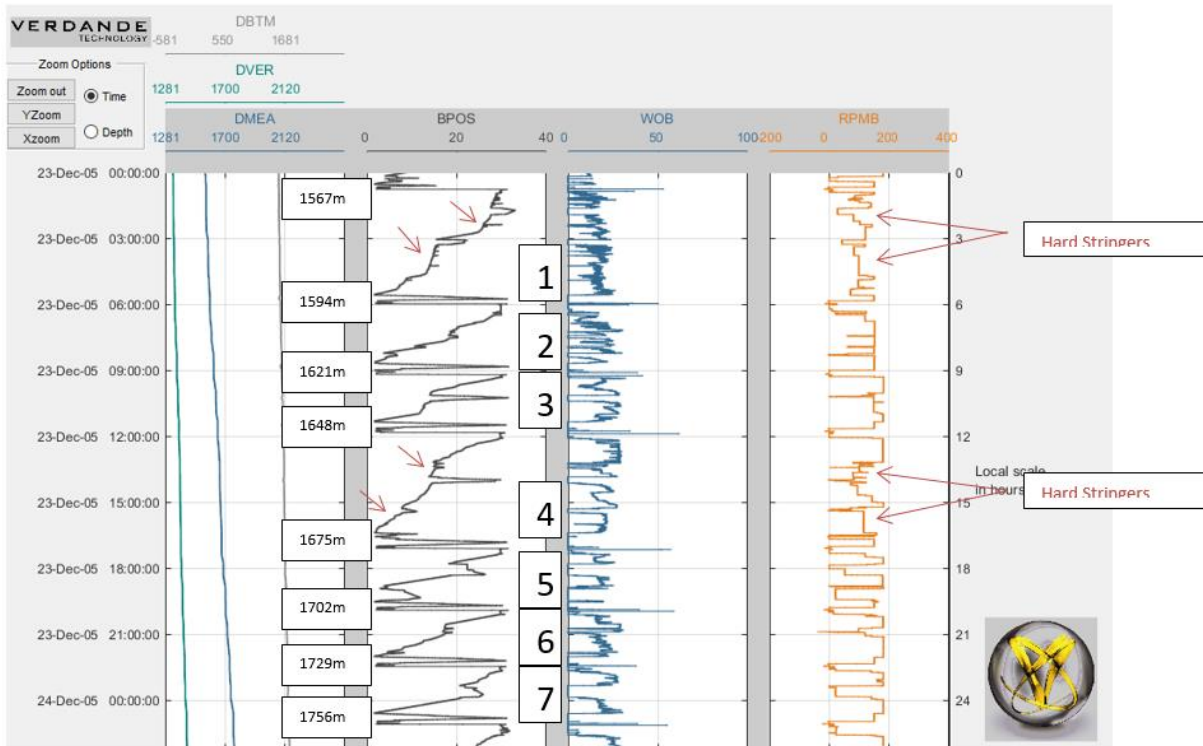
Figure 5.2: RTDD from Well C-47 bit section 17 ½'' dated 23 December 2005. DBTM, DVER and DMEA are drilling depth data measured vs. time. BPOS, WOB and RPM are also plotted vs. time in different real-time drilling windows. During this day, 7 sections or stands were drilled, totaling 189 meters. BPOS speed indicates that section 1 and 4 were drilled at a lower rate compared to the others. This can be caused by the occurrence of hard stringers (red arrows) within softer formations.

However there seem to be some differences between the two drilling situations taking place in section 1 and 4. If examining the RPMB of both sections, the highest average bit rotations seems to be overall lower in section 1 compared to section 4. In fact, after completing stand number 2, there is a small increase in the highest average RPMB ratings. This seems to indicate a change in formation type from what can be described as a medium soft to a soft formation. Comparing the BPOS speed of section 2 to that of section 3, 5, 6 and 7, the BPOS speed of section 2 is slightly lower than the others, which support this theory. This is shown in figure 5.3, where RPMB-baselines are drawn for a medium soft formation in section 1 and 2, and for a soft formation in section 3,4,5,6 and 7. Figure 5.3 also show a suggested hardness-classification for the type of stringers found in section 1 and 4. In section 1 there are one hard and one medium hard formation, while in section 4 there are one medium hard and one slightly hard formation.

Figure 5.3: RTDD from Well C-47 bit section 17 ½'' dated 23 December 2005. DBTM, DVER and DMEA are drilling depth data measured vs. time. BPOS, WOB and RPM are also plotted vs. time in different real-time drilling windows. Green stapled lines indicate RPMB baselines for a soft (dark green) and medium soft (light green) formation. Red right triangles (showing BPOS speed by their inclination/steepness) and red arrows (showing corresponding RPMB) indicate where hard stringers are located. Bright red marks a stringer for a hard formation (section 1 only), dark red marks stringers for a medium hard formation (section 1 and 4) while pink marks stringers for a slightly hard formation (section 4 only).

ROP-data is provided in the RTDD from Statoil. However, an alternative method to calculate penetration rate is used, which also can verify if the provided ROP-data is acceptable. As seen by the inclination or steepness of the right triangles in figure 5.3, the positioning and speed of the block is an important variable for determining penetration rate. The block positioning can be differentiated with respect to time (ΔBPOS/ΔT) to estimate rate of penetration. Figure 5.4 shows the original ROP-data plotted versus the calculated derivative, dBPOS, for the relevant sections containing hard stringers, section 1 (1565-1590 m) and 4 (1645-1680 m).
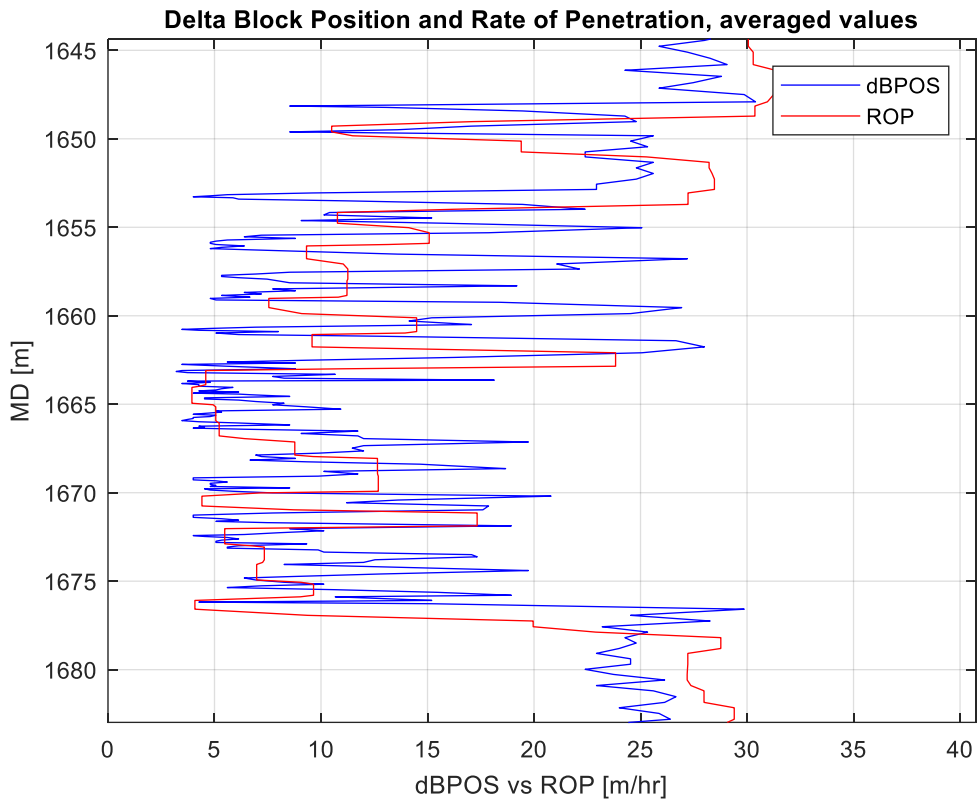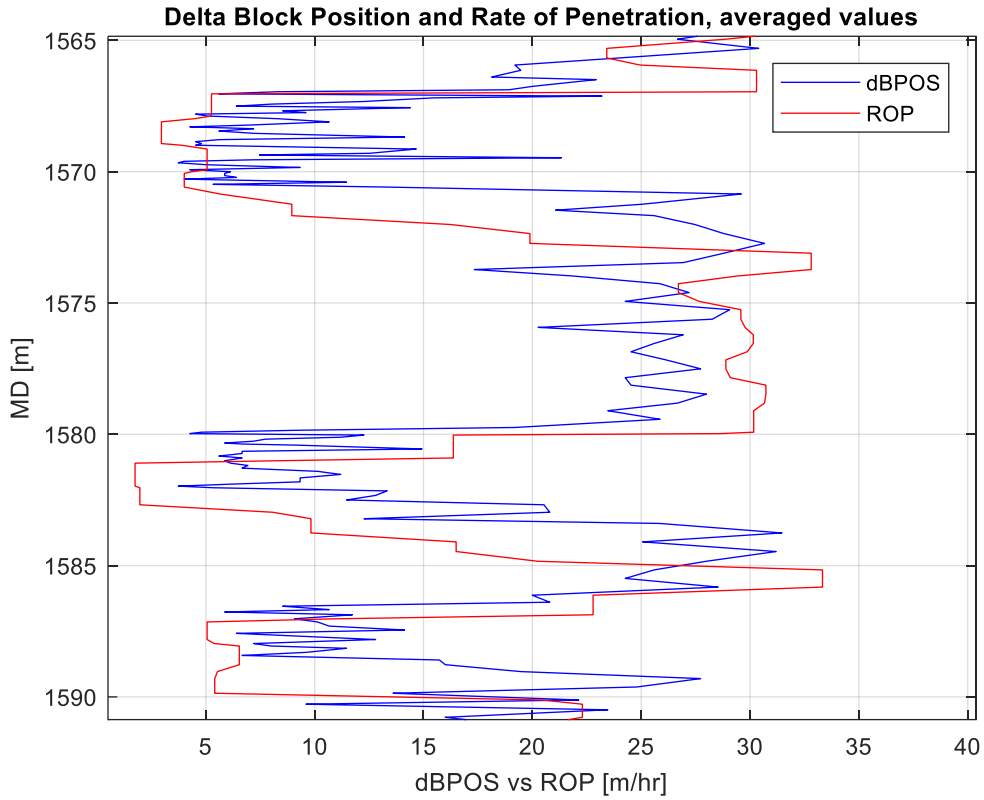
Figure 5.4: Calculated dBPOS values plotted vs. ROP for the sections 1 (upper image, 1565-1590 m) and 4 (lower image, 1645-1680m) in Well C-47 bit section 17 ½'' dated 23 December 2005.

From the figures, it is clear that the dBPOS follows the same trend as the ROP. The graph for the ROP is notably smoother than the graph for dBPOS, which is because a 3-point average for the ROP-data has been taken twice, compared to only once for the dBPOS. However, for further drillability calculations, dBPOS has been chosen as the preferred parameter. This is because the hardness or drillability of the formations will have better correspondence with the correct depth by using dBPOS. The original ROP-data delivered will estimate the hard formations deeper than where they actually are positioned.

5.1.3 Quantitative method: Computing drillability with help of agent

This section will present the result from the drillability agent performed on the 17 ½" section of Well 34/10-C-47. First there will be a section explaining how the program works, also illustrated graphically by means of a flowchart. Then, the following section will present the actual outcome from the program. The quantitative results will mostly be described through the use of hardness and drillability-plots, so the reader can gain a good understanding of the material.

5.1.3.1 The program for Bourgoyne-Young drilling model

This program will calculate drillability from RTDD using the simplified Bourgoyne-Young drilling equation derived in section 4.1.4.3.a (eqn. 4.1ii). An overview of the commands used, and the overall "flow" of the program are shown in the flowchart in Figure 5.5. Primarily the script consists of executing functions. The Matlab codes are attached in Appendix B.
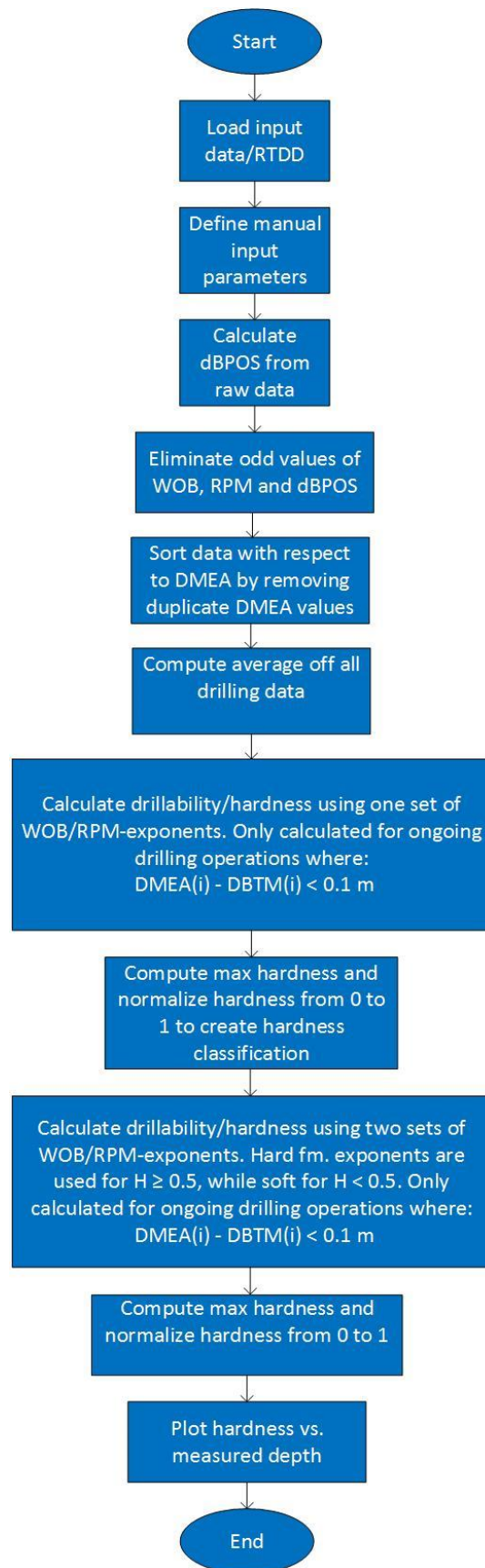
Figure 5.5: Sketched flowchart for the Bourgoyne-Young method, indicating the commands and flow of data. The output is hardness and hardness plotted vs. measured depth.

The script is started by loading the correct folder for the data gathering and loads the real-time drilling data of the correct interval into Matlab (17 ½" section). After this, parameters being constant throughout the agent are defined, such as the drill bit being 17 ½", gravity being 9.81 m/s², and the average a_5-a_6 exponents being 1.25 and 0.70 (eqn. 4.3-4.4). The a_5 and a_6 exponents for moderately hard ($a_{5\_mod\_hard}$ = 0.875, $a_{6\_mod\_hard}$ = 0.55) and moderately soft formations ($a_{5\_mod\_soft}$ = 1.626, $a_{6\_mod\_soft}$ = 0.85), given by equations 4.5-4.8, are also defined here. Whether moderately hard or moderately soft exponents are chosen in the calculations, are however up to the hardness classification made after the initial drillability results using only one exponent. This hardness classification will be decided later in the script.

The eight relevant drilling parameters being described in section 5.1.1, are then loaded into the script. Again, these are vertical depth (DVER), measured depth (DMEA), drill bit depth (DBTM), time, block position (BPOS), penetration rate (ROP), bit rotations per minute (RPMB) and weight on bit (WOB). As mentioned, ROP is not preferred as the variable for penetration rate and is replaced by the derivate of block positioning (dBPOS) during the main programming. However, ROP is used during plotting and comparisons of ROP with dBPOS, so it will be loaded into the agent for those reasons. The next step in the program is to compute the dBPOS.

The first step in doing so is defining the position of a point BPOS$_{average}$(j), which is the average of the computations of the block position of three points:

$$BPOS_{average}(j) = \frac{BPOS(i) + BPOS(i+1) + BPOS(i+2)}{3} \tag{5.1}$$

This procedure must also be done with the other seven relevant drilling parameters as these need to correspond to the new average BPOS values. The time increment between each data point is now increased to 15 seconds from the original 5 seconds. Performing these average readings reduce the amount of data between each recording, which also reduces the total amount of work done by the agent.

The speed of the block, dBPOS, which should be equal to the drilling rate, can now be calculated. This is done by calculating the slope of two block positions from the previous step:

$$dBPOS(k) = \frac{BPOS_{average}(j-1) + BPOS_{average}(j)}{15} * 3600 \tag{5.2}$$

The equation is multiplied by 3600 to convert the units for dBPOS from m/s to m/h, which are the units used for ROP, as was seen earlier in the plot comparing dBPOS with ROP (Figure 5.4).

The next step is to eliminate odd values of dBPOS, WOB and RPMB. The block velocity is set to range between 2.5 and 40 m/h, so values outside this range is eliminated. The bit weight is set to remove values less than 2.5 tonnes. Finally bit rotations per minute is set to rotate at least 25 rpm, so all values less than this are not being considered during calculations.

To make sure computations are only made when there is an active drilling operation, data are sorted with respect to measured depth. This can be done in two ways. The first is the one mentioned earlier, which is to check that the bit depth DBTM matches or is very close to the measured hole depth DMEA before starting to sort data. The specified distance between these two parameters can be set to be no less than for example 0.1 meters, as shown in eqn. (5.3):

$$DMEA(i) - DBTM(i) \leq 0.1 \, m \tag{5.3}$$

Only entities when this condition is fulfilled is then saved for further use. The problem with this method, is that it will not work properly for sorting in datasets containing duplicate DMEA-values. When there is more than one value for DMEA (a specific measured depth value occurring twice or more) in the set, the DMEA-value can be linked with multiple entities and values for DBTM. This situation was problematic in the dataset for the 17 ½'' section, as the measured depth values, after first increasing normally with depth, suddenly reversed and started decreasing to lower depth values again. This caused the occurrence of duplicate DMEA-values in the data set. The reason for this discrepancy remains unclear and is here considered as anomalies. According to the FWR, there are no undesirable circumstances reported during drilling of the interval, such as side-tracking, which could explain the condition.

Instead, to solve the issues with the duplicate DMEA-values, it has been opted for an alternative method for sorting and filtering out non-relevant drilling data. This is done by using a continuous loop that is only storing the data in the next step if it contains drilling data correlated to the deepest depth in the hole (highest DMEA-value), meaning the depth value of the current step must be of a larger value than that of the previous step. Done in this way, there is no real reason to check the conditions of eqn. (5.3), because it is given that measured well depth, which represents the deepest position of the open hole at all time, can only increase by the means of performing a drilling operation drilling an even deeper wellbore. Credit should be given to (assistant supervisor) Isak Swahn, for help solving the programming required in this alternative method.

However, eqn. (5.3) is still used in the script as an extra safety measure, not to sort data with respect to measured depth, but rather for verifying that there is an active drilling process. The conditions of eqn. (5.3) will be checked by an if-function in the script just before computations on drillability is

commenced by eqn. (4.1ii). This means that the drillability calculations by the Bourgoyne-Young formulas will only be executed if eqn. (5.3) is fulfilled.

The next step in the agent will be to perform another averaging of data. Further reduction of data size will lessen the number of calculations for the agent, as well as it helps for plotting reasons. The averaging is done in exactly the same way as during the method of eqn. (5.1). Having now performed an averaging of the initial data twice, this means the time-increment between data readings have increased from the original 5 seconds, to (5x3 =) 15 seconds in the first averaging-step, to (15x3=) 45 seconds in this step.

Now everything is set up to start implementing the formulas of the simplified Bourgoyne-Young drilling model. The next function will first calculate drillability using one a_5 and one a_6 exponent (the average exponents, 1.25 and 0.70, respectively) and then find maximum drillability along the complete well section. The maximum drillability is essential to be able to normalize and define the drillability values in different formation types and sets up the foundation for the hardness classification system proposed in this method. The normalized drillability is then computed in the next function by the following equation:

$$Normalized\ Drillability(i) = \frac{Drillability(i)}{Max\ Drillability} \tag{5.4}$$

This calculation makes the drillability range from 0 to 1. If the drillability < 0.5, it is assumed that the drillability is calculated in a hard formation. However, in this thesis, is has been decided to base the classification system around the inverse of drillability, namely formation hardness. Hardness can be obtained straight after calculating drillability, by applying the simple relation:

$$Formation\ Hardness\ (i) = \frac{1}{Drillability\ (i)} = \frac{1}{K} \tag{5.5}$$

Maximum hardness is found by applying the built-in max-function in Matlab on eqn. (5.5), while normalized hardness is obtained by using hardness instead of drillability in eqn. (5.4). Now, having obtained normalized hardness, the classification is such that if hardness > 0.5, it is assumed to be a hard formation type, while hardness ≤ 0.5, represents a soft formation. The normalization process performed in this step now makes it possible to apply more than one exponent for WOB (a_5) and RPM (a_6).

The next function will calculate drillability using two types of a_5 and a_6 exponents. If drillability < 0.5 (corresponding to hardness > 0.5), moderately hard formation exponents will be used; a_5 will be set to $a_{5\_mod\_hard}$ = 0.875, and a_6 will be set to $a_{6\_mod\_hard}$ = 0.55, before starting on the calculations. On the

other hand, if drillability ≥ 0.5 (corresponding to hardness ≤ 0.5) moderately soft formation exponents are chosen; a_5 will be set to $a_{5\_mod\_soft} = 1.625$, and a_6 set to $a_{6\_mod\_soft} = 0.85$. The calculation of maximum drillability/hardness and the normalization process done in the previous step is then repeated, only now hardness is normalized having used two sets of drilling exponents.

5.1.3.2 Hardness results

This section will test the program for the simplified Bourgoyne-Young drilling model presented in the previous section. As mentioned, the program is tested on drilling data from the 17 ½" interval of Well 34/10-C-47. More specifically, it is the interval drilled on 23 December 2005, between approximately 1567 and 1756 m MD, which has been chosen for further inspection. Here, two sub-intervals between 1567 to 1594 m MD and 1648 to 1675 m MD are especially interesting. This is the portion of the well where hard stringers were reported in the FWR, and the two intervals highlighted are those who were examined by log interpretation in section 5.1.2. From now on, the uppermost interval 1567-1594 m MD will be referred to as Section 1, while the deeper interval 1648-1675 m MD will be referred to as Section 4. This labelling is based on the intervals respective position among the total number of stands drilled during this day (7 in total), as seen in Figure 5.2 in section 5.1.2.

For the hardness detection to be as accurate as possible, it is important to follow the steps explained in the previous section. This includes calculating and using dBPOS as a parameter for penetration rate, eliminating odd values of BPOS, WOB and RPMB, only computing drillability during an active drilling operation, using 3-point averaging of data, normalizing drillability/hardness, and applying two sets of exponents for the final hardness computation.

Figure 5.6 shows calculated hardness from the relevant interval 1567-1756 m MD, using the non-modified or "raw" data delivered from Statoil.
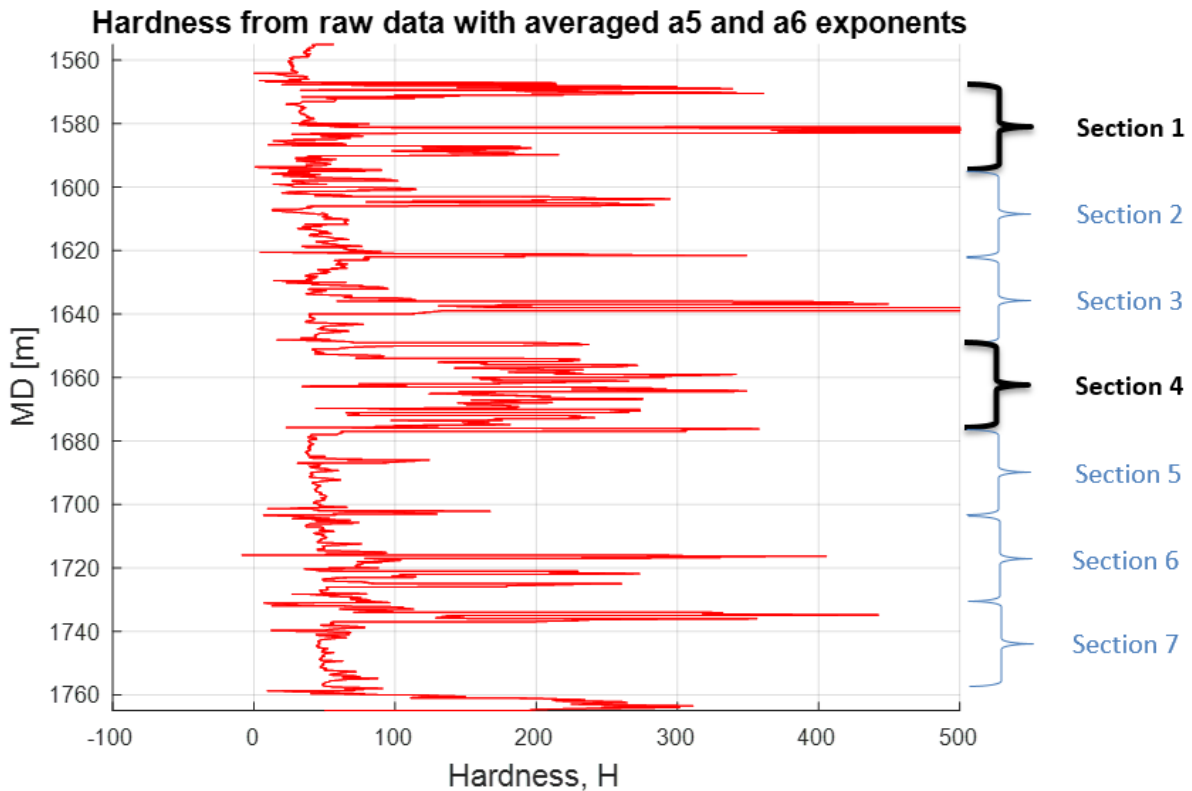
Figure 5.6: Calculated hardness, H, plotted vs. measured depth, MD, from raw RTDD in Well C-47, bit section 17 ½'', interval 1560-1760 meters, dated 23 December 2005. No filtering is done, so spikes of "negative" and "positive" hardness values are noticeable. To give as "raw" image as possible, ROP is used instead of dBPOS as the parameter for penetration rate.

Looking more closely at Figure 5.6, some specific trends can be seen in both Section 1 (1567-1594 m MD) and Section 4 (1648-1675 m MD). It is clear that Section 1 contains two very large "positive" spikes in Hardness, while Section 4 has spikes with smaller values, yet seem to have average hardness values generally higher than that of Section 1 (and the rest of the interval). These trends might indicate that hard stringers are situated in between a softer formation type in Section 1, causing the large and sudden spikes in hardness. For Section 4, there seem to be a more of a shift to generally higher hardness values from the section's situated above, perhaps indicating a shift in formation type from a soft to harder formation. However, observations during the log interpretation examining correlations between BPOS, WOB and RPMB in section 5.1.2, suggested the presence of hard stringers also in Section 4. Thus, it should be further explored whether it is hard stringers or a general shit to higher average hardness values which are causing the hardness trends in Section 4.

Still, remember this is just early signs taken from raw data. Forthcoming modifications in the agent will alter the initial image given from Figure 5.6. Incorporating dBPOS instead of ROP in the calculations, elimination of odd values and sorting of values should for instance significantly improve

the readability of the plot. These are the stepwise adjustments made to enhance the hardness result and which are illustrated further in this section:

1. Replacing ROP with dBPOS and eliminating odd values of dBPOS, WOB and RPMB
2. Sorting data with respect to measured depth by removing duplicate DMEA values (includes checking for active drilling operation) and computing 3-point average
3. Normalizing hardness to make hardness range from 0 to 1
4. Introducing hardness classification using two sets of exponents for both WOB and RPMB exponents
5. Varying the exponent values; using moderate versus extreme values
6. Changing definition of hardness in hard formations

Step 1 introduces dBPOS as the parameter for penetration rate instead of ROP and removes abnormally high and low values of dBPOS, WOB and RPMB. The results of these modifications are shown in Figure 5.7. The top image still represents raw data as in Figure 5.6, however dBPOS has now replaced ROP in the computations. The lower image represents modified data, after the removal of unrealistic values of the drilling parameters dBPOS, WOB and RPMB.
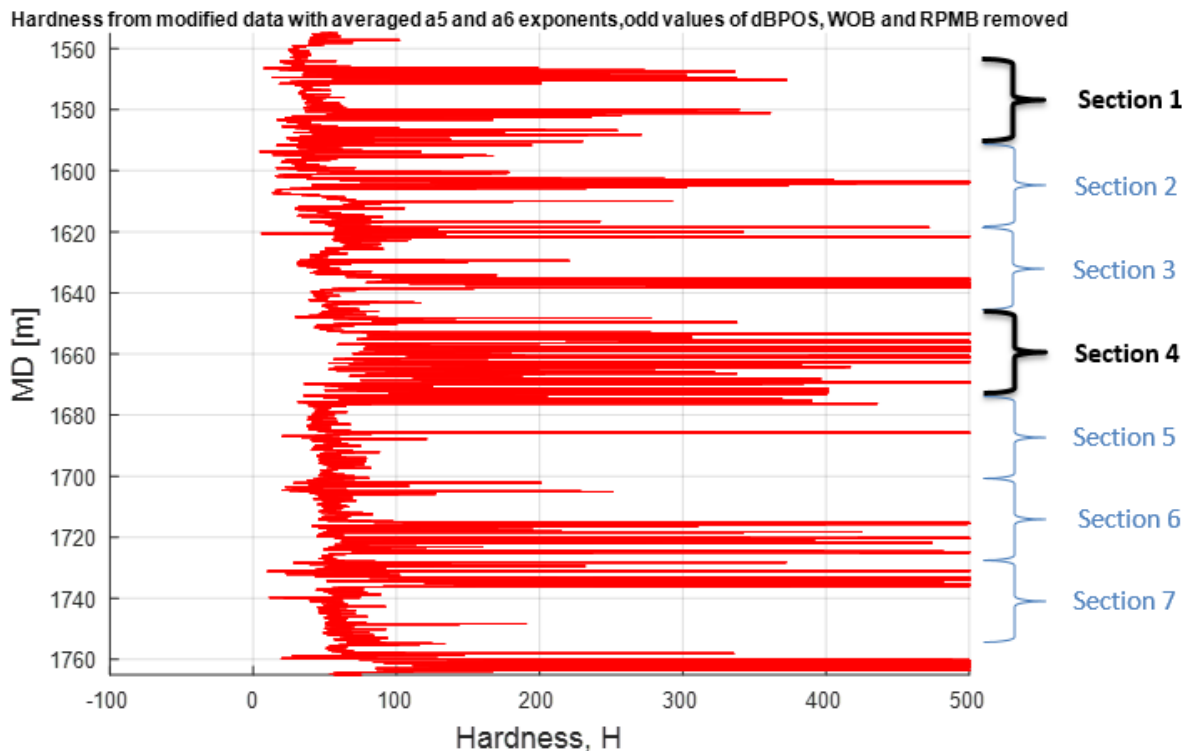

Hardness from raw data with averaged a5 and a6 exponents, dBPOS introduced
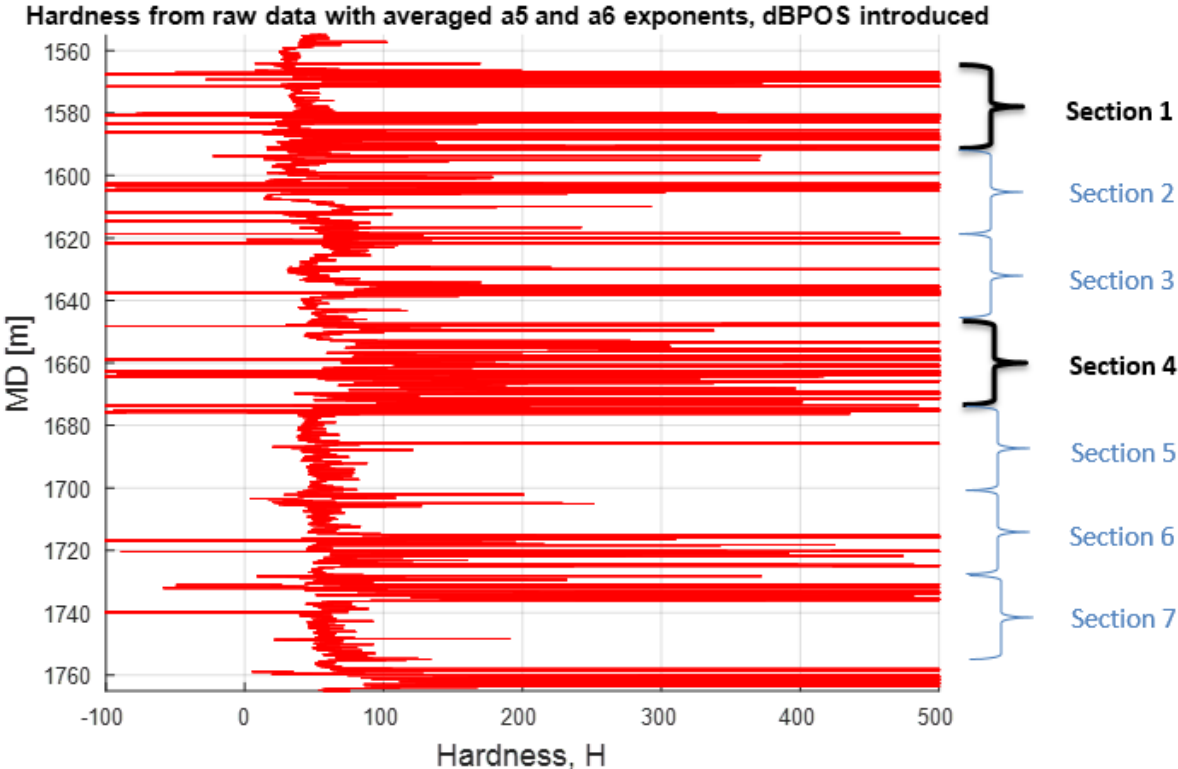
Figure 5.7: Calculated hardness, H, plotted vs. measured depth, MD, from RTDD in Well C-47, bit section 17 ½'', interval 1560-1760 meters, dated 23 December 2005. The difference between the upper and lower image is that the upper image still contains "raw" data, as dBPOS only has replaced ROP in the hardness calculations. In the lower image, the RTDD has been modified, as abnormal values of dBPOS, WOB and RPMB have been removed.

Notice that more "negative" spikes of hardness appear in the top image of Figure 5.7 compared to in Figure 5.6. This is caused by abnormal BPOS and dBPOS values within the RTDD which have affected the calculation of hardness when dBPOS is used instead of ROP. In the lower image, there are no negative spikes or negative values of hardness whatsoever. This is a result of the elimination of odd values for dBPOS, but also WOB and RPMB. There are also fewer "positive" spikes of hardness, and with the same spikes having lesser values, then in the lower compared to the upper image. The lower image still remains somewhat unclear and should be refined in the next step. However, with dBPOS replacing ROP, the hardness is now computed at the correct depth position, as was discussed in section 5.1.2.

In step 2, data will be sorted with respect to measured depth by removing duplicate DMEA-values, which ensures that hardness calculations are only done when there is an ongoing drilling process. Then, a 3-point average is made, reducing data size and setting up for graphically smoother plotting. Figure 5.8 show the computed hardness plot after taking these measures:
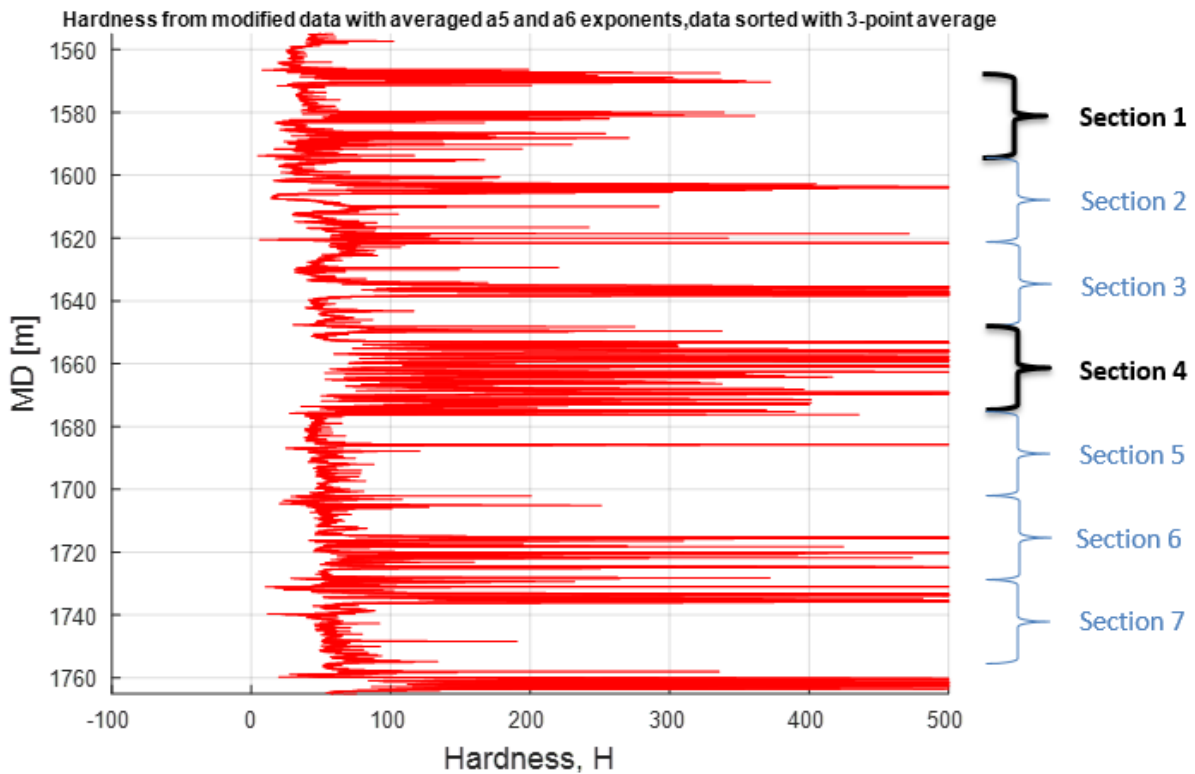
Figure 5.8: Calculated hardness, H, plotted vs. measured depth, MD, from RTDD in Well C-47, bit section 17 ½'', interval 1560-1760 meters, dated 23 December 2005. Data has been sorted with respect to measured depth by removing duplicate DMEA values. There has also been taken a 3-point average, which means a considerable reduction in the number of data points. No noticeable difference is seen from Figure 5.7, which can indicate that the "positive" hardness spikes are not caused by data anomalies.

There is no noticeable difference between the plots of Figure 5.8 and the lower image of Figure 5.7. This is an unexpected result given that the number of data entries for the complete 17 ½" interval have been severely reduced from 13299 in Figure 5.7 to 4165 in Figure 5.8. So, less than one third (4165/13299 = 0.31), of the entries are remaining after the removal of duplicate DMEA-values (number of points reduced from 13299 to 12623), taking 3-point average (number of points reduced from 12623 to 4207, which is one third) and checking whether if it was an active drilling operation by $DMEA(i) - DBTM(i) \leq 0.1$ before calculating drillability (number of points reduced from 4207 to 4165). This can indicate that the large "positive" spikes of hardness seen in Figure 5.8 are not data anomalies, as this filtering process should have removed them from the image if this was the case. However, the graph remains very vague and blurry compared to the graph of Figure 5.6 which were using raw data and computed drillability with ROP and not dBPOS as the parameter for penetrate rate. Normalizing the hardness, which should scale the hardness values and thus "compress" the plot, can address this problem.

In step 3, the data has been normalized to make hardness range from 0 to 1, where 0 represents extremely soft formations and 1 extremely hard formations. As can be seen from Figure 5.9,

normalizing the hardness has helped with plot readability. It is now easier to identify where the low hardness values are located, as well as the "positive" hardness spikes are more refined. Overall the hardness values are better scaled compared to each other.
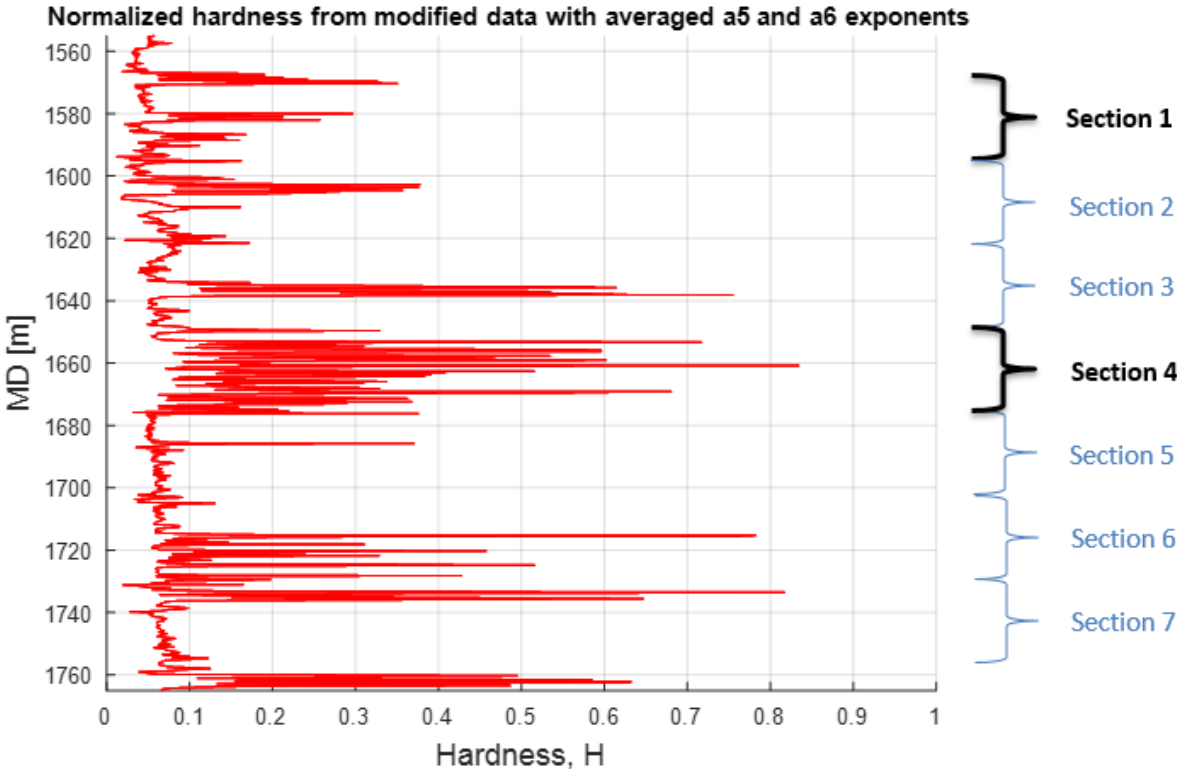

Figure 5.9: Calculated and normalized hardness, H, plotted vs. measured depth, MD, from RTDD in Well C-47, bit section 17 ½'', interval 1560-1760 meters, dated 23 December 2005. Normalization of hardness values have resulted in a much smoother plot compared to in Figure 5.8.

The scaling improvement of the plot in Figure 5.9 compared to in Figure 5.8 has made it possible to find which of the harder sections contain the most "positive" spikes and seems to be most troublesome to drill. So far, Section 4 seems to be the most problematic one based on average hardness ratings and number and value of spikes. However, Section 3, 6 and 7, though softer in general hardness than Section 4, may also contain hard stringers, indicated by large spikes. There is also a smaller spike in Section 2, with the same value or amplitude as the one in Section 1. We already know that Section 1 contains hard stringers based on the information in the final well report, so the spike in the top part of Section 2 may be an extension of the troublesome area of Section 1. Section 1 and Section 4 was selected for log interpretation based on the FWR information and initial hardness signs (most easily spottable signs) during log interpretation, however the spikes in the other sections can be interesting to take note off for future evaluations.

So far, the calculations of drillability and hardness have been calculated using only one type of exponent value for the WOB and RPBM terms. These were the average exponents of $a_{5\text{-avg}} = 1.25$ and $a_{6\text{-avg}} = 0.70$. In step 4, hardness classification is introduced based on the normalization in the previous step. This means that for values of hardness > 0.5, moderately hard formation type exponents of $a_{5\_mod\_hard} = 0.875$, and $a_{6\_mod\_hard} = 0.55$ are utilized, while for values of hardness ≤ 0.5, moderately soft formation type exponents of $a_{5\_mod\_soft} = 1.625$, and $a_{6\_mod\_soft} = 0.85$ are utilized. Figure 5.10 shows hardness computed with two sets of exponents.
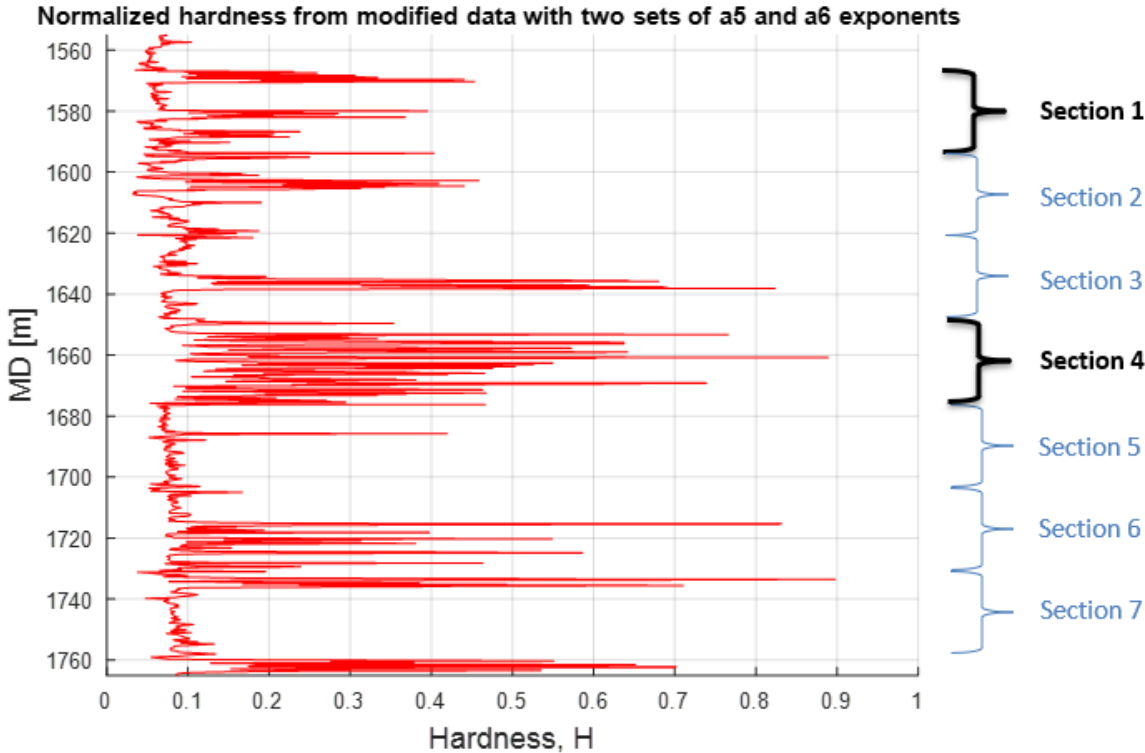

Figure 5.10: Calculated and normalized hardness, H, plotted vs. measured depth, MD, from RTDD in Well C-47, bit section 17 ½'', interval 1560-1760 meters, dated 23 December 2005. Hardness, H, has been classified such that it is calculated with two different sets of a_5 and a_6 exponents. For H > 0.5, moderately hard formation type exponents are used, while for H ≤ 0.5 moderately soft formation type exponents are used.

Comparing the plot of Figure 5.10 to Figure 5.9, there are some notable differences. The plot has become more defined, which is most easily seen in the "dense" region around H = 0.2-0.4 in Section 4. The image is clearer because the highest hardness values have become "stretched" towards even higher values, now touching the H = 0.9 mark compared to only reaching about H = 0.83 in Figure 5.9. However, though the plot is more stretched, lower hardness values have also become higher, moving the baseline interval consisting of the lowest values from 0.3-0.8 in Figure 5.9 to 0.5-1.0 in Figure 5.10. Another difference is that the highest "positive" spike was located in Section 4 in Figure 5.9, while now the highest spike is located in Section 7, barely higher than the one in Section 4.

The more distinct separation seen in the plot between low and high hardness values, especially in the zones with high discrepancy between lower and higher values such as in Section 4 and Section 7, may be caused by that the new exponents are more suited to these zones of mixed lithology. Further varying the values of the formation exponents, and especially increasing the difference between a_5 and a_6, can perhaps cause an even clearer and more easily readable image.

In step 5, using extreme cases of formation exponents will be tested versus using only moderate ones. In Figure 5.11, very hard formation exponents and moderately soft formation exponents (blue graph), in addition to moderately hard formation exponents and very soft formation exponents (green graph) are added to the plot of the moderately hard and moderately soft exponents used in Figure 5.10 (red graph).

Figure 5.11: Calculated and normalized hardness, H, plotted vs. measured depth, MD, from RTDD in Well C-47, bit section 17 ½'', interval 1560-1760 meters, dated 23 December 2005. Hardness, H, is calculated with two different sets of a_5 and a_6 exponents. The values of the formation exponents are being varied, such that blue graph shows very hard formation exponents and moderately soft formation exponents, green graph shows very soft formation exponents and moderately hard formation exponents, while red graph shows the previous case of moderately hard and moderately soft formation exponents.

This graph may look very blurry and hard to interpret at first. However, if one decides to only focus on Section 1 and Section 4, it becomes much more refined. Figure 5.12 shows zoomed images of these two sections.

Normalized hardness from modified data with two sets of a5 and a6 exponents

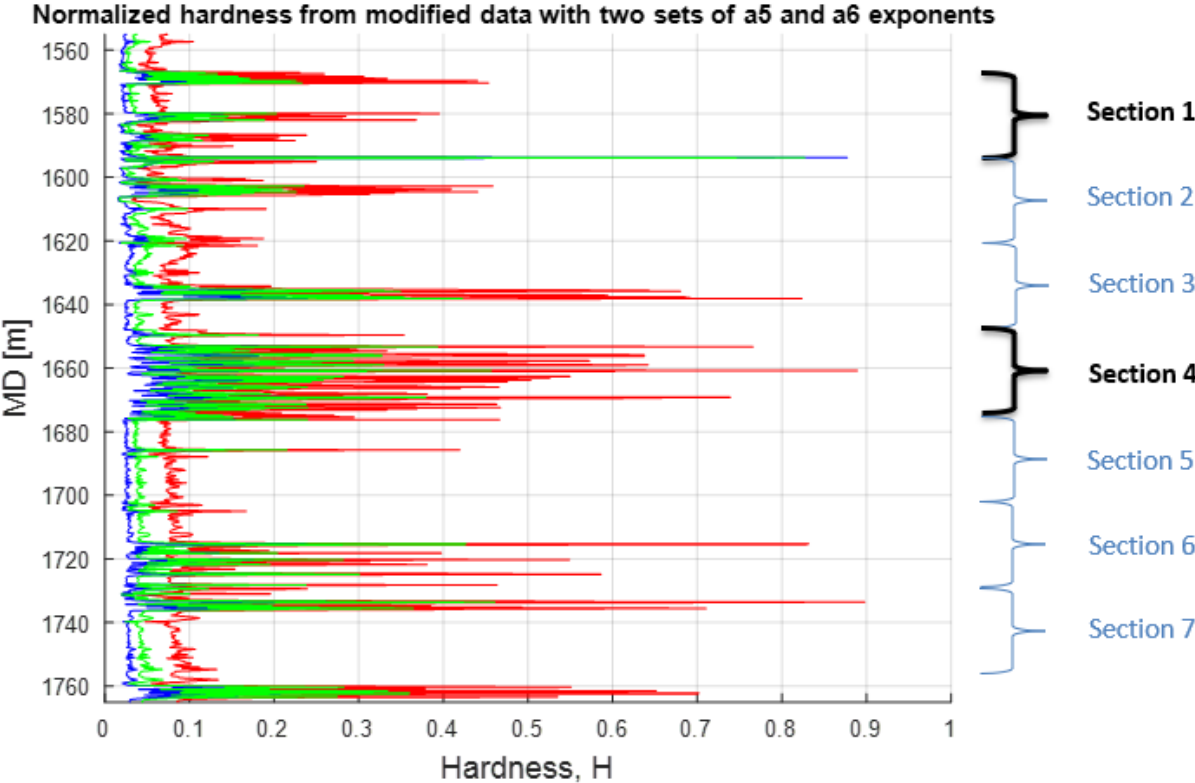**Normalized hardness from modified data with two sets of a5 and a6 exponents**

Figure 5.12: Calculated and normalized hardness, H, plotted vs. measured depth, MD, from RTDD in Well C-47, bit section 17 ½'', dated 23 December 2005. **The upper image shows** *Section 1 (1567-1594 m MD), while* **the lower image shows** *Section 4 (1648-1675 m MD). Hardness, H, is calculated with two different sets of a₅ and a₆ exponents. The values of the formation exponents are being varied, such that blue graph shows very hard formation exponents and moderately soft formation exponents, green graph shows very soft formation*

From the two images of Figure 5.12, the largest and most distinct variation in hardness are obtained by using the original sets of moderately hard and moderately soft formation exponents (red graph). After this, calculations of hardness using very soft and moderately hard formation exponents (green graph) shows better variation compared to calculations with very hard and moderately soft formation exponents (blue graph). This result is perhaps a little surprising, given one could expect formation type exponents suited for very hard formations, such as what the blue graph represents, would show more distinct spikes when hard sections or stringers were encountered. However, the general trend is that this does not seem to be the case. The blue graph is in all but one instance the graph showing the least variation in readings.

The only anomaly in this trend is the large spike situated at around 1594 m MD, just at the boundary between Section 1 and Section 2. Here, the trend is reversed, the blue graph shows the highest peak (H = 0.87), followed by the green (barely noticeable in Figure 5.12, but H = 0.82 when zoomed in) and lastly the red (H = 0.4). A zoomed image of this anomaly is shown in Figure 5.13. This situation should be checked for correlating behaviours of BPOS, WOB and RPMB with log interpretation, deciding whether it is a hard stringer, or some anomaly caused in the hardness plots when tripping pipe.

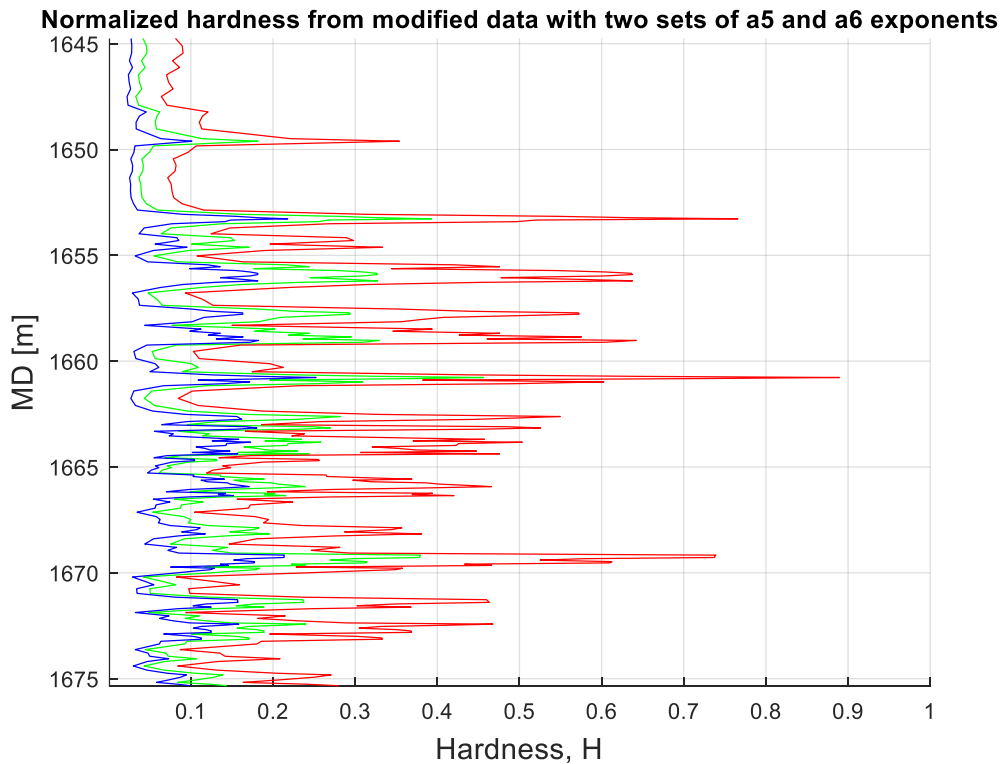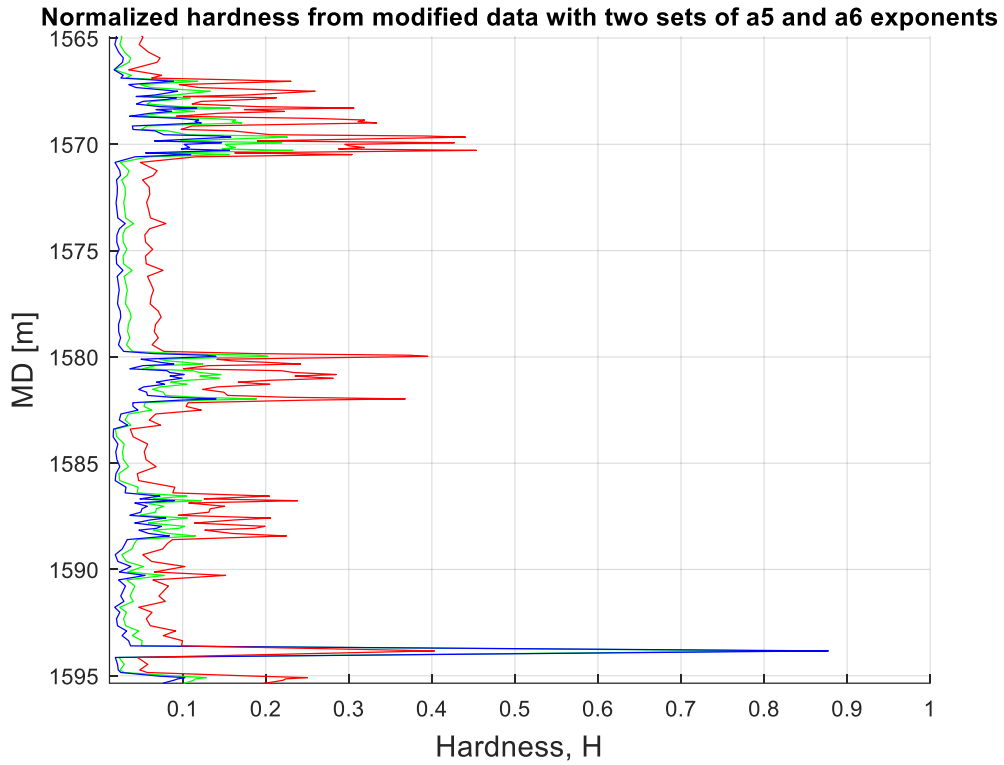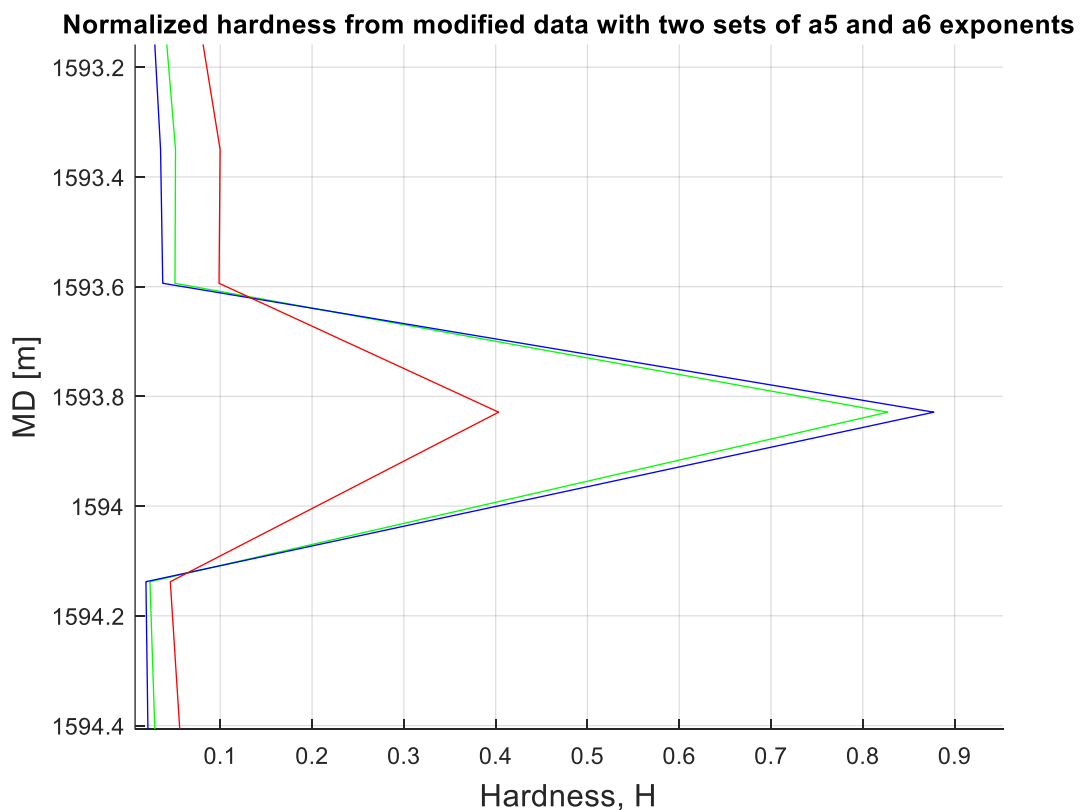**Normalized hardness from modified data with two sets of a5 and a6 exponents**

Figure 5.13: Calculated and normalized hardness, H, plotted vs. measured depth, MD, from RTDD in Well C-47, bit section 17 ½'', dated 23 December 2005. **The image shows an abnormal peak in hardness at the border between** *Section 1 (1567-1594 m MD)* **and** *Section 2 (1594-1621).* **Hardness, H, is calculated with two different sets of** *a₅* **and** *a₆* **exponents. The values of the formation exponents are being varied, such that blue graph shows very hard formation exponents and moderately soft formation exponents, green graph shows very soft formation exponents and moderately hard formation exponents, while red graph shows the original case of moderately hard and moderately soft formation exponents. This situation needs further inspection by log interpretation to determine whether it is caused by a hard stringer or from pipe tripping.**

Excluding the discussed anomaly in Figure 5.13, Figure 5.12 showed that the largest variation in hardness with two exponents were obtained by using the original sets of moderately hard and moderately soft formation exponents (red graph). These exponents are thus considered to most accurately reflect the formation, producing hardness results that can be used for further analysis.

The last step, step 6, will investigate the hardness classification limit. When using two different sets of formation exponents this limit was set at 0.5. This meant formations with hardness > 0.5 calculated with one set of exponents was classified as hard formations, and later re-calculated with moderately hard formation exponents when two different sets of exponents were used. Formations with hardness ≤ 0.5 were classified as soft formations and later re-calculated with moderately soft formation exponents. The classification limit of H > 0.5, was not necessarily optimal. Too many formations may be classified as hard when using this system, as can be seen by looking more closely at Figure 5.9. A more suitable limit could be to use H > 0.75. This will define more of the formations as being soft, which can produce a different hardness plot. Figure 5.14 shows computed hardness when the limit is set at H > 0.75 (black graph) versus when it is set at the original H > 0.5 (red graph).

Figure 5.14: Calculated and normalized hardness, H, plotted vs. measured depth, MD, from RTDD in Well C-47, bit section 17 ½'', interval 1560-1760 meters, dated 23 December 2005. Hardness, H, is calculated with two different sets of a_5 and a_6 exponents. The hardness limit is being varied, such that the red graph shows the original case of H > 0.5, while the black graph represents a situation where the hardness limit is increased to 0.75.

Again, like seen earlier, because of the fuzziness of the plot in Figure 5.14, results will be hard to interpret unless the plot is zoomed in. In Figure 5.15, Section 1 has been selected for further inspection.

Normalized hardness from modified data with two sets of a5 and a6 exponents

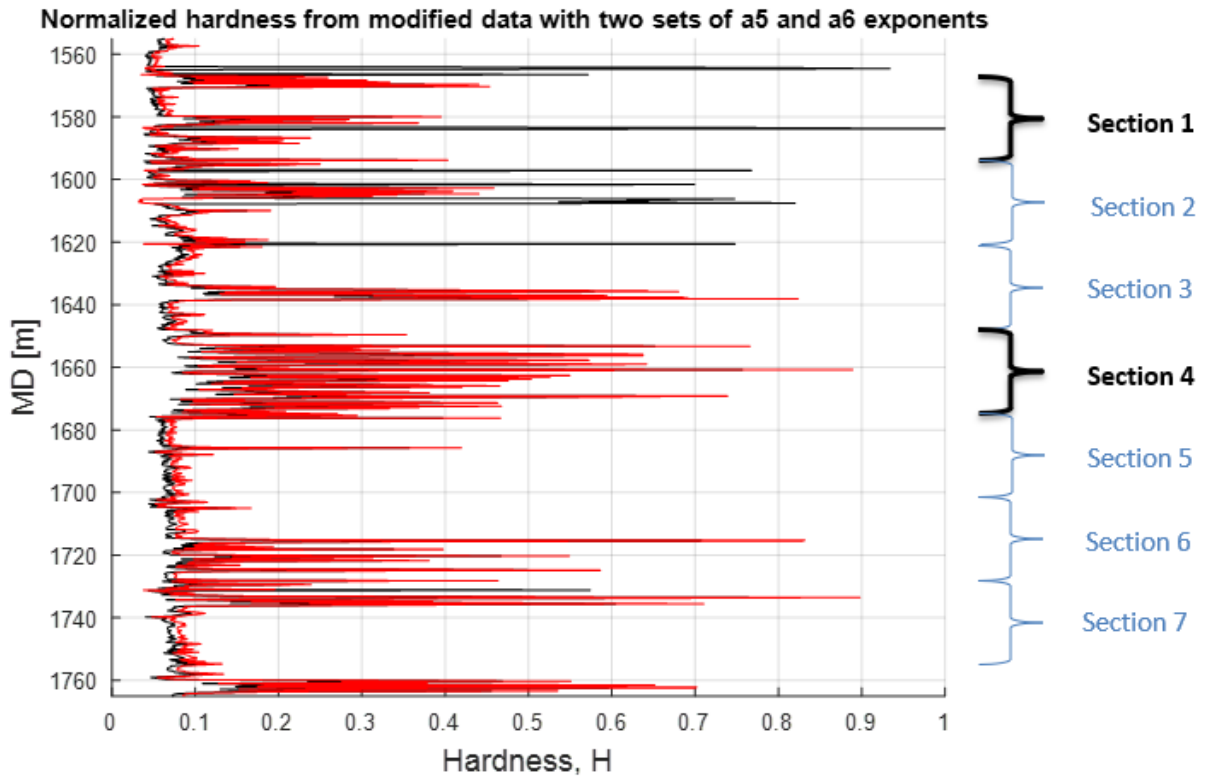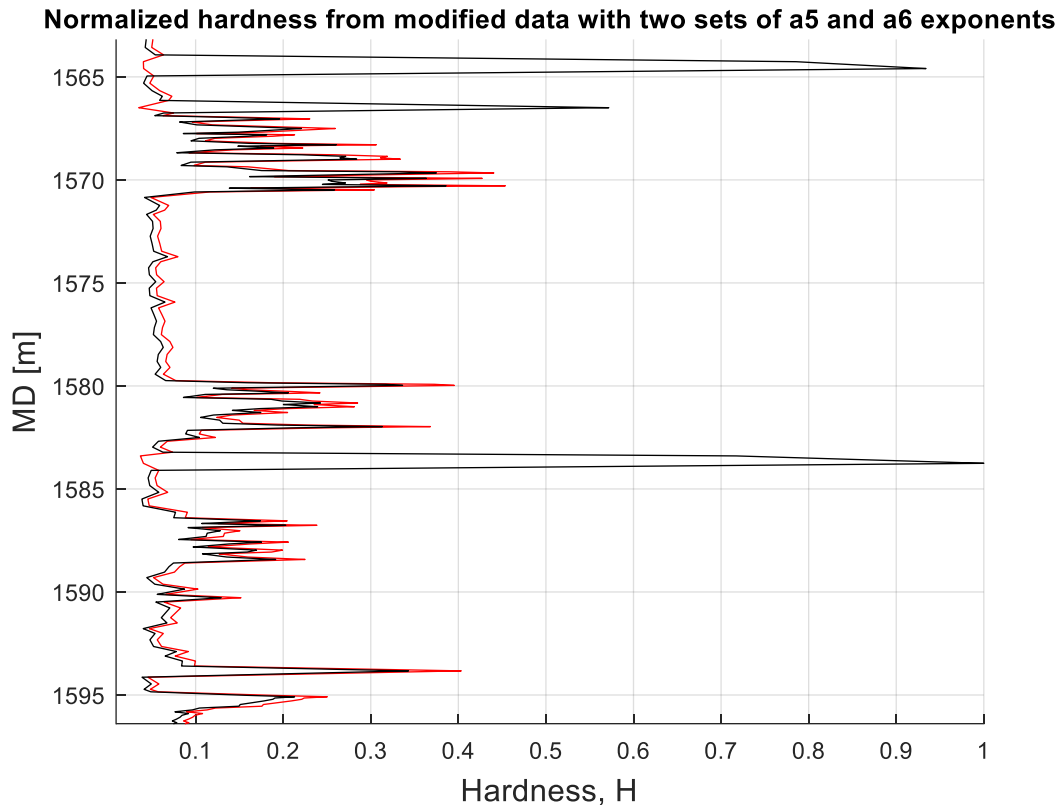*Figure 5.15: Calculated and normalized hardness, H, plotted vs. measured depth, MD, from RTDD in Well C-47, bit section 17 ½'', dated 23 December 2015. The image shows Section 1 (1567-1594 m MD). Hardness, H, is calculated with two different sets of a_5 and a_6 exponents. The hardness limit is being varied, such that the red graph shows the original case of H > 0.5, while the black graph represents a situation where the hardness limit is increased to H > 0.75.*

As seen from Figure 5.15, the difference between the two graphs are minimal. However, the original case of H > 0.5 (red graph), still represent a slightly more distinct variation in hardness than the case of H > 0.75 (black graph). Again, like earlier, there seem to be some anomalies in the plots where the general trend is reversed. In this case, there are three spikes of hardness in the graph for H > 0.75 at around 1563, 1567, and 1584 m MD. The H > 0.5 graph is not responding to these spikes at all, so this seems to be a data or computing irregularity rather than something caused by a difference in hardness (or tripping). The fact that these spikes are situated at depths where no other plots have previously indicated any harder formations or hard stringers supports this assessment. Because the definition of hardness with H > 0.5 has more distinct transitions (and less data anomalies) than for H > 0.75, H > 0.5 will be continued to be applied as the hardness classification limit.

5.1.4 Correlating the results from qualitative and quantitative method

This section will explore the relationship between the results obtained from the qualitative method with the results obtained from the quantitative method. The aim is to confirm the location of hard formations or hard stringers within the different intervals.

5.1.4.1 Section 1

Starting with Section 1, the interval from 1567-1594 m MD, this should be the easiest one to identify any harder formation types as the FWR already states that several hard stringers were hit within this interval. From the log interpretation, as was shown in the overview image of Figure 5.3, hard stringers were indicated at least at three locations. Figure 5.16 shows an enlarged image of Section 1 (and partly Section 2) taken from Figure 5.3.

Figure 5.16: RTDD from Section 1, 1567-1594 m MD. DBTM, DVER and DMEA are drilling depth data measured vs. time. BPOS, WOB and RPM are also plotted vs. time in different real-time drilling windows. Green stapled lines indicate RPMB baselines for a soft (dark green, not shown here) and medium soft (light green) formation. Red right triangles (showing BPOS speed by their inclination/steepness) and red arrows (showing corresponding RPMB) indicate where hard stringers are located. Bright red marks a stringer for a hard formation (section 1 only), dark red marks stringers for a medium hard formation (section 1 and 4) while pink marks stringers for a slightly hard formation (section 4 only, not shown here). Hard stringers are indicated at least at three locations in Section 1.

Indications of stringers were made by looking at the corresponding behavior of BPOS, WOB and RPM. The steeper the BPOS-curve (shown by the inclination of the triangles), the slower is the BPOS speed with time, which together with an increase in WOB and decrease in RPM can be attributed to harder formations causing a decrease in penetration rate and drillability. During the log interpretation the stringers were informally classified as hard, medium hard and slightly hard. Hard and medium hard stringers were identified in Section 1, with the one classified as hard appearing in the lower part of the section and the two classified as medium hard appearing in the uppermost part.

The decrease in penetration rate when encountering harder formations means that dBPOS, which was calculated and chosen to be used instead of ROP as a measure of penetration rate, should then also decrease when hitting harder formations. Plotting dBPOS together with BPOS can illustrate the relationship between the velocity of the block and the steepness of the BPOS curve. In Figure 5.17, dBPOS and BPOS are plotted versus time. The three indicators for hard stringers which was spotted and shown in Figure 5.16 are marked with bright red (one indicator) and dark red (two indicators). There are also several new indicators, each being marked in green. However, the general trend seems to be that the indicators are separated in three clusters, with each cluster having softer formations in between those. These clusters of signs are potentially the composite of one hard stringer. The two uppermost clusters contain at least 4 indicators each, while the lower contain at least 1. The number of indicators in each cluster is being marked in parenthesis.

Figure 5.17: dBPOS and BPOS plotted vs. time in Section 1 from 1567-1594 m MD. Arrows marks indicators of hard stringers found according to a combination of decrease in penetration rate/block velocity and steeper BPOS curve. Bright red and dark red arrows marks the three previously identified indicators. Green arrows are newly identified indicators. The indicators appear in three larger clusters, each cluster potentially making up one hard stringers. Softer formations are situated in between clusters/stringers. The number in parenthesis indicate the minimum number of indications of stringers identified in each cluster.

Adding the computed hardness curve from the previous section to the plot above should verify whether the spotted indicators for hard stringers are correct. This step is made in Figure 5.18 below. Notice the negative correlating behavior between the curves of the dBPOS and the hardness.

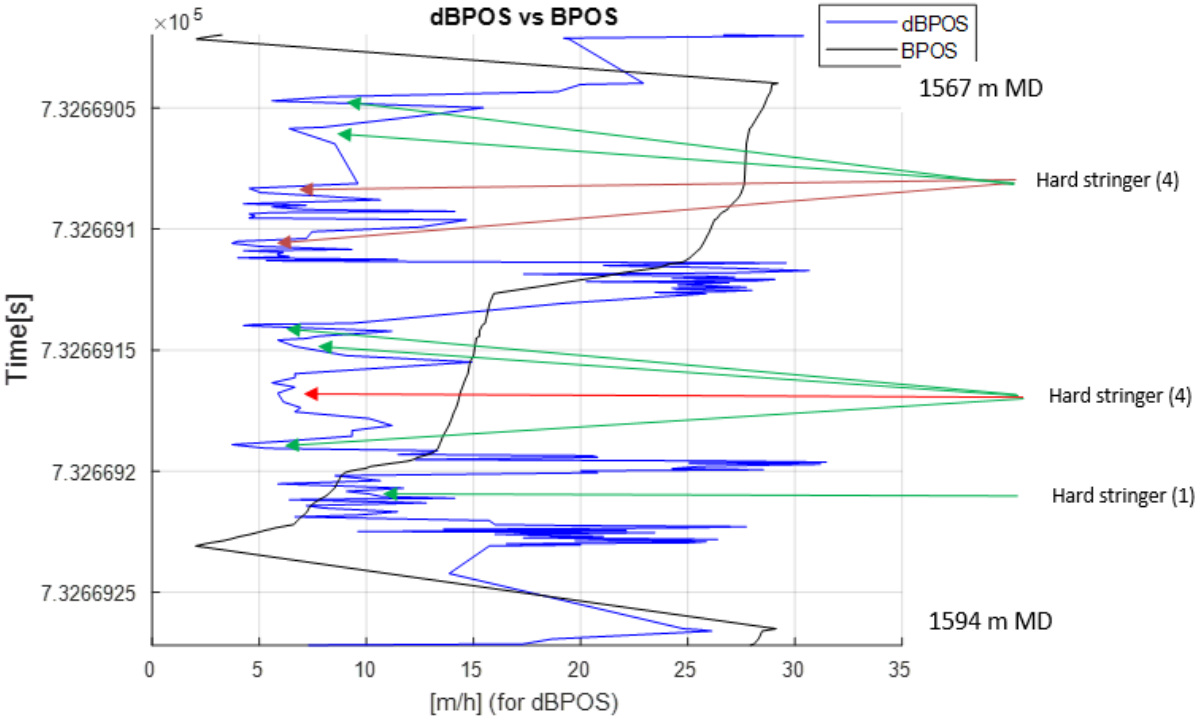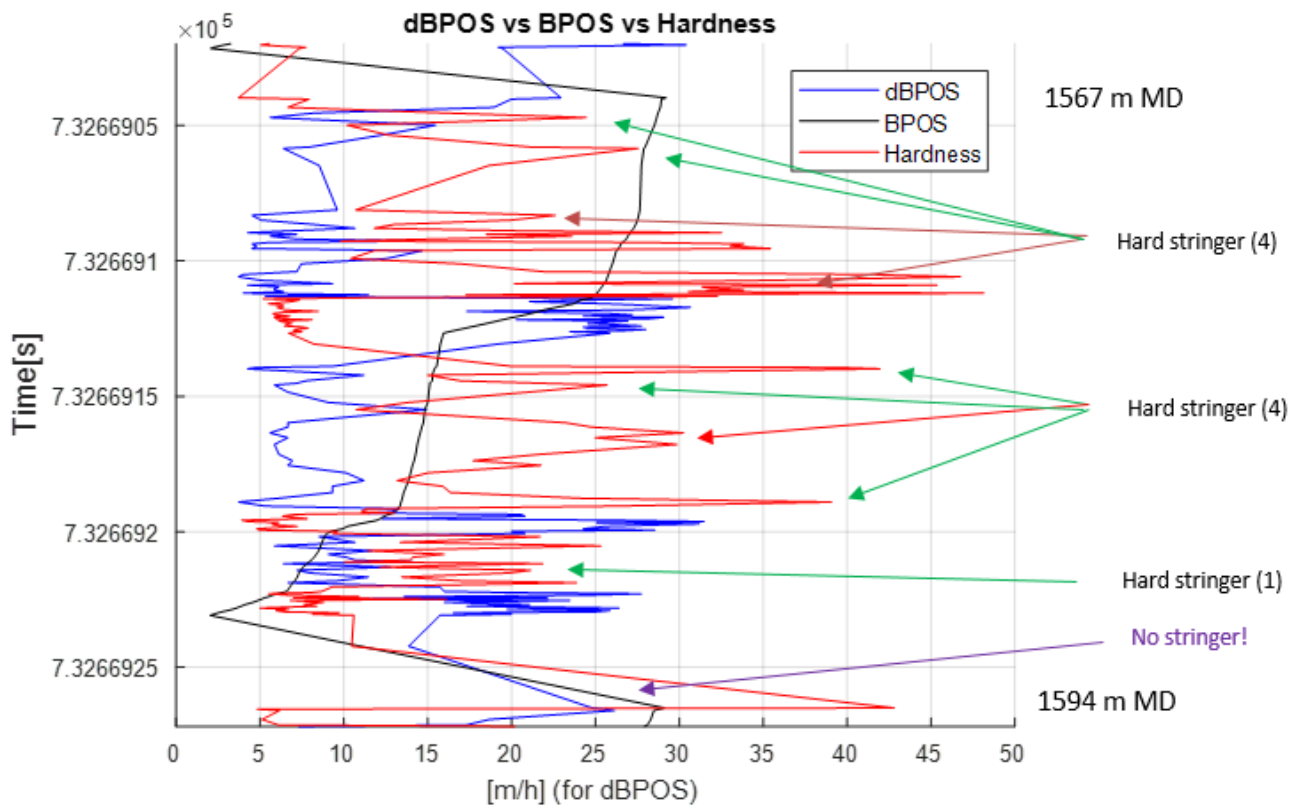*Figure 5.18: dBPOS, BPOS and hardness plotted vs. time in Section 1 from 1567-1594 m MD. Arrows marks indicators of hard stringers found according to a combination of increase in hardness, decrease in penetration rate/block velocity and steeper BPOS curve. Bright red and dark red arrows marks the three previously identified indicators. Green arrows are newly identified indicators. The indicators appear in three larger clusters, each cluster potentially making up one hard stringer. Softer formations are situated in between clusters/stringers. The number in parenthesis indicate the minimum number of indications of stringers identified in each cluster. The previously discussed anomaly at around 1594 m MD is marked with a purple arrow and is not being considered a hard stringer as there are increases in all parameters.*

The hardness curve confirms that the indications for hard stringers by the dBPOS and BPOS curves seems to be correct. The anomaly that was discussed in the previous section at around 1594 m MD can now also be excluded as a hard stringer as there is an increase in dBPOS together with an increase in both hardness and block positioning.

Plotting hardness and dBPOS vs. measured depth instead of time will enable for a better overview of the thickness of the hard stringers or harder formations. This also makes it possible to draw formation boundaries. In Figure 5.19 hardness and dBPOS are plotted vs. measured depth, with formation boundaries drawn between hard and soft formations. Three hard stringers and three soft formations are being marked. The soft formations seem to be part of the same formation type, which has a normalized hardness value of around 0.05-0.07. The hard stringers have varied hardness, ranging from about 0.15 to 0.45 at the most. The thickness of the stringers is approximately 3.5, 2.0 and 2.25 meters. It should be noted that in section 2.1.1.3, a hard stringer was originally defined to vary in thickness from 0.5 up to 2 meters. If strict by this definition, the uppermost and lowermost

116

stringer, and especially the uppermost, should perhaps more correctly be classified as hard formations rather than hard stringers. However, the term hard stringer is used for all three in this occasion, as there is a trend that one soft formation is being "pierced" by three hard stringers, rather than a general shift in formation type towards harder formations.
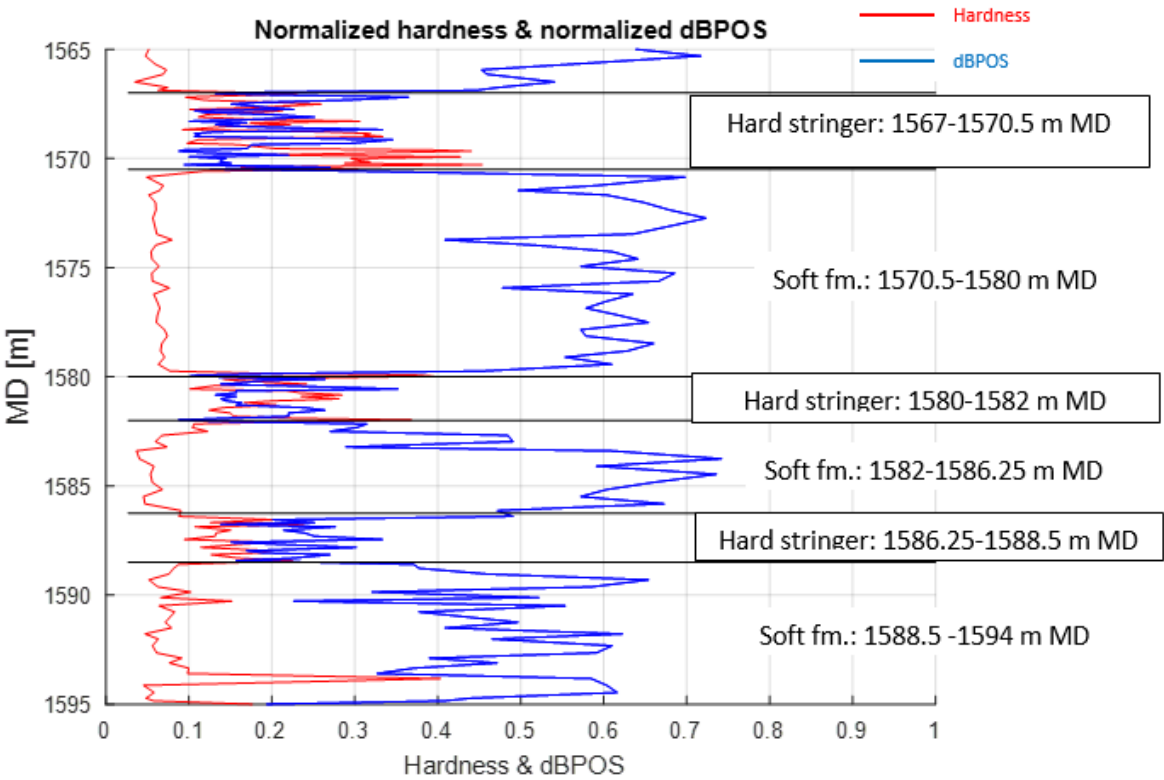
Figure 5.19: Normalized hardness and dBPOS plotted vs. measured depth in Section 1 from 1567-1594 m MD. The negative correlating behavior between the graphs of hardness (red graph) and dBPOS (blue graph), have been used to identify three hard stringers at positions where hardness values are high and dBPOS values are low. Formation boundaries are drawn (black horizontal lines) between hard stringers and softer formation types.

5.1.4.2 Section 4

Next is the other interval in focus, Section 4, situated at depths of 1648-1675 m MD. Figure 5.20 is an enlarged cut of this section taken from Figure 5.3.
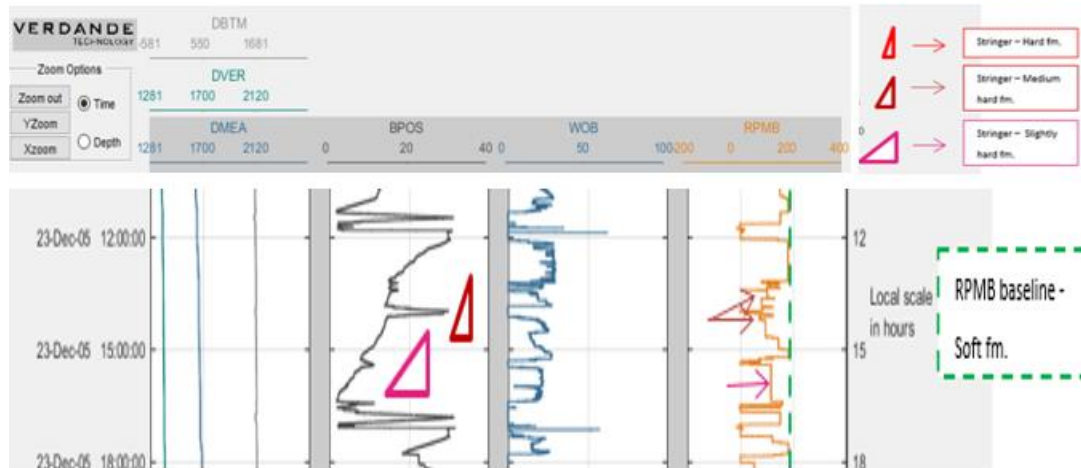
Figure 5.20: RTDD from Section 4, 1648-1675 m MD. DBTM, DVER and DMEA are drilling depth data measured vs. time. BPOS, WOB and RPM are also plotted vs. time in different real-time drilling windows. Green stapled lines indicate RPMB baselines for a soft (dark green) and medium soft (light green, not shown here) formation. Red right triangles (showing BPOS speed by their inclination/steepness) and red arrows (showing corresponding RPMB) indicate where hard stringers are located. Bright red marks a stringer for a hard formation (section 1 only, not shown here), dark red marks stringers for a medium hard formation (section 1 and 4) while pink marks stringers for a slightly hard formation (section 4 only). Hard stringers are indicated at least at two different locations in Section 4.

In section 4, continuing with the informal hardness classification from the log interpretation section, a medium hard (dark red) and slightly hard stringer (pink) were identified. The one classified as medium hard Is appearing in the uppermost part of the section while the one classified as slightly hard is appearing in the lower part. Notice that the RPMB-baseline (light green stapled line), which is also an indicator for formation hardness, is of a higher value than what was the case for Section 1 (dark green stapled line, see Figure 5.16). The value of this baseline has increased from about 16 to 20 RPM. Thus, the soft formation types of Section 4 may be expected to be softer than those of Section 1, which were classified as medium soft according to this classification.

As in the previous section, the next step to identify any potential hard stringers will be to investigate the relationship between the graphs of dBPOS and BPOS, looking for decreases in dBPOS together with a higher steepness of the BPOS curve. In Figure 5.21, dBPOS and BPOS are plotted versus time.

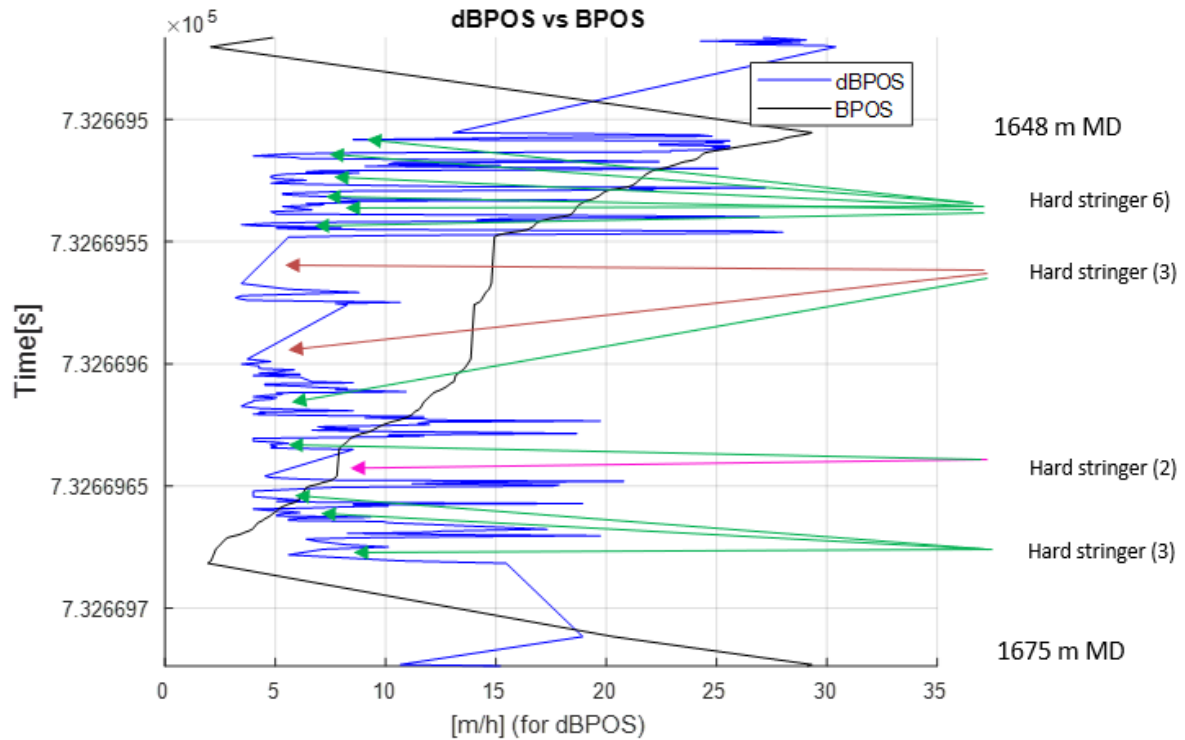*Figure 5.21: dBPOS and BPOS plotted vs. time in Section 4 from 1648-1675 m MD. Arrows marks indicators of hard stringers found according to a combination of decrease in penetration rate/block velocity and steeper BPOS curve. Dark red and purple arrows mark the three previously identified indicators. Green arrows are newly identified indicators. The indicators appear in four clusters, each cluster potentially making up one hard stringer. The top and bottom cluster may also potentially be transitional hardness intervals. Softer formations are situated in between clusters/stringers. The number in parenthesis indicate the minimum number of indications of stringers identified in each cluster.*

In Figure 5.21, there are several new indicators of hard stringers in addition to the three that was spotted in Figure 5.20. However, the new indicators are vaguer, and it is difficult to confirm whether these really are indicators of hard stringers before the hardness graph is also evaluated. Especially the upper part of the section has an area where the dBPOS is going quickly back and forth between values of 5 m/h to around 27 m/h. In the same time interval, the BPOS is not rapidly decreasing but rather "zigzagging". Right after this part the BPOS abruptly turns very steep, which is a clearer sign of harder formations types. The BPOS in this middle part is also combined with low dBPOS values of around 4-8 m/h (dark red arrows indicate this area). Further down, the dBPOS graph starts to fluctuate again, now between values of 5-20 m/h. The BPOS graph is also once more zigzagging, but over a longer time-frame than in the upper part. The BPOS becomes stable in the middle of this lower part, accompanied by very low dBPOS, making this a more obvious indicator for a harder formation (marked with a pink arrow). Since the more clearer indicators for hard formations are positioned in the middle of this interval, it may seem that the "zigzagging parts" of BPOS and high fluctuating dBPOS at the top and bottom of the interval could represent hardness transitions from a soft to a hard formation (at the top) and hard to soft formation (at the bottom).

In Figure 5.22, hardness is added to the plot of Figure 5.21.
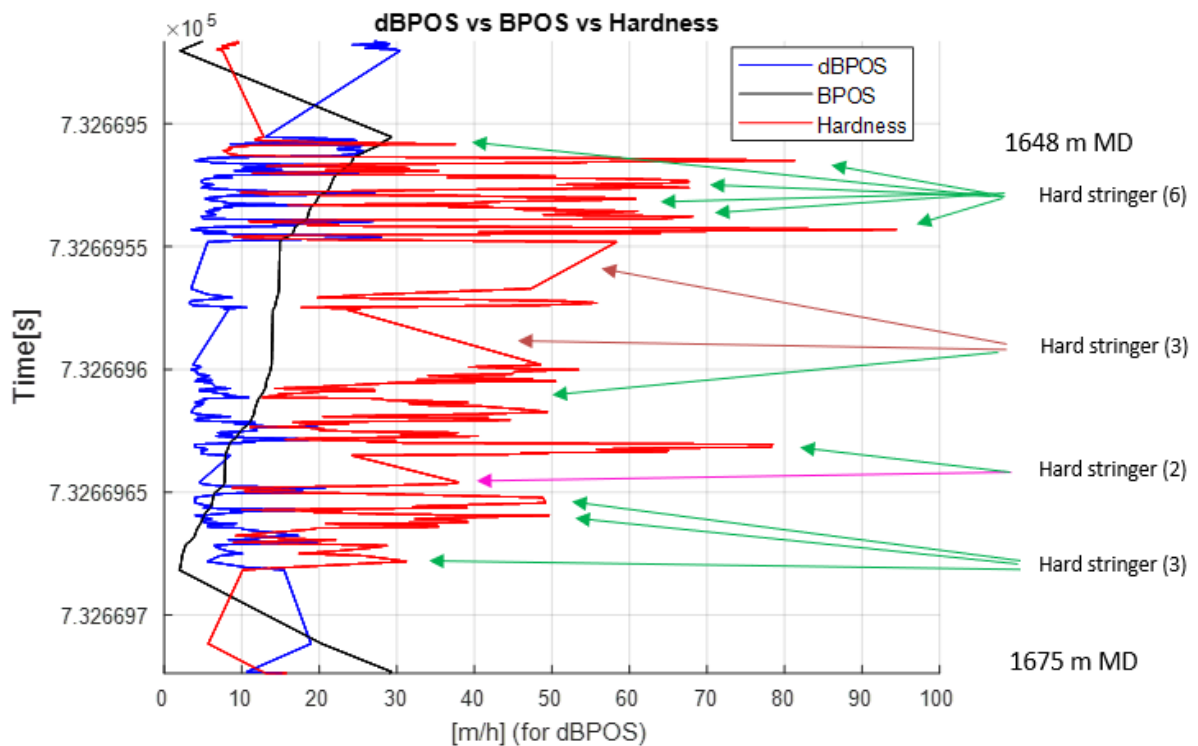
Figure 5.22: dBPOS, BPOS and hardness plotted vs. time in Section 4 from 1648-1675 m MD. Arrows marks indicators of hard stringers found according to a combination of increase in hardness, decrease in penetration rate/block velocity and steeper BPOS curve. Dark red and dark pink arrows mark the three previously identified indicators. Green arrows are newly identified indicators. The indicators appear in four larger clusters, each cluster potentially making up one hard stringer. The top and bottom cluster may also potentially be transitional hardness intervals. Softer formations are situated in between clusters/stringers. The number in parenthesis indicate the minimum number of indications of stringers identified in each cluster.

The negative correlating behavior between the dBPOS and Hardness graph, plus the peaks of the hardness curve, seems to confirm that the indications for harder formations by the dBPOS and BPOS curves are correct.

In Figure 5.23, hardness and dBPOS are plotted vs. measured depth. This plot is a lot more unclear than the equivalent plot for Section 1, so it makes sense to first highlight and identify the different stringers or transition areas from Figure 5.21 and 5.22 with arrows before drawing formation boundaries. The reason the plot is so vague is because the graphs for hardness and dBPOS are situated close together, in addition to that the graphs are oscillating back and forth between readings. All indicators of harder formations (arrows) from Figure 5.22 have been identified in Figure 5.23. There is also possibly one new hard stringer, which is being marked in black (top area of interval).

120

Figure 5.23: Normalized hardness and dBPOS plotted vs. measured depth in Section 4 from 1648-1675 m MD. The negative correlating behavior between the graphs of hardness (red graph) and dBPOS (blue graph), have been used to identify harder formations at positions where hardness values are high and dBPOS values are low. The indicators are showed by the same arrows as in the previous two figures. The indicators appear in four larger clusters, each cluster potentially making up one hard stringer. The top and bottom cluster may also potentially be transitional hardness intervals. The number in parenthesis indicate the minimum number of indications of stringers identified in each cluster. A new possible hard stringer is identified at around 1649 m MD.

In Figure 5.24, suggested formation boundaries are added and drawn into the image from Figure 5.23. There are four formations labeled as hard and five labelled as soft. Based on the characteristics and thickness of the different hard formations, only one (from 1669-1970 m MD, with H = 0.74) is being considered as a hard stringer. Starting from the top of the interval, there is a soft formation (H = 0.06) situated down to a depth of 1653 m MD. As mentioned above, this formation may possibly contain a hard stringer as there is a spike in hardness to H = 0.35 at around 1649 m MD. Below this formation is a harder formation from 1653-1661.25 m MD. This formation could be characterized as a transitional interval towards a harder formation type situated further below, or it may also be characterized as a softer formation with multiple hard stringers. There are spikes in hardness towards very high values such as H = 0.77 and H = 0.89 within this interval. From 1661.25-1662.5 m MD there is another soft formation. Then from 1662.5-1665.5 m MD, comes another hard section, which is labelled as a hard formation rather than a hard stringer because of its thickness of 4 meters. Below this interval comes a soft formation from 1666.5-1669 m MD. This interval may also

potentially contain a hard stringer as there is a peak towards H = 0.375 in the middle of the interval. From 1669-1670 comes the most obvious characteristic of a hard stringer within Section 4. As mentioned, H is here peaking towards H = 0.74. After this stringer comes a soft low-thickness interval of 1 meter. Situated from 1671-1673.25 m MD is a hard formation, however this interval could also be interpreted as a soft formation pierced with two hard stringers (both with H around 0.55), or possibly a hard formation with one soft stringer as the two peaks in hardness are separated by a peak in dBPOS (dBPOS = 0.45). It could also be characterized as a transitional interval towards a softer formation. This is because, below and at the bottom of Section 4, from 1673.25 m MD downwards, comes a soft formation with H= 0.08.
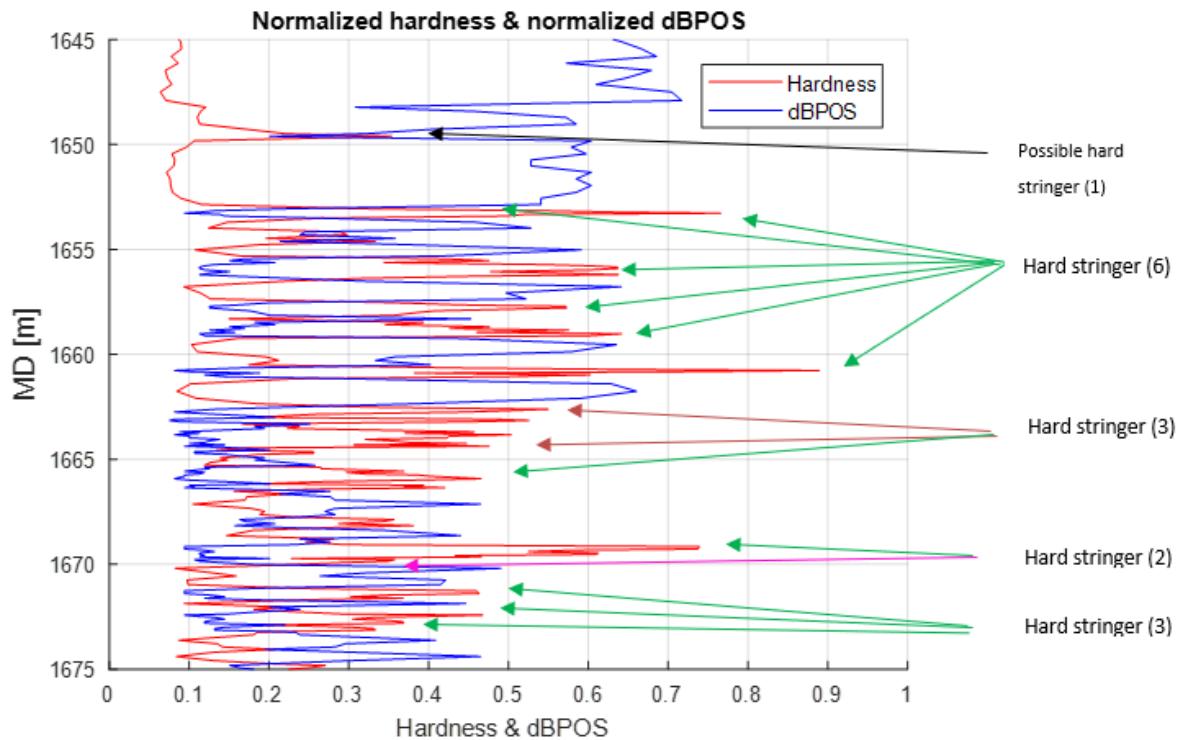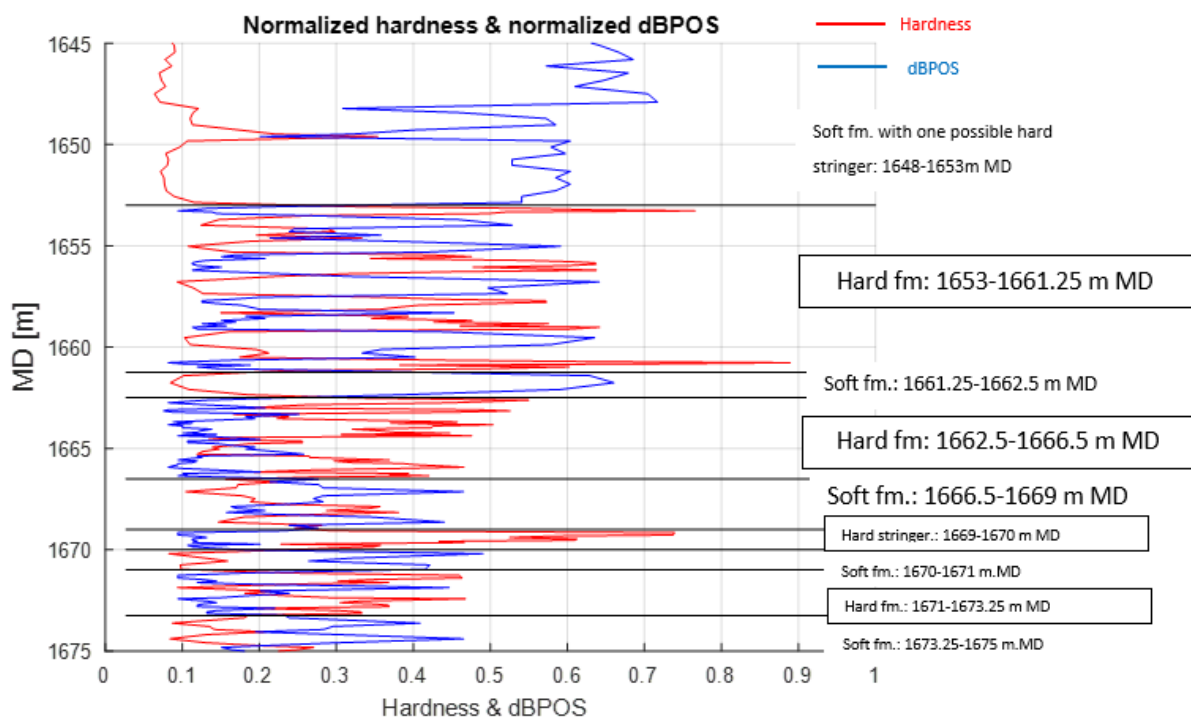

Figure 5.24: Normalized hardness and dBPOS plotted vs. measured depth in Section 4 from 1648-1675 m MD. The negative correlating behavior between the graphs of hardness (red graph) and dBPOS (blue graph), have been used to identify harder formations at positions where hardness values are high and dBPOS values are low. Formation boundaries are drawn (black horizontal lines) between hard stringers and softer formation types.

Though Section 4 has been difficult to interpret because of the oscillating values in hardness, the hardness baseline of this section has been raised compared to Section 1. This was not what was expected based on the log analysis, and the increase seen in ROP from 16 to 20 RPM. For instance, the hardness among the softer formation types were H = 0.05-0.07 in section 1 (same as in top of Section 4) while they have increased closer to H = 0.1 in this section. Thus Section 4 can be considered as a harder stand-section than Section 1. This transition in hardness is related to an

important shift in lithology, something that will be explained more thoroughly in the following chapters.

5.1.5 Formation boundaries

Figure 5.2.5, below, shows the computed hardness for the whole 17 ½" section of Well C-47 plotted vs. TVD. The formation boundaries presented in section 3.2 have been drawn.
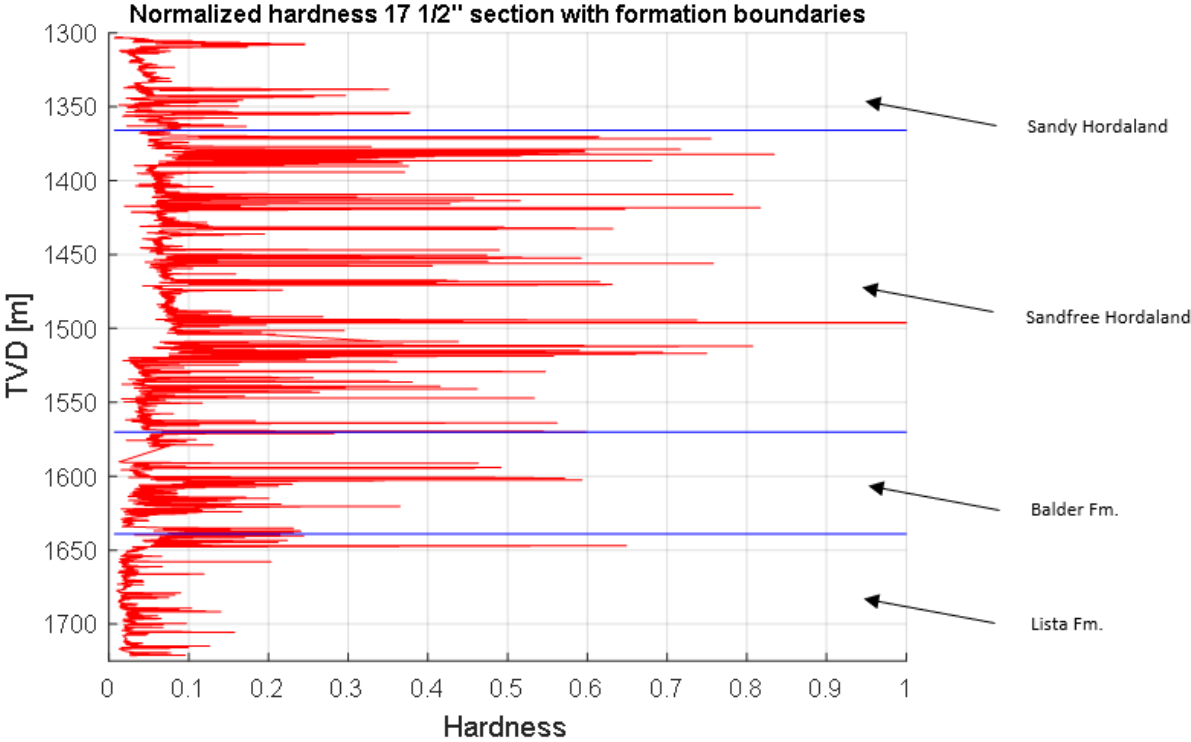
Figure 5.25: Normalized hardness (red graph) plotted vs. TVD for the 17 ½" bit section. Blue lines are formation tops for the Sandfree Hordaland, Balder and Lista formations.

The highest baseline of hardness is seen in the Sandfree Hordaland formation. This formation has also the highest peaks in hardness values. The Balder and Lista formations have the lowermost hardness baselines and appear to be the softest formations.

For selecting an ideal interval to base the task of separating between the effect of hardness vs. pore pressure on penetration rate, there need to be some variation in hardness. Selecting the lowermost part of the Sandy Hordaland, where the FWR had reported the occurrence of hard stringers, will likely not be productive. The stringers are mostly linked to changes in formations hardness and can skew the results. The test interval should also be located in or below the transition zone where the pore pressure starts increasing to abnormal values. However, before deciding on a test interval, the

results of the pore pressure calculations should be evaluated. This will help to locate the transition zone.

5.2 Results from pore pressure model

This section presents the results from the pore pressure model. The models have been tested on the same interval as the hardness model, the 17 ½" interval (1302-1724 m TVD / 1495-2380 m MD) of the Gullfaks C Well 34/10-C-47. The decision to select this interval was based on that the pore pressure is here reported to start departing from the normal pressure trend line towards abnormal values. As such, there will be variance in both pore pressure (ρ_{pore}), and well pressure (ρ_{ecd}). This increases the effect of overbalance (ρ_{ecd}-ρ_{pore}) on penetration rate which should make the study of comparing the effects of formations hardness vs. pore pressure on penetration rate easier.

First the pore pressure will be calculated without having decided the value of some important parameters. Lastly, after having decided the parameters, final results should be obtained. The goal here is to obtain as precise results as possible for the ρ_{pore}. The result will be compared with the pore pressure gradient found in the final well report.

5.2.1 Initial results

The pore pressure was in section 4.2 defined as:

$$p_{pore} = \frac{\log\left(\frac{ROP}{\left(\frac{WOB}{4d_{bit}}\right)^{a_5}\left(\frac{RPM}{60}\right)^{a_6}}\right) - a_1 - a_2(D_{ref} - D) + a_3 D^{0.69} p_{normal} + a_4 D \rho_{ecd}}{a_3 D^{0.69} + a_4 D} \tag{4.12}$$

Plotting the pore pressure against depth should reveal where the transition zone to abnormal pore pressure values is situated within the 17 ½" section. First, let us try to plot the pore pressure without the effect of the real drillability, represented through the coefficient a_1, such that $a_1 = 0$. Also, let us set the reference depth, D_{ref}, to the value D_{ref} = 4272 ft TVD (1302 m TVD). The D_{ref} should be positioned in a zone of normal pore pressure, not in or below the transition zone. The selected value, which is positioned at the very top of the 17 ½" section, will ensure this.

Figure 5.26 shows the pore pressure plotted according to eqn. (4.12), with $a_1 = 0$ and $D_{ref} = 4272$.
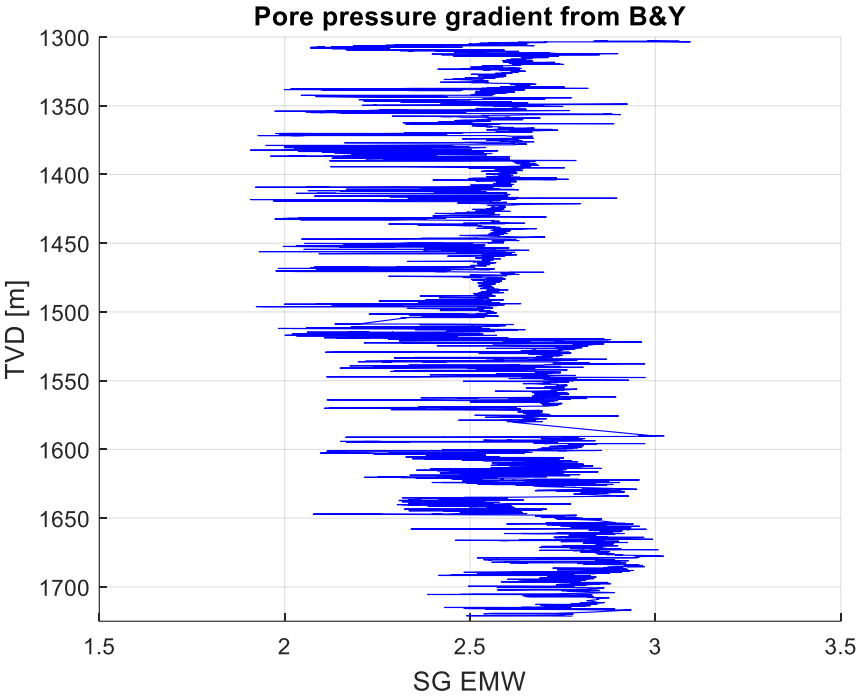
Figure 5.26: Pore pressure plotted vs. TVD for the 17 ½" bit section. The effect of real drillability, represented through a_1 is here neglected. The reference depth D_{ref} is set at 4272 ft TVD (1302 m TVD).

The initial pore pressure results presented in Figure 5.26 shows that pore pressure is calculated too high. If the uppermost part of the 17 ½" section is representable of a normal pore pressure zone, values here should be close to 1.044 SG EMW, the typical North Sea pore pressure gradient. Instead the calculated values are approximately 2.6 SG EMW in the upper region.

These high pore pressure values are caused by the fact that the real drillability, represented through a_1 was neglected. A positive value for a_1 in eqn. (4.12) would have reduced the pore pressure, shifting the graph towards lower values. These results indicate that for obtaining precise values of pore pressure through the Bourgoyne-Young method, the real drillability or a_1, must be determined.

Also, the reference depth, D_{ref}, was here set as 4272 ft TVD (1302 m TVD). This was an assumption, ensuring it would be positioned in a normal pore pressure zone. Ideally, D_{ref} should be located just slightly above the transition zone, marking the lowest depth with normal pore pressure before the pore pressure starts increasing. According to Figure 5.26, it may seem like the transition zone is located closer to 1500 m TVD, such that D_{ref} was selected too high. However, the pore pressure graph is not steadily increasing towards 1500 m TVD, which would have been natural for a normal

compaction zone (it is rather slightly decreasing). A method for determining D_{ref} and the position of the transition zone will be proposed in the next section.

5.2.2 Determining a_1, D_{ref} and the location of the transition zone

From the initial results in the previous section it is clear that for obtaining precise values for pore pressure, the real drillability, represented through a_1 need to be determined. As well, we need a better method for obtaining D_{ref} and the location of the transition zone. This can be achieved by solving the pore pressure eqn. (4.12) for a_1, while making a few assumptions.

We know that D_{ref} should be situated in the normal pore pressure zone. This means that when the depth is equal to the reference depth, $D = D_{ref}$, the pore pressure should be equal to the normal pore pressure, $\rho_{pore} = \rho_{normal}$. Inserting this into eqn. (4.12), and solving for a_1, yields:

$$a_1 = \log\left(\frac{ROP}{\left(\frac{WOB}{4d_{bit}}\right)^{a_5}\left(\frac{RPM}{60}\right)^{a_6}}\right) + a_4 D_{ref}(\rho_{ecd} - p_{normal}) \qquad (5.1)$$

This expression shows two things. First, a_1 will be a function of the common logarithm of the simplified drillability K = $\frac{ROP}{\left(\frac{WOB}{4d_{bit}}\right)^{a_5}\left(\frac{RPM}{60}\right)^{a_6}}$ at the reference depth. Second, given that pore pressure is equal to the normal pore pressure ($\rho_{pore} = \rho_{normal}$), a_1 is a function of an overbalance factor ($\rho_{ecd} - \rho_{normal}$).

In a normal overbalanced drilling operation, the mud weight (ρ_{ecd}) is chosen close to the pore pressure gradient to optimize penetration rate. This means the overbalance factor ($\rho_{ecd} - \rho_{normal}$) will be relatively small. As such, at the reference depth, D_{ref}, located in the normal pore pressure zone, the second term of eqn. (5.1) is mainly dominated by the depth-value and less so by the overbalance factor.

In the transition zone, as the pore pressure starts increasing to abnormal values, the mudweight is gradually increased. Consequently, there will be a significant overbalance between the ρ_{ecd} and ρ_{normal}, such that the second term in eqn. (5.1) will grow rapidly with depth. This fact was exploited by

126

Bourgoyne and Young, who introduced a more general form of eqn. (5.1) where D_{ref} is replaced by D. They named the parameter the modified drillability, K_{mod}:

$$K_{mod} =$$

$$\log\left(\frac{ROP}{\left(\frac{WOB}{4d_{bit}}\right)^{a_5}\left(\frac{RPM}{60}\right)^{a_6}}\right) + a_4 D(\rho_{ecd} - p_{normal}) = \log(K) + a_4 D(\rho_{ecd} - p_{normal}) \quad (5.2)$$

For $D \leq D_{ref}$, thus in normally compacted formations where $\rho_{pore} = \rho_{normal}$, K_{mod} will follow a normal trendline called $K_{mod-normal}$ which is proportional to the negative slope of a_2. This can be shown by inserting the definition of ROP by the Bourgoyne-Young method given by eqn. (4.11) with $\rho_{pore} = \rho_{normal}$ into the K_{mod} equation in (5.2). This gives:

$$K_{mod-normal} = (a_1 + a_2 D_{ref}) - a_2 D \qquad \text{(for D} \leq \text{D}_{ref}) \qquad (5.3)$$

Equation (5.3) shows that at the reference depth, where $D = D_{ref}$, $K_{mod} = a_1$. From the surface, K_{mod} is decreasing towards this value. However, according to eqn. (5.2), below D_{ref}, K_{mod} will start departing from this normal trendline towards higher values because of the overbalance effect of $(\rho_{ecd}- \rho_{normal})$. This means that a_1, the value of K_{mod} at the reference depth, is the lowest value K_{mod} can have; thus $K_{mod} \geq a_1$. As such, for determining D_{ref}, we are looking for a deflection point for which the K_{mod} curve alters its trend from slightly decreasing (remember; $K_{mod-normal}$ proportional to the negative slope of a_2 = 9.0 x 10^{-5}) to notably increasing.

K_{mod} is plotted against depth in Figure 5.27 below:
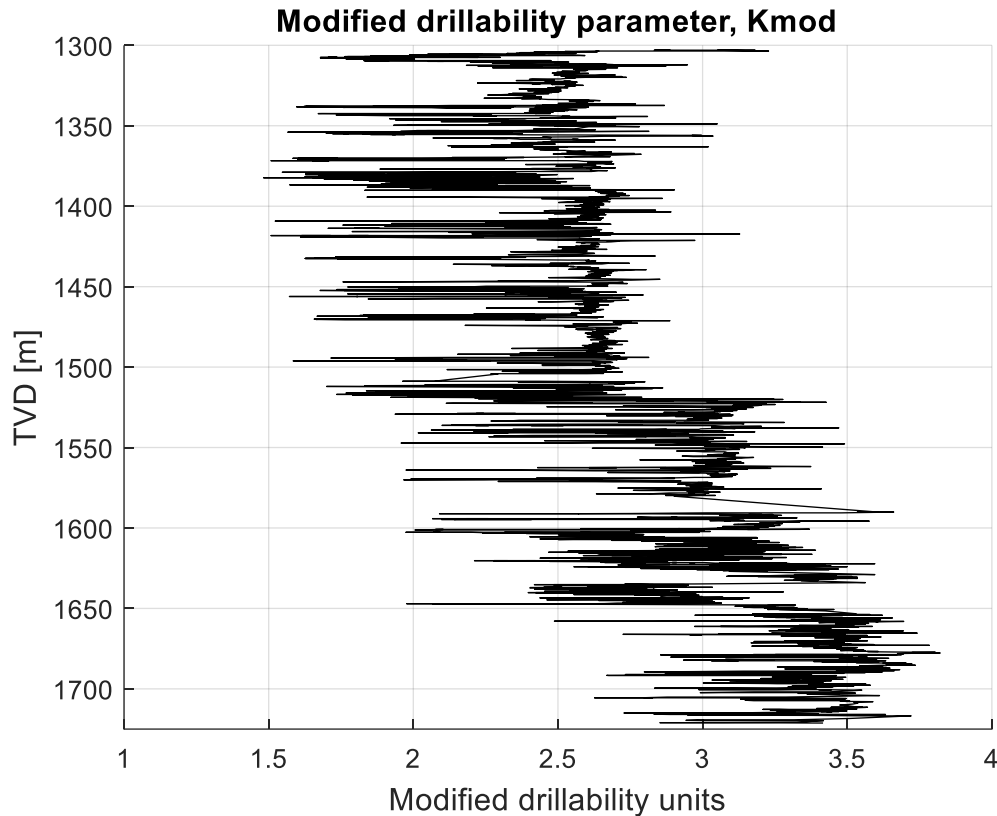
Figure 5.27: Modified drillability parameter, K_{mod}, plotted vs. TVD for the 17 ½" bit section.

From the plot of Figure 5.27 the largest change in K_{mod} is seen around a depth of 1500 m TVD. This was the same observations as for the plot of the initial pore pressure results in Figure 5.26. The change at this depth is even more significant in the K_{mod} plot. However, as was pointed out in the pore pressure plot, in the section above this depth, from 1400-1500 m TVD, K_{mod} is not showing the correct trend. K_{mod} should be slightly decreasing towards the reference depth. Here, as K_{mod} reaches the depth of 1500 m TVD, it is already somewhat increasing, meaning this may not be an optimal reference depth.

Since the K_{mod} is showing a slightly increasing trend between 1400-1500 m TVD, the reference depth presumably should be set at 1400 m TVD or somewhere in the top region between 1302-1400 m TVD. The lowest values of K_{mod} is found in this region, but It is difficult to spot a clearly defined deflection point, as the graph is oscillating between low and high values. There is a decline in K_{mod} from 1310 towards 1330 m TVD, but this decline is too steep given that the normal trendline for K_{mod} is proportional to the negative slope of $a_2 = 9.0 \times 10^{-5}$. There is also very low K_{mod} values from 1380 to 1390 m TVD, but these values are too low compared to the general trend in K_{mod} seen for the rest of the interval in the upper region.

With supplementing data from the 24" section, the trend of K_{mod} should be easier to evaluate as the $K_{mod-normal}$ trendline can be followed from the top of the well down to the deflection point at D_{ref}. Solely based on the K_{mod} results from the 17 ½" section, it cannot be confirmed whether D_{ref} is positioned at the top of the 17 ½" section or near the bottom of the 24" section. In fact, the K_{mod} can be evaluated as having an increasing trend for the whole 17 ½" interval. This may indicate the complete interval is situated within an abnormal pressured zone. However, based on the data available, and to calculate pore pressure, it is necessary to assume that D_{ref} is positioned in the 17 ½" interval.

So, based on the K_{mod} plot, the reference depth (or deflection point of the K_{mod} curve) cannot be determined with any higher accuracy than that it is located somewhere between 1302 and 1400 m TVD. The best option to ensure that D_{ref} is located within a normal pore pressure zone, is to use the initial guess that D_{ref} is positioned at 1302 m TVD, which is at the very top of the section.

The penetration rate can also be utilized to estimate where the transition zone is located. This is however a less than optimal approach because there are more variables involved. Changes in these variables can mask the effect of changing lithology or increasing formation pore pressure. However, penetration rate can be used as a second-order tool in conjunction with the obtained results for hardness and modified drillability. In Figure 5.28 penetration rate (dBPOS) is plotted for the 17 ½" bit section with formation boundaries also drawn:
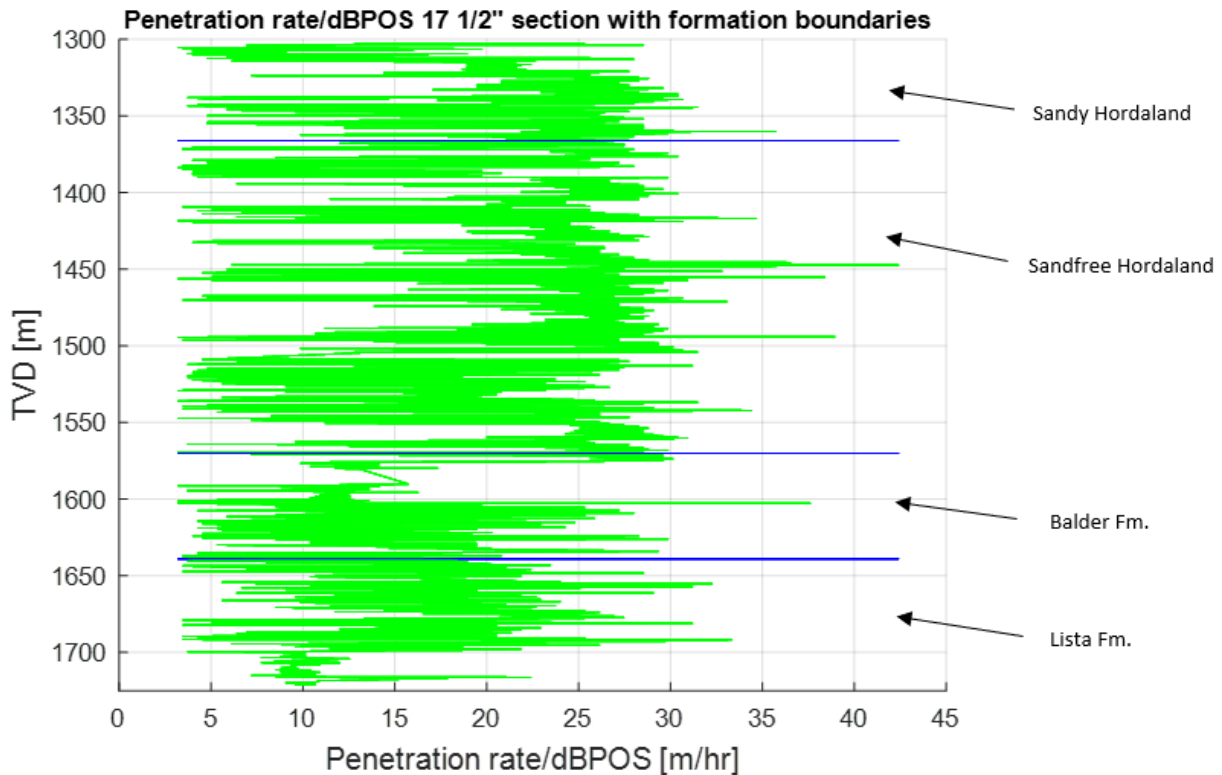
Figure 5.28: Penetration rate (dBPOS) plotted vs. TVD for the 17 ½" bit section. Blue lines are formation tops for the Sandfree Hordaland, Balder and Lista formations.

From Figure 5.28, it is observed high values of penetration rate from the top of the 17 ½" section down towards the top of the Balder formation at 1570 m TVD. According to the K_{mod} plot in Figure 5.27, pore pressure continues to increase rapidly below this depth. This may indicate that the reduced penetration rates in the Balder and Lista formations can be attributed to other factors, as increasing pore pressure in theory should have an increasing effect on the penetration rate. However, based on the hardness plot in Figure 5.25, the reduced penetration rate cannot be caused by changes in the formation hardness, as these formations have very low average hardness. It is possible that factors such as bit wear or reductions in WOB and RPM have attributed to the low drilling rate in the Balder and Lista formations.

Increases in penetration rate are associated with changing lithology, especially those changes caused by formation hardness and pore pressure (which includes the effect of overbalance and under-compaction). The only lithology boundary within the 17 ½" interval which is not located in or below the transition zone, as indicated by K_{mod}, is the boundary between the Sandy Hordaland and Sandfree Hordaland formation. This boundary is located at 1366 m TVD according to the FWR. This lithology change is likely what cause the increase seen in K_{mod}. The penetration rate is also high throughout the Sandfree Hordaland formation. However, the hardness values are higher here than in both the Lista

130

and Balder formations, with several peaks in hardness. This may indicate that the increased pore pressure is the main cause for the high penetration rates in the Sandfree Hordaland formation.

If assuming the start of the transition zone corresponds to the depth of the Sandy Hordaland-Sandfree Hordaland boundary, D_{ref} can be set to 1366 m TVD. Inserting this value for D_{ref} in eqn. (4.3) gives $a_1 = 2.63$. Note that during this calculation, to avoid anomalies, this was the average value of six different a_1 values taken for depth points within one meter above and below 1366 m TVD. Another method for obtaining a_1 would be to read of the graph of K_{mod} at D_{ref}, but this is a less precise method. However, it is required to check the graph of K_{mod}, to avoid selecting D_{ref} and a_1 at a point where there is a spike in the K_{mod} values.

5.2.3 Final pore pressure results

Having decided the reference depth D_{ref} and the real drillability factor a_1, it is now possible to calculate pore pressure more accurately. First, to help evaluate the results, it is useful to re-write the pore pressure formula in eqn. (4.12). Substituting the definition of K_{mod} given by eqn. (5.2) into the pore pressure equation, gives:

$$p_{pore} = p_{normal} + \frac{K_{mod} - a_1 - a_2(D_{ref} - D)}{a_3 D^{0.69} + a_4 D}$$

$$= p_{normal} + \frac{\log(K) + a_4 D(\rho_{ecd} - p_{normal}) - a_1 - a_2(D_{ref} - D)}{a_3 D^{0.69} + a_4 D} \tag{5.4}$$

These expressions highlight that the pore pressure is equal to the normal pore pressure gradient and a term which is dominated by the difference between the modified drillability K_{mod} and the real drillability factor a_1. For $D \leq D_{ref}$, K_{mod} should follow the normal compaction trendline, $K_{mod\text{-}normal}$, meaning $K_{mod} = K_{mod-normal} = (a_1 + a_2 D_{ref}) - a_2 D$. Inserting this into eqn. (5.4) means the second term is canceled and $\rho_{pore} = \rho_{normal}$ for all values of $D \leq D_{ref}$. However, note that this represents an idealistic situation.

The term $a_2(D_{ref}-D)$, which accounts for the effect from rock strength increases due to normal compaction with depth, will become positive inside the abnormal pressured zone where $D > D_{ref}$. However, its effect on pore pressure in the Bourgoyne-Young method is small compared to the effect of changes in the other variables such as drillability and mudweight.

In Figure 5.29, pore pressure is plotted against TVD using D_{ref} = 1366 m TVD and a_1 = 2.63:
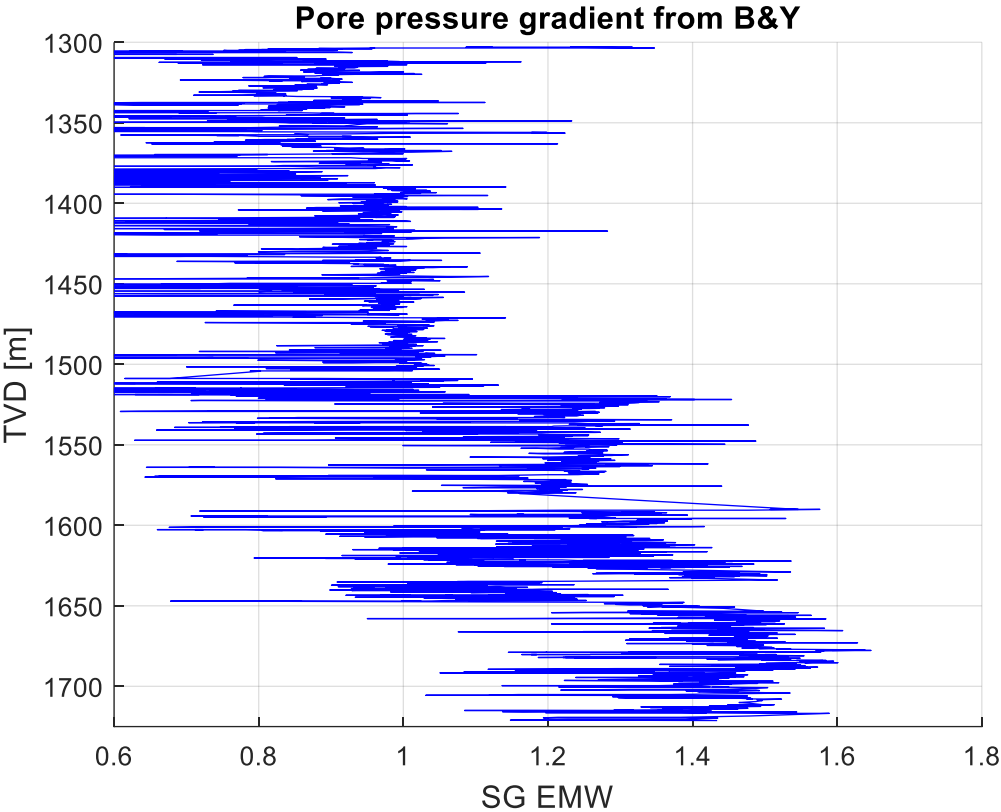
Figure 5.29: Pore pressure plotted vs. TVD for the 17 ½" bit section. The reference depth D_{ref} is set at 4482 ft TVD (1366 m TVD) and the real drillability parameter a_1 to 2.63.

The pore pressure results of Figure 5.29 are an improvement of the initial results of Figure 5.26. This can be seen by the range of the pore pressure values, now situated from about 0.9 at the top of the 17 ½" interval to 1.5 at the bottom (if neglecting negative and positive spikes). However, in the top region from 1300-1400 m TVD, the pore pressure is estimated very low compared to the region 1400-1500 m TVD situated below. It is also unstable in this area, oscillating from negative to positive values. The K_{mod} had the same type of behavior in the top region, but the negative spikes are even more noticeable in the pore pressure plot. This is attributed to the pore pressure readings sensitivity to the $(K_{mod}-a_1)$ factor. A sudden reduction in drillability, means K_{mod} can become significantly lower than a_1, which will yield negative and abnormal pore pressure readings lower than the ρ_{normal}.

The pore pressure results can be compared with those found in the FWR. In Figure 5.30, pressure gradients from the FWR in addition to mudweight (ρ_{ecd}) from the RTDD is plotted vs. TVD
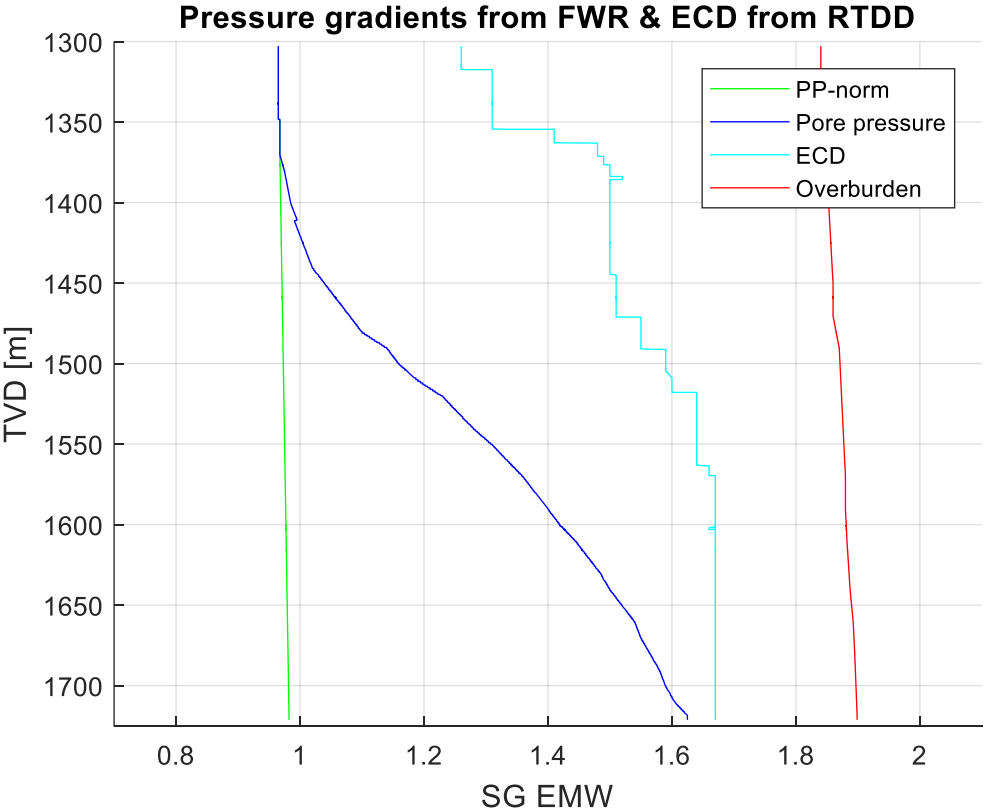
Figure 5.30: Pressure gradients from the final well report plotted vs. TVD for the 17 ½" bit section. ECD from the RTDD is also shown.

From this, two things can be observed. First, below the reference depth at D_{ref} = 1366 m TVD and in the zone of abnormal pore pressure, the pore pressure is estimated too low. For example, at 1550 m TVD the calculated pore pressure is about 1.2, while it should be closer to 1.3 according to the FWR. This should be attributed to that the a_1 was set too high. Second, above 1366 m TVD, where it is reported a normal pore pressure regime in the FWR, it has been made changes in the mud density with ECD going from 1.26 to 1.48 SG EMW.

Substantial increases in mudweight is natural in the abnormal pressured zone and affects the K_{mod} parameter, $K_{mod} = \log(K) + a_4 D(\rho_{ecd} - p_{normal})$. This again, will affect the pore pressure readings. Above the reference depth, K_{mod} should ideally follow the $K_{mod-normal}$ trendline, decreasing with the slope of -a_2, before being equal to its minimum value of $K_{mod-min}$ = a_1 as it reaches the reference depth. However, if noteworthy increases are made to the mudweight in a normal compacted zone, such that the overbalance (ρ_{ecd}- ρ_{normal}) becomes substantial, K_{mod} will be recorded

too high and the accuracy of the straight-line representation of $K_{mod-normal}$ for D < D_{ref} diminishes. It was not possible to spot any turning point for the K_{mod} in the upper region, and this change in ECD may have attributed to this, along with the many negative spikes in drillability.

Thus, it cannot be confirmed that the section above 1366 m TVD is a normally pressured zone, such as stated in the FWR. The most secure option is therefore to set the reference depth at 1302 m TVD, located at the very top of the 17 ½" section, where it is the highest probability that a normal compacted zone is found. This depth was selected for the initial pore pressure results of Figure 5.26. However, the initial calculations were done without the a_1 factor. The K_{mod} is oscillating heavily at this point, making it impossible to decide the a_1. A more stable part of the graph must be chosen. From 1312-1334 m TVD, there is a section where K_{mod} is decreasing steadily from 2.6 to 2.4. Using the average of these values, meaning setting D_{ref} = 1323 m TVD and a_1 = 2.5, is a valid approach as this the most stable interval found in the upper region. The 2.5 value is also an appropriate average for K_{mod} from 1323 m down to 1400 m TVD. In Figure 5.31 the pore pressure has been recalculated with these modifications. The figure also shows the normal pressure trendline and pore pressure gradient taken from the FWR.
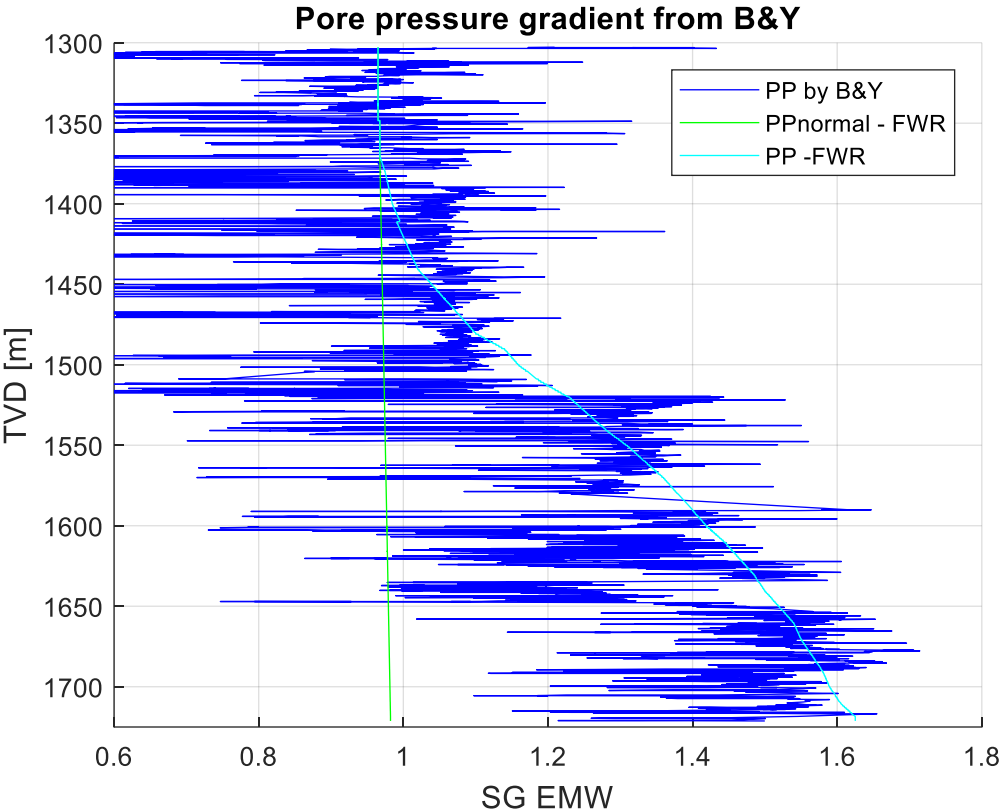
Figure 4.7: Pore pressure calculated by the Bourgoyne-Young method plotted vs. TVD for the 17 ½" bit section. The reference depth D_{ref} is set at 4341 ft TVD (1323 m TVD) and the real drillability parameter a_1 to 2.5. The normal pore pressure gradient and pore pressure gradient from the FWR is also shown.

The final pore pressure result is somewhat compatible with that of the FWR. However, the result is characterized by the highly fluctuating values. These oscillations are correlated both to sudden changes in hardness and other drilling parameters, such as the WOB. The effect of these changes on the result will be discussed in in the next chapter.

6 Study of Hardness vs. Lithology and Hardness vs. Pore Pressure

In this chapter the results from the previous chapter will be utilized to study the relation between hardness and lithology changes, as well as the effect of hardness vs pore pressure on penetration rate.

6.1 Comparing hardness with lithology

Having obtained the hardness results, the lithology described in section 3.2 can now be compared with the hardness by drawing formation boundaries. Changes in hardness caused by a lithology change should be possible to detect from the hardness graph.

The position of the formations in Well C-47 are described in Figure 6.1 below, taken from the FWR.

Formation	Measured Depth	True Vertical Depth [m MSL]	TVD deviation from prognosis
Top Utsira Fm.	995	882	+4
Top sandy Hordaland	1050	927	
Top sandfree Hordaland	1655	1282	
Top Balder Fm.	2050	1486	-1
Top Lista Fm.	2200	1555	
Top Shetland Gp.	2411	1655	-6
Top Kyrre Fm.	2833	1842	
Top Krans Mb.	2892	1865	+11
Top S10	2929	1878	+13
Top S9	3028	1914	N/A
Top S8	3047	1920	+20
Top S7	3058	1925	N/A
Top S6	3075	1930	N/A
Top S5	3150	1957	N/A
Top S3	3202	1973	N/A
Top S2	3810	2000	+40
Top S2/Base S3	4220	1994	+4
TD	4399	1982	+2

Figure 6.1: Formation tops with measured depth and true vertical depth for Well C-47. TVD deviation from prognosis is also shown. (Christophersen, Gjerde and Valdem, 2007).

To simplify matters, only the formations within the 17 ½" section will be chosen for interpretation. The 17 ½" section is positioned from 1495-2380 m MD. This means that formation boundaries for top Sandfree Hordaland, top Balder Fm. and top Lista Fm., can be drawn.

Figure 6.2 below shows a hardness plot for the 17 ½" section with drawn formation boundaries.
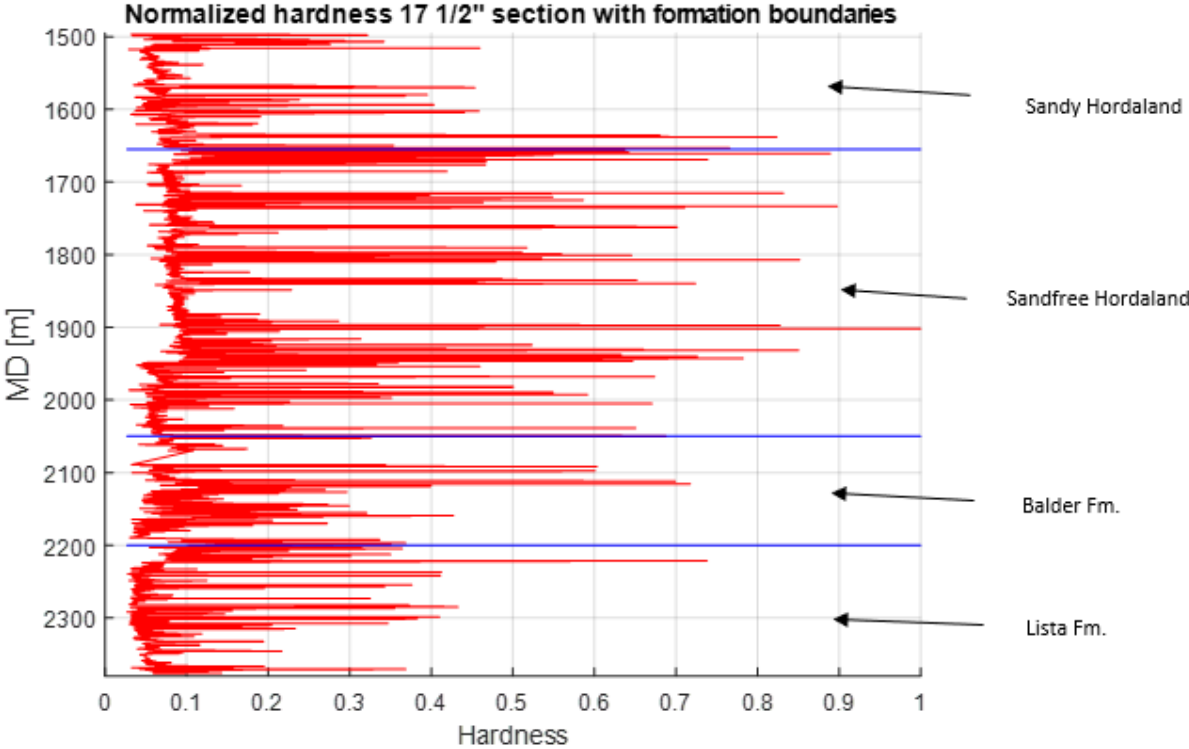
Figure 6.2: Normalized hardness (red graph) plotted vs. measured depth for the entire 17 ½" bit section. Blue lines are formation tops for the Sandfree Hordaland, Balder and Lista formations.

The first or uppermost formation top representing the transition between the Sandy Hordaland and Sandfree Hordaland formations were in fact studied in the previous chapter, as it is located within one of the selected intervals, namely Section 4. So, this lithology change should explain the increase in hardness and oscillating hardness values which were observed while studying Section 4. Figure 6.3 shows a hardness plot from Section 4 which highlights the top position of the Sandfree Hordaland formation.
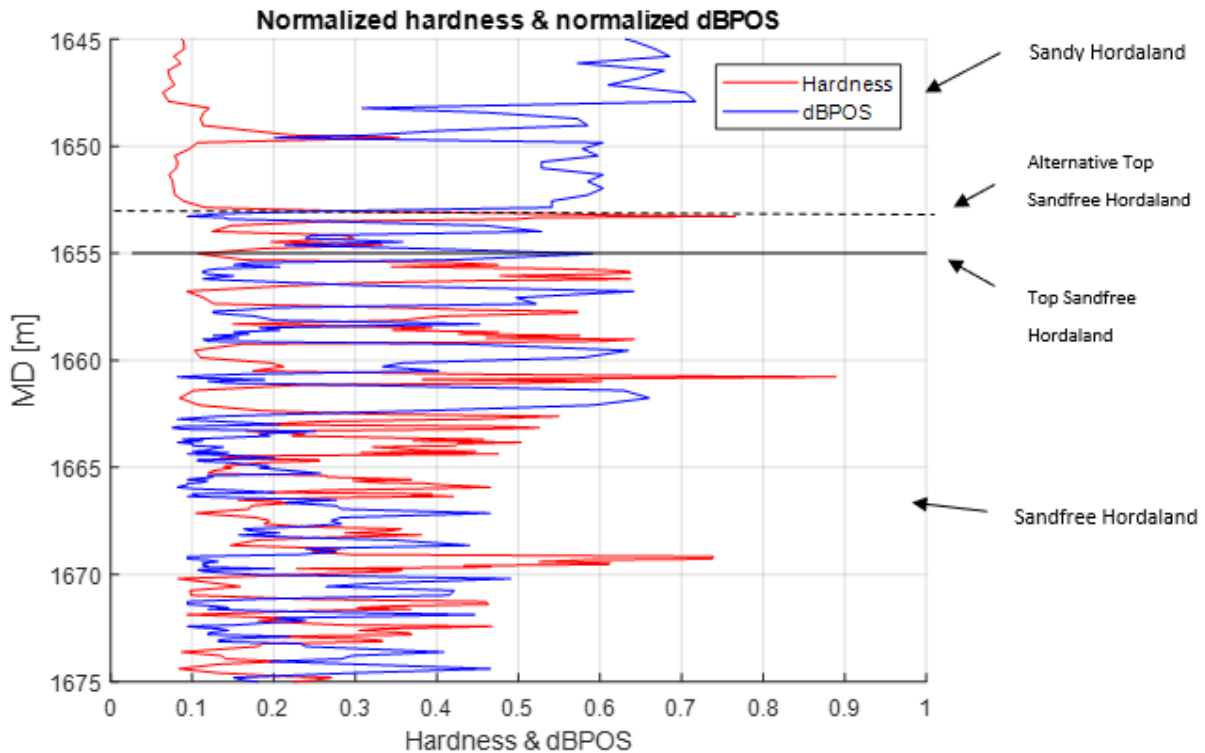
Figure 6.3: Normalized hardness (red graph) and dBPOS (blue graph) plotted vs. measured depth for the interval 1645-1675 m MD (Section 4). Black solid line is the formation top for the Sandfree Hordaland formation. Black dashed line shows an alternative formation top.

The boundaries of the formation are located at 1655 m MD according to the FWR, however, an alternative formation top can be drawn at 1653 m MD. This boundary shows better correlation with the hardness and dBPOS graphs.

When entering the Balder formation there is no distinctive change in formation hardness. This can be seen in Figure 6.4, which shows hardness and dBPOS plotted versus measured depth for the interval 2000 – 2100 m MD. This is perhaps expected as the Balder formation, like the Sandfree Hordaland formation above, is also mostly consisting of claystones. The top Balder formation boundary is positioned at 2050 m MD, however the boundary could be positioned 10 meters further down at 2060 m MD, as there is a small increase in hardness and notable decrease in dBPOS at this position. The slow decrease of hardness (or slow increase of dBPOS) at 2070 m MD is not related to any lithology changes, but to a 5-day stop in drilling caused by a downhole problem reducing the directional response of the rotary steerable system (RSS). The hole later packed off which required backreaming (this problem is described in detail in the final well report).
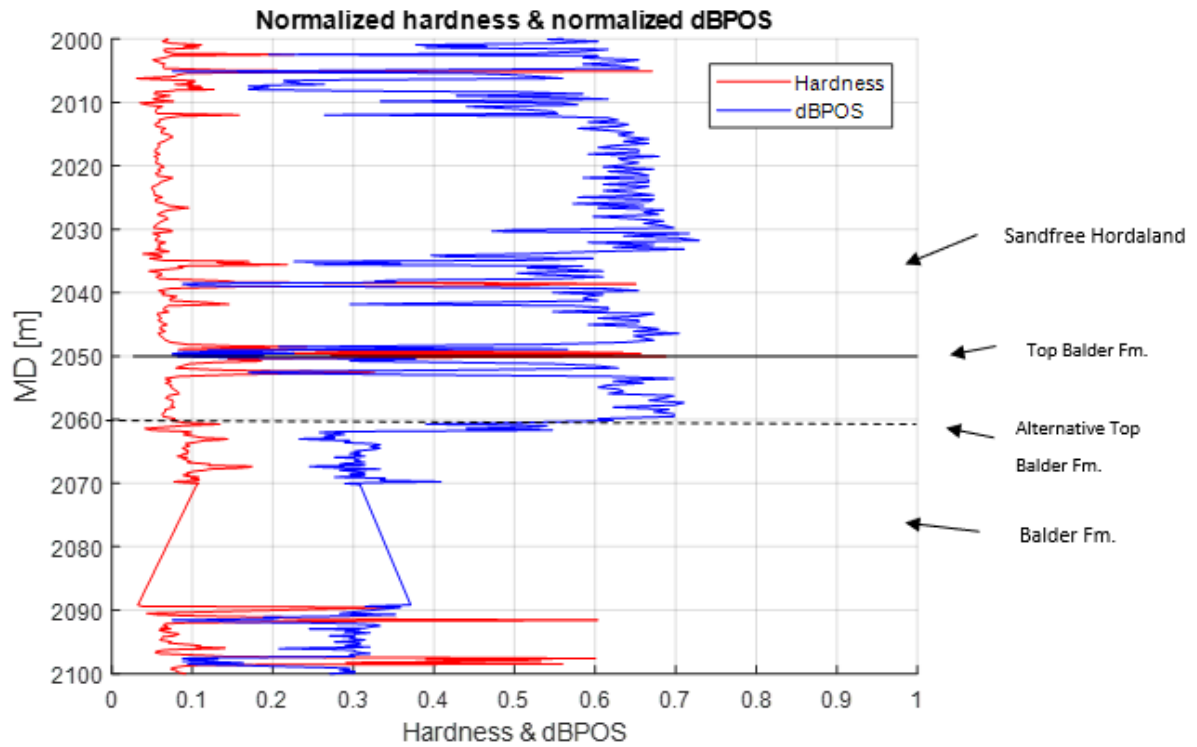
Figure 6.4: Normalized hardness (red graph) and dBPOS (blue graph) plotted vs. measured depth for the interval 2000 – 2100 m MD. Black solid line is the formation top for the Balder Fm. Black dashed line shows an alternative formation top.

Finally, the boundary between the Balder Fm. and Lista Fm. will be investigated. Figure 6.5 shows the boundary for the top Lista Fm.
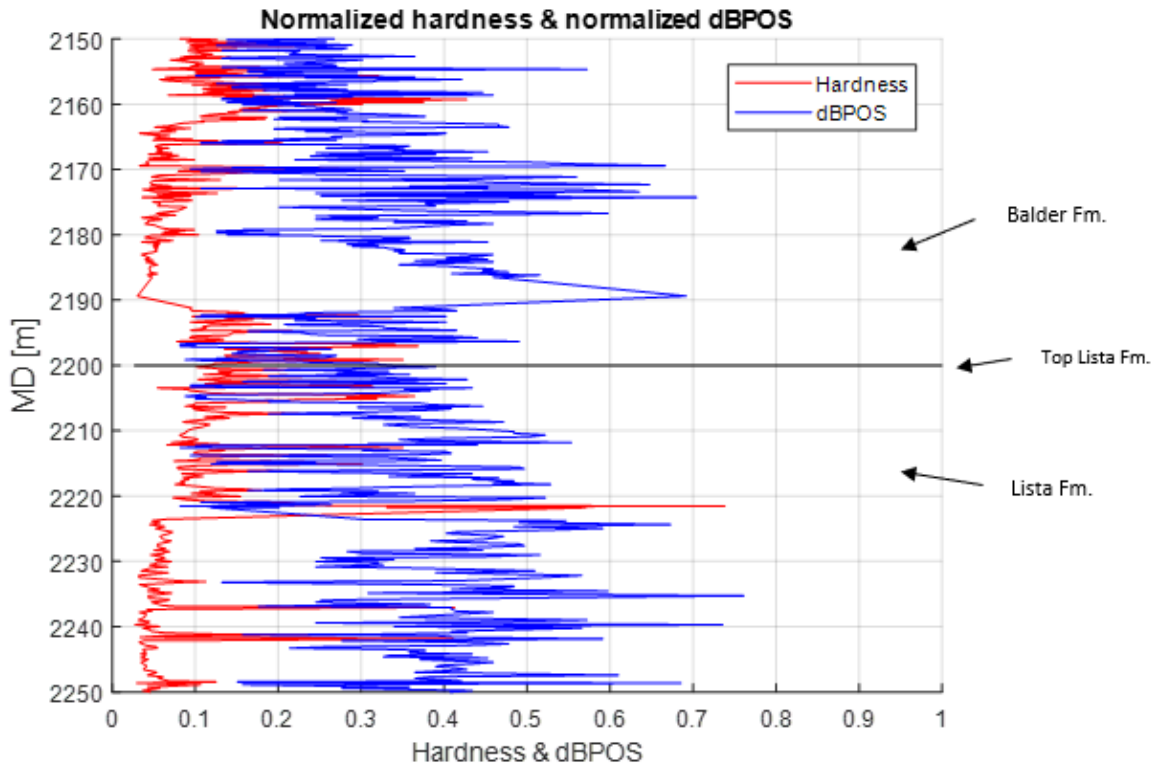
Figure 6.5: Normalized hardness (red graph) and dBPOS (blue graph) plotted vs. measured depth for the interval 2150 - 2250 m MD. Black solid line is the formation top for the Lista Fm.

During the transition into the the Lista Fm. there is a lot of oscillations in the hardness and dBPOS values. This makes It difficult to draw any alternative formation top, so this step has been omitted for this last boundary. After the transition interval, the hardness is again stabilized and is comparable to the hardness of the Balder Fm. above, so no noticeable difference in hardness has occurred when entering the Lista Fm.

6.2 Effect of formation hardness vs. pore pressure on penetration rate

In this section the obtained hardness and pore pressure results will be evaluated to see if there is a correlation with the ROP. The method used dissects the 17 ½" interval into the top region and the lower region. The top region is situated from 1302-1400 m TVD, where normal pore pressure is found above 1366 m TVD according to the pressure regime in the FWR. The lower region is from 1400 – 1724 m TVD, thus inside the transition zone having abnormal pressure.

6.2.1 Top region (1302-1400 m TVD)

The normal pore pressure zone in the top region coincides with the bottom part of the Sandy Hordaland formation. This section was studied in detail (Section 1 and 4 from the hardness study) and several hard stringers were identified. However, the general hardness of the zone is relatively low, as can be seen in the hardness plot of Figure 6.2. It also has high average penetration rate, as seen in Figure 6.3. In Figure 6.6, normalized data for hardness, pore pressure and penetration rate (dBPOS) are plotted for the top region from 1302 – 1400 m TVD.
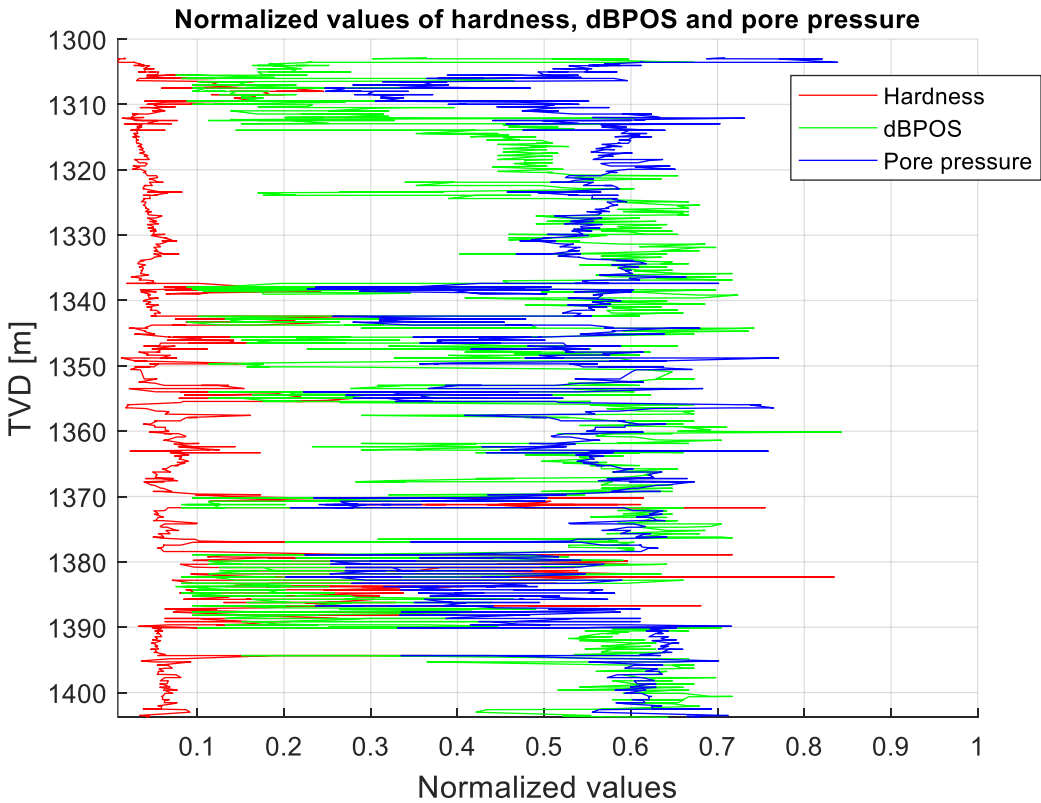
Figure 6.6: Normalized values of hardness, penetration rate (dBPOS) and pore pressure plotted vs. TVD for the 1302-1400 m TVD interval of the 17 ½" bit section.

It was experienced difficulties in determining the reference depth and a_1 in the top region as there was a lack of a clear turning point in the modified drillability parameter signaling a shift from a normal compacted zone with hydrostatic pressure towards an under-compacted zone with abnormal pore pressure. The unstable K_{mod} can be attributed to that the hard stringers found here induce sudden decreases in drillability. As well the mudweight was raised, which also affects the K_{mod}.

Testing the method along with data from the 24" interval would probably make the job of determining a reference depth and a_1 easier. The top section of a well is normally drilled in an

141

interval of normal pore pressure with constant mud weight. This means K_{mod} is likely to follow the $K_{mod-normal}$ trendline from the top of the well down to the abnormal pressured zone, where it starts increasing. Seeing the "bigger picture" would therefore make it easier to spot the exact depth of the turning point in the K_{mod} graph. With data from the 24" interval it would also be possible to exert the option of setting the reference depth higher, inside the lower part of the 24" interval, given a zone of stable K_{mod} could have been found there. Ideally there is very little change in K_{mod} in the last few 100 meters of the bottom part of the normal compacted zone (K_{mod} is here decreasing with the slope of -$a_2 = 9.0 \times 10^{-5}$) before it starts increasing when entering the transition zone. By setting D_{ref} higher, this problem zone protruded with hard stringers just above the transition zone would have been avoided in the process of determining a_1.

According to Bourgoyne et. al, such problem zones just above the transition zone to a higher formation pore pressure gradient are frequently encountered: "These formations are hard, often limey and yields a lower-than-normal penetration rate. Many people feel that these formations are extremely low permeability formations that form the pressure seal for the abnormal pressure gradients. These seals may vary in thickness from a few feet to several hundred feet" (Bourgoyne et. al, 1986). These statements are in line with the experienced results. Supplemented with the presence of calcium carbonite (CaCO), the high-pressure conditions existing in these caprocks will be ideal for the formation of ROP-reducing hard stringers.

The fluctuating and high hardness, with corresponding fluctuating and low pore pressure and penetration rate between 1380-1390 m TVD, may indicate such a seal which Bourgoyne et. al. is referring to. The WOB was also increased and the RPM reduced in this 10-meter interval (see Figures 6.8 and 6.9 in the next section). The interval is too thick to be considered a hard stringer, as the thickness of hard stringers may vary from half a meter up to two meters (Personal comments, Skalle, 2016). If this is a major seal, it may be the real boundary between the Sandy and Sandfree Hordaland formations. However, this is not in accordance with the information in the FWR, which sets the boundary at 1366 m TVD. How the process of setting this depth was done by the operating company is unknown. According to the FWR there is not reported any drilling incident between 1380-1390 m TVD, which may confirm whether these are anomalies. There is one incident situated at 1347 m TVD which may have had an effect which has carried over to this interval, as drilling continued from 1347 to 1453 m TVD. The reported incident at 1347 m TVD was: "Power drive hold inclination "hold inclination" mode not working. Communication with power drive improved during the night".

The effect of hard stringers on penetration rate is seen in Figure 6.6. Assuming there is a normal pore pressure regime above 1366 m TVD, as according to the FWR, it must be the hard stringers situated at 1307, 1338 and 1343 m TVD, that are affecting the penetration rate, not the pore pressure. When the hard stringers are passed, the pore pressure quickly retract back to a steady baseline of about 0.5-0.6. The penetration rate also moves back to baseline, although not as quick as the pore pressure.

6.2.2 Lower region (1400-1724 m TVD)

When entering the transition zone, pore pressure starts increasing from the baseline of 0.6. This is seen in Figure 6.7, where normalized data are plotted for the bottom region from 1400 – 1724 m TVD. From 1400, until about 1500 m TVD, all parameters, including the hardness (high values of WOB), are slowly increasing. This must indicate that the pore pressure, and the overbalance effect, has the largest effect on penetration rate in this interval. This can also be seen by studying the hardness graph of Figure 5.25 with the modified drillability parameter of Figure 5.27 for this interval; both parameters are slowly increasing.
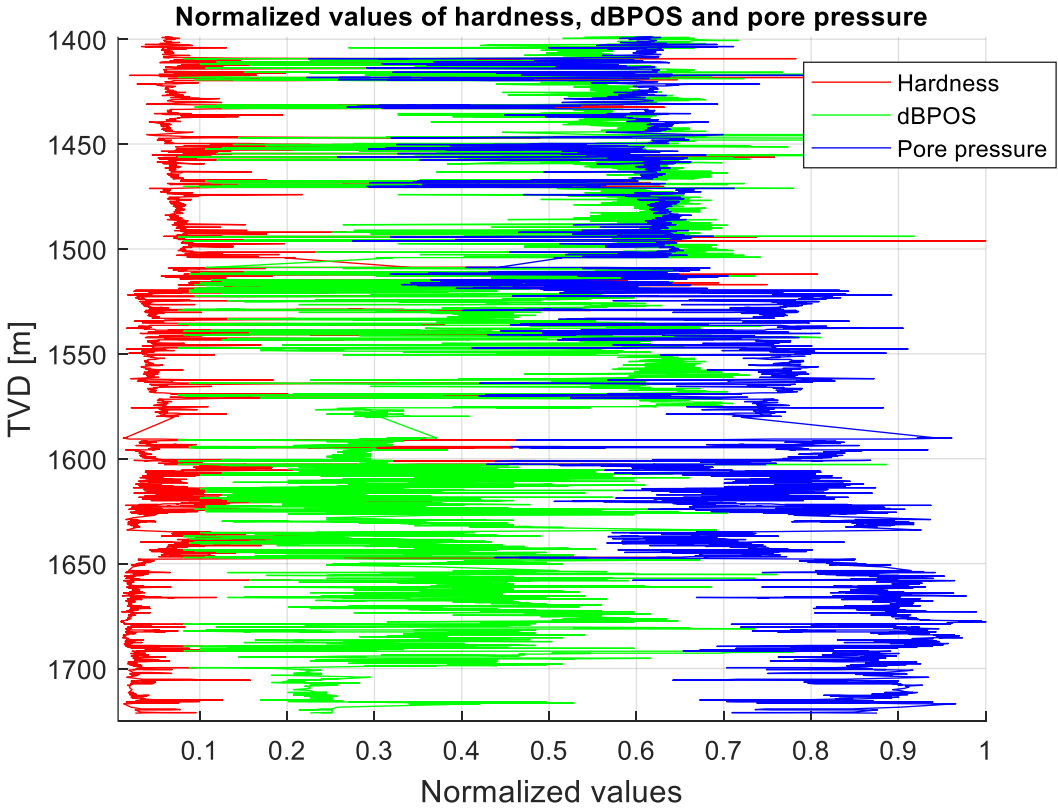
Figure 6.7: Normalized values of hardness, penetration rate (dBPOS) and pore pressure plotted vs. TVD for the 1400-1724 m TVD interval of the 17 ½" bit section.

143

The penetration rate and pore pressure look normal down to 1500 m TVD, considering this is in the start of the transition zone. Slightly below this depth, at 1520 m TVD, there is a notable reduction in penetration rate, and jumps both in the computed hardness (reduced) and pore pressure (increased). There are heavy oscillations inn all parameters until they are stabilized again at 1550 m TVD. According to the FWR, there is reported an incident of "Erratic torque/stalling of the top drive" in the 1520-1550 m interval. The RPM is increased from 180 to 200 during this interval as seen in Figure 6.8:
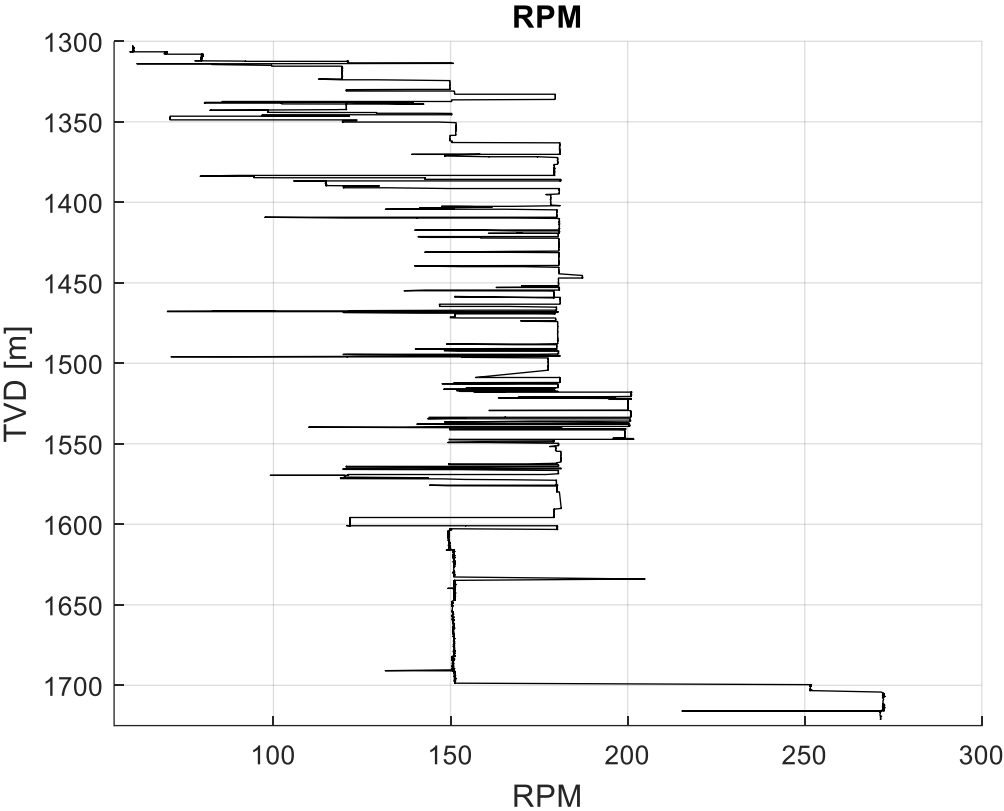
Figure 6.8: RPM plotted vs. TVD for the 1302-1724 m TVD interval of the 17 ½" bit section.

This incident, leading to increased and unstable RPM can somewhat explain the heavy oscillations in the ROP, hardness and drillability between 1520 – 1550 m TVD. However, it cannot explain the severe reduction seen in penetration rate and subsequent jumps in the hardness and pore pressure graphs at these depths. As seen in Figure 6.9, the WOB was, as the ROP and pore pressure, slowly increasing towards 1520 m TVD:

144
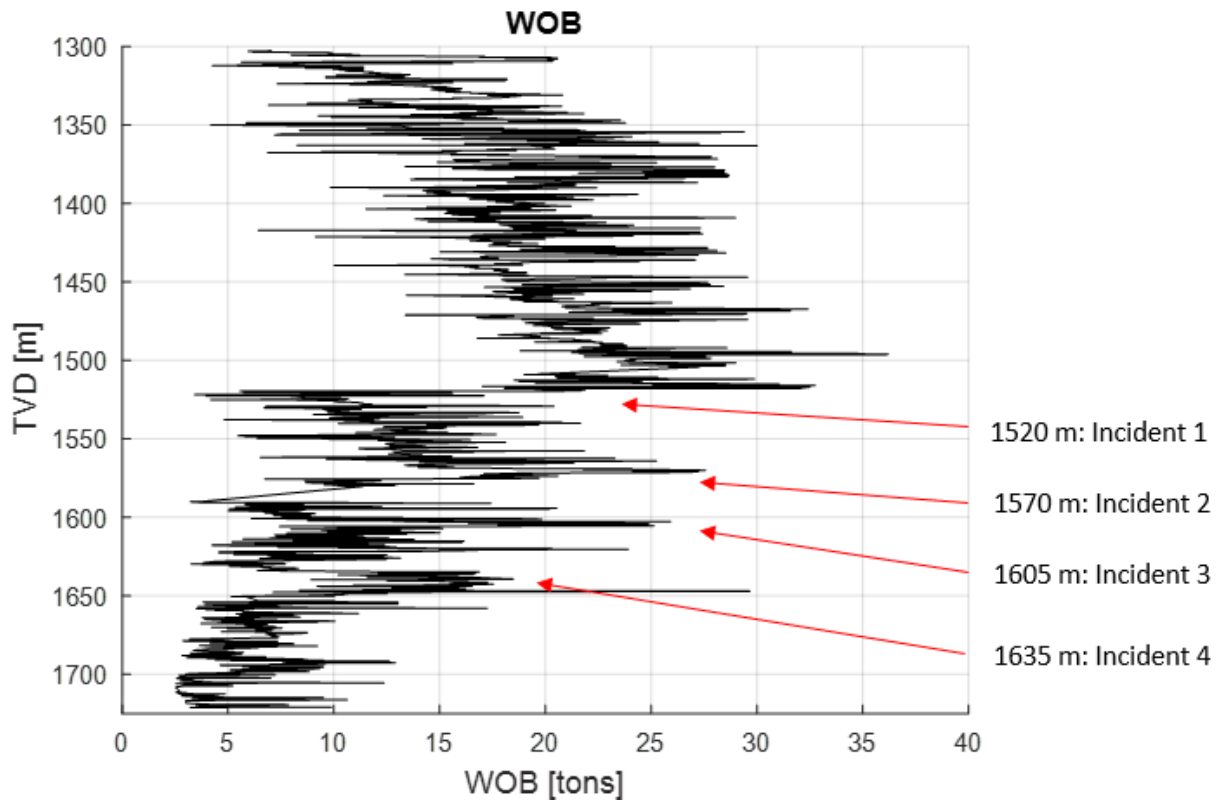
Figure 6.9: WOB plotted vs. TVD for the 1302-1724 m TVD interval of the 17 ½" bit section. Depth of drilling incidents are indicated.

The WOB is notably reduced at 1520 m TVD, slightly increasing towards 1570 m TVD, before being reduced again at 1570 m TVD. From here it is slowly increasing towards 1605 m TVD, where it peaks. Thereafter it is reduced in steps towards very low weights at the bottom of the 17 ½" section, except at the position of incident 4 from 1635-1650 m TVD, where it remains high. The reduction in WOB at 1520 m TVD from about 25 to 10 tons, severely reduces the penetration rate. This explains the jumps seen in both hardness (lowered) and pore pressure (increased) at this depth. After 1550 m TVD, when the RPM is brought down from 200 to 180 again, the ROP is again stabilized, and continues to increase towards 1570 m TVD.

At 1570 m TVD, there is then reported another incident: "…lack of directional response from power drive". This required POOH to change the BHA, an operation which took several days as the hole packed off and backreaming was required. After this second incident at 1570 m TVD, WOB is reduced, and stable and increasing until 1605 m TVD where a third incident strikes: "Not able to follow planned well path. POOH with 17 ½" RSS BHA. Found failure on RSS…". This incident gave a spike in the WOB readings at 1605 m TVD, giving also very notable changes in the hardness and pore pressure graphs.

From 1605 m TVD the WOB is then kept at a low weight and is relatively stable until 1635 m TVD, where a fourth and final incident occurs: "Had washout on discharge module on MP 1 cylinder 2. Started to change same. Meanwhile circulated/backreamed to improve hole cleaning". The WOB is here increased and staying so until 1650 m TVD, which also gives increased values in hardness and decreased values in pore pressure for these depths.

The effect these four drilling incidents has on WOB, which again affects penetration rate, hardness and pore pressure, makes it difficult to evaluate the effect of hardness vs. pore pressure on penetration rate in the abnormal pressure zone. Particularly, the first incident at 1520 m TVD, where WOB is reduced from about 25 to 10 tons, making penetration rate drop significantly, disrupts the natural development or expected increase in penetration rate most often seen in an abnormal pressured zone because of the overbalance effect. By studying Figure 5.30, it is observed that the (ρ_{ecd}-ρ_{pore}) factor becomes smaller with depth in the abnormal pressure zone, such that it was expected the ROP would increase continuously with depth. Instead, because of the reduced WOB in the lowermost part of the section, the penetration rate is kept very low.

This is a signal that it is the effect of the overall reduction in WOB rather than the increase in ROP, which has led to the produced hardness and pore pressure results in the lowermost section. This can also be seen by the low average hardness and low ROP in the Balder (1570 – 1639 m TVD) and Lista (1639 – 1724 m TVD) formations compared to the high pore pressure. In a more normal situation, the penetration rate would also have been high.

Whether this reduction in WOB was planned or not, to perhaps lower wear on the BHA or decrease energy input, the reduced WOB has certainly affected the hardness and pore pressure results in the abnormal pressure zone. According to Skalle (personal comments, 2018), the reduction in WOB was more likely done to reduce production of cuttings. Whatever the cause, the reduction in WOB made it difficult to evaluate the effect of hardness and pore pressure on penetration rate. However, from 1400 – 1500 m TVD, at the start of the transition zone and before the sudden decrease in WOB, it was possible to spot the overbalance effect on penetration rate. This was indicated by an increase in all parameters; hardness (because of high WOB), modified drillability, pore pressure and penetration rate. In the top region above 1366 m TVD, inside the normal pressured zone, the effect of hardness on penetration rate could be seen. This was shown through hard stringers, which caused negative spikes in hardness and penetration rate, thus also affecting the pore pressure. However, the pore pressure moved quickly back to the normal and steady baseline values it had before the depth of the hard stringer. The stable pore pressure signals it was the spike in hardness rather than changes in pore pressure which caused the change in penetration rate in the normal pressure zone.

7 Discussion

The obtained results indicated that both hardness and pore pressure can be quantified based on a simplistic approach to the Bourgoyne-Young method. However, the results also show that when the drilling process is disrupted, such that the recorded input parameters become irregular, the pore pressure method will not produce accurate results.

7.1 Hardness model

During the work done in this thesis, hard stringers were identified in bit section 17 ½" of Well C-47. This was done by first looking at log data using a qualitative model and then computing drillability and hardness through a simplified (quantitative) model of the Bourgoyne-Young drilling equation (eqn. 4.1ii). Real-time drilling data provided by Statoil were used as input parameters in both models. The original Bourgoyne-Young drilling equations requires several input parameters which were not possible to obtain and the equation in full is quite complex. The simplifications done to the equation to obtain the results in this thesis will be discussed below. Results obtained using the simplified equation will also be discussed. Finally, the correlations between hardness and lithology have been evaluated.

7.1.1 Quality of mathematical model

7.1.1.1 Derivation of model

The quality of the results obtained are related to the quality of the mathematical (quantitative) model. The mathematical model has been developed using a quite simplistic approach, however improvements can be made to make the model more realistic and thus reflect real world drilling operations.

The original Bourgoyne-Young drilling equation is as mentioned above quite complex, with a large range of drilling parameters and formation exponents. After evaluation of available data and what variables would have an immediate effect on penetration rate, only those which were a function of WOB and RPM were considered essential to model the hardness. Thus, only the formation exponents related to the WOB and RPM were needed in the final simplified equation (eqn. 4.1ii). At its most

simplistic form only one set of formation exponents were used to calculate hardness, this being the average formation exponents based on the extreme of the ranges, taken from eqn. (4.3) and (4.4).

The effect of bit weight on ROP, is as mentioned essential and therefore included in the simplified model. However, the parameter called threshold bit weight factor, $\left(\frac{WOB}{d_{bit}}\right)_t$, was considered insignificant. This factor represents the minimum weight on bit to produce cuttings and can be neglected in relatively soft formations. For harder formations, it can be computed with the help of drilloff test data, but since no such data were available, the factor was overlooked in the drillability calculations.

Bit selection, bit performance and bit failure were discussed in section 2.1.2.1 b). The effect of tooth wear on penetration rate is important as it can lead to a significant reduction in penetration rate. However, the wearing process is gradual and will not affect sudden changes in hardness. This, including the lack of available data on the parameter fractional tooth dullness (h), lead to that the effect of bit wear was neglected in calculations. The effect of bit hydraulics on penetration is also not being considered in the final equation. This was also due to lack of available data, as the parameter hydraulic impact force beneath the bit (F$_j$) could not be obtained.

The effect of overbalance, together with the variables caused by drillability, bit weight and rotary speed has been shown to be of importance for immediate changes in penetration rate. As such, the factor of overbalance should ideally have been included in the final simplified equation. The problem was that the overbalance factor could not be considered real-time as there were no RTDD made available for the pore pressure gradient, ρ$_{pore}$. Data on pore pressure could only be obtained from the FWR, which were predicted in advance and read from the pressure gradients in Figure 3.4. An improvement on the agent would be to use the predicted or calculated pore pressure data and see whether this would affect the final results obtained to any large degree. This is further discussed under "Future improvements".

Mud weights effect on hardness is also overlooked. RTDD on ρ_{ecd} were available, but these could only be included in the model through the overbalance term, which in terms of densities, is $\left(p_{pore} - \rho_{ecd}\right)$. The alternative methods based on the d$_c$-exponents would include the effect of mud weight on hardness. This is also further discussed under "Future Improvements".

Normal compaction and under-compaction were not among those factors considered having any immediate effect on penetration rate and was therefore omitted from the final simplified equation. The function modelling under-compaction in abnormally pressured formations had the same issues as the function for overbalance, meaning it would require the ρ$_{pore}$ parameter. As was stated in

section 2.3.1.1, the effect of overbalance is considered much more important than the effect of under-compaction for penetration rate. Thus, it was only natural to neglect the effect of under-compaction when (initially at least) the effect of overbalance was decided to be neglected.

The function for normal compaction is dependent on the true vertical depth, which was available among the RTDD. Thus, this function could in theory have been included in the model and not affect results too such a large degree. However, this function also depends on the formation coefficient a_2, which should ideally be decided based on specific formation type characteristics, which can be a difficult process. This would add unnecessary complexity and as the goal was to keep the equation as simplistic as possible, the effect of normal compaction was thus decided not to be considered.

So, the simplification done to the Bourgoyne-Young drilling model resulted in the following equation (in terms of drillability K):

$$K = \frac{ROP}{WOB^{a_5} RPM^{a_6}} \tag{4.1ii}$$

7.1.1.2 Testing of model

During testing of the hardness model, a classification system separating soft and hard formations was proposed. This system also enabled the use of two separate sets of formation exponents such that the exponents are fitted to the formation types being drilled. First hardness was computed using only one formation exponent for both the WOB and RPM parameters. This made it possible to find maximum hardness. Hardness could then be normalized from 0 to 1 by dividing all hardness values on the maximum value. The hardness scale was then used to classify the formations with respect to hardness. The formations were classified according to:

1. Soft formations: Hardness ≤ 0.5
2. Hard formations: Hardness > 0.5

E.g. this meant formations with Hardness > 0.5, were classified as hard formations and moderately hard formation exponents given according to Eq. (4.5) and (4.6) were used in the hardness calculations thereafter. For soft formations the case was vice versa and moderately soft formations exponents according to Eq. (4.7) and (4.8) were used. The calculation of maximum drillability/hardness and the normalization process done in the previous step was then repeated, so hardness could now be normalized having used two sets of drilling exponents.

For the evaluated formation, the two sets of formation exponents were varied to try to refine and produce a clearer and more readable image of hardness. Three different cases of varying formation exponents were tested, two extreme cases versus a more moderate approach. The most distinct separation in hardness values were seen using (1) two moderate exponents. This was opposed to (2) the case of using a very hard formation exponent for hard formations and a moderately soft formation exponent for soft formations, in addition to (3) the case of using a moderately hard formation exponent for hard formations and very soft formation exponents for soft formations. This trend is exemplified in Figures 5.11 and 5.12. However, in all three cases, the transitions between soft and hard formations were easily detected.

The hardness classification limit set at H = 0.5 were not necessarily optimal. Setting the limit too low could classify too many formations as hard formations. The effect of increasing the limit such that hard formations were defined for H > 0.75 was thus investigated. Figure 5.14 and 5.15 showed the results from this alteration. The impact on the hardness curve was however minimal, and the original case of H > 0.5 showed more distinct transitions in hardness (in addition to less data anomalies) than what was the case for H > 0.75. Thus, H > 0.5 was continued to be applied as the hardness classification limit for the rest of the work in the thesis.

To correlate the results from the log analysis (qualitative method) with the hardness detection (quantitative method), two different sections of the 17 ½" interval was chosen for closer inspection. These were:

- o "Section 1": 1567-1594 m MD
- o "Section 4": 1648-1675 m MD

These two sections were chosen particularly because the log analysis indicated hard stringers in both sections, as well as their respective hardness curves showed some distinct variations in hardness compared to each other, with one section having more stable hardness values (Section 1) and the other having more oscillating values in hardness (Section 4).

During the log analysis, the correlating behavior of the parameters BPOS, WOB and RPM with respect to time, were used to detect hard stringers. When evaluating the hardness curves, the goal was to identify these stringers and other potential hard formations, as well as map out the general hardness of the sections. This could be achieved with the help of various hardness plots. The steps made to accomplish this was as follows:

- First, a plot showing dBPOS and BPOS versus time (See e.g. Figure 5.17), was used to confirm the location of the already identified stringers. Indicators of other new potential stringers or harder formations could also be reveled through this plot.

- Second, the hardness graph was added to the plot of dBPOS and BPOS versus time (See e.g. Figure 5.18). For both sections, the negative correlating behavior between the dBPOS and the hardness graph, plus the peaks of the hardness curve, helped confirm that the indications for harder formations by the dBPOS and BPOS curves in the previous plot was correct.

- Third, dBPOS and hardness was plotted vs. measured depth instead of time to enable for a better overview of the thickness of the hard stringers or harder formations. This step also made it possible to draw formation boundaries (See e.g. Figure 5.19).

Based on the characteristics of the hardness plot, some conclusions could be drawn for each of the sections:

- The lithology of Section 1 seems to consist of a softer formation type (with a normalized hardness value of around 0.05-0.07) being "pierced" by three hard stringers with normalized hardness varying from about 0.15 to 0.45 at most. Thickness of the hard stringers were approximately 3.5, 2.0 and 2.25 meter (See Figure 5.19).

- The lithology of Section 4 was more difficult to interpret than that of Section 1. This was because of larger parts of the interval consists of oscillating hardness values. In the top quarter part of the section there is a soft formation with normalized hardness of about 0.06, which corresponds to the same hardness as in the soft formation of Section 1. However, after the first quarter part and throughout the rest of the section the general hardness (lowest baseline) is raised to about 0.1, while the hardness is oscillating between low and high values and peaking towards very high values (e.g. such as H = 0.74, 0.35, 0.77, 0.89) multiple times. An attempt to draw formation boundaries and separate the oscillating part of the interval in minor formations was made, which concluded in four formations being labeled as hard and five labelled as soft (See Figure 5.24).

7.1.1.3 Correlations between hardness and lithology

The effect of lithology change on the hardness curve was also tested. The known transitions occurring in the 17 ½" section of Well C-47 was investigated closer. These three transitions were:

- Sandy Hordaland → Sandfree Hordaland (1655 m MD)

- Clear effect of lithology change seen, and an alternative boundary was drawn at 1653 m MD, as this boundary shows better correlation with the hardness and dBPOS graphs than that of the boundary of 1655 m MD stated in the FWR. The soft formation (with normalized hardness of about 0.06) that was considered in Section 1 and in the top quarter part of Section 4 was the Sandy Hordaland formation. The lithology changes experienced when investigating Section 4, marked with an increase in hardness to around 0.1 and more oscillating hardness values, correlates with the transition into the Sandfree Hordaland formation at 1653 m MD (See Figure 6.3).
- Sandfree Hordland → Balder Fm (2050 m MD)
  - No distinctive change in formation hardness is seen at 2050 m MD. However, an alternative boundary is drawn 10 meters further down at 2060 m MD, as there is a small increase in hardness and notable decrease in dBPOS at this position (See Figure 6.4).
- Balder Fm → Lista Fm (2200 m MD)
  - There is seen a lot of oscillation in the hardness and dBPOS values during the transition into the Lista Fm. This made it difficult to draw any alternative boundaries. After the transition interval, the hardness stabilizes and is comparable to the hardness of the Balder Fm. above, so no noticeable difference in general hardness occurred when entering the Lista Fm.

7.1.2 Quality of data

The RTDD provided by Statoil have been mostly of good quality. During the logging interpretation it was clear that RPM and WOB showed good correspondence with the BPOS velocity. However, when constructing the hardness plots there was seen some abnormal values of RPM and WOB. These instances have been attributed to times were drilling was at a halt, such as during tripping operations, installing new pipe or when casing is installed and cemented. As only data during ongoing drilling operations were relevant for the hardness calculations, these abnormalities was thus sorted out and removed.

The ROP-data provided were not considered accurate. This was highlighted in Figure 5.4, were ROP from the data package was plotted against the block velocity, dBPOS, which was manually estimated. The graphs showed some correspondence and the same general trend, but the ROP provided in the RTDD were positioned too deep compared to dBPOS. There is no information on how the ROP-data delivered from Statoil were estimated.

dBPOS was estimated by differentiating the block position (using the average of three block positions) with respect to time (ΔBPOS/ΔT). This method may not be exact and can induce some erroneous values, but none were noticed during the work, such that accuracy of the method seems acceptable.

No gamma ray data were available. This was unfortunate as having access to gamma ray could have helped to separate between which lithology was drilled in, that is decide whether drilling was happening in shale or sand etc. Thus, no qualified efforts to decide the lithology type were made, it was only decided whether the lithology was soft or hard. Other methods to name the lithology type could have been decided through correlations between hardness and gamma ray or sonic logs from other wells nearby Well C-47. However, this was not prioritized but may be a possible improvement for the future.

The gamma ray data was also needed to establish a clean shale zone to make trend line calculations in for the methods based on pore pressure and the d_c-exponent. These methods were thus not possible to proceed with, but they can be used in a future thesis if gamma ray data becomes available. This is also discussed under "Future improvements of hardness model" below.

7.1.3 Future improvements of hardness model

The method presented does not represent the "finished article" and there is room for further improvements. Still the simplistic equation derived has been proven to be capable of separating between soft and hard formations in the example well, and to quantify formation hardness. The method can also be seen as a cost-effective way to help mitigate serious down hole problems related to the occurrence of soft and hard formations. However, potential improvements that can refine and improve the accuracy of the method, include:

1. More testing on formation intervals having different lithologies or testing on a different well. Result obtained can be difficult to evaluate properly as there has been little room for comparison with other lithologies than those represented in the example intervals. Testing the method with data from other wells would also help correlate real hardness with hardness indicated by the program.

2. Developing a method with less simplifications. Only parameters considered essential for immediate changes in penetration rate and which were available among the RTDD were

included in the simplified method. Hardness calculations can thus not be considered to be 100 percent exact, as each simplifying step made may have contributed to a degree of error. The simplicity of the hardness model means that it is only relying on a few variables: ROP (dBPOS), WOB, RPM, in addition to the constants d_{bit} and formation exponents a_5 and a_6, which are hard to determine exact. Another drawback is thus that the hardness become very sensitive to changes in one of the three main variables, such was evidently in the WOB reduction in the abnormally pressured zone. Factors such as threshold bit weight, bit wear and bit hydraulics were neglected because of lack of data. For evaluating immediate changes in hardness, a simplistic model based on the included parameters is sufficient. However, when hardness needs to be accurately quantified, a more complex model will be beneficial given the additional input data is of good quality.

3. Testing on a well with exact data on formation type exponents or on a well having data which exponents could have been extracted from. The formation type exponents in the Bourgoyne-Young drilling equation should ideally be chosen based on local drilling conditions and historical drilling data, e.g. from nearby wells. Alternatively, they can be determined through methods such as multiple regression analysis (requires prior drilling data) or analyzing drilloff test data. Unfortunately, no such data were available, so it was opted to use averages taken from the ranges of exponents values. In the simplistic method used in this thesis only formation exponents from the WOB and RPM terms were used, so the degree of error affecting the final results may have been limited. However, if more parameters were included in the equation it would certainly have been beneficial for the precision of the results having a more accurate method for determining formation exponents.

4. The effect of overbalance on penetration rate need to be included in the equation as it is one of the variables shown to be essential for immediate changes in penetration rate. This is problematic to do because it is a function of the pore pressure, which were not among the RTDD. Tests should be done using the estimated pore pressure in new hardness calculations. However, since the pore pressure is a function of the simplified drillability K, the pore pressure is sensitive to changes in hardness and results may be less than optimal. Else, predicted (or established) values for pore pressure could have been utilized (found in the FWR), but this contradicts mimicking a real-time detection of hardness. The effect of overbalance on hardness using predicted pore pressure can be evaluated if compared against the results obtained in this thesis.

5. Considering the effect of mud weight on hardness detection. Normally the pore pressure will increase with depth in a formation. Increases in mud weight is thus made for drilling to remain overbalanced. However, if the pore pressure remains the same or an abnormally pressured formation leads to a reduction in pore pressure, while the mud weight is increased, the pressure differential, $\Delta P = P_{ECD} - P_{pore}$, will increase. This will lead to a decrease in penetration rate (because of the Hold Down Effect), which may appear as a hard formation on the hardness plot. Distinguishing between changes in hardness vs. changes in mud weight and pore pressure thus remains a challenge. Basically, this is the same as the effect of overbalance on penetration rate discussed above, and since data for mud weight were available (while pore pressure was not), one issue is how to incorporate the effect of mud weight into the drilling equation. For the method with the Bourgoyne-Young drilling equation this is not possible, as there are no functions which considers the effect of mud weight alone, it is only considered in accordance with the effect of pore pressure in the ΔP term, which is only natural according to the physical laws. Hence, further tests also including the effect of mud weight on the hardness curve should be implemented in a future model.

6. Obtaining gamma ray or other logging parameters such as acoustic and sonic logs. Such data would not only help indicate hard formations and to correlate results with the calculated hardness, but could also help to separate and decide which rock type is drilled in, e.g. if the indicated formation types are sand, shale, carbonates etc.

7.2 Pore pressure model

The computed hardness, or drillability, is an important input parameter in the pore pressure model. The other required parameters are the normal pore pressure gradient (ρ_{normal}), the mudweight/ECD (ρ_{ecd}), the real drillability factor (a_1), the formation coefficients a_2, a_3, a_4, and the depths, D and D_{ref}, measured in TVD. Because of the many input variables (9) in the model, there are many potential sources for error.

7.2.1 Quality of mathematical model

7.2.1.1 Testing of model

The results obtained highlighted the issue of having many input variables, and the pore pressure was seen to be especially sensitive to changes in hardness (drillability). When drillability abruptly changed, there were large associated pore pressure responses. This happens throughout the test well, adding noise to the calculated pore pressure.

For accuracy, the pore pressure method was also shown to be very dependent on determining the correct value of a_1, the real drillability factor. This factor should be set at a depth of normal compaction above the transition zone and represent the minimum value of the modified drillability parameter K_{mod}. However, as was experienced, if the zone of normal pore pressure is a problem zone protruded with hard stringers, such that there are sudden decreases in drillability, the K_{mod} will not follow the $K_{mod-normal}$ trendline. This makes it challenging to determine a_1. Another reason for the difficulty on settling on a correct value for a_1 was that the mudweight (ECD) had been increased in the normal pore pressure zone, which also affects the K_{mod}.

Results was able at multiple instances to exemplify the vulnerability of the pore pressure method to drilling problems causing irregular recordings of input parameters. For instance, in the test well, BHA-related issues caused a severe reduction in WOB and subsequent low ROP in the abnormally pressured Balder and Lista formations. This overall low and decreasing WOB, rather than continuously high and increasing ROP, have most likely led to low and decreasing values of computed formation hardness. So even though pore pressure was computed to increase throughout the Balder and Lista formations, as expected, these results may have been more attributed to the low WOB and hardness, rather than the high ROP caused by the overbalance effect. However, though low values of ROP in the lowermost section, it is still increasing somewhat, which is a sign of abnormal pore pressure and the overbalance factor. This is in accordance with the pressure gradients in the FWR in Figure 5.30, where the overbalance factor ($\rho_{ecd} - \rho_{pore}$) becomes lower with depth in the abnormal pressure zone. However, because of the overall decreasing WOB it is hard to assess whether hardness or pore pressure had the most significant effect on penetration rate in the Balder and Lista formations.

7.2.1.2 Effect of formation hardness vs. pore pressure on penetration rate

In the start of the transition zone, from 1400-1500 m TVD, before the sudden decrease in WOB, the overbalance effect on penetration rate could be seen. Here there was an interval with an increase in hardness (caused by high WOB), modified drillability, pore pressure and penetration rate.

The effect of hardness on penetration rate, was also seen. This happened in the top region above 1366 m TVD, inside the normal pressure zone. Hard stringers caused negative spikes in hardness and penetration rate, which also affected the pore pressure. However, the pore pressure moved quickly back to the normal and steady baseline values it had before the depth of the hard stringer. The stable pore pressure signals it was the spike in hardness rather than changes in pore pressure which caused the change in penetration rate in the normal pressure zone.

Testing the pore pressure method for the transition zone in another well not so troubled by drilling related issues, would likely produce better results. This would then make it easier to evaluate the effect of hardness vs. pore pressure on penetration rate. But the tested well has managed to highlight the many weakness related to this method. This shows that pore pressure estimations should not be made solely based on drilling parameters. However, the method is seen as a viable tool if run together with other pore pressure detection methods such as seismic data (acoustic velocity/interval transit time), drilling mud properties and drilled cuttings.

7.2.2 Future improvements of pore pressure model

Suggested future improvements are:

1. More testing on data from other wells, especially on wells containing data for the full length of the well. Results were affected by the difficulties on accurately setting D_{ref} and a_1, as this had to be done in a problem zone just above the transition zone. With full well data, the K_{mod} parameter can be tracked from surface, making it easier to spot the turning point marking the depth of D_{ref}. As well, the D_{ref} can then also be set above a potential problem zone. To progress from deciding a_1 from logical interpretation, an automatic method which saves the minimum K_{mod} value as a_1, with restraints such that as the depth for a_1 must be found in a normal compacted zone with normal pore pressure, would also be beneficial.

2. Developing a method with less simplifications. Effects from parameters such as threshold bit weight, bit wear and bit hydraulics were not accounted for. Thus, the hardness is not precisely quantified. In turn, this affects the pore pressure calculations.

3. Testing on a well with exact data on formation type exponents or on a well having data which exponents could have been extracted from. The formation type exponents in the Bourgoyne-Young drilling equation should ideally be chosen based on local drilling conditions and historical drilling data, e.g. from nearby wells. Alternatively, they can be determined through methods such as multiple regression analysis (requires prior drilling data) or analyzing drilloff test data. Unfortunately, no such data were available. The exponents a_3 and a_4 were thus based on average values of coefficients for shale formations in the U.S Gulf of Mexico area. For the exponents a_5 and a_6 it was opted to use averages taken from the ranges of exponents values. Not having an accurate method for determining formation exponents means there is an uncertain degree of error linked to the results.

4. Obtaining gamma ray or other logging parameters such as acoustic and sonic logs. Such data would not only help indicate hard formations and to correlate results with the calculated hardness, but could also help to separate and decided which rock type is drilled in, e.g. if the indicated formation types are sand, shale, carbonates etc. Providing a reliable detection of shale sections is especially important as the reference depth should be set in a normally compacted shale section.

5. Perform an evaluation of the quality of the pore pressure gradient in the FWR. There is no information which methods has been utilized to create the pore pressure gradient in the FWR. Thus, the quality of this pore pressure gradient should be assessed more thoroughly. Also, the start of the transition zone is set at 1366 m TVD in the FWR. This depth also coincides with the reported boundary between the Sandy Hordaland – Sandfree Hordaland formations. The obtained results did not show drastic changes in parameters at this depth. An evaluation should thus also be made on how the depth of this boundary could be determined with such a high degree of precision in the FWR.

6. Include monitoring of drilling torque. Torque, which is an energy-based parameter, can also be useful for identifying abnormal pore pressure zones. It is affected by the change in differential pressure and mechanical behavior of the shales when entering the transition zone. Unfortunately, torque is very sensitive to other phenomena such as hole geometry, deviation and BHA make-up – therefore it is being viewed as more of a second-order parameter for diagnosing abnormal pore pressure. Nevertheless, some studies should be made on torque behavior in relation to the observed results.

7. Measure the drilling efficiency. This can be done by using the concept of Mechanical Specific Energy (MSE), which is the energy required to remove a unit volume of rock. The goal in this method is to minimize MSE and maximize the ROP. Drillers can do this by controlling the WOB, torque, ROP and RPM. The WOB was significantly reduced in the abnormal pressure zone. Whether this was done to lessen the wear on the BHA or save input energy as ROP is expected to increase in the abnormal pressure zone, is unknown. Monitoring MSE could help to see how the drilling efficiency evolves throughout the transition zone, and before and after this WOB reduction. Studying MSE in relation to hard stringers, would also be interesting. This may also help in the study of separating between the effects of formation hardness vs. pore pressure on penetration rate.

8. Develop a real-time method which can measure the effect of hardness vs. pore pressure on penetration rate. In this report, the results had to be manually interpreted to identify the cause of increased ROP. By computing the percentage increase in drillability vs. that in pore pressure when ROP increases from a set baseline, it may be possible to decide whether hardness or pore pressure is the main contributor. The problem is that the pore pressure is very sensitive to changes in hardness. More studies should be done to see if there is a way to work around this problem.

8 Conclusion

The work done in this thesis have led to that the following conclusions can be drawn;

Hard formations need to be detected to mitigate hardness induced equipment and downhole problems and ensure a safe drilling operation. Efforts to map out and calculate formation hardness has been made in the industry. One of the most popular methods was put to test in this thesis.

Pore pressure is also related to drilling problems, especially dangerous kicks and blowouts. Continuous pore pressure detection is essential to hinder such circumstances. A simplistic approach for computing pore pressure was developed and tested on real-time drilling data.

Hardness model:

- The simplified hardness detection method proved cable of separating between soft and hard formations (or hard stringers) and quantify formation hardness.

- Hardness calculations were based on Bourgoyne-Young drilling equation. The simplistic approach gave reliable but to some degree inaccurate results.

- Matlab programming was utilized to perform calculations. Input and RTDD parameters needed in the simplified equation were WOB, RPM, and dBPOS (calculated from $\Delta BPOS/\Delta T$). The output parameter was calculated hardness, shown in hardness plots against depth.

- The transitions of the hardness graph were more distinctive when using two different sets of formation exponents, compared to only using one set of exponents. A hardness classification was also attempted but did not have the wanted effect.

- Provided input data were of sufficient quality, except for the ROP-data, which was not accurate and instead calculated by using block movement ($\Delta BPOS/\Delta T$). The manually computed block velocity showed better correspondence with depth and was able to produce more accurate results.

- Because gamma ray and alternative logging data such as acoustic and sonic logs were not available, no efforts were made to decide on the rock lithology drilled in. Also because of the lack of gamma ray data, no d_c-exponent trendline could be established and the methods based on the d_c-exponent were dropped for the present thesis.

- Hard stringers were identified in two separate test intervals. The deepest interval is regarded as a transition interval, indicating a shift from a softer (Sandy Hordaland) to a harder (Sandfree Hordaland) formation type.

- When investigating the known lithology transitions in the 17 ½" section, it was possible to draw alternative formation boundaries which showed better correlation with the hardness and dBPOS graphs.

Pore pressure model:

- Based on a simplified version of the Bourgoyne-Young equation the model for pore pressure was derived. The simplified pore pressure model was proven able to quantify pore pressure when tested on RTDD from a North Sea well. The pore pressure results were partly in compliance with those of the FWR of the operating company.

- The pore pressure model has many variables, thus many sources for errors, which the results indicate. Accuracy during testing was especially sensitive to changes in formation hardness and WOB. Determining correct values for the reference depth D_{ref}, and the real drillability constant a_1, was also shown to be very important.

- Accuracy is thought to improve if the model is tested on wells with more complete sets of data, given the additional data is of good quality. For example, formation type exponents were not provided along with the RTDD for the test well and had to be based on average values.

- Access to full well length data in addition to a lithology indicator such as gamma ray would make it easier to decide D_{ref} and a_1 more accurately. If tested on wells with complete sets of data, it is also possible to make the model more complex and include for the effects from parameters such as threshold bit weight, bit wear and bit hydraulics.

- The effect of hardness vs. pore pressure on ROP was manually studied. In the normal pressure zone, hardness was found to have the most significant effect. In the start of the transition zone, the effect of increased pore pressure was seen. The lower part of the

transition zone was difficult to study because of the impact the severely reduced WOB had on ROP, hardness and pore pressure.

o   Work should be done to develop a real-time method which can measure the effect of hardness vs. pore pressure on ROP and at the same time bypass the problem of the sensitivity of the pore pressure method to changes in hardness.

o   The results indicate that quantifying pore pressure accurately by drilling parameter-based methods such as the Bourgoyne-Young method is difficult. However, the method is a viable tool if run together with other pore pressure detection methods such as seismic data (acoustic velocity/interval transit time), drilling mud properties and drilled cuttings.

9 References

Abdollahi J. 2003. Abnormal Drillstring Wash-out and Fatigue Experienced When Drilling Hazardous Formation in Iranian Oil Field. Paper SPE-85327-MS presented at SPE/IADC Middle East Drilling Technology Conference and Exhibition, Abu Dhabi, 20-22 October

Agwu, O.E. and Akpabio, J.U. 2012. Assessment of Drill Cuttings Behaviour in Wellbore Washouts. Paper IRACST – Engineering Science and Technology: An International Journal (ESTIJ), ISSN: 2250-3498, Vol.2, No.6, December 2012

ATHY L.F., 1930. Density, porosity and compactation of sedimentary rocks, *Bull. Amer. Assoc. Petrol. Geol.* v. 14, pp. 1-24.

Bahari M.H., Bahari A., Moharrami F.N., Sistani M.B.N., 2008. Determining Bourgoyne and Young Model Coefficients Using Genetic Algorithm to Predict Drilling Rate. Paper Journal of Applied Sciences **8**: 3050-3054. DOI: 10.3923/jas.2008.3050.3054. Available at http://scialert.net/abstract/?doi=jas.2008.3050.3054. Cited 2017. 8:3050-3054.

Bestcrystals.com. Mohs Hardness Scale, Available at: https://www.bestcrystals.com/hardness.html. Cited 2017

Bourgoyne, A.T., Millhelm, K.K., and Chenevert, M.E. et al. 1986. Applied Drilling Engineering, Textbook Series Vol.2, SPE, Richardson Texas

Christophersen L., Gjerde J., Valdem S., 2007. Final Well Report. Statoil, Bergen

Directional Drilling Technology. Dog Leg Severity, Available at: http://directionaldrilling.blogspot.no/2011/07/dog-leg-severity-dls.html. Cited 2017

Eaton B.A., 1975. The Equation for Geopressure Prediction from Well Logs. Paper SPE 5544 presented at SPE AIME Annual fall meeting, Dallas, 28 September – 1 October

Fjær E., Holt R.M., Horsrud P., Raaen A.M., Risnes R. Petroleum Related Rock Mechanics. 2nd ed. Amsterdam: Elsevier; 2008: 311-312

Flexible Learning, The University of Auckland. Metamorphic rocks, Available at https://flexiblelearning.auckland.ac.nz/rocks_minerals/rocks/metamorphic.html. Cited 2016

Geology.com. Shale, Available at http://geology.com/rocks/shale.shtml. Cited 2017

Glossary. Stringer, Available at http://geomaps.wr.usgs.gov/parks/misc/glossarys.html. Cited 2016

Head, A.L. 1951. A Drillability Classification of Geological Formations. Paper WPC 4105 presented at the 3rd World Petroleum Congress, Hague, 28 May – 6 June

Hoseinie S.H., Ataie M., Aghababaei H., Pourrahimian Y. Iran. 2007. RDi – A new method for evaluating of rock mass drillability.

Morris R.I., 1969. Rock Drillability Related to a Roller Cone Bit. Paper SPE-2389-MS presented at the Drilling and Rock Mechanics Symposium, Austin, 14 -15 January

Norwegian Petroleum Directorate, Article at http://www.npd.no/en/Publications/Norwegian-Continental-Shelf/No1-2014/Turning-the-tide-for-drilling/. Cited 2016

NPD[1]. Fact pages, Nordland Group, http://factpages.npd.no/ReportServer?/FactPages/PageView/strat_Litho_level1_group_formation&rs:Command=Render&rc:Toolbar=false&rc:Parameters=f&NpdId=113&IpAddress=95.34.224.64&CultureCode=en. Cited 2017

NPD[2]. Fact pages, Hordaland Group, http://factpages.npd.no/ReportServer?/FactPages/PageView/strat_Litho_level1_group_formation&rs:Command=Render&rc:Toolbar=false&rc:Parameters=f&NpdId=67&IpAddress=95.34.224.64&CultureCode=en 2017). Cited 2017

NPD[3]. Fact pages, Rogaland Group, http://factpages.npd.no/ReportServer?/FactPages/PageView/strat_Litho_level1_group_formation&rs:Command=Render&rc:Toolbar=false&rc:Parameters=f&NpdId=131&IpAddress=95.34.224.64&CultureCode=en. Cited 2017

NPD[4]. Fact pages, Balder Formation, http://factpages.npd.no/ReportServer?/FactPages/PageView/strat_Litho_level1_group_formation&rs:Command=Render&rc:Toolbar=false&rc:Parameters=f&NpdId=6&IpAddress=95.34.224.64&CultureCode=en. Cited 2017

NPD[5]. Fact pages, Lista Formation, http://factpages.npd.no/ReportServer?/FactPages/PageView/strat_Litho_level1_group_formation&rs:Command=Render&rc:Toolbar=false&rc:Parameters=f&NpdId=95&IpAddress=95.34.224.64&CultureCode=en. Cited 2017

NPD[6]. Fact pages, Shetland Group, http://factpages.npd.no/ReportServer?/FactPages/PageView/strat_Litho_level1_group_formation&rs:Command=Render&rc:Toolbar=false&rc:Parameters=f&NpdId=143&IpAddress=95.34.224.64&CultureCode=en. Cited 2017

NPD[7]. Fact pages, Kyrre Formation, http://factpages.npd.no/ReportServer?/FactPages/PageView/strat_Litho_level1_group_formation&rs:Command=Render&rc:Toolbar=false&rc:Parameters=f&NpdId=92&IpAddress=95.34.224.64&CultureCode=en. Cited 2017

NPD[8]. Fact pages, Statfjord Group, http://factpages.npd.no/ReportServer?/FactPages/PageView/strat_Litho_level1_group_formation&rs:Command=Render&rc:Toolbar=false&rc:Parameters=f&NpdId=157&IpAddress=95.34.224.64&CultureCode=en. Cited 2017

Odfjell. Pipe buckling, Article at: http://blog.odfjellwellservices.com/what-is-drill-pipe-buckling-and-how-to-prevent-it-from-happening. Cited 2017

Petrowiki[1]. Drillpipe failures, Available at petrowiki.org/Drillpipe_failures. Cited 2017

Petrowiki[2]. Mechanical pipe-sticking, petrowiki.org/Mechanical_pipe_sticking. Cited 2017

Petrowiki[3]. Lost circulation, petrowiki.org/Lost_circulation. Cited 2017

Petrowiki[4]. Borehole instability, petrowiki.org/Borehole_instability. Cited 2017

Petrowiki[5]. Roller cone bit classification, http://petrowiki.org/Roller_cone_bit_classification#IADC_classification. Cited 2017

Petrowiki[6]. Kicks, petrowiki.org/Kicks. Cited 2019

Prasad U., 2009. Drillability of a Rock in Terms of its Physico-Mechanical And Micro-Structural Properties. Paper ARMA-09-040 presented at the 43rd U.S. Rock Mechanics Symposium & 4th U.S. – Canada Rock Mechanics Symposium, Asheville, 28 June – 1 July

Schlumberger[1]. Source rock, Available at http://www.glossary.oilfield.slb.com/Terms/s/source_rock.aspx. Cited 2016

Schlumberger[2]. Round trip, http://www.glossary.oilfield.slb.com/Terms/r/round_trip.aspx. Cited 2016

Schlumberger[3]. Washout, http://www.glossary.oilfield.slb.com/Terms/w/washout.aspx. Cited 2017

Schlumberger[4]. Dog leg, http://www.glossary.oilfield.slb.com/Terms/d/dog_leg.aspx. Cited 2017

Sclumberger[5]. Keyseat, http://www.glossary.oilfield.slb.com/en/Terms/k/keyseat.aspx. Cited 2017

Sclumberger[6]. Abnormal pressure, https://www.glossary.oilfield.slb.com/en/Terms/a/abnormal_pressure.aspx. Cited 2019

Skalle P., 2015. Pressure Control During Oil Well Drilling. 6th edition. Bookboon.com.

Wijk G., 1989. The stamp test for rock drillability classification. Int. J Rock Mech Min. Sci & Geomech Abst. 26(1):37-44.

Wikipedia[1]. Diagenesis, Available at https://en.wikipedia.org/wiki/Diagenesis. Cited 2016

Wikipedia[2]. Lamination, https://en.wikipedia.org/wiki/Lamination. Cited 2016

Wikipedia[3]. Shale, https://en.wikipedia.org/wiki/Shale. Cited 2017

Wikipedia[4]. Knoop hardness test, https://en.wikipedia.org/wiki/Knoop_hardness_test. Cited 2017

Wikipedia[5]. Porosity, https://en.wikipedia.org/wiki/Porosity. Cited 2019

Wikipedia[6]. Blowout, https://en.wikipedia.org/wiki/Blowout_(well_drilling). Cited 2019

Yoshida C., Ikeda S., Eaton B.A., 1996. An Investigative Study of Recent Technologies Used for Prediction, Detection and Evaluation of Abnormal Formation Pressure and Fracture Pressure in North and South America. Paper IADC/SPE 36381 presented at IADC/SPE Asia Pacific Drilling Technology Conference, Kuala Lumpur, September

10 Abbreviations

BHA	Bottomhole assembly
BPOS	Block position
dBPOS (ΔBPOS/ΔT)	Block position velocity
DCN	Drillability classification number
DST	Drill stem test
ECD	Equivalent circulating density
EMW	Equivalent mud weight
Fm.	Formation
FWR	Final well report
HK	Knoop hardness
IADC	International association of drilling contractors
IPT	Department of Petroleum Technology and Applied Geophysics
LCM	Loss of circulation materials
MD	Measured Depth
MOP	Margin of overpull
MWD	Measurements while drilling
OBM	Oil-based mud
PCD	Polycrystalline compact diamond
POOH	Pull out of hole
RDi	Rockmass Drillability index
RKB	Rotary kelly bushing
ROP	Rate of penetration
ROV	Remotely operated underwater vehicle
RPM	Revolutions per minute
RSS	Rotary steerable system
RTDD	Real-time drilling data
SG	Specific gravity
SW	Water saturation
TVD	True vertical depth [m]
UCS	Uniaxial compressive strength
WBM	Water-based mud
WL	Wire-line
WOB	Weight on bit

11 Appendix A - Graphs

A.1   ROP vs. MD

A.2   RPM vs. MD

A.3   WOB vs. MD
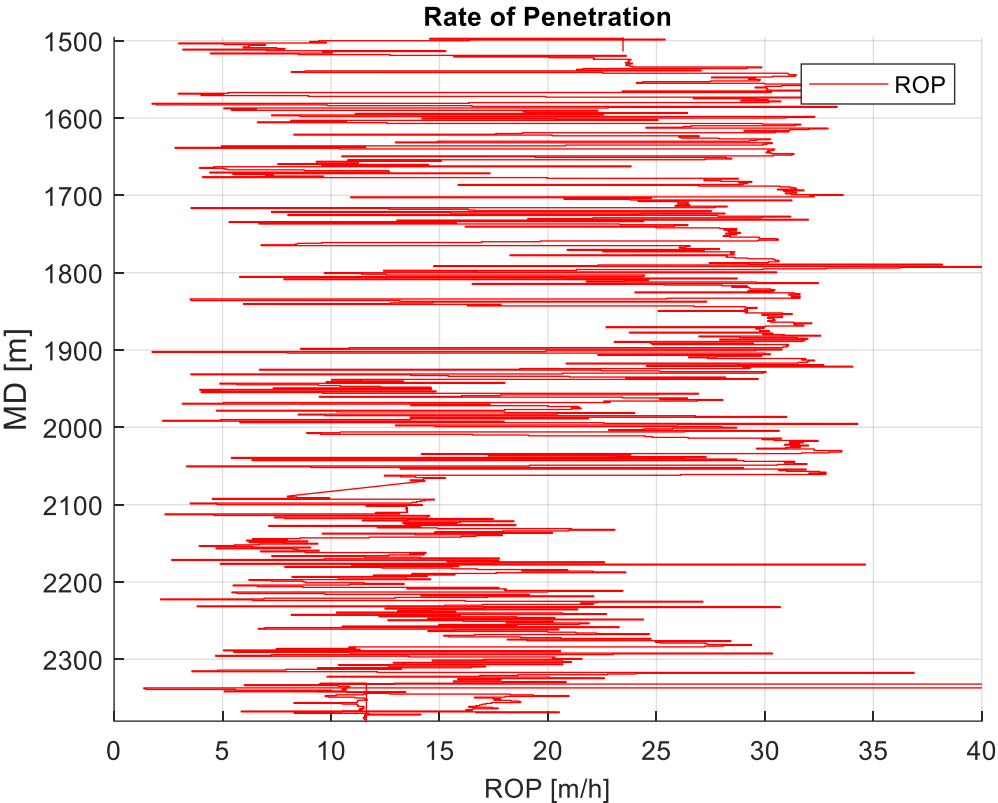
Figure A.1: ROP plotted vs. MD for the 17 ½" interval of Well C-47. This is the original ROP-data from the RTDD.
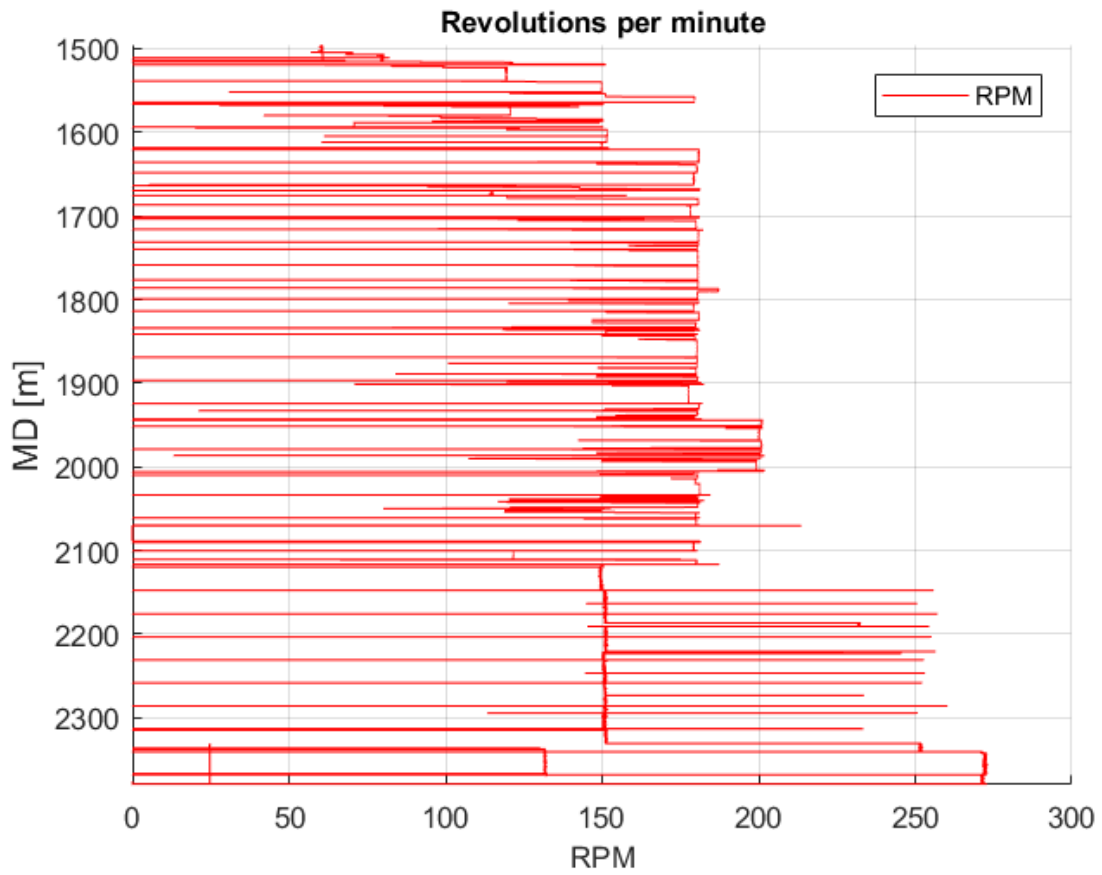
Figure A.2: RPM plotted vs. MD for the 17 ½" interval of Well C-47. This is the original RPM-data from the RTDD. Before being used in computing hardness, some of the data (for RPM < 25) were eliminated, in addition to that only data when there was an active drilling operation was used.
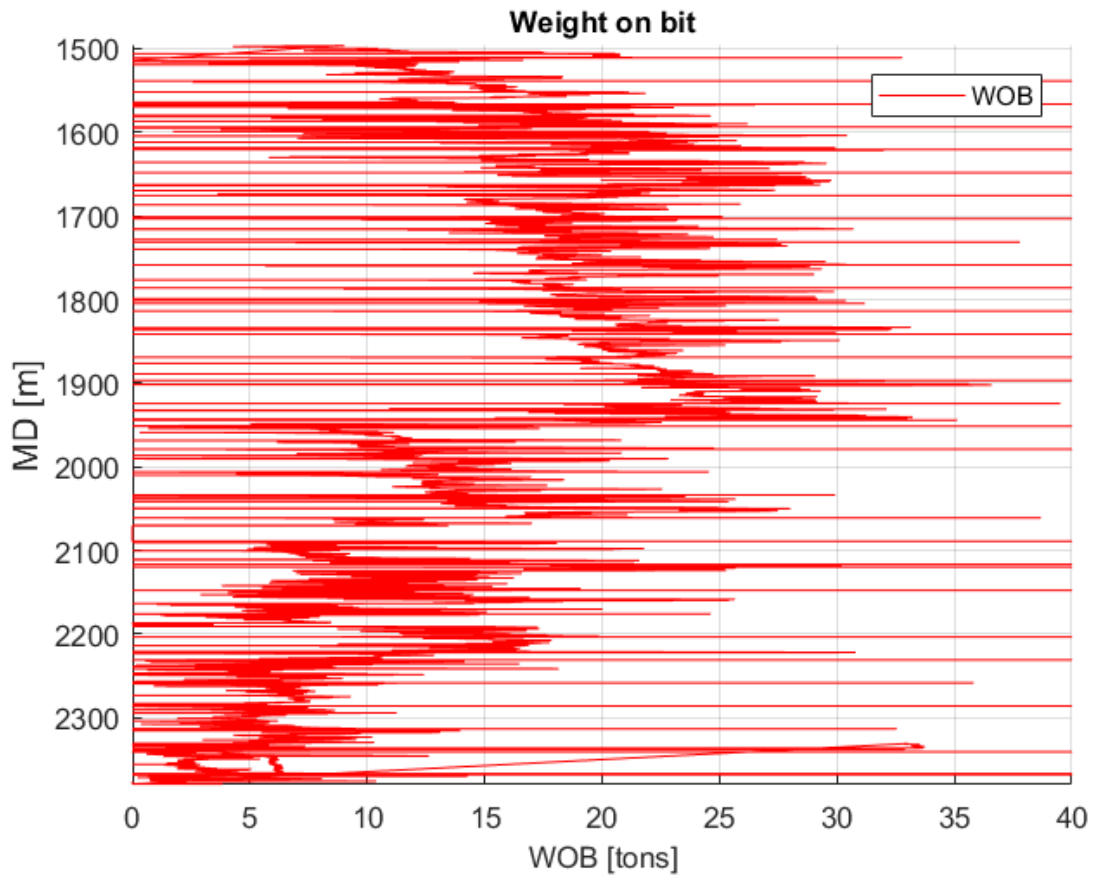
Figure A.3: WOB plotted vs. MD for the 17 ½" interval of Well C-47. This is the original WOB-data from the RTDD. Before being used in computing hardness, some of the data (for WOB < 2.5) were eliminated, in addition to that only data when there was an active drilling operation was used.

12 Appendix B - Matlab agents

12.1 Hardness agent

```matlab
% Hardness Agent %
% Made by Bertil Osheim for his master thesis %

clc
clear

% Load the correct folder for the data gathering %

cd('C:\Users\berti\Desktop\Prosjektoppgave\Matlab');

% Load drilling data of correct interval into matlab %

rtdd = xlsread('interval17_5.xlsx');

% Length of drilling data %

rtddlength = length(rtdd);

% Inputs %

% Variables %
% Diameter of drillbit being used in interval %

dbit = 17.5;

% Constant values %
% Gravity %

g = 9.81;

% Drilling coefficients for Bourgoyne-Young drilling model %

a5_avg = 1.25;
a6_avg = 0.70;

a5_soft = 1.625; %2.0 = Extremely Soft; %a5-Range: (0.5-2.0 Bourgoyne)
a6_soft = 0.85; %1.0 = Extremely Soft; %a6-Range: (0.4-1.0 Bourgoyne)

a5_hard = 0.875; %0.5 = Extremely Hard;
a6_hard = 0.55; %0.4 = Extremely Hard;


    DVER = rtdd(:,1);
    DMEA = rtdd(:,2);
    DBTM = rtdd(:,3);
    Time = rtdd(:,4);
    BPOS = rtdd(:,5);
    ROP  = rtdd(:,6);
    RPMB = rtdd(:,7);
    WOB  = rtdd(:,8);
```

```matlab
    % Calculate drillability from original(Raw)data

 j = 1;

for i = 1:1:rtddlength

    if (DMEA(i) - DBTM(i)) < 0.1

        f5_1_raw(j) = WOB(i)^a5_avg;
        f6_1_raw(j) = RPMB(i)^a6_avg;

        K_1_raw(j) = ROP(i)./(f5_1_raw(j).*f6_1_raw(j));
        H_1_raw(j) = 1/K_1_raw(j);

        DVERraw(j) = DVER(i);
        DMEAraw(j) = DMEA(i);
        DBTMraw(j) = DBTM(i);
        Timeraw(j) = Time(i);
        BPOSraw(j) = BPOS(i);
        ROPraw(j)  = ROP(i);
        RPMBraw(j) = RPMB(i);
        WOBraw(j)  = WOB(i);

        j = j + 1;
    end

  end

 % Calculate dBPOS from original BPOS and Time data

 k = 1;

for i = 1:3:(rtddlength-2)
    DVERavg(k) = (DVER(i) + DVER(i+1) + DVER(i+2))/3;
    DMEAavg(k) = (DMEA(i) + DMEA(i+1) + DMEA(i+2))/3;
    DBTMavg(k) = (DBTM(i) + DBTM(i+1) + DBTM(i+2))/3;
    Timeavg(k) = (Time(i) + Time(i+1) + Time(i+2))/3;
    BPOSavg(k) = (BPOS(i) + BPOS(i+1) + BPOS(i+2))/3;
    ROPavg(k)  = (ROP(i)  + ROP(i+1)  + ROP(i+2))/3;
    RPMBavg(k) = (RPMB(i) + RPMB(i+1) + RPMB(i+2))/3;
    WOBavg(k)  = (WOB(i)  + WOB(i+1)  + WOB(i+2))/3;

    k = k + 1;
end

rtddavglength = length(WOBavg);

 j = 1;

    for i = 2:1:rtddavglength
        dBPOS1(j) = ((BPOSavg(i-1) - BPOSavg(i))./15.*3600);
        DVER1(j) = DVERavg(i);
        DMEA1(j) = (DMEAavg(i)+DMEAavg(i-1))/2; %DMEAavg(i)
        DBTM1(j) = DBTMavg(i);
        Time1(j) = Timeavg(i);
        BPOS1(j) = (BPOSavg(i)+BPOSavg(i-1))/2; %=BPOSavg(i)
        ROP1(j)  = ROPavg(i);
        RPMB1(j) = RPMBavg(i);
        WOB1(j)  = WOBavg(i);

        j = j + 1;
```

```matlab
    end

rtdd1length = length(WOB1);

% Calculate drillability after replacing ROP with dBPOS as drilling rate
parameter (contains extreme negative values/spikes because of unfiltered
dBPOS)

 j = 1;

for i = 1:1:rtdd1length

     if (DMEA1(i) - DBTM1(i)) < 0.1

         f5_1_raw_dBPOS(j) = WOB1(i)^a5_avg;
         f6_1_raw_dBPOS(j) = RPMB1(i)^a6_avg;

          K_1_raw_dBPOS(j) =
                  dBPOS1(i)./(f5_1_raw_dBPOS(j).*f6_1_raw_dBPOS(j));
         H_1_raw_dBPOS(j) = 1/K_1_raw_dBPOS(j);

         DVERraw_dBPOS(j) = DVER1(i);
         DMEAraw_dBPOS(j) = DMEA1(i);
         DBTMraw_dBPOS(j) = DBTM1(i);
         Timeraw_dBPOS(j) = Time1(i);
         BPOSraw_dBPOS(j) = BPOS1(i);
         ROPraw_dBPOS(j)  = ROP1(i);
         RPMBraw_dBPOS(j) = RPMB1(i);
         WOBraw_dBPOS(j)  = WOB1(i);

         j = j + 1;
     end

   end

% Eliminate odd values of WOB, RPM and dBPOS

% Eliminate odd values of WOB

j = 1;
for i = 1:rtdd1length
    if WOB1(i) > 2.5 % [tonne]

        dBPOSelWOB(j) = dBPOS1(i);
        DVERelWOB(j) = DVER1(i);
        DMEAelWOB(j) = DMEA1(i);
        DBTMelWOB(j) = DBTM1(i);
        TimeelWOB(j) = Time1(i);
        BPOSelWOB(j) = BPOS1(i);
        ROPelWOB(j)  = ROP1(i);
        RPMBelWOB(j) = RPMB1(i);
        WOBelWOB(j)  = WOB1(i);

        j = j + 1;
    end
end

rtddelWOBlength = length(WOBelWOB);

% Eliminate odd values of RPMB
```

```matlab
j = 1;
for i = 1:rtddelWOBlength
    if  RPMBelWOB(i) > 25 %[rpm]

        dBPOSelRPMB(j) = dBPOSelWOB(i);
        DVERelRPMB(j) = DVERelWOB(i);
        DMEAelRPMB(j) = DMEAelWOB(i);
        DBTMelRPMB(j) = DBTMelWOB(i);
        TimeelRPMB(j) = TimeelWOB(i);
        BPOSelRPMB(j) = BPOSelWOB(i);
        ROPelRPMB(j)  = ROPelWOB(i);
        RPMBelRPMB(j) = RPMBelWOB(i);
        WOBelRPMB(j)  = WOBelWOB(i);

        j = j + 1;
    end
end

rtddelRPMlength = length(WOBelRPMB);

%Eliminate odd values of dBPOS

j = 1;

  for i = 1:1:rtddelRPMlength
      if dBPOSelRPMB(i) > 2.5 && dBPOSelRPMB(i) < 45 % [m/h]

        dBPOSeldBPOS(j) = dBPOSelRPMB(i);
        DVEReldBPOS(j) = DVERelRPMB(i);
        DMEAeldBPOS(j) = DMEAelRPMB(i);
        DBTMeldBPOS(j) = DBTMelRPMB(i);
        TimeeldBPOS(j) = TimeelRPMB(i);
        BPOSeldBPOS(j) = BPOSelRPMB(i);
        ROPeldBPOS(j)  = ROPelRPMB(i);
        RPMBeldBPOS(j) = RPMBelRPMB(i);
        WOBeldBPOS(j)  = WOBelRPMB(i);

        j= j + 1;
      end
  end

  rtddeldBPOSlength=length(WOBeldBPOS);

  % Updating RTDD-data after sorting of values

        dBPOS2 = dBPOSeldBPOS;
        DVER2 = DVEReldBPOS;
        DMEA2 = DMEAeldBPOS;
        DBTM2 = DBTMeldBPOS;
        Time2 = TimeeldBPOS;
        BPOS2 = BPOSeldBPOS;
        ROP2  = ROPeldBPOS;
        RPMB2 = RPMBeldBPOS;
        WOB2  = WOBeldBPOS;

rtdd2length =length(WOB2);

% Calculate drillability after replacing ROP with dBPOS as drilling rate
parameter + elimination of odd values

 j = 1;
```

```matlab
for i = 1:1:rtdd2length

    if (DMEA2(i) - DBTM2(i)) < 0.1

        f5_1_odd_removed(j) = WOB2(i)^a5_avg;
        f6_1_odd_removed(j) = RPMB2(i)^a6_avg;

        K_1_odd_removed(j) =
dBPOS2(i)./(f5_1_odd_removed(j).*f6_1_odd_removed(j));
        H_1_odd_removed(j) = 1/K_1_odd_removed(j);

        dBPOSodd_removed(j) = dBPOS2(i);
        DVERodd_removed(j) = DVER2(i);
        DMEAodd_removed(j) = DMEA2(i);
        DBTModd_removed(j) = DBTM2(i);
        Timeodd_removed(j) = Time2(i);
        BPOSodd_removed(j) = BPOS2(i);
        ROPodd_removed(j)  = ROP2(i);
        RPMBodd_removed(j) = RPMB2(i);
        WOBodd_removed(j)  = WOB2(i);

        j = j + 1;
    end

  end


% Sort list of data with respect to measured depth by removing
% duplicate DMEA values

        dBPOSsortDMEA = []; dBPOSsortDMEA(1) = dBPOS2(1);
        DVERsortDMEA = []; DVERsortDMEA(1) = DVER2(1);
        DMEAsortDMEA = []; DMEAsortDMEA(1) = DMEA2(1);
        DBTMsortDMEA = []; DBTMsortDMEA(1) = DBTM2(1);
        TimesortDMEA = []; TimesortDMEA(1) = Time2(1);
        BPOSsortDMEA = []; BPOSsortDMEA(1) = BPOS2(1);
        ROPsortDMEA =  []; ROPsortDMEA(1)  = ROP2(1);
        RPMBsortDMEA = []; RPMBsortDMEA(1) = RPMB2(1);
        WOBsortDMEA =  []; WOBsortDMEA(1)  = WOB2(1);

        deepest_depth = -999999;
        for i = 2:rtdd2length
            if DMEA2(i) > deepest_depth
                deepest_depth = DMEA2(i);

                dBPOSsortDMEA = [dBPOSsortDMEA dBPOS2(i)];
                DVERsortDMEA = [DVERsortDMEA DVER2(i)];
                DMEAsortDMEA = [DMEAsortDMEA DMEA2(i)];
                DBTMsortDMEA = [DBTMsortDMEA DBTM2(i)];
                TimesortDMEA = [TimesortDMEA Time2(i)];
                BPOSsortDMEA = [BPOSsortDMEA BPOS2(i)];
                ROPsortDMEA =  [ROPsortDMEA ROP2(i)];
                RPMBsortDMEA = [RPMBsortDMEA RPMB2(i)];
                WOBsortDMEA =  [WOBsortDMEA WOB2(i)];
            end
        end

 % Updating RTDD-data after sorting of values
```

```matlab
            dBPOS3 = dBPOSsortDMEA;
            DVER3 = DVERsortDMEA;
            DMEA3 = DMEAsortDMEA;
            DBTM3 = DBTMsortDMEA;
            Time3 = TimesortDMEA;
            BPOS3 = BPOSsortDMEA;
            ROP3  = ROPsortDMEA;
            RPMB3 = RPMBsortDMEA;
            WOB3  = WOBsortDMEA;

        rtdd3length = length(WOB3);


% Computing average of all drilling data

k = 1;

for i = 1:3:(rtdd3length-2)
    dBPOS3avg(k) = (dBPOS3(i) +dBPOS3(i+1) + dBPOS3(i+2))/3;
    DVER3avg(k) = (DVER3(i) + DVER3(i+1) + DVER3(i+2))/3;
    DMEA3avg(k) = (DMEA3(i) + DMEA3(i+1) + DMEA3(i+2))/3;
    DBTM3avg(k) = (DBTM3(i) + DBTM3(i+1) + DBTM3(i+2))/3;
    Time3avg(k) = (Time3(i) + Time3(i+1) + Time3(i+2))/3;
    BPOS3avg(k) = (BPOS3(i) + BPOS3(i+1) + BPOS3(i+2))/3;
    ROP3avg(k)  = (ROP3(i)  + ROP3(i+1)  + ROP3(i+2))/3;
    RPMB3avg(k) = (RPMB3(i) + RPMB3(i+1) + RPMB3(i+2))/3;
    WOB3avg(k)  = (WOB3(i)  + WOB3(i+1)  + WOB3(i+2))/3;

    k = k + 1;
end

rtdd3avglength = length(WOB3avg);


% Updating drilling parameters after the elimination of odd values,
% sorting of depth data, and averaging of all values.

dBPOS4 = dBPOS3avg;
DVER4 = DVER3avg;
DMEA4 = DMEA3avg;
DBTM4 = DBTM3avg;
Time4 = Time3avg;
BPOS4 = BPOS3avg;
ROP4  = ROP3avg;
RPMB4 = RPMB3avg;
WOB4  = WOB3avg;

rtdd4length = length(WOB4);

% Compute Drillability/Hardness and maximum Drillability/Hardness using one
a5/a6-exponent

  j = 1;

  for i = 1:1:rtdd4length

      if (DMEA4(i) - DBTM4(i)) < 0.1

          f5_1(j) = WOB4(i)^a5_avg;
          f6_1(j) = RPMB4(i)^a6_avg;
```

```matlab
        K_1(j) = dBPOS4(i)./(f5_1(j).*f6_1(j));
        H_1(j) = 1/K_1(j);

        dBPOS5(j) = dBPOS4(i);
        DVER5(j) = DVER4(i);
        DMEA5(j) = DMEA4(i);
        DBTM5(j) = DBTM4(i);
        Time5(j) = Time4(i);
        BPOS5(j) = BPOS4(i);
        ROP5(j) = ROP4(i);
        RPMB5(j) = RPMB4(i);
        WOB5(j) = WOB4(i);

        j = j + 1;
    end

end

K_1max = max(K_1);
H_1max = max(H_1);
rtdd5length = length(K_1);

 % Normalize Hardness using one a5/a6-exponent

for i=1:rtdd5length

    K1_norm(i) = K_1(i)/K_1max;
    H1_norm(i) = H_1(i)/H_1max;

end

% Compute Drillability/Hardness and Max Drillability/Hardness using two
a5/a6 exponents


for i = 1:rtdd5length

    if K1_norm(i) < 0.5
        a5 = a5_hard;
        a6 = a6_hard;
    else
        a5 = a5_soft;
        a6 = a6_soft;
    end

        f5_2(i) = WOB5(i)^a5;
        f6_2(i) = RPMB5(i)^a6;

        K_2(i) = dBPOS5(i)./(f5_2(i).*f6_2(i));
        H_2(i) = 1/K_2(i);

end

K_2max = max(K_2);
H_2max = max(H_2);
rtdd6length = length(K_2);

% Normalize Hardness using two a5/a6 exponents

for i= 1:rtdd6length
```

```matlab
        K2_norm(i) = K_2(i)/K_2max;
        H2_norm(i) = H_2(i)/H_2max;

    end

% Normalize dBPOS
    dBPOS5max = max(dBPOS5);

    for i= 1:rtdd5length

        dBPOS5norm(i)= dBPOS5(i)/dBPOS5max;

    end


% Average Hardness (computed with 9 points) for smoother plotting

j = 1;

for i= 1:3:rtdd6length-2

    K2_plot(j) =  (K_2(i) + K_2(i+1) + K_2(1+2))/3;
    H2_plot(j) =  (H_2(i) + H_2(i+1) + H_2(1+2))/3;
    DVER_plot(j) = (DVER5(i) + DVER5(i+1) + DVER5(i+2))/3;
    DMEA_plot(j) = (DMEA5(i) + DMEA5(i+1) + DMEA5(i+2))/3;
    ROP5_plot(j) = (ROP5(i) + ROP5(i+1) + ROP5(i+2))/3;
    RPMB5_plot(j) = (RPMB5(i)  + RPMB5(i+1)  + RPMB5(i+2))/3;
    WOB5_plot(j) = (WOB5(i)  + WOB5(i+1)  + WOB5(i+2))/3;
    dBPOS5_plot(j) = (dBPOS5(i)  + dBPOS5(i+1)  + dBPOS5(i+2))/3;

    j = j + 1;
end

K2_avg1max = max(K2_plot);
H2_avg1max = max(H2_plot);
rtdd6avg1length = length(H2_plot);

j = 1;

for i= 1:3:rtdd6avg1length-2

    K2_plot2(j)    = (K2_plot(i) +   K2_plot(i+1) +  K2_plot(1+2))/3;
    H2_plot2(j)    = (H2_plot(i) +   H2_plot(i+1) +  H2_plot(1+2))/3;
    DVER_plot2(j) = (DVER_plot(i) + DVER_plot(i+1) + DVER_plot(i+2))/3;
    DMEA_plot2(j) = (DMEA_plot(i) + DMEA_plot(i+1) + DMEA_plot(i+2))/3;
    ROP5_plot2(j) = (ROP5_plot(i) + ROP5_plot(i+1) + ROP5_plot(i+2))/3;
    RPMB5_plot2(j) = (RPMB5_plot(i)  + RPMB5_plot(i+1)  +
RPMB5_plot(i+2))/3;
    WOB5_plot2(j) = (WOB5_plot(i)  + WOB5_plot(i+1)  + WOB5_plot(i+2))/3;
    dBPOS5_plot2(j) = (dBPOS5_plot(i)  + dBPOS5_plot(i+1)  +
dBPOS5_plot(i+2))/3;

    j = j + 1;
end

K2_avg2max = max(K2_plot2);
H2_avg2max = max(H2_plot2);
rtdd6avg2length = length(H2_plot2);

% Normalize Average Hardness (computed with 2 exponents)
```

```matlab
for i=1:rtdd6avg2length
     K2avg_norm(i) = K2_plot2(i)/K2_avg2max;
     H2avg_norm(i) = H2_plot2(i)/H2_avg2max;
end

% Drawing formation boundaries

% "Section 1"
Boundary1 = 1567;
Boundary2 = 1570.5;
Boundary3 = 1580;
Boundary4 = 1582;
Boundary5 = 1586.25;
Boundary6 = 1588.5;

% "Section 4"
Boundary7 = 1653;
Boundary8 = 1661.25;
Boundary9 = 1662.5;
Boundary10 = 1666.5;
Boundary11 = 1669;
Boundary12 = 1670;
Boundary13 = 1671;
Boundary14 = 1673.25;

for i=1:rtdd5length
    fmdepthBoundary1(i) = Boundary1;
    fmdepthBoundary2(i) = Boundary2;
    fmdepthBoundary3(i) = Boundary3;
    fmdepthBoundary4(i) = Boundary4;
    fmdepthBoundary5(i) = Boundary5;
    fmdepthBoundary6(i) = Boundary6;

    fmdepthBoundary7(i) = Boundary7;
    fmdepthBoundary8(i) = Boundary8;
    fmdepthBoundary9(i) = Boundary9;
    fmdepthBoundary10(i) = Boundary10;
    fmdepthBoundary11(i) = Boundary11;
    fmdepthBoundary12(i) = Boundary12;
    fmdepthBoundary13(i) = Boundary13;
    fmdepthBoundary14(i) = Boundary14;
end

%17.5 Section - Overview:
topSandfreeHordalandMD = 1655; topSandfreeHordalandTVD = 1366;
topBalderMD = 2050; topBalderTVD = 1570;
topListaMD = 2200; topListaTVD = 1639;

for i= 1:rtdd5length
    fmdepthSandfreeHordaland(i) = topSandfreeHordalandMD;
    fmdepthBalder(i) = topBalderMD;
    fmdepthLista(i) = topListaMD;
end

for i= 1:rtdd6length
    fmdepthSandfreeHordaland(i) = topSandfreeHordalandMD;
    fmdepthBalder(i) = topBalderMD;
    fmdepthLista(i) = topListaMD;
end

for i= 1:rtdd6avg2length
```

```matlab
        fmdepth_avg_SandfreeHordaland(i) = topSandfreeHordalandMD;
        fmdepth_avg_Balder(i) = topBalderMD;
        fmdepth_avg_Lista(i) = topListaMD;
    end



% Plot functions

 figure(1);
 grid on;
 hold on;
 set(gca,'YDir','Reverse');
 xlabel('Hardness, H','fontsize',12);
 ylabel('MD [m]','fontsize',12);
 title ('Hardness from raw data with averaged a5 and a6
exponents','fontsize',12);
 axis([-100 500, 1555 1765]) %axis([-100 500, 1495 2380])
 plot(H_1_raw,DMEAraw,'r');

saveas(figure(1),'C:\Users\berti\Desktop\Prosjektoppgave\Matlab\Plots2\H_1_
raw.jpg');

figure(2);
 grid on;
 hold on;
 set(gca,'YDir','Reverse');
 xlabel('Hardness, H','fontsize',12);
 ylabel('MD [m]','fontsize',12);
 title ('Hardness from raw data with averaged a5 and a6 exponents, dBPOS
introduced','fontsize',10);
 axis([-100 500, 1555 1765]) %axis([-100 500, 1495 2380])
 plot(H_1_raw_dBPOS,DMEAraw_dBPOS,'r');

saveas(figure(2),'C:\Users\berti\Desktop\Prosjektoppgave\Matlab\Plots2\H_1_
raw_dBPOS.jpg');

 figure(3);
 grid on;
 hold on;
 set(gca,'YDir','Reverse');
 xlabel('Hardness, H','fontsize',12);
 ylabel('MD [m]','fontsize',12);
 title ('Hardness from modified data with averaged a5 and a6 exponents,odd
values of dBPOS, WOB and RPMB removed','fontsize',8);
 axis([-100 500, 1555 1765]) %axis([-100 500, 1495 2380])
 plot(H_1_odd_removed,DMEAodd_removed,'r');

saveas(figure(3),'C:\Users\berti\Desktop\Prosjektoppgave\Matlab\Plots2\H_1_
odd_removed.jpg');

 figure(4);
 grid on;
 hold on;
 set(gca,'YDir','Reverse');
 xlabel('Hardness, H','fontsize',12);
 ylabel('MD [m]','fontsize',12);
 title ('Hardness from modified data with averaged a5 and a6 exponents,data
sorted with 3-point average','fontsize',8);
 axis([-100 500, 1555 1765]) %axis([-100 500, 1495 2380])
 plot(H_1,DMEA5,'r');
```

```matlab
saveas(figure(4),'C:\Users\berti\Desktop\Prosjektoppgave\Matlab\Plots2\H_1.
jpg');

figure(5);
grid on;
hold on;
set(gca,'YDir','Reverse');
xlabel('Hardness, H','fontsize',12);
ylabel('MD [m]','fontsize',12);
title ('Normalized hardness from modified data with averaged a5 and a6
exponents','fontsize',10);
axis([0 1, 1555 1765]) %axis([-100 500, 1495 2380])
plot(H1_norm,DMEA5,'r');

saveas(figure(5),'C:\Users\berti\Desktop\Prosjektoppgave\Matlab\Plots2\H1_n
orm.jpg');

figure(6);
grid on;
hold on;
set(gca,'YDir','Reverse');
xlabel('Hardness, H','fontsize',12);
ylabel('MD [m]','fontsize',12);
title ('Normalized hardness from modified data with two sets of a5 and a6
exponents','fontsize',10);
axis([0 1, 1555 1765]) %axis([-100 500, 1495 2380])
plot(H2_norm,DMEA5,'r');

saveas(figure(6),'C:\Users\berti\Desktop\Prosjektoppgave\Matlab\Plots2\H2_n
orm.jpg');

figure(7);
grid on;
hold on;
set(gca,'YDir','Reverse');
xlabel('[m/h] (for dBPOS)','fontsize',10);
ylabel('Time[s]','fontsize',12);
title ('dBPOS vs BPOS vs Hardness','fontsize',10);
axis([0 50, Time5(371) Time5(529)]); %axis([-100 500, 1495 2380])
plot(dBPOS5,Time5,'b',BPOS5,Time5,'k',H_2,Time5,'r');
legend('dBPOS','BPOS','Hardness');

saveas(figure(7),'C:\Users\berti\Desktop\Prosjektoppgave\Matlab\Plots2\dBPO
SvsBPOSSection1.jpg');

figure(8);
grid on;
hold on;
set(gca,'YDir','Reverse');
xlabel('Hardness & dBPOS','fontsize',10);
ylabel('MD [m]','fontsize',12);
title ('Normalized hardness & normalized dBPOS','fontsize',10);
axis([0 1, 1565 1595]) %axis([-100 500, 1495 2380])
plot(H2_norm,DMEA5,'r',dBPOS5norm,DMEA5,'b');
legend('Hardness','dBPOS');
hold on
plot(H2_norm,fmdepthBoundary1,'k');
hold on
plot(H2_norm,fmdepthBoundary2,'k');
hold on
```

```matlab
 plot(H2_norm,fmdepthBoundary3,'k');
 hold on
 plot(H2_norm,fmdepthBoundary4,'k');
 hold on
 plot(H2_norm,fmdepthBoundary5,'k');
 hold on
 plot(H2_norm,fmdepthBoundary6,'k');

saveas(figure(8),'C:\Users\berti\Desktop\Prosjektoppgave\Matlab\Plots2\H2_n
ormAndBoundariesSection1.jpg');

 figure(9);
 grid on;
 hold on;
 set(gca,'YDir','Reverse');
 xlabel('[m/h] (for dBPOS)','fontsize',10);
 ylabel('Time[s]','fontsize',12);
 title ('dBPOS vs BPOS','fontsize',10);
 axis([0 35, Time5(759) Time5(985)]); %axis([-100 500, 1645 1675+])
 plot(dBPOS5,Time5,'b',BPOS5,Time5,'k'); %,H_2,Time5,'r');
 legend('dBPOS','BPOS'); %,'Hardness');

saveas(figure(9),'C:\Users\berti\Desktop\Prosjektoppgave\Matlab\Plots2\dBPO
SvsBPOSSection4.jpg');

 figure(10);
 grid on;
 hold on;
 set(gca,'YDir','Reverse');
 xlabel('Hardness & dBPOS','fontsize',10);
 ylabel('MD [m]','fontsize',12);
 title ('Normalized hardness & normalized dBPOS','fontsize',10);
 axis([0 1, 1645 1675]) %axis([-100 500, 1495 2380])
 plot(H2_norm,DMEA5,'r',dBPOS5norm,DMEA5,'b');
 hold on
 plot(H2_norm,fmdepthSandfreeHordaland,'k');
 %plot(H2_norm,fmdepthBoundary7,'--k')
 legend('Hardness','dBPOS');

saveas(figure(10),'C:\Users\berti\Desktop\Prosjektoppgave\Matlab\Plots2\nor
malizeddBPOSvsBPOSSection4.jpg');

 figure(11);
 grid on;
 hold on;
 set(gca,'YDir','Reverse');
 xlabel('Hardness','fontsize',10);
 ylabel('MD [m]','fontsize',12);
 title ('Normalized hardness 17 1/2" section with formation
boundaries','fontsize',10);
 axis([0 1, 1495 2380]) %axis([-100 500, 1495 2380])
 plot(H2_norm,DMEA5,'r');
 legend('Hardness','dBPOS');
 hold on
 plot(H2_norm,fmdepthSandfreeHordaland,'b');
 hold on
 plot(H2_norm,fmdepthBalder,'b');
 hold on
 plot(H2_norm,fmdepthLista,'b');
```

```matlab
saveas(figure(11),'C:\Users\berti\Desktop\Prosjektoppgave\Matlab\Plots2\who
lesection.jpg');

 figure(12);
 grid on;
 hold on;
 set(gca,'YDir','Reverse');
 xlabel('Hardness & dBPOS','fontsize',10);
 ylabel('MD [m]','fontsize',12);
 title ('Normalized hardness & normalized dBPOS','fontsize',10);
 axis([0 1, 2000 2100]) %axis([-100 500, 1495 2380])
 plot(H2_norm,DMEA5,'r',dBPOS5norm,DMEA5,'b');
 hold on
 plot(H2_norm,fmdepthBalder,'k');
 %plot(H2_norm,fmdepthBoundary7,'--k')
 legend('Hardness','dBPOS');

saveas(figure(12),'C:\Users\berti\Desktop\Prosjektoppgave\Matlab\Plots2\Bal
derFmBoundary.jpg');

 figure(13);
 grid on;
 hold on;
 set(gca,'YDir','Reverse');
 xlabel('Hardness & dBPOS','fontsize',10);
 ylabel('MD [m]','fontsize',12);
 title ('Normalized hardness & normalized dBPOS','fontsize',10);
 axis([0 1, 2150 2250]) %axis([-100 500, 1495 2380])
 plot(H2_norm,DMEA5,'r',dBPOS5norm,DMEA5,'b');
 hold on
 plot(H2_norm,fmdepthLista,'k');
 %plot(H2_norm,fmdepthBoundary7,'--k')
 legend('Hardness','dBPOS');

saveas(figure(13),'C:\Users\berti\Desktop\Prosjektoppgave\Matlab\Plots2\Lis
taFmBoundary.jpg');

 figure(14);
 grid on;
 hold on;
 set(gca,'YDir','Reverse');
 xlabel('ROP [m/h]','fontsize',10);
 ylabel('MD [m]','fontsize',12);
 title ('Rate of Penetration','fontsize',10);
 axis([0 40, 1495 2380]) %axis([0 30, 1495 2380])1565 1595
 plot(ROP,DMEA,'r');
 legend('ROP');

saveas(figure(13),'C:\Users\berti\Desktop\Prosjektoppgave\Matlab\Plots2\ROP
vsMD.jpg');

 figure(15);
 grid on;
 hold on;
 set(gca,'YDir','Reverse');
 xlabel('RPM','fontsize',10);
 ylabel('MD [m]','fontsize',12);
 title ('Revolutions per minute','fontsize',10);
 axis([0 300, 1495 2380]) %axis([0 30, 1495 2380])1565 1595
 plot(RPMB,DMEA,'r');
```

```matlab
 legend('RPM');

saveas(figure(13),'C:\Users\berti\Desktop\Prosjektoppgave\Matlab\Plots2\RPM
vsMD.jpg');

figure(16);
 grid on;
 hold on;
 set(gca,'YDir','Reverse');
 xlabel('WOB [tons]','fontsize',10);
 ylabel('MD [m]','fontsize',12);
 title ('Weight on bit','fontsize',10);
 axis([0 40, 1495 2380]) %axis([0 30, 1495 2380])1565 1595
 plot(WOB,DMEA,'r');
 legend('WOB');

saveas(figure(13),'C:\Users\berti\Desktop\Prosjektoppgave\Matlab\Plots2\WOB
vsMD.jpg');
```

12.2 Pore pressure agent

```matlab
% Pore Pressure Agent %
% Made by Bertil Osheim for his master thesis %

clc
clear

% Load the correct folder for the data gathering %

cd('C:\Users\berti\Desktop\Prosjektoppgave\Matlab');

% Load drilling data of correct interval into matlab %

rtdd = xlsread('int17_5.xlsx');

% Length of drilling data %

rtddlength = length(rtdd);

% Inputs %

% Variables %
% Diameter of drillbit being used in interval %

dbit = 17.5; % [inch]

% Constant values %
% Gravity %

g = 9.81;

% Drilling coefficients for Bourgoyne-Young drilling model %
a2 = 0.000090;  % From average values of B-Y drilling coefficients, from
shale fm. in GoM area
```

```matlab
a3_avg = 0.000100; % From average values of B-Y drilling coefficients, from
shale fm. in GoM area
a4_avg = 0.000035; % From average values of B-Y drilling coefficients, from
shale fm. in GoM area

a5_avg = 1.25;      % From average of ranges      a5-Range: (0.5-2.0)
Bourgoyne et al.
a6_avg = 0.70;      % From average of ranges      a6-Range: (0.4-1.0)
Bourgoyne et al.

a5_soft = 1.625; %2.0 = Extremely Soft;
a6_soft = 0.85; %1.0 = Extremely Soft;
a5_hard = 0.875;  %0.5 = Extremely Hard;
a6_hard = 0.55;  %0.4 = Extremely Hard;


    DVER    = rtdd(:,1);
    DMEA    = rtdd(:,2);
    DBTM    = rtdd(:,3);
    Time    = rtdd(:,4);
    BPOS    = rtdd(:,5);
    ROP     = rtdd(:,6);
    RPMB    = rtdd(:,7);
    WOB     = rtdd(:,8);
    ECDB    = rtdd(:,9);


 % Calculate drillability and pore pressure from orginal(Raw)data

 j = 1;

for i = 1:1:rtddlength

    if (DMEA(i) - DBTM(i)) < 0.1

        f5_1_raw(j) = ((WOB(i)*2.20462262/dbit)/4)^a5_avg;    % [1000
lbf/in]
        f6_1_raw(j) = (RPMB(i)/60)^a6_avg;          % [1/min]

        K_1_raw(j) = (ROP(i)*3.2808)./(f5_1_raw(j).*f6_1_raw(j));
        H_1_raw(j) = 1/K_1_raw(j);

        f3_1_raw(j) = (ROP(i)*3.2808)./(f5_1_raw(j).*f6_1_raw(j));
        f4_1_raw(j) = (ROP(i)*3.2808)./(f5_1_raw(j).*f6_1_raw(j));
        f3f4_1_raw(j) = (ROP(i)*3.2808)./(f5_1_raw(j).*f6_1_raw(j));

        rho_pore_raw_f3_US(j) =
log(f3_1_raw(j))./(2.303*a3_avg.*(DVER(i)*3.2808).^0.69) + 9.0; % [lbm/gal]
        rho_pore_raw_f4_US(j) =
log(f4_1_raw(j))./(2.303*a4_avg.*DVER(i)*3.2808) + ECDB(i)*8.345404; %
[lbm/gal]
        rho_pore_raw_f3f4_US(j) = (log(f3f4_1_raw(j)) +
20.727*a3_avg.*(DVER(i)*3.2808).^0.69 +
2.303*a4_avg.*DVER(i)*3.2808.*ECDB(i)*8.345404)/(2.303*a3_avg.*(DVER(i)*3.2
808).^0.69 + 2.303*a4_avg.*DVER(i)*3.2808); % [lbm/gal]

        rho_pore_raw_f3(j) = rho_pore_raw_f3_US(j)/8.345404; % [g/cm3]
        rho_pore_raw_f4(j) = rho_pore_raw_f4_US(j)/8.345404; % [g/cm3]
        rho_pore_raw_f3f4(j) = rho_pore_raw_f3f4_US(j)/8.345404; %[g/cm3]

        DVERraw(j) = DVER(i);
```

184

```matlab
            DMEAraw(j) = DMEA(i);
            DBTMraw(j) = DBTM(i);
            Timeraw(j) = Time(i);
            BPOSraw(j) = BPOS(i);
            ROPraw(j)  = ROP(i);
            RPMBraw(j) = RPMB(i);
            WOBraw(j)  = WOB(i);
            ECDBraw(j) = ECDB(i);

            j = j + 1;
        end

end

% Calculate dBPOS from orginal BPOS and Time data

 k = 1;

for i = 1:3:(rtddlength-2)
    DVERavg(k) = (DVER(i) + DVER(i+1) + DVER(i+2))/3;
    DMEAavg(k) = (DMEA(i) + DMEA(i+1) + DMEA(i+2))/3;
    DBTMavg(k) = (DBTM(i) + DBTM(i+1) + DBTM(i+2))/3;
    Timeavg(k) = (Time(i) + Time(i+1) + Time(i+2))/3;
    BPOSavg(k) = (BPOS(i) + BPOS(i+1) + BPOS(i+2))/3;
    ROPavg(k)  = (ROP(i)  + ROP(i+1)  + ROP(i+2))/3;
    RPMBavg(k) = (RPMB(i) + RPMB(i+1) + RPMB(i+2))/3;
    WOBavg(k)  = (WOB(i)  + WOB(i+1)  + WOB(i+2))/3;
    ECDBavg(k) = (ECDB(i) + ECDB(i+1) + ECDB(i+2))/3;
    k = k + 1;
end

rtddavglength = length(WOBavg);

 j = 1;

    for i = 2:1:rtddavglength
        dBPOS1(j) = ((BPOSavg(i-1) - BPOSavg(i))./15.*3600);
        DVER1(j) = DVERavg(i);
        DMEA1(j) = (DMEAavg(i)+DMEAavg(i-1))/2; %DMEAavg(i)
        DBTM1(j) = DBTMavg(i);
        Time1(j) = Timeavg(i);
        BPOS1(j) = (BPOSavg(i)+BPOSavg(i-1))/2; %=BPOSavg(i)
        ROP1(j)  = ROPavg(i);
        RPMB1(j) = RPMBavg(i);
        WOB1(j)  = WOBavg(i);
        ECDB1(j) = ECDBavg(i);

        j = j + 1;
    end

rtdd1length = length(WOB1);

% Eliminate odd values of WOB, RPM and dBPOS

% Eliminate odd values of WOB

j = 1;
for i = 1:rtdd1length
    if WOB1(i) > 2.5 % [tonne]
        %>5 && WOB1(i) < 30
```

185

```matlab
            dBPOSelWOB(j) = dBPOS1(i);
            DVERelWOB(j) = DVER1(i);
            DMEAelWOB(j) = DMEA1(i);
            DBTMelWOB(j) = DBTM1(i);
            TimeelWOB(j) = Time1(i);
            BPOSelWOB(j) = BPOS1(i);
            ROPelWOB(j)  = ROP1(i);
            RPMBelWOB(j) = RPMB1(i);
            WOBelWOB(j)  = WOB1(i);
            ECDBelWOB(j) = ECDB1(i);

            j = j + 1;
    end
end

rtddelWOBlength = length(WOBelWOB);

% Eliminate odd values of RPMB

j = 1;
for i = 1:rtddelWOBlength
    if  RPMBelWOB(i) > 25 %[rpm]
        %>50 && RPMBelWOB(i) < 250

        dBPOSelRPMB(j) = dBPOSelWOB(i);
        DVERelRPMB(j) = DVERelWOB(i);
        DMEAelRPMB(j) = DMEAelWOB(i);
        DBTMelRPMB(j) = DBTMelWOB(i);
        TimeelRPMB(j) = TimeelWOB(i);
        BPOSelRPMB(j) = BPOSelWOB(i);
        ROPelRPMB(j)  = ROPelWOB(i);
        RPMBelRPMB(j) = RPMBelWOB(i);
        WOBelRPMB(j)  = WOBelWOB(i);
        ECDBelRPMB(j) = ECDBelWOB(i);

        j = j + 1;
    end
end

rtddelRPMlength = length(WOBelRPMB);

%Eliminate odd values of dBPOS

j = 1;

  for i = 1:1:rtddelRPMlength
      if dBPOSelRPMB(i) > 2.5 && dBPOSelRPMB(i) < 45 % [m/h]

        dBPOSeldBPOS(j) = dBPOSelRPMB(i);
        DVEReldBPOS(j) = DVERelRPMB(i);
        DMEAeldBPOS(j) = DMEAelRPMB(i);
        DBTMeldBPOS(j) = DBTMelRPMB(i);
        TimeeldBPOS(j) = TimeelRPMB(i);
        BPOSeldBPOS(j) = BPOSelRPMB(i);
        ROPeldBPOS(j)  = ROPelRPMB(i);
        RPMBeldBPOS(j) = RPMBelRPMB(i);
        WOBeldBPOS(j)  = WOBelRPMB(i);
        ECDBeldBPOS(j) = ECDBelRPMB(i);

        j= j + 1;
      end
```

```matlab
        end

    rtddeldBPOSlength=length(WOBeldBPOS);

    % Updating RTDD-data after sorting of values

            dBPOS2 = dBPOSeldBPOS;
            DVER2 = DVEReldBPOS;
            DMEA2 = DMEAeldBPOS;
            DBTM2 = DBTMeldBPOS;
            Time2 = TimeeldBPOS;
            BPOS2 = BPOSeldBPOS;
            ROP2  = ROPeldBPOS;
            RPMB2 = RPMBeldBPOS;
            WOB2  = WOBeldBPOS;
            ECDB2 = ECDBeldBPOS;

rtdd2length =length(WOB2);

% Sort list of data with respect to measured depth by removing
 % duplicate DMEA values

            dBPOSsortDMEA = []; dBPOSsortDMEA(1) = dBPOS2(1);
            DVERsortDMEA = []; DVERsortDMEA(1) = DVER2(1);
            DMEAsortDMEA = []; DMEAsortDMEA(1) = DMEA2(1);
            DBTMsortDMEA = []; DBTMsortDMEA(1) = DBTM2(1);
            TimesortDMEA = []; TimesortDMEA(1) = Time2(1);
            BPOSsortDMEA = []; BPOSsortDMEA(1) = BPOS2(1);
            ROPsortDMEA =  []; ROPsortDMEA(1)  = ROP2(1);
            RPMBsortDMEA = []; RPMBsortDMEA(1) = RPMB2(1);
            WOBsortDMEA =  []; WOBsortDMEA(1)  = WOB2(1);
            ECDBsortDMEA = []; ECDBsortDMEA(1) = ECDB2(1);

            deepest_depth = -999999;
            for i = 2:rtdd2length
                if DMEA2(i) > deepest_depth
                    deepest_depth = DMEA2(i);

                    dBPOSsortDMEA = [dBPOSsortDMEA dBPOS2(i)];
                    DVERsortDMEA = [DVERsortDMEA DVER2(i)];
                    DMEAsortDMEA = [DMEAsortDMEA DMEA2(i)];
                    DBTMsortDMEA = [DBTMsortDMEA DBTM2(i)];
                    TimesortDMEA = [TimesortDMEA Time2(i)];
                    BPOSsortDMEA = [BPOSsortDMEA BPOS2(i)];
                    ROPsortDMEA =  [ROPsortDMEA ROP2(i)];
                    RPMBsortDMEA = [RPMBsortDMEA RPMB2(i)];
                    WOBsortDMEA =  [WOBsortDMEA WOB2(i)];
                    ECDBsortDMEA = [ECDBsortDMEA ECDB2(i)];
                end
            end

 % Updating RTDD-data after sorting of values

            dBPOS3 = dBPOSsortDMEA;
            DVER3 = DVERsortDMEA;
            DMEA3 = DMEAsortDMEA;
            DBTM3 = DBTMsortDMEA;
            Time3 = TimesortDMEA;
            BPOS3 = BPOSsortDMEA;
            ROP3  = ROPsortDMEA;
            RPMB3 = RPMBsortDMEA;
```

```matlab
        WOB3  = WOBsortDMEA;
        ECDB3 = ECDBsortDMEA;

    rtdd3length = length(WOB3);

% Computing average of all drilling data

k = 1;

for i = 1:3:(rtdd3length-2)

    dBPOS3avg(k) = (dBPOS3(i) +dBPOS3(i+1) + dBPOS3(i+2))/3;
    DVER3avg(k) = (DVER3(i) + DVER3(i+1) + DVER3(i+2))/3;
    DMEA3avg(k) = (DMEA3(i) + DMEA3(i+1) + DMEA3(i+2))/3;
    DBTM3avg(k) = (DBTM3(i) + DBTM3(i+1) + DBTM3(i+2))/3;
    Time3avg(k) = (Time3(i) + Time3(i+1) + Time3(i+2))/3;
    BPOS3avg(k) = (BPOS3(i) + BPOS3(i+1) + BPOS3(i+2))/3;
    ROP3avg(k)  = (ROP3(i)  + ROP3(i+1)  + ROP3(i+2))/3;
    RPMB3avg(k) = (RPMB3(i) + RPMB3(i+1) + RPMB3(i+2))/3;
    WOB3avg(k)  = (WOB3(i)  + WOB3(i+1)  + WOB3(i+2))/3;
    ECDB3avg(k) = (ECDB3(i) + ECDB3(i+1) + ECDB3(i+2))/3;

    k = k + 1;
end

rtdd3avglength = length(WOB3avg);


% Updating drilling parameters after the elimination of odd values,
% sorting of depth data, and averaging of all values.

dBPOS4 = dBPOS3avg;
DVER4 = DVER3avg;
DMEA4 = DMEA3avg;
DBTM4 = DBTM3avg;
Time4 = Time3avg;
BPOS4 = BPOS3avg;
ROP4  = ROP3avg;
RPMB4 = RPMB3avg;
WOB4  = WOB3avg;
ECDB4 = ECDB3avg;

rtdd4length = length(WOB4);

% Import of excel pressure data originating from Final well report

file_excel = 'Pressure-data-17.5.xlsx';

dver_eow_temp = xlsread(file_excel,'A10:A417');
rho_pore_eow_temp = xlsread(file_excel, 'C10:C417');
rho_ovb_eow_temp = xlsread(file_excel, 'E10:E417');
rho_pore_norm_eow_temp = xlsread(file_excel,'G10:G417');

eowlength = length(dver_eow_temp);

% Aligning of the excel data to other field data, with respect to vertical
% depth and array length


  dver_eow = zeros(1,rtdd4length);
  rho_pore_eow = zeros(1,rtdd4length);
```

```matlab
    rho_ovb_eow = zeros(1,rtdd4length);
    rho_pore_norm_eow = zeros(1,rtdd4length);

for i = 1:rtdd4length
    for j = 1:eowlength

        if  DVER4(i) > dver_eow_temp(j)

            rho_pore_eow(i) = rho_pore_eow_temp(j);
            rho_ovb_eow(i) = rho_ovb_eow_temp(j);
            rho_pore_norm_eow(i) = rho_pore_norm_eow_temp(j);
        end
    end
end

  for i= 1:1:525
      rho_pore_eow(i) = 0.9650;
      rho_ovb_eow(i) = 1.8403;
      rho_pore_norm_eow(i) = 0.9650;
  end

% Calculate drillability and pore pressure from modified data with B&Y

for i= 1:rtdd4length
rho_pore_norm_US(i)= rho_pore_norm_eow(i)*8.34540445;
DVER4_US(i) = DVER4(i)*3.2808399;
WOB4_US(i) = WOB4(i)*2.20462262;
dBPOS4_US(i) = dBPOS4(i)*3.2808399;
ECDB4_US(i) = ECDB4(i)*8.34540445;

end

j = 1;

for i = 1:1:rtdd4length

    if (DMEA4(i) - DBTM4(i)) < 0.1

        f2_1(j) = exp(2.303*a2*(4272-DVER4_US(i)));

        f5_1(j) = ((WOB4_US(i)/dbit)/4)^a5_avg;    % [1000 lbf/in]
        f6_1(j) = (RPMB4(i)/60)^a6_avg;            % [1/min]

        K_1(j) = (dBPOS4_US(i))./(f5_1(j).*f6_1(j));
        H_1(j) = 1/K_1(j);

        PPnormal(j) = rho_pore_norm_eow(i);
        PP(j) = rho_pore_eow(i);

        Kp_mark_mod(j) = log(K_1(j))/2.303 +
a4_avg.*DVER4_US(i).*(ECDB4_US(i)-rho_pore_norm_US(i));

        a1 = 2.5;
        Dref = 1323*3.2808399;


        Kp_mark(j) = log10(K_1(j)) + a4_avg.*DVER4_US(i).*(ECDB4_US(i)-
rho_pore_norm_US(i));

        Kp_mark_normal(j) = (a1 + a2*Dref) - a2*DVER4_US(i);
```

```matlab
            rho_pore_BY_US(j) = rho_pore_norm_US(i) + (Kp_mark(j) - a1 -
a2*(Dref-DVER4_US(i)))/(a3_avg.*DVER4_US(i)^0.69 + a4_avg.*DVER4_US(i));
            rho_pore_BY(j) = rho_pore_BY_US(j)/8.34540445;

            rho_pore_BY_ecd_US(j) = rho_pore_norm_US(i) +
(a4_avg.*ECDB4_US(i).*(DVER4_US(i)-Dref) - a2*(Dref-
DVER4_US(i)))/(a3_avg.*DVER4_US(i)^0.69 + a4_avg.*DVER4_US(i));
            rho_pore_BY_ecd(j) = rho_pore_BY_ecd_US(j)/8.34540445;

            rho_pore_f3f4_mod_US_2(j) = (log(K_1(j)) - 2.303*1.7368 -
2.303*a2*(Dref-DVER4_US(i)) +
rho_pore_norm_US(i)*2.303*a3_avg.*DVER4_US(i)^0.69 +
2.303*a4_avg.*DVER4_US(i).*ECDB4_US(i))/(2.303*a3_avg.*DVER4_US(i)^0.69 +
2.303*a4_avg.*DVER4_US(i)); % [lbm/gal]
            rho_pore_f3f4mod_2(j) = rho_pore_f3f4_mod_US_2(j)/8.34540445; %
[g/cm3]

            % Uten noe modifikasjonoer
             rho_pore_f3f4_US(j) = (log(K_1(j)))/2.303 - a2*(4271-DVER4_US(i))
+ rho_pore_norm_US(i)*a3_avg.*DVER4_US(i).^0.69 +
a4_avg.*DVER4_US(i).*ECDB4_US(i))/(a3_avg.*DVER4_US(i).^0.69 +
a4_avg.*DVER4_US(i)); % [lbm/gal]
             rho_pore_f3f4(j) = rho_pore_f3f4_US(j)/8.34540445;


            dBPOS5(j) = dBPOS4(i);
            DVER5(j) = DVER4(i);
            DMEA5(j) = DMEA4(i);
            DBTM5(j) = DBTM4(i);
            Time5(j) = Time4(i);
            BPOS5(j) = BPOS4(i);
            ROP5(j)  = ROP4(i);
            RPMB5(j) = RPMB4(i);
            WOB5(j)  = WOB4(i);
            ECDB5(j) = ECDB4(i);

            j = j + 1;
        end

end
  K_1max = max(K_1);
  H_1max = max(H_1);
  dBPOS5max = max(dBPOS5);
  rho_pore_BYmax = max(rho_pore_BY);
  PPnormalmax = max(PPnormal);

  rtdd5length = length(K_1);

   % Normalize Hardness using one a5/a6-exponent

  for i=1:rtdd5length

      K1_norm(i) = K_1(i)/K_1max;
      H1_norm(i) = H_1(i)/H_1max;
      dBPOS5_norm(i) = dBPOS5(i)/dBPOS5max;
      rho_pore_BY_norm(i)= rho_pore_BY(i)/rho_pore_BYmax;
      PPnormal_norm(i) = PPnormal(i)/PPnormalmax;

  end

  % Drawing formation boundaries
```

```matlab
    % 17.5 Section - Overview:
    topSandfreeHordalandMD = 1655; topSandfreeHordalandTVD = 1366;
    topBalderMD = 2050; topBalderTVD = 1570;
    topListaMD = 2200; topListaTVD = 1639;

    for i= 1:rtdd5length
        fmdepthSandfreeHordaland(i) = topSandfreeHordalandTVD;
        fmdepthBalder(i) = topBalderTVD;
        fmdepthLista(i) = topListaTVD;
    end

% Plotting

%  figure(1);
%  grid on;
%  hold on;
%  set(gca,'YDir','Reverse');
%  xlabel('SG EMW','fontsize',12);
%  ylabel('TVD [m]','fontsize',12);
%  title ('Drillability','fontsize',12);
%  axis([0 750, 1300 1725])
%  plot(K_1,DVER5,'b');
%
saveas(figure(1),'C:\Users\berti\Desktop\Prosjektoppgave\Matlab\Plots3\dril
lability.jpg');

figure(2);
 grid on;
 hold on;
 set(gca,'YDir','Reverse');
 xlabel('Hardness','fontsize',12);
 ylabel('TVD [m]','fontsize',12);
 title ('Normalized hardness 17 1/2" section with formation
boundaries','fontsize',10);
 axis([0 1, 1500 2400])
 plot(H1_norm,DMEA5,'r');

saveas(figure(2),'C:\Users\berti\Desktop\Prosjektoppgave\Matlab\Plots3\hard
nessvsMD.jpg');

 figure(3);
 grid on;
 hold on;
 set(gca,'YDir','Reverse');
 xlabel('RPM','fontsize',12);
 ylabel('TVD [m]','fontsize',12);
 title ('RPM','fontsize',12);
 axis([55 300, 1300 1725])
 plot(RPMB5,DVER5,'k');

saveas(figure(3),'C:\Users\berti\Desktop\Prosjektoppgave\Matlab\Plots3\RPM.
jpg');

 figure(4);
 grid on;
 hold on;
 set(gca,'YDir','Reverse');
 xlabel('WOB [tons]','fontsize',12);
 ylabel('TVD [m]','fontsize',12);
 title ('WOB','fontsize',12);
```

```matlab
 axis([0 40, 1300 1725])
 plot(WOB5,DVER5,'k');

saveas(figure(4),'C:\Users\berti\Desktop\Prosjektoppgave\Matlab\Plots3\WOB.
jpg');


 figure(5);
 grid on;
 hold on;
 set(gca,'YDir','Reverse');
 xlabel('Hardness','fontsize',12);
 ylabel('TVD [m]','fontsize',12);
 title ('Normalized hardness 17 1/2" section with formation
boundaries','fontsize',10);
 axis([0 1, 1300 1725])
 plot(H1_norm,DVER5,'r');
 hold on
 plot(H1_norm,fmdepthSandfreeHordaland,'b');
 hold on
 plot(H1_norm,fmdepthBalder,'b');
 hold on
 plot(H1_norm,fmdepthLista,'b');

saveas(figure(5),'C:\Users\berti\Desktop\Prosjektoppgave\Matlab\Plots3\hard
ness.jpg');

 figure(6);
 grid on;
 hold on;
 set(gca,'YDir','Reverse');
 xlabel('Penetration rate/dBPOS [m/hr]','fontsize',12);
 ylabel('TVD [m]','fontsize',12);
 title ('Penetration rate/dBPOS 17 1/2" section with formation
boundaries','fontsize',10);
 axis([0 45, 1300 1725])
 plot(dBPOS5,DVER5,'g');
 hold on
 plot(dBPOS5,fmdepthSandfreeHordaland,'b');
 hold on
 plot(dBPOS5,fmdepthBalder,'b');
 hold on
 plot(dBPOS5,fmdepthLista,'b');

saveas(figure(6),'C:\Users\berti\Desktop\Prosjektoppgave\Matlab\Plots3\dBPO
S.jpg');

 figure(7);
 grid on;
 hold on;
 set(gca,'YDir','Reverse');
 xlabel('SG EMW','fontsize',12);
 ylabel('TVD [m]','fontsize',12);
 title ('Pressure gradients from FWR & ECD from RTDD','fontsize',12);
 axis([0.7 2.1, 1300 1725])
 plot(rho_pore_norm_eow,DVER4,'g');
 hold on
 plot(rho_pore_eow,DVER4,'b');
 hold on
 plot(ECDB4,DVER4,'c');
 hold on
```

```matlab
 plot(rho_ovb_eow,DVER4,'r');
 legend('PP-norm','Pore pressure','ECD','Overburden');

saveas(figure(7),'C:\Users\berti\Desktop\Prosjektoppgave\Matlab\Plots3\pres
sure_gradients_eow.jpg');

 figure(8);
 grid on;
 hold on;
 set(gca,'YDir','Reverse');
 xlabel('SG EMW','fontsize',12);
 ylabel('TVD [m]','fontsize',12);
 title ('Pore pressure gradient from B&Y','fontsize',12);
 axis([0.6 1.8, 1300 1725]);
 plot(rho_pore_BY,DVER5,'b');
 hold on
 plot(PPnormal,DVER5,'g');
 hold on
 plot(PP,DVER5,'c');
 legend('PP by B&Y','PPnormal - FWR','PP -FWR');

saveas(figure(8),'C:\Users\berti\Desktop\Prosjektoppgave\Matlab\Plots3\rho_
pore.jpg');

 figure(9);
 grid on;
 hold on;
 set(gca,'YDir','Reverse');
 xlabel('Modified drillability units','fontsize',12);
 ylabel('TVD [m]','fontsize',12);
 title ('Modified drillability parameter, Kmod','fontsize',12);
 axis([1 4, 1300 1725])
 plot(Kp_mark,DVER5,'k');
%  hold on
%  plot(Kp_mark_normal,DVER5,'b');

saveas(figure(9),'C:\Users\berti\Desktop\Prosjektoppgave\Matlab\Plots3\K_mo
d.jpg');

 figure(10);
 grid on;
 hold on;
 set(gca,'YDir','Reverse');
 xlabel('Normalized values','fontsize',12);
 ylabel('TVD [m]','fontsize',12);
 title ('Normalized values of hardness, dBPOS and pore
pressure','fontsize',10);
 axis([0 1, 1300 1725])
 plot(H1_norm,DVER5,'r');
 hold on
 plot(dBPOS5_norm,DVER5,'g');
 hold on
 plot(rho_pore_BY_norm,DVER5,'b');
%  hold on
%  plot(PPnormal_norm,DVER5,'k');
 legend('Hardness','dBPOS','Pore pressure');

saveas(figure(10),'C:\Users\berti\Desktop\Prosjektoppgave\Matlab\Plots3\K1+
rho_pore_norm.jpg');
```

NTNU

Norwegian University of
Science and Technology